

TALLINN UNIVERSITY OF TECHNOLOGY
DOCTORAL THESIS
66/2018

Structure and Variability of Currents in the Stratified Gulf of Finland

IRINA SUHHOVA

TALLINN UNIVERSITY OF TECHNOLOGY

School of Science

Department of Marine Systems

This dissertation was accepted for the defence of the degree 03/10/2018

Supervisor:

Dr Taavi Liblik
Department of Marine Systems
Tallinn University of Technology
Tallinn, Estonia

Advisor:

Prof Victor Zhurbas
P.P. Shirshov Institute of Oceanology
Russian Academy of Sciences
Moscow, Russia

Opponents:

Dr Daniel Rak
Observational Oceanography Laboratory
Institute of Oceanology of Polish Academy of Sciences
Sopot, Poland

Dr Piia Post
Institute of Physics
Faculty of Science and Technology
University of Tartu
Tartu, Estonia

Defence of the thesis: 10/12/2018, Tallinn

Declaration:

Hereby I declare that this doctoral thesis, my original investigation and achievement, submitted for the doctoral degree at Tallinn University of Technology has not been submitted for doctoral or equivalent academic degree.

Irina Suhhova

signature



Copyright: Irina Suhhova, 2018

ISSN 2585-6898 (publication)

ISBN 978-9949-83-354-2 (publication)

ISSN 2585-6901 (PDF)

ISBN 978-9949-83-355-9 (PDF)

TALLINNA TEHNIKAÜLIKOO
DOKTORITÖÖ
66/2018

Hoovuste muutlikkus ja struktuur stratifitseeritud Soome lahes

IRINA SUHHOVA

Contents

List of Publications.....	6
Author's Contribution to the Publications.....	7
Introduction.....	8
1 Motivation and Objectives	10
2 Material and Methods.....	11
3 Results and Discussion.....	15
3.1 Mean lateral flow structure in the upper layer.....	15
3.2 Mean vertical flow structure.....	16
3.3 Linkage between stratification and vertical current structure.....	18
3.4 Alterations of flow regime by atmospheric forcing.....	21
3.4.1 Current spectra	21
3.4.2 Prominent wind-driven processes	25
3.5 Influence of the deep layer current dynamics on biogeochemistry	30
4 Conclusions.....	34
References.....	36
Acknowledgements	42
Abstract	43
Lühikokkuvõte	44
Appendix.....	45
Curriculum vitae	127
Elulookirjeldus	129

List of Publications

The list of author's publications, on the basis of which the thesis has been prepared:

I Suhhova, I., Liblik, T., Lilovert, M.-J. and Lips, U. 2018. A descriptive analysis of the linkage between the vertical stratification and current oscillations in the Gulf of Finland. *Boreal Env. Res.* 23: 83–103.

II Suhhova, I., Pavelson, J. and Lagemaa, P. 2015. Variability of currents over the southern slope of the Gulf of Finland. *Oceanologia*, 57, 132–143.

III Lilovert, M.-J., Elken, J., Suhhova, I., Liblik, T. 2017. Observed flow variability along the thalweg, and on the coastal slopes of the Gulf of Finland, Baltic Sea. *Estuarine Coastal and Shelf Science*, 195, 23–33.

IV Liblik, T., Laanemets, J., Raudsepp, U., Elken, J., Suhhova, I. 2013. Estuarine circulation reversals and related rapid changes in winter near-bottom oxygen conditions in the Gulf of Finland. *Baltic Sea. Ocean Science*, 9, 917–930.

V Lips, U., Laanemets, J., Lips, I., Liblik, T., Suhhova, I., Suursaar, Ü. 2017. Wind-driven residual circulation and related oxygen and nutrient dynamics in the Gulf of Finland (Baltic Sea) in winter. *Estuarine Coastal and Shelf Science*, 195, 4–15.

Author's Contribution to the Publications

Contribution to the papers in this thesis are:

I – The author was responsible for collecting data, data analysis and writing the manuscript.

II – The author was responsible for collecting, processing and analysing the data, and for writing the manuscript.

III-V – The author participated in the field measurements, processed and analysed current velocity data and participated in writing the manuscripts.

Introduction

The Baltic Sea is a large brackish inland sea with restricted water exchange with the North Sea. The average depth of the Baltic Sea is 52 m, with a surface area of 415 200 km² and volume of 21 700 km³ (HELCOM 2009). The Baltic Sea can be considered as a strongly stratified estuarine system with remarkably high freshwater flux from the rivers and saline water inflow through the Danish Straits (Leppäranta and Myrberg 2009; Geyer and MacCready 2014). The bottom of the Baltic Sea is one of the largest dead zones in the world; the hypoxic water covers up to 20% of the total area (Conley et al. 2002; Diaz and Rosenberg 2008).

The Gulf of Finland is an elongated estuarine basin, located in the northeastern part of the Baltic Sea (Fig. 1). The Gulf is about 400-km long, its width varies between 48 and 135 km, and its depth decreases from the entrance to the easternmost part (Alenius et al. 1998). The Gulf has a free water exchange with the Baltic Proper through the western border, and freshwater discharge is mainly concentrated to the eastern part of the Gulf through the Neva River. Surface layer salinity increases from 0–3 g kg⁻¹ in the easternmost area up to 5–7 g kg⁻¹ at the entrance area, while the deep layer salinity below the quasi-permanent halocline (60–70 m) exceeds 8–10 g kg⁻¹ (Alenius et al. 1998). The freshwater input in the east and saltier water in the west create the typical estuarine circulation with an inflow in the deep layer and an outflow in the upper layer in the Gulf. As the estuarine circulation is intensified by the northeasterly and northerly winds (Elken et al. 2003; Liblik and Lips 2012) the alterations or even reversals of the estuarine circulation (inflow in the surface layer and outflow in the deep layer) can occur in the case of strong westerly winds (Elken et al. 2003). The mean surface circulation in the Gulf of Finland is weak and cyclonic, with the eastward flow of the northern Baltic Proper water along the southern coast and the westward flow along the northern coast (Palmén 1930; Alenius et al. 1998; Andrejev et al. 2004). At shorter time-scales, the circulation is more complicated and mainly caused by the changes in the wind forcing.

The thermohaline stratification in the Gulf of Finland is variable and reveals clear seasonality. The water body in deep enough areas is well mixed down to quasi-permanent halocline during the winter period and has mostly two-layer structure (Alenius et al. 1998). However, the wind-induced strong estuarine circulation reversals may cause occasional stratification weakening (Elken et al. 2003) and collapse events (Elken et al. 2014) in the Gulf, while estuarine circulation results in stronger stratification (Elken et al. 2003; Liblik and Lips 2012). The seasonal thermocline develops at a depth of 10–20 m from the beginning of May and starts to erode by the end of August (Alenius et al. 1998; Liblik and Lips 2011). Therefore, during the summer, a three-layer vertical structure appears in the deeper areas of the Gulf of Finland.

The coastal upwelling and downwelling events remarkably affect the vertical thermohaline structure in the Gulf. Strong enough alongshore wind impulses cause the coupled upwelling-downwelling events along southern/northern coasts (Zhurbas et al. 2008; Lips et al. 2009). Owing to the prevailing south-westerly winds in the region (Mietus 1998; Soomere and Keevallik 2003) the upwelling is mainly expected at the Finnish coast as it was shown by the model simulations (Myrberg and Andrejev 2003; Andrejev et al. 2004). However, the recent studies revealed that the frequencies of upwelling events are similar near the northern and southern coast of the Gulf (Uiboupin and Laanemets 2009; Lehmann et al. 2012; Kikas and Lips 2016). Both

upwelling and downwelling events are usually accompanied by the intense jet-like along-shore currents, with speeds reaching 30 cm s^{-1} (Laanemets et al. 2005). The width of downwelling jet can reach up to 12 km (Laanemets et al. 2005) and upwelling cross-shore extent can exceed 30 km, with temperature drop of up to 11°C (Lips et al. 2009).

Seiches and inertial oscillations have high contribution to the kinetic energy and vertical mixing in the Gulf (Arneborg and Liljebladh 2001; Lorke et al. 2002; Lilover et al. 2011), while the energy input of tidal forcing is considered to be low (Reissmann et al. 2009). The energy maxima of current oscillations are usually revealed at a broad semi-diurnal frequency band (BSD), broad diurnal frequency band (BD) and/or low-frequency seiches band (LFS) (Wübbler and Krauss 1979; Jönsson et al. 2008; Lilover et al. 2011). Wübbler and Krauss (1979) revealed presence of seiches with periods of 19 (20) h – 4th mode, 24 (22) h – 3rd mode and 28 (26) h – 2nd mode and diurnal tidal constituents K1 (23.93 h) and O1 (25.82 h), which are the contributors into the BD frequency band. Strong oscillations close to the 2nd and 3rd mode were also observed using model simulation by Jönsson et al. (2008). The energy maximum revealed at the seiche period of 31 hours belongs to the LFS band.

Changes in salinity and oxygen conditions in the deep layers of the Baltic Sea are influenced by major inflows from the North Sea (Matthäus and Franck 1992). Such inflow events transport highly saline oxygen-rich water into the Baltic Proper. However, the water coming from the Baltic Proper to the Gulf of Finland originates from the sub-halocline layer and induces stronger stratification and increasing hypoxic conditions in the deep layers of the Gulf of Finland (Laine et al. 2007; Conley et al. 2009; Liblik et al. 2018), as well an increase in phosphorus concentration (Lips et al. 2008). Changes in the near-bottom oxygen concentrations can lead to the release of phosphorus from sediments and transportation it to the upper layers (Viktorsson et al. 2012).

1 Motivation and Objectives

The circulation in the Gulf of Finland is complicated and variable. There are no steady currents or permanent dominant forces (such as tides) that would determine the current field in the Gulf. Circulation in the Gulf is very sensitive to wind forcing (e.g., Elken et al. 2003, Liloer et al. 2011, Liblik and Lips 2012). Therefore, the wind variability in various temporal scales presumably has consequences to current fields. Previous current profiling experiments in the Baltic Sea (e.g., Liblik and Lips 2012, Bulczak et al. 2016) and in other stratified marine areas (e.g., van Haren 2000) indicate that current structure is linked to pycnoclines. Variable wind forcing and stratification makes the current dynamics difficult to model and predict. On the other hand, advective fluxes of physical (e.g., heat, salt, buoyancy), biogeochemical (e.g., nutrients, oxygen), biological (e.g., plankton, fish larvae) or anthropogenic pollution (oil, dredging caused suspended matter) have a major impact to the conditions in the sea. Eutrophication caused consequences, such as hypoxia or harmful algal blooms are still actual topics in the Gulf of Finland. Lack of knowledge in the current dynamics is one source of uncertainty in the understanding of eutrophication-related processes, e.g., it is difficult to give adequate estimates of nutrient budgets, and it is not clear, what are the fluxes between the Gulf of Finland and the Baltic Proper. Prior to the present thesis, only a few acoustic current profile measurements in the Gulf are published in literature: episodic shipboard measurements (e.g., Pavelson et al. 1999, Laanemets et al. 2005); time-series in shallow coastal areas (Suursaar and Aps 2007, Liloer et al. 2011, Rasmus et al. 2015), and one time-series in the central, deeper part of the Gulf (Liblik and Lips 2012). The present work relies on 11 bottom-mounted current profiler deployments in the Gulf of Finland. The main aim of the thesis is to investigate temporal variability of vertical current structure from hours to months in different stratification conditions and seasons.

The main objectives of the thesis are:

- To describe the lateral and vertical mean current structure, compare it with earlier studies and relate it to the mean wind patterns;
- To show the linkage between the current shear maxima and the two pycnoclines;
- To describe the effect of wind forcing on the current structure through the water column;
- To relate variability of dominant oscillation frequencies with the presence of pycnoclines and wind forcing (or their variability);
- To relate the changes in the oxygen and nutrient conditions in the near-bottom layer to the deep layer current dynamics.

2 Material and Methods

The bottom-mounted Acoustic Doppler current profiler (ADCP) data analysed in the present thesis were collected in the Gulf of Finland in the frame of different research projects of the Department of Marine Systems at TUT (Tallinn University of Technology) from March 2009 until May 2014. Acoustic current profilers apply the Doppler Effect by transmitting short pulses (pings) at a fixed frequency and receiving the echoes from small particles such as plankton and suspended sediments in the water. While most of the sound goes forward, unaffected by scatters, the reflected backscattered sound is Doppler shifted expressed as the difference in frequency between the waves the profiler sends out and the waves it receives. By measuring the Doppler shift and the time series of returning acoustic echoes, the device calculates current velocities at many different depths, providing a current profile. Several different companies produce ADCPs, and one of them is Teledyne RD Instruments, who produced their first ADCPs in 1982 (Teledyne RD Instruments 2006).

One of the first ADCP measurements in the Gulf of Finland was made by Estonian and Finnish marine researchers in 1990-s, mainly as a background data for biological process studies (Pavelson et al. 1999, Laanemets et al. 2005). Suursaar and Aps (2007) made measurements in Estonian coastal waters in summer 2006 and Lilover et al. (2011) in summer 2008. Since 2008, approximately 30 measurements using a self-contained ADCP were made by the Department of Marine Systems at TUT in the different parts of the Gulf (deep areas and coastal areas). Liblik and Lips (2012) described the temporal variations of vertical current structure in the central, deeper part of the Gulf during summer 2009 (depth 85 m) and showed that a strong outflow and inflow could occur in the upper and deeper layers.

The ADCP data collected in 2009–2014 were used to investigate different aspects of the flow pattern and variability: 1) lateral structure of current (Papers II and III), 2) vertical structure of current (Paper I, III), 3) linkage between stratification and vertical current structure (Papers I, IV, V), 4) influence of variable atmospheric forcing on flow regime (Papers I, II, III, IV, V) and 5) impact of the deep layer current dynamics on biogeochemistry (Papers IV and V).

The first study (Paper I) analysed the five time-series of bottom-mounted ADCP data in the period 2009–2014 (Fig. 1). For the second study (Paper II), the current velocity measurements using bottom-mounted ADCP were carried out at the southern coast of the Gulf of Finland from 13 March to 30 June 2009 (Fig. 1). For the third study (Paper III), multi-monthly current measurements were conducted in different locations in the period from 2009 until 2014 (Fig. 1). For the fourth study (Paper IV) two bottom-mounted ADCP were located along the thalweg of the Gulf: one in the eastern part and the second in the western part of the study area, approximately 100 km apart (Fig. 1). Six surveys along the thalweg performed from December 2011 until May 2012 included ten stations of CTD (conductivity, temperature, depth) profiles and sampling for calibration of sensors. For the fifth study (Paper V), two bottom-mounted acoustic Doppler current profilers were used: ADCP at the thalweg of the Gulf and RDCP (Recording Doppler Current Profiler) in the shallow area near the southern coast of the Gulf (Fig. 1). Water samples for nutrient analyses and vertical CTD profiles were collected at 12 stations during surveys from December 2013 to May 2014. Additionally, water samples were used for quality control of oxygen data.

The current velocity data were obtained with a bottom-mounted acoustic Doppler current profiler 307.2 kHz broadband ADCP (Workhorse Sentinel, Teledyne RD Instruments), except one measurement where the RDCP 600 (Aanderaa) was used. Current profilers were deployed on the seafloor with a trawl-resistant platform. The profilers were set to collect the measurements with a vertical increment of 2 m depth bins and sampling interval from 10 min to 1 h. The echo from the sea surface is much stronger than the echo from scatters in the water, therefore, the data from the last 6% (transducer beam angles were oriented 20° from the vertical) near the surface can be contaminated due to the surface side lobe effect (Teledyne RD Instruments 2006) and were eliminated from the dataset. Thus, the uppermost reliable measurements were at a depth range of 5 m to 10 m from the surface. In the near-bottom layer, the deepest 5 m were lost due to the blanking distance between the instrument and the first layer from which correct data could be used. Velocity accuracy is 0.5 % of the water velocity relative to ADCP. The quality of the data at each level was checked using certain criteria for the internal quality parameters of ADCP following the procedure developed by Book et al. (2007). The location of current profilers and study periods for each publication is given in Table 1.

The time series of currents were filtered with a 1-h moving average filter to get hourly values for some descriptive and statistical analysis purposes, such as the vertical distribution of current velocity components, polar histograms of currents, rotary spectral analysis, average and maximum current velocity values. For the low-frequency current analysis in all papers, the time series were filtered with a 36 h cut-off Butterworth filter (Butterworth 1930).

For spectral structure investigations of current oscillations, rotary spectral analysis technique introduced by, Emery and Thomson (2004) was applied. The exact calculation procedures can be found in Paper I.

The CTD and oxygen data were collected aboard the research vessel Salme by Idronaut S.r.l CTD probe Ocean Seven 320plus. The quality of the salinity data was checked against the water sample analyses using a high-precision salinometer 8410A Portasal (Guildline). Salinity values were expressed as Absolute Salinity (g kg^{-1}) in the thesis, but Practical Salinity Scale (PSS-78) was used in figures 10 and 11. Salinity scale PSS-78 do not have units and the values for the Baltic Sea are about 0.1 smaller than in the Absolute Salinity scale. The dissolved oxygen sensor was calibrated before each survey and the data quality was checked against water sample analyses. The dissolved oxygen concentration was measured using the OX 4000 L DO meter (WWR International, LLC). The exact calibration procedures can be found in Paper IV and Paper V.

Table 1. Mooring positions, deployment periods and depth range of ADCP data used in presented publications.

Paper	ID	Latitude (N)	Longitude (E)	Period	Depth range (m)	Sea depth (m)
II, III	L3	59°27.40'	24°09.96'	13.03.2009–30.06.2009	7–45	50
III	P4	59°41.20'	24°37.40'	23.07.2009–24.09.2009	8–80	85
III	K8	59°42.10'	26°24.23'	12.01.2010–27.04.2010	6–58	63
I*, III	P9	59°41.02'	24°37.45'	14.04.2010–31.08.2010	9–79	84
I	NS11	59°58.80'	26°20.80'	30.09.2010–28.10.2010	8–62	67
I, III	NS16	59°50.34'	24°49.90'	13.07.2011–05.09.2011	9–73	78
I, III, IV	RW21	59°29.60'	23°54.10'	21.12.2011–09.05.2012	10–86	91
III, IV	RE20	59°45.05'	24°27.19'	21.12.2011–09.05.2012	8–82	87
III	P22	59°41.00'	24°37.50'	28.05.2012–09.10.2012	8–80	85
I, III, V	R25	59°35.13'	24°15.64'	09.12.2013–06.05.2014	10–82	87
III, V**	C25	59°28.98'	24°20.82'	09.12.2013–28.04.2014	7–19	21

*In Paper I, measurements from the period 01.06.2010–31.08.2010 were used

** RDCP data

Additionally, the following data sets were used in the thesis

- Wind data from the Kalbådagrund (Paper I, III and IV), Tallinnamadal lighthouse (Paper I, II, IV and V) and Utö (Paper III) meteorological stations were used.
- The sea level data from Pakri gauge and ADCP's pressure sensor were used in Paper II; sea level data from Kunda coastal station were used in Paper IV.
- Circulation model HIROMB (High Resolution Operational Model for the Baltic Sea) results were used in Paper II.

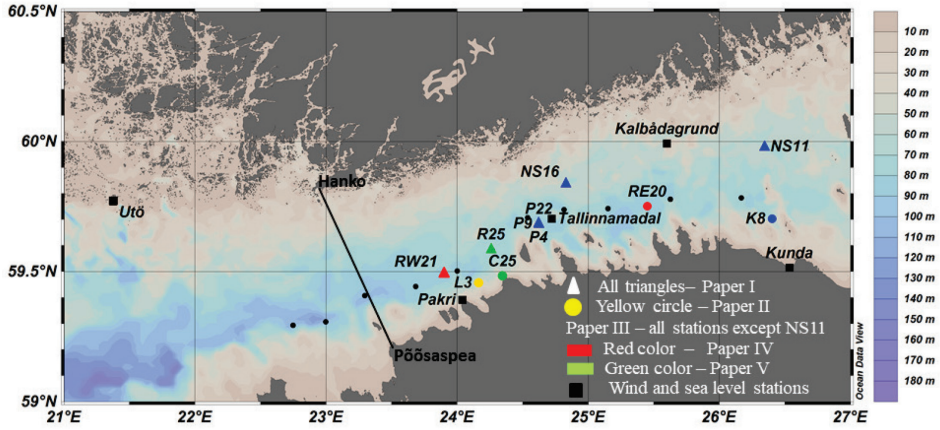


Figure 1. Map of the study area in the Gulf of Finland. Locations of ADCP deployments (Table 1), wind measurements locations at Kalbådagrund, Utö, Tallinnamadal Lighthouse and sea level stations in Pakri and Kunda are shown. Black dots represent the locations of the CTD stations along the thalweg. The western border of the Gulf is defined as the black line from Pöösaspea to Hanko.

3 Results and Discussion

3.1 Mean lateral flow structure in the upper layer

The long-term average circulation pattern in the upper layer of the Gulf of Finland is cyclonic – with fresher water outflow along the northern coast and saltier water inflow along the southern coast (Palmén 1930; Alenius et al. 1998, Stipa 2004, Kikas and Lips 2016). Such a mean flow scheme is mainly caused by the prevailing wind force, salinity gradient and the Coriolis Effect (Alenius et al. 1998). The wind field over the Baltic Sea is mostly promoted by eastward moving atmospheric cyclones, with dominant wind direction from the southwest (Mietus 1998, Soomere and Keevallik 2001, Keevallik and Soomere 2014). The freshwater inflow into the Gulf mostly comes from the Neva River which is located in the easternmost part of the basin (the annual freshwater run-off is about $114 \text{ km}^3 \text{ y}^{-1}$), while the saline water inflow from the Baltic Proper comes through the western border with annual inflow of about 600 km^3 (Alenius et al. 1998). The combination of the freshwater run-off from the rivers and saltier water inflow from the Baltic Proper has a major impact on the salinity distribution of the Gulf. The presence of the westward-directed surface layer current near the northern coast in the entrance area of the Gulf can be seen from the recent long-term measurements made by Rasmus et al. (2015). The mean flow structure is a mixed result of temporal variability of forcing (wind, buoyancy) and spatial variability (e.g., travelling of eddies, meandering of coastal currents). The most variable forcing factor, especially for the uppermost layer, in the area is wind. Anyhow, it can be expected that the resulting mean of time-series gives an estimate of residual currents in the location.

The observations carried out on the thalweg (Fig. 1, locations RE20, RW21, R25, P22) together with historical observations demonstrated well the known cyclonic circulation showing eastward current direction (Fig. 2) in the uppermost measured bins (8–10 m depth). However, the inflow was located further offshore from the southern coast compared to results obtained by Palmén (1930) and Andrejev (2004). Interesting circulation features were found close to the southern coastal slope in the Gulf, mean current vectors in three stations showed across-gulf directed flow (Paper II, III) (Fig. 2a). Mean offshore current (from the southern coast) component (at C25, Figs. 1–2) and onshore current (at L3) were found in the western part of the Gulf while in the eastern part (at K8) mean offshore current was revealed in the upper layer. It should be noted, that wind conditions during these observations deviated from the climatological mean (Fig. 3). Mean wind vector was from the north-west during the observations at station L3 while it was from the south during observations at K8 (Fig. 3). Mean air flow direction matched with the climatological mean (southwest) at C25, but the magnitude of the mean vector was greater during current observations (Fig. 3). However, the results obtained at the stations L3 and K8 support simulations of numerical models, which suggested the presence of anticyclonic loops in the mean circulation pattern in the central and western part of the southern Gulf (Elken et al. 2011, their Fig. 2; Lagemaa 2012, his Fig. 12). Mean offshore current component at station C25 was present only for the period 2010–2011 (Lagemaa 2012, his Fig. 12a).

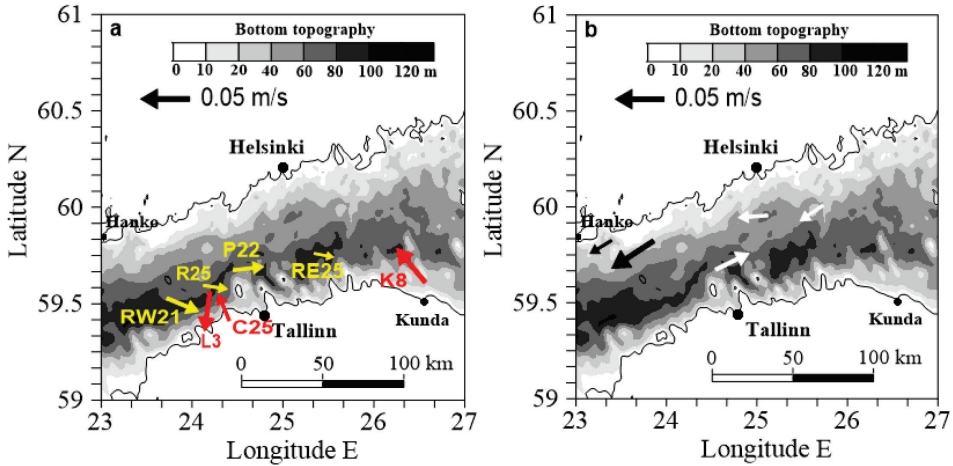


Figure 2. Maps of resultant vectors of current at the 10 m depth. (a) New ADCP measurements and (b) historical measurements. The exact calculation procedure can be found in Paper III. Arrows are centred on the measurements sites. Yellow arrows indicate new measurements along the thalweg (4 locations) and the red arrows indicate new measurements along the southern coast (3 locations). The historical data are marked by white (years 1923–1927, Palmén 1930) and black (year 1979, Laakkonen et al. 1981) arrows.

3.2 Mean vertical flow structure

The vertical current structure of the Gulf of Finland is rather complex and depends on the wind forcing and stratification.

Six observations were carried out along the thalweg in different years, three of them during the winter period and the other three during the summer period. All winter measurements were acquired in various locations, while summer measurements had the same location on the thalweg (Fig. 1, locations P4, P9, P22). Vertical profiles of mean current vectors revealed nearly unidirectional vertical distribution throughout the water column in winter (Paper III) (Fig. 3b). In all three locations, the inflow to the Gulf prevailed through the water column. Simultaneously with an inflow at the thalweg, an outflow was observed near the southern coast in winter 2013–2014 (Paper V). The vertical profiles of mean current vectors had similar two-layer structure with an inflow in the upper layer and an outflow in the deep layer in summers 2009 (station P4, Fig. 3c) and 2012 (station P22, Fig. 3c), while in summer 2010 the three-layer flow was revealed (station P9, Fig. 3c). It must be noted that during 2010 observations, the magnitude of the mean wind vector from south-west agreed closely with the long-term mean, while during observations made in 2009 and 2012, airflow from the southwest was stronger (Fig. 3c, upper panel). Therefore, the mean current profile in 2010 likely represents the long-term mean flow regime at thalweg in summer while the years 2009 and 2012 describe the reversed flow structure in the case of higher (than the climatic mean) prevalence of airflow from the southwest (Paper III). The resultant current in the coastal zone and northward from the thalweg revealed a multi-layer structure with an outflow in the upper layer for all stations (Fig. 3a).

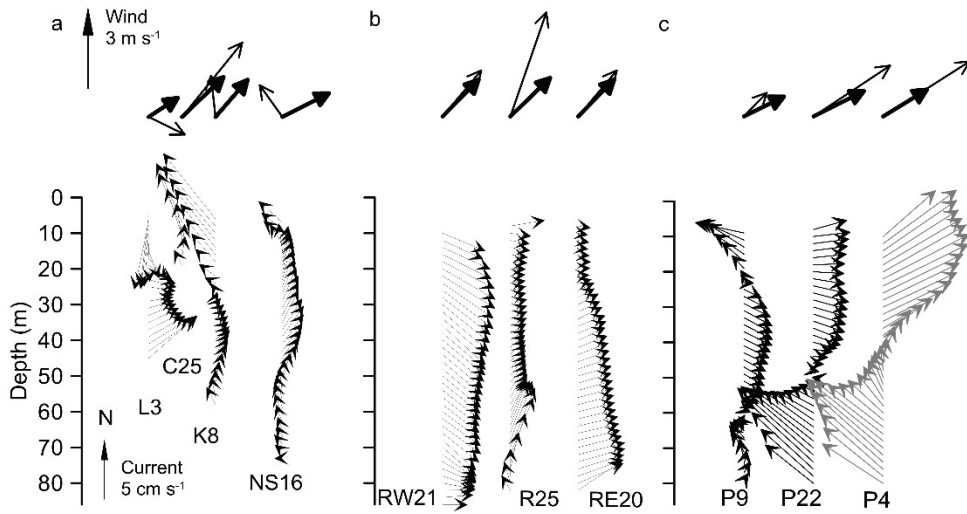


Figure 3. The resultant vectors of wind (upper arrows) and currents (a) at coastal stations and along the thalweg (b) in winter and (c) in summer. The thin arrows are the means of the measurement periods and bold arrows are the long-term (1981–2015) mean wind vectors in the same period during the year, respectively. Two time series (RW21 and R25) were measured towards the west from central station P (where three series P4, P9, P22 were acquired) and one (RE20) towards the east (see Fig. 1).

At all stations located in the western part of thalweg, the mean current speed was stronger in the upper (10.7–12.1 cm s^{-1}) and deeper layers (8.9–12.1 cm s^{-1}), while station RE20, located in the eastern part of the thalweg, revealed a continuous decrease of the mean speed with the depth (from 10.9 cm s^{-1} in the upper layer to 7.3 cm s^{-1} in the deep layer) (Table 2). The maximum average speed values were recorded in the near-bottom layer at station P22, being 12.1 cm s^{-1} . At the coastal stations L3, C25, K8 as well as the stations located closer to the northern slope NS11 and NS16, the mean current speed had highest values in the upper layer and decreased with the depth (Table 2). Except for the coastal station K8, the mean current speed in the upper layer was approximately in the same order (about 11–12 cm s^{-1}) as current observations made by Rasmus et al. (2015) at the northern slope of the Gulf. Stations NS11 and NS16 located close to the northern coast had a current speed of about 4 cm s^{-1} in the near-bottom layer, which is similar to the values obtained by Rasmus et al. (2015).

The strongest (1-hour mean) current in the upper layer (64.6 cm s^{-1}) was registered during winter 2011/2012 and in the deep layer (58.5 cm s^{-1}) during winter 2013/2014 measurements (Table 2).

It has to be noted that the present results miss the measurements in the uppermost 7–10 m layer, therefore the currents in the surface layer could not be described in the present study. However, the measurements made by Alenius et al. (1998) in the upper layer showed higher current speeds in the range of 10–20 cm s^{-1} . A recent study carried out in the Gulf of Finland using drifters (Tuomi et al. 2018) and the model simulations (Alari et al. 2016) suggested even higher current speeds due to the surface Stokes drift contribution.

The measurements in the closest 4 meters above the seabed were also not performed; therefore, the flow conditions in the bottom boundary layer are not known. To describe current velocities in the bottom boundary layer the Ekman theory is widely used in physical oceanography based on the balance of the frictional and the Coriolis forces. The dynamics of the bottom boundary layer also depends on the bottom roughness, strength of the flow and stratification. Measurements made in the waters of Lake Michigan had a median current speed of 2.7 cm s^{-1} at 1 m above the bottom (Troy et al. 2016). The results revealed by the observations (Rasmus et al. 2015) for the western and eastern Gulf of Finland had slightly higher values showing that the mean current speed at 2 m above bottom was in the range of $4.5\text{--}5 \text{ cm s}^{-1}$.

Table 2. Average and maximum values (1 h average) of current speed (cm s^{-1}) for the selected depth range: near-bottom layer, intermediate layer (20–50 m) and upper layer (8–11 m) at the eleven locations and average wind speed (m s^{-1}) during the measurement periods.

ID	Mean speed (cm s^{-1})			Maximum speed (cm s^{-1})			Wind speed (m s^{-1})
	Deep layer (m)	20–50 m	8–11m	Deep layer	20–50 m	8–11m	10 m height
L3	- (max depth 45m)	7.7	11.4	-	33.5	39.5	6.1
P4	11.3 (72–80)	9.2	12.1	44.7	44.4	51.4	6.0
K8	3.5 (50–58)	4.5	8.8	21.2	26.5	51.8	5.8
P9	8.9 (71–79)	8.0	11.5	34.9	39.7	55.4	6.1
NS11	5.6 (54–62)	8.4	10.7	25.8	41.7	35.0	7.3
NS16	5.0 (65–73)	7.3	11.1	29.3	23.2	41.3	5.7
RW21	11.2 (78–86)	9.8	12.0	36.7	48.9	64.6	8.5
RE20	7.3 (74–82)	8.7	10.9	34.8	44.5	49.4	8.5
P22	12.1 (72–80)	9.6	11.1	46.2	48.8	41.5	6.6
R25	11.9 (74–82)	9.7	10.7	58.5	50.6	55.1	8.6
C25	- (max depth 19m)	-	11.7	-	-	53.1	8.5

3.3 Linkage between stratification and vertical current structure

The vertical current structure is dependent on the presence of stratification. There are several studies, which show the coincidence in the vertical location of pycnoclines and current shear maxima (e.g. van Haren 2000, Janout et al. 2013, Li et al. 2016, Pu et al. 2017). Barotropic flow exists in the vertically mixed water column (Koue et al. 2018; Allahdadi and Li 2017; Lilover 1989). Hence, the presence or absence of stratification and location of pycnoclines determine the vertical current structure (Csanady 1973; Saenko 2006; Shivaprasad et al. 2013).

Vertical stratification in the Gulf of Finland is variable and has a highly seasonal character. In winter, the water body is rather well mixed down to the halocline at the depths of 60–80 m (Haapala and Alenius 1994, Alenius et al. 2003). Starting from May, the solar heating and wind mixing form a sharp seasonal thermocline at the depths of

10–20 m, it develops during summer and starts to erode by the end of August (Alenius et al. 1998; Liblik and Lips 2011). Therefore, in deep enough areas, mostly two-layer structure exists in winter and three-layer structure during summer.

Two winter measurements located in the western part of the Gulf (RW21, R25) had a similar pattern of the vertical flow structure with the current shear remaining weak until the first half of January (Fig. 4d and 4e). During both measurements, the reversed estuarine circulation (inflow in the upper layer and strong outflow in the deeper layer) was a result of strong SW winds. The reversal of estuarine circulation destroyed the stratification (because this layered transport caused a density increase in the upper layer and decrease in the deep layer), and as a consequence, a barotropic flow system formed in the weakly stratified conditions. Such events can weaken stratification also in the Northern Baltic Proper (Elken et al. 2006). Starting from 1990, the breakdowns of stratifications during the winter periods occur more commonly due to the shift in the wind regime: increase of the westerly-southwesterly wind impulses (Elken et al. 2014; Lehtoranta et al. 2017). At the beginning of January 2012 and 2014, the wind force weakened and changed direction creating favourable conditions for re-establishment of estuarine circulation. Starting from the second half of January, a strong current shear near the bottom was associated with saltwater wedge intrusion into the Gulf, which resulted in the re-establishment of the halocline (Paper IV, V). The shear maximum in the upper 10–20 m layer during the period when the seasonal thermocline did not exist was associated with the secondary halocline, which developed due to the westward transport of fresher water (Paper I, IV). Thus, both two-layer and three-layer flow regimes occur during winters in the Gulf.

During the first half of the observation period in autumn 2010, a strong shear maximum was observed at around 25 m depth and it deepened down to 40 m by the end of October (Fig. 4c). The current shear maxima coincided with the location of the seasonal thermocline, which deepened due to autumn convection (Paper I). Deepening of the seasonal thermocline during the summer periods in the Gulf is on average from 24 m in June down to 32 m in August (Liblik et al. 2011; Liblik and Lips 2017). Deepening and weakening of the seasonal thermocline continue in autumn until it is vanished (Lehtoranta et al. 2017).

Summer measurements acquired at the central station P9 and the station N16, northward from the thalweg, revealed the strongest current shear in the seasonal thermocline. The other maximum was occasionally observed at the depth of halocline around 60 m, which implies the existence of a three-layer flow in the water column during both summer measurements (Fig. 4a and 4b). Thus, the flow structure is closely related to stratification and one-, two- or three-layer vertical structure may occur in the Gulf depending on the presence of the pycnoclines.

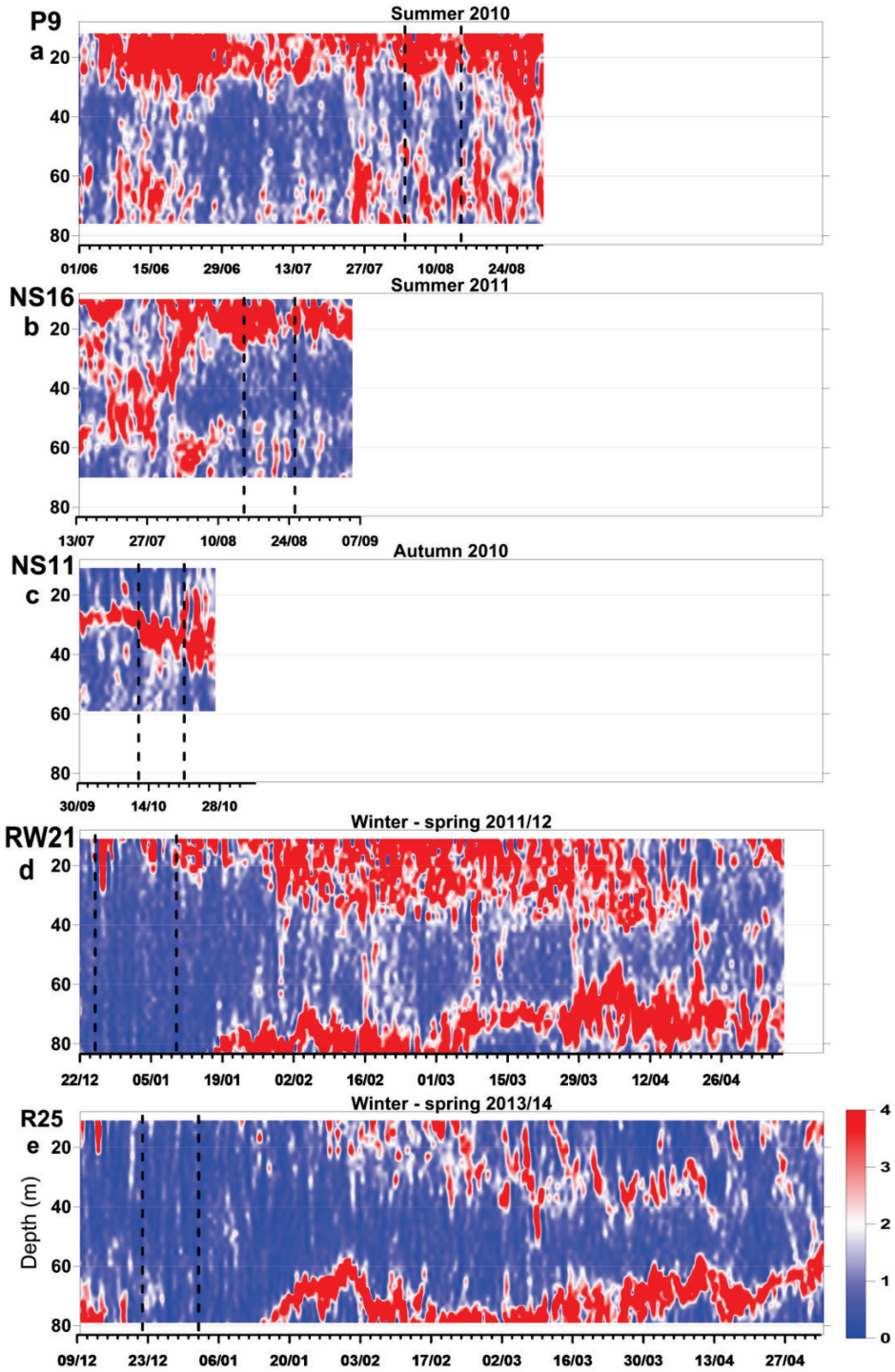


Figure 4. Low-pass filtered time series of the current shear square (in 10^{-4} s^{-2}): a) in summer 2010 (P9), b) summer 2011 (NS16), c) autumn 2010 (NS11), d) winter–spring 2011/12 (RW21), and e) winter–spring 2013/14 (R25). The vertical dashed lines indicate the selected periods, which were analysed in more detail.

The vertical location and strength of the two pycnoclines vary a lot. The seasonal thermocline is at 10–30 m depth during the spring and summer period; it deepens and weakens during autumn until it vanishes (Alenius et al. 2003; Liblik and Lips 2011). The quasi-permanent halocline is present during the whole year (except the reversal events, when stratification is destroyed) at the depths of 60–80 m, being the weakest in the winter period (Alenius et al. 1998; Lehtoranta et al. 2017). Liblik and Lips (2011) concluded that starting from the mid-1990s, the halocline became much stronger compared to the previous years, which could be explained by the major Baltic inflows during the last decade of the 20th century (Mohrholz et al. 2015). The strength and location of the pycnoclines across the Gulf strongly depend on the wind forcing and the pycnoclines have variations in inclination associated with upwelling/downwelling events (Liblik and Lips 2017). During the upwelling events in the southern part of the Gulf, pycnoclines have shallower position compared to the northern part and *vice versa* during the downwelling events (Talpsepp et al. 1994; Laanemets et al. 2005; Lips et al. 2009; Liblik and Lips 2017). For instance, the core of the seasonal thermocline was observed at the depth of 46 m during downwelling at the southern coast on 20 July 2012 (Liblik and Lips 2017).

For further analysis of vertical current profiles during different stratification conditions, selected periods (10–17 days) of time-series were chosen in the following measurement sites: P9 and NS16 (three-layer flow), NS11 (two-layer flow), and RW21 and R25 (one-layer flow) (Paper I). Relaying on stratification and current shear maxima time-series, three depth horizons were selected for describing the currents during the selected periods.

Wind conditions during the selected winter periods were characterized by the strong air flow from the southwest. Polar histograms of current direction (Paper I, Fig. 9) showed that the barotropic up-wind flow directed to the SW was present in the whole vertical range of measurements during the selected winter periods in winters 2011–2012 and 2013–2014.

During the selected period of the two-layer flow in autumn 2010, the northwesterly and southerly winds prevailed. The flow in the upper layer had a uniform distribution while in the deep layer, the flow was dominated by southwesterly currents.

The summer periods were characterized by weaker and variable along-gulf winds. The flow in the upper layer and deep layer during the selected period in summer 2010 was directed to the northwest and northeast, respectively, while the intermediate layer was characterized by weak currents to the ESE or WNW. Polar histograms of currents during the selected period in summer 2010 were rather dissimilar in all three depth horizons (Paper I, Fig. 9). Upper layer revealed a uniform directional distribution, while the flow in the intermediate layer and the deep layer was dominated by westward and northward currents, respectively.

3.4 Alterations of flow regime by atmospheric forcing

3.4.1 Current spectra

To estimate the vertical distribution of kinetic energy throughout the water column during one- (two winter periods), two- (one autumn period) and three-layer (two summer periods) flow regimes, five current velocity time series were selected depending on the stratification conditions. Kinetic energy spectra of non-smoothed

current velocity time series revealed that the presence of kinetic energy maxima could differ depending on the stratification and external forcing.

The prominent spectral peaks with periods from 14 h to 31 h (winter measurements) and 12.4 h to 26 h (summer measurements), which comprise the current oscillations due to seiches, tides, and inertial currents were present in the water column. These peaks correspond well to the local inertial period (13.9 h), semidiurnal (12.42 h) and diurnal (25.8 h) tidal period (Lilover 2012), as well as seiches-driven current oscillation periods of 16 h (Lilover 2011), 23 h (Jönsson 2008), 26.4 h, and 31 h (Wübbler and Kraus 1979).

Two periods with barotropic flow structure were selected for further spectral analysis (Paper I). In winter 2011/12, significant peaks close to the periods of the 1st and 3rd mode seiche were revealed, while in 2013/14, the periods of the 2nd and 3rd mode seiche were present (Fig. 5). During both periods, significant peaks were observed throughout the water column with the highest energy level recorded in the upper layer with the amplitude of 5.6 cm s^{-1} for the 1st seiche mode (2011/12) and 7.2 cm s^{-1} for the 2nd seiche mode (2013/14). Strong wind events and weak stratification (Paper IV, V) created favourable conditions for seiches (Simpson et al. 2014, Breaker et al. 2010).

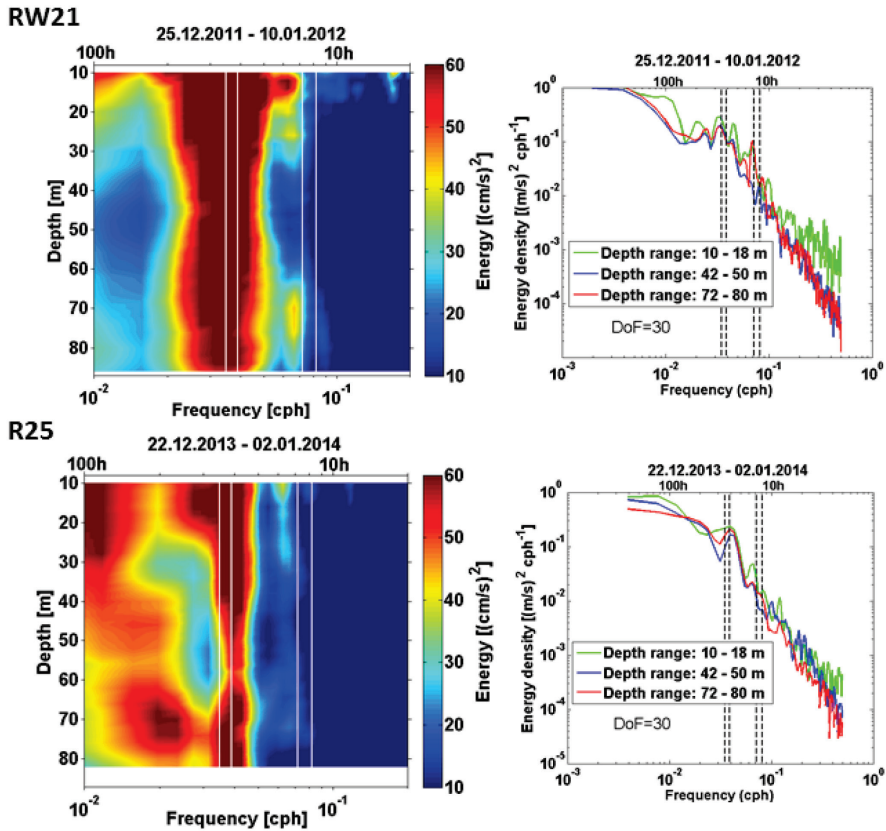


Figure 5. (Left panels) Vertical distributions of kinetic energy spectra during one-layer flow (RW21, R25). (Right panels) Depth-averaged kinetic energy density for the upper, intermediate, and near-bottom layer. Vertical white lines (left panels) and dashed lines (right panels) indicate the oscillation periods of 28.6 h, 25.6 h, 13.9 h, and 12.42 h.

Higher spectral energy was concentrated close to the local inertial period (13.9 h) during the selected two-layer flow structure in October 2010 (Fig. 6). Kinetic energy spectra revealed stronger current oscillations in the upper and intermediate layers with an amplitude of 8.5 cm s^{-1} and 5.5 cm s^{-1} , respectively. The presence of the near-inertial frequency could be associated to the pycnocline, which caused the baroclinic flow (Maas and van Haren 1987). Baroclinic flow was also seen from the phase shift of current oscillations between the upper and intermediate layer at the pycnocline. Lass et al. (2003) showed that the phase shift of current oscillations was caused by stratification in the water column that separates different layers.

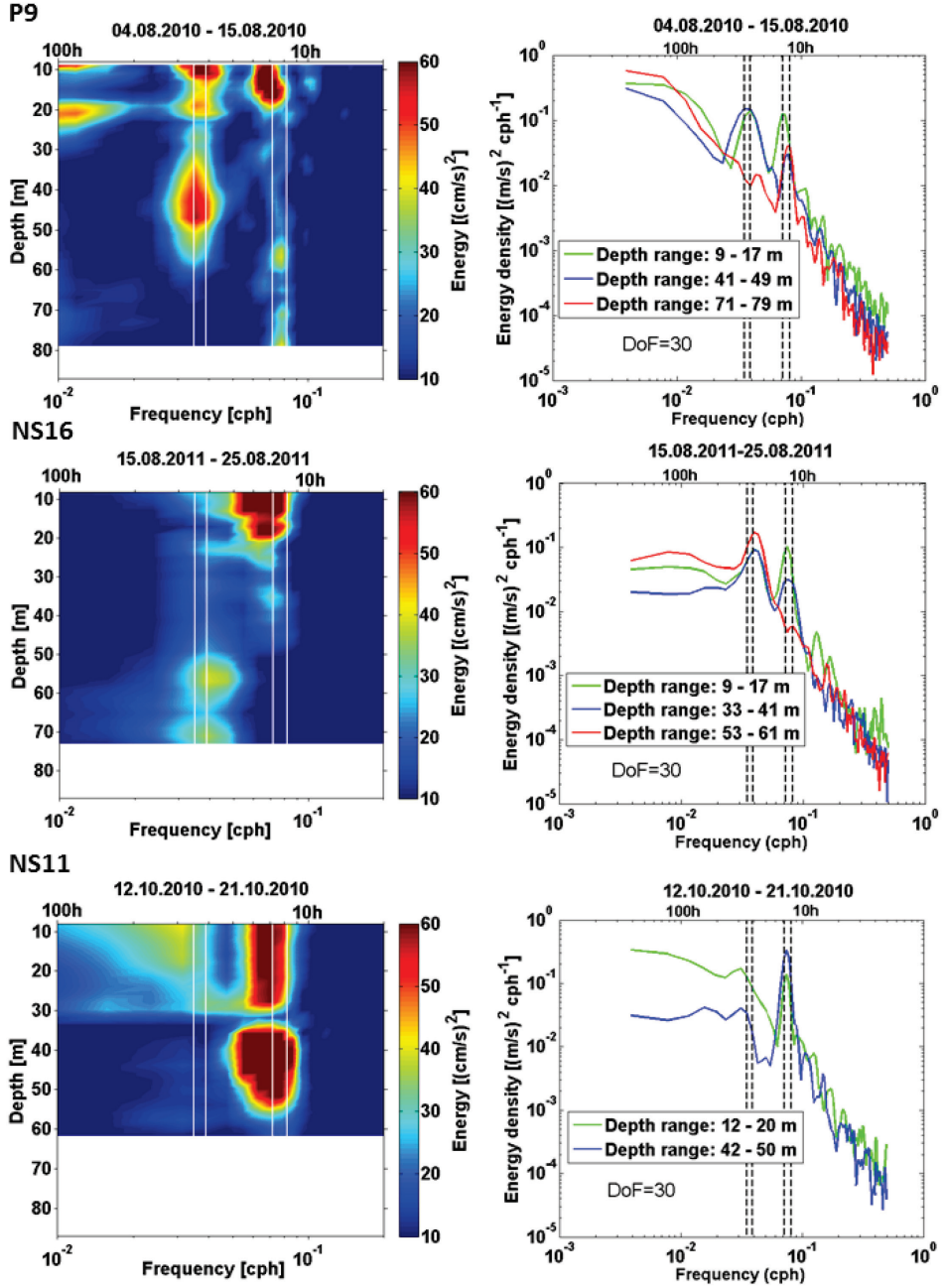


Figure 6. (Left column) Vertical distributions of kinetic energy spectra during three-layer flow (P9, NS16) and two-layer flow (NS11). (Right column) Depth-averaged kinetic energy density for the upper, intermediate, and near-bottom layer. Vertical white lines (left column) and dashed lines (right column) indicate the oscillation periods of 28.6 h, 25.6 h, 13.9 h, and 12.42 h.

Current spectra were influenced by inertial oscillations, seiches and tides during summer periods. The vertical distribution of kinetic energy in summer periods revealed the same energy peaks, but in different depth ranges. BD and BSD frequencies had almost equal energy in the upper 20 m layer, with a maximum current oscillation amplitude of 5.5 cm s^{-1} and 5.1 cm s^{-1} respectively in summer 2010 (Fig. 6). A prominent BD frequency peak was present in the intermediate layer, while at the same time, the BSD band energy peak was present in the entire water column, but with lower energy in the intermediate layer. In summer 2011, the BSD frequencies had higher energy in the upper 20 m depth and BD frequencies had their maximum in the near-bottom layer with the current oscillation amplitude of 4.8 cm s^{-1} and 6.1 cm s^{-1} , respectively. Both frequency bands were present in the depth range from 21 m to 51 m, but had lower energy.

The spectra calculated from the data sets during stratified periods show that the vertical distributions of kinetic energy spectra are linked to the locations of pycnoclines in the water column and highly influenced by inertial oscillations and seiches. In contrast to the open ocean and many seas in the world, tides are generally small and do not play an important role in the Baltic Sea dynamics (Alenius et al. 1998; Leppäranta and Myrberg 2009). Inertial waves generated by the inertial oscillations over an inclined bottom together with near-internal waves and topographic waves are suggested being the main contributors to vertical mixing in the bottom boundary layer in the Baltic Sea (Lass et al. 2003; Meier et al. 2006; Holtermann et al. 2012; Lappe and Umlauf 2016). The generated kinetic energy of internal waves may be transported to deeper layers, but can be lost against stable stratification (Lass et al. 2003).

3.4.2 Prominent wind-driven processes

The shorter time scale currents are more complex and to a great extent driven by the changes in the wind field. The upwelling and downwelling events in the coastal zones develop as a response to alongshore wind impulses and can impact the long-term mean circulation (Paper II). Uiboupin and Laanemets (2009) found that along-gulf cumulative wind stress larger than $0.1 \text{ N m}^{-2} \text{ d}$ is needed for generating the upwelling events.

Using the combination of an along-isobath wind and current pulses with modelled temperature contours, the four upwelling events and four downwelling events were identified during spring/summer measurements 2009 (Fig. 7). Only few sufficiently clear sky SST images reflecting upwelling events in the region of our interest were found during the study period. Two events on 17 May and 29 June were found in the southern coast of Gulf. Based on available data, two upwelling events (14–24 May and 21–30 June) and one downwelling event (15–20 June) were chosen to estimate the displacements of fronts from the coast.

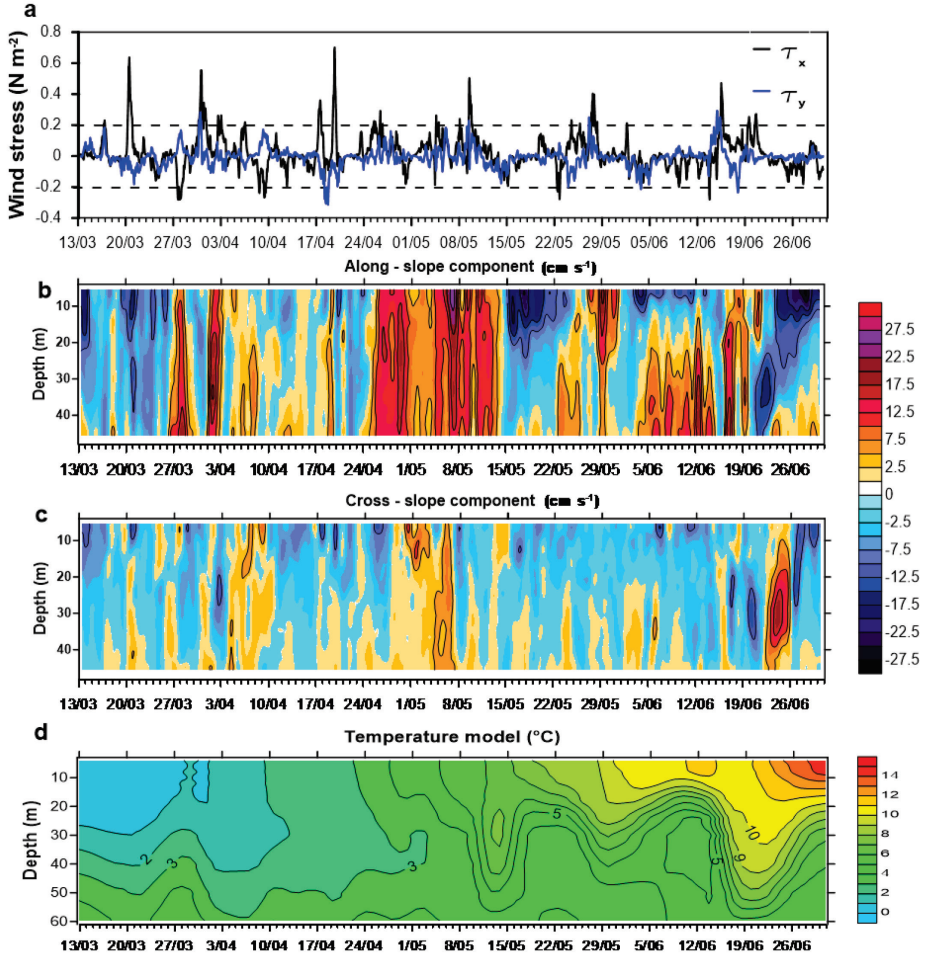


Figure 7. (a) Hourly time series of along-coast (black line) and cross-coast (blue line) wind stress components. Time series of the low-pass filtered along-isobaths (b) and cross-isobaths (c) current velocity components. Positive velocities (red) display the inflow into the Gulf (along-isobaths component) or offshore flow (across-isobaths component), and negative velocities (blue) display the opposite flow respectively. (d) Time series of the modelled temperature.

Strong, downwelling-favourable alongshore wind stress (cumulative wind stress $0.6 \text{ N m}^{-2} \text{ d}$) created the eastward flow throughout the whole water column from 15 until 20 June 2009. The estimated displacement of the centre of downwelling front from the coast was calculated according to Austin and Lenz (2002) and was approximately 11 km. The displacement of the upwelling-associated front was calculated using a non-linear model with impulsively exerted wind stress introduced by Csanady (1977). The result obtained from the data gave the outcrop of pycnocline (position of the front center) approximately 10 km and 6 km from the coast for the upwelling event of 21–30 June and 14–24 May, respectively. According to measurements made by Lips et al. (2009), the cross-shore upwelling front in the surface layer may extend more than 30 km off-shore in the southern part of the Gulf. Very

intense upwelling events were also seen from satellite data during different years in the Gulf of Finland (Uiboupin and Laanemets 2009).

The upwelling/downwelling jet width is scaled by a few baroclinic Rossby deformation radii, which for the Gulf of Finland is about 2–4 km (Alenius et al. 2003); therefore, the width of the jet is expected to be around 10 km, what coincides well with our calculations and earlier observations made by Laanemets et al. (2005).

Wind forcing also plays an important role in modifications of estuarine circulation in the Gulf. Elken et al. (2003) concluded that northeasterly and northerly winds support estuarine circulation, while stronger southwesterly wind forcing causes the reversal of estuarine circulation in the Gulf (the surface layer flows into the estuary and the deep layer flows out). During the earlier observations based on velocity measurements (Liblik and Lips 2012) and CTD measurements together with model simulations (Elken et al. 2003), the estuarine circulation reversal events were examined in the summer period. In this study we analysed well-developed reversals of estuarine circulation (Paper **IV**, **V**) observed in two winter periods (2011/12 Fig. 8 and 2013/14 Fig.9) using bottom-mounted ADCP data at locations RE20, RW21 and R25 (see Fig. 1) complemented with CTD and oxygen, wind and nutrient data. The estuarine circulation reversals as a response to the strong southwesterly wind impulses lasted from 0.5 to 1.5 month. The cumulative wind stress for the 1.5-month long reversal event was approximately $11 \text{ N m}^{-2} \text{ d}$ while for the shorter period reversals, the cumulative wind stress was much weaker – $2 \text{ N m}^{-2} \text{ d}$. Westerly winds, which cause reversal events, are positively correlated with the NAO (North Atlantic Oscillation) index in the Baltic Sea region. The historical wind and NAO index data analysis showed that the 1.5-month long, strong reversal events are rather extraordinary and do not occur every winter. Though, stratification collapse events have become more frequent in recent decades (Elken et al. 2014). Shorter reversal events and consequent temporary weakening of the halocline are common and occur every year.

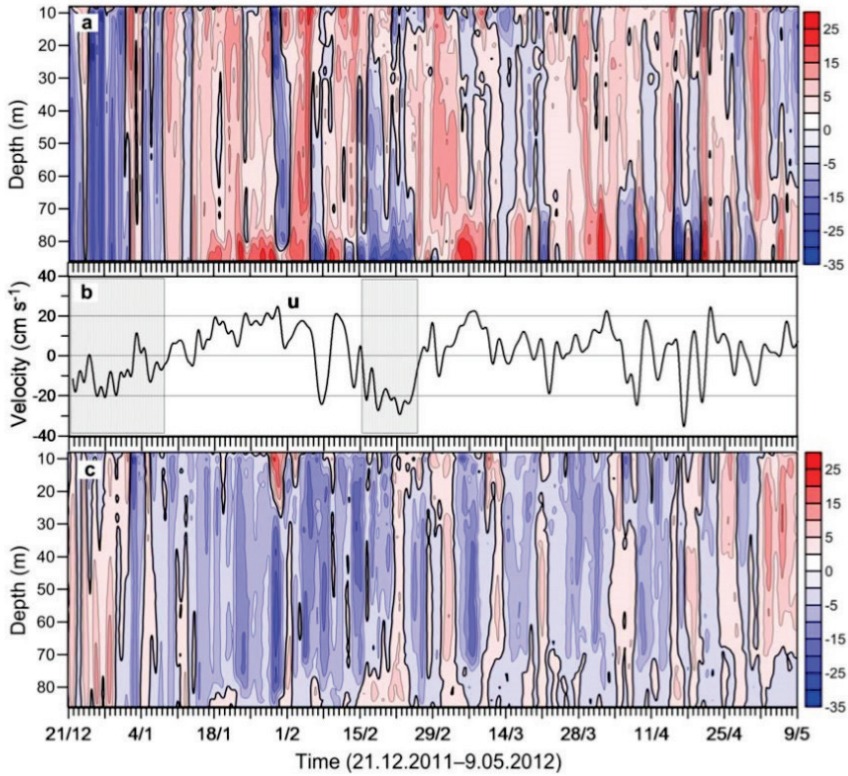


Figure 8. (a) Temporal course of vertical distribution of low-pass filtered along-gulf current velocity component (u) and (c) cross-gulf current velocity component (v) in cm s^{-1} at the location of mooring station A3/RW21 from 21 December 2011 to 9 May 2012. Positive velocities (red) display the inflow into the Gulf or northward flow, and negative velocities (blue) display the opposite flow, respectively. (b) Temporal course of along-gulf current velocity component (u) at the depth of 85 m. The shaded areas mark the time intervals when developed estuarine circulation reversals were observed at location A3/RW21.

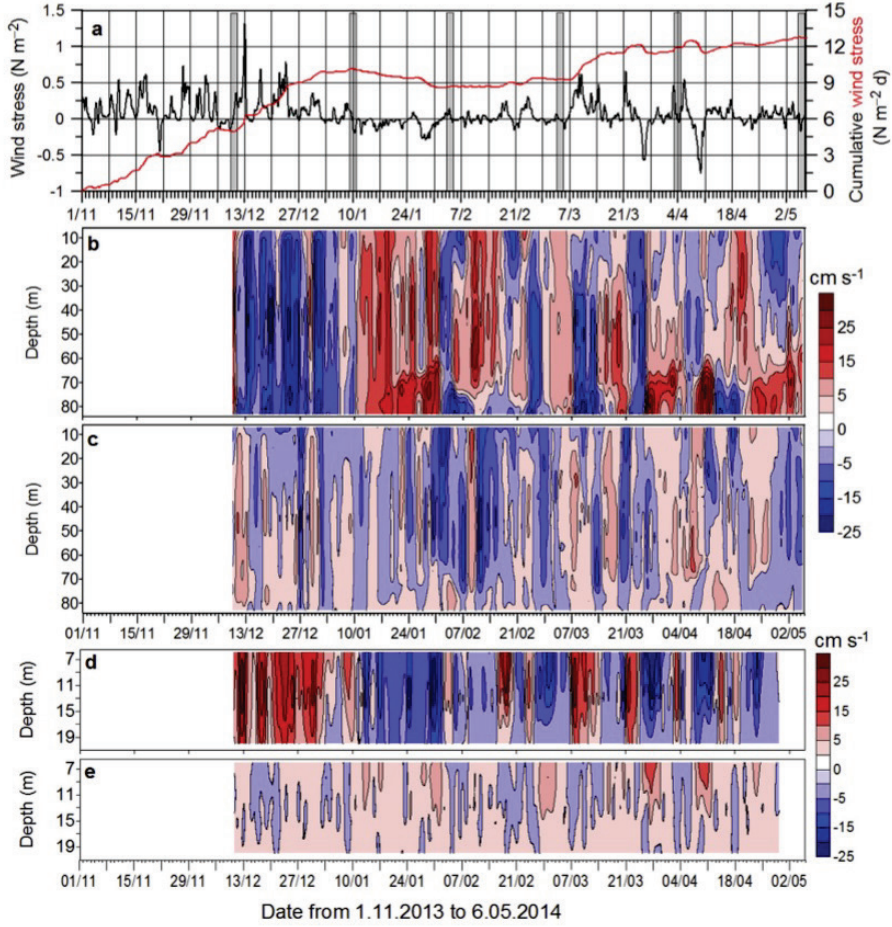


Figure 9. (a) Time series of along-gulf component of wind stress (black curve, positive eastward) and cumulative along-gulf wind stress (red curve) based on wind data from 1 November 2013 to 9 May 2014 at Tallinnamadal Lighthouse in the Gulf of Finland. Time series of vertical distribution of low-pass filtered (b) along-thalweg and (c) cross-thalweg current velocity component at station A6/R25 from 9 December 2013 to 6 May 2014 and (d) along-coast and (e) cross-coast current velocity component at station C25 from 9 December 2013 to 28 April 2014. Positive values (red) display the inflow to the Gulf for the along-gulf component and north-northwestward flow for the cross-gulf (cross-coast) component.

Barotropic flow regimes were observed during the winter-spring 2013/14 and it can be divided into two periods: from 9 December 2013 until 10 January 2014 and from 11 January until 31 January (Fig. 9). Within the first period, the formed barotropic flow consisted first of an outflow (up-wind flow) in the central Gulf and an inflow (down-wind flow) along the coasts, which is similar to the wind-driven circulation in the lakes (Bennet 1974; Winant et al. 2014). Thus, the barotropic inflow along the coast should create simultaneous upwind barotropic flow along the thalweg, which is common for the semi-enclosed homogeneous basins (Sanay and Valle-Levinson 2005). During the second period, when wind weakened and changed direction from the southwest to the east, the barotropic inflow occurred in the central Gulf and outflow

along the coast (Paper V) (Fig. 9); this flow pattern is similar to the weakly stratified estuarine dynamics (Burchard et al. 2011). Highest values of inflow/outflow events were recorded mainly in the deep layers below the 70 m depth during the alternation of estuarine and reverse circulation. Current speed maxima recorded during this events were 58.5 cm s^{-1} for outflow case and 38.3 cm s^{-1} for inflow case. In the coastal area, the current speed maximum in the near-bottom layer was 35.9 cm s^{-1} during the first period and 23.6 cm s^{-1} during the second period.

Flow in the coastal area was mostly two-layer in summer 2009, with stronger currents in the upper 15 m layer (Paper II). A pronounced up-wind current event below the seasonal thermocline occurred during the easterly winds in the first half of June 2009. Westward winds raised the sea level on the northern coast and dropped on the southern coast of the Gulf creating the downwind jet-like currents at both coasts and upwind flow in the central area of the Gulf (Paper II). Such an upwind flow is common for the elongated basins and estuaries (e.g., Csanady 1973).

3.5 Influence of the deep layer current dynamics on biogeochemistry

The Baltic Sea has one of the largest hypoxic areas in the world that has been systematically observed over the decades (Diaz 2001; Diaz and Rosenberg 2008). Salinity stratification in the Baltic Sea (Lepäranta and Myrberg 2009) prevents the direct ventilation of the deep layers below the quasi-permanent halocline. Replenishment of the oxygen conditions in the deep water of the Baltic Proper mainly occurs by spreading of oxygen-rich, dense waters of saline inflow events from the North Sea (Matthäus and Franck 1992). The Gulf of Finland receives its sub-halocline water from the northern Baltic Proper (Liblik et al. 2018).

Winter measurements 2011/2012 (Paper IV) and 2013/2014 (Paper V) showed that oxygen concentration in the near-bottom layer is highly influenced by the alternation between the stratified and mixed conditions. Present study showed that the reversal events during winter destroy stratification and temporarily improve the near-bottom oxygen conditions (Fig. 10). The deep layer along the thalweg in the western and central part of the Gulf had an average oxygen concentration of 11.7 mg l^{-1} during the largest reversal event in December 2011. This reversal event created favourable conditions for complete mixing of the water column. At the easternmost stations, the water was completely mixed even at the end of January, while in the western and central part of the Gulf, the hypoxic conditions were already again well developed.

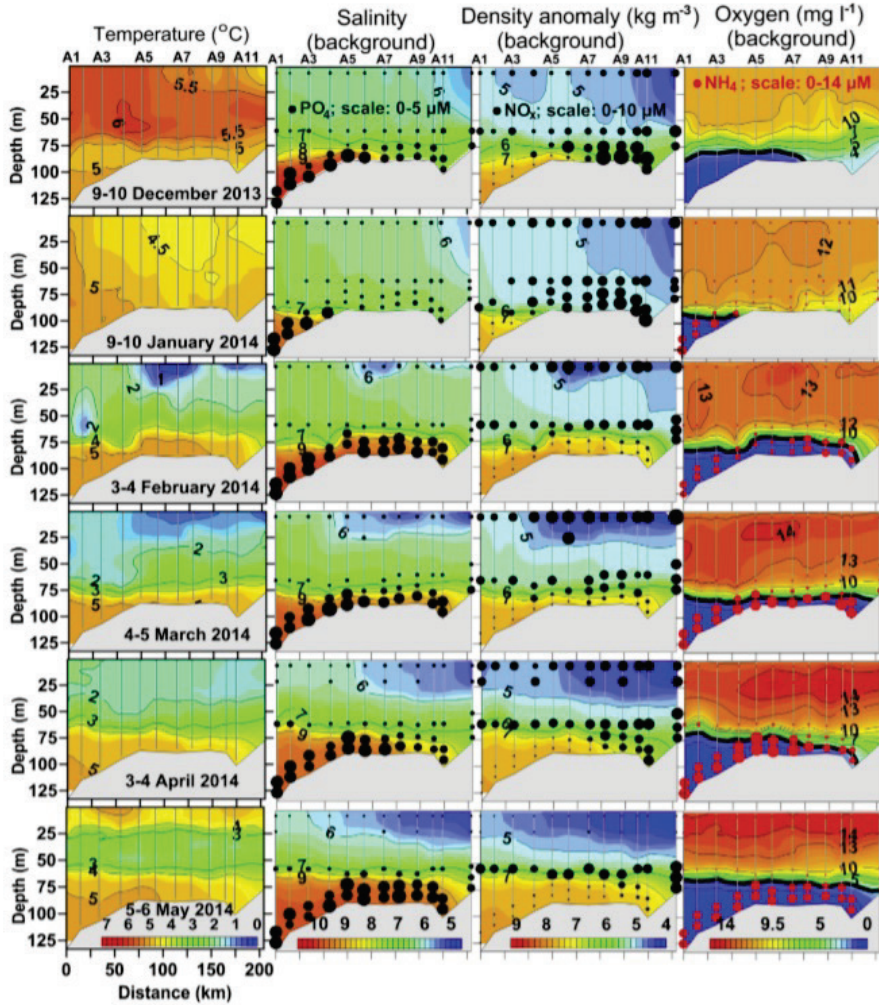


Figure 10. Vertical sections of temperature, salinity (in PSS-78 scale), density anomaly, and dissolved oxygen concentration on 9–10 December 2013 and 9–10 January, 3–4 February, 4–5 March, 3–4 April and 5–6 May 2014 along the thalweg of the Gulf of Finland from station A1 to station A12 (see Fig. 1, Paper V). Colour scales are shown in the lower panels. A black bold contour line (panels in the right column) marks the dissolved oxygen concentration of 2.9 mg l^{-1} (threshold concentration for hypoxia). Concentrations of PO_4^{3-} and NO_x are indicated as black dots and concentrations of NH_4^+ as red dots varying in size; scales are shown in the upper panels. Note that concentrations of NH_4^+ were not measured on 9–10 December 2013. Values on the x-axis indicate the distance from the westernmost station A1.

The re-establishment of strong haline stratification and hypoxia may occur very rapidly after the reversal events at the western end of the Gulf, within 12 h (Paper IV). A strong link between dynamics of saltwater wedge intrusion to the Gulf and disappearance of oxygen in the near-bottom layer was found for winter 2013/2014 using linear regression between salinity and oxygen ($r^2=0.86$) (Fig. 11). As a result of saltwater wedge intrusion, hypoxic conditions were observed approximately 130 km

eastward from the western border of the Gulf in March and May 2012 (Paper IV). The saltwater wedge had even larger horizontal (~170 km) and vertical extent, resulting in hypoxic conditions at a depth of about 60 m in May 2014 (Fig. 10). The hypoxic area formed by May 2014 was estimated as large as 2620 km² and oxygen depletion below the 60–70 m depth remained in the Gulf until the beginning of November 2014 (Paper V). Unusually to the most estuarine marine systems (where deep layer circulation brings water with higher oxygen concentrations from open sea/ocean to estuary), the intensification of estuarine circulation transports hypoxic water from the deeper sub-halocline layers of the Northern Baltic Proper into the Gulf. A similar estuarine process was found by Gilbert et al. (2005) in St. Lawrence estuary.

The increase of hypoxic conditions enhances phosphorus release from the sediment and decreases nitrogen removal (Vahtera et al. 2007; Tamminen and Andersen 2007). The high correlation ($r^2=0.83$) between oxygen and phosphate concentration (Fig. 11) and between salinity and oxygen indicated that the movement of hypoxic saltwater wedge had high influence on the phosphorus level in the near-bottom layer of the Gulf (Paper V). However, the long-term measurements during the period 1992–2014 at the depth of 70 m indicated that the concentrations of the phosphate were markedly higher in the Gulf than in the Northern Baltic Proper (Lehtoranta et al. 2017). This indicates that the bottom of the Gulf continues to consume oxygen and releases additional phosphorus into the water that comes from the Northern Baltic Proper (Lehtoranta et al. 2017). Taking into account that during winter periods the reversal of estuarine circulation could temporarily lead to intensive vertical mixing (Elken et al. 2014; Paper IV, V), the phosphorus released from the sediment will be transported to the upper layers (Paper V). Lehtoranta et al. (2017) found that the major locations for delivering the phosphorus released from the sediment and import to the surface layer during winter mixing are the shallower, eastern and central areas of the Gulf. Increased phosphorus concentration in the water column will stimulate primary production and probability of occurrence of cyanobacteria blooms, which leads to even higher depletion of oxygen (Pitkänen et al. 2001; Vahtera et al. 2007). The surveys along the thalweg (Paper V) revealed that NO_x concentrations were related to the extent of the hypoxic saltwater wedge (Fig. 10). NO_x concentrations were very low in the hypoxic water and were highest in the eastern part of the Gulf and the water column above 75 m in the well-oxygenated areas. In addition, Jäntti and Hietanen (2012) found that in hypoxic conditions, the nitrogen instead of being removed from the system is recycled into a bioavailable form, which intensifies eutrophication. Therefore, the lateral transport of the salt wedge in conjunction with increased frequency of complete vertical mixing events (Elken et al. 2014) have a major impact on the environmental conditions in the Gulf.

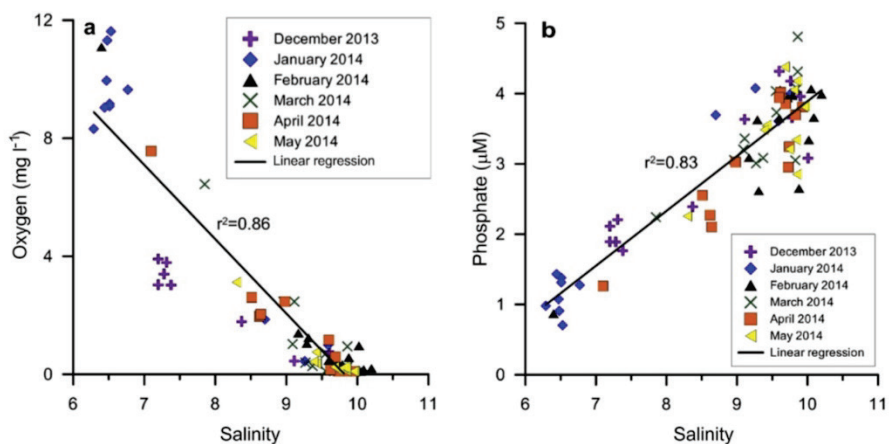


Figure 11. (a) Near-bottom oxygen concentration versus salinity (in PSS-78 scale) and (b) near-bottom phosphate concentration versus salinity with corresponding linear regression lines based on the measurements at stations A1–A12 (see Fig. 1, Paper V) in the Gulf of Finland during six surveys from December 2013 to May 2014.

4 Conclusions

The main aim of the present work was to improve the knowledge on the variability of the vertical structure of currents in the Gulf of Finland and relate it to the wind forcing and stratification conditions. Influence of current dynamics to the biogeochemical fields in the deep layer of the Gulf was analysed as well. There is a lack of current-measurement time-series in the Gulf of Finland, particularly in the deeper part of the water column. The present thesis is the first rigorous investigation that deals with the vertical structure of currents through both pycnoclines in the Gulf of Finland. The main data source of the thesis was 11 time-series of acoustic current measurements in 2009-2014, which were supported by thermohaline structure and wind measurements. The obtained results showed that a strong interplay between the currents and stratification exists in the Gulf, resulting in the different vertical structure of the currents depending on the season and wind forcing.

The main results of the present thesis can be summarized as follows:

- General mean cyclonic circulation occurs in the upper layer in the Gulf, but local loops in the mean circulation might exist as suggested by recent modelling studies.
- Mean vertical current structure at the thalweg revealed typical estuarine circulation in summers when wind forcing was similar to the climatic average – westward current (outflow from the Gulf) in the upper layer and eastward flow (inflow to the Gulf) below the seasonal thermocline. Reversed mean vertical flow structure (inflow in the upper layer, outflow in the deep layer) was revealed in summers when airflow from the southwest was stronger than the climatic average.
- The mean current speed of all time-series was in the range of 9–12 cm s⁻¹ in the upper layer and below 70 m depth. The flow was weaker in the intermediate layer.
- One-, two- or three-layer current structure might occur in the Gulf of Finland, realization of the regime depends on the presence of pycnoclines. Pycnoclines determine the vertical locations of current shear maxima and separation of the layers with different kinetic energy spectra of currents.
- Estuarine circulation reverses and the halocline weakens during strong westerly-southwesterly wind events. In extreme cases, this process led to the collapse of vertical stratification during winters and the creation of the barotropic flow system, consisting of the mean upwind flow in the central, deep area of the Gulf and opposite flow near the southern coast.
- Strong reversal events that destroy stratification for weeks are rather extraordinary and do not occur every winter. Shorter reversal events and consequent temporary weakening of the halocline are common in the Gulf.
- The energy maxima of current oscillations occurred at a broad semi-diurnal frequency band, broad diurnal frequency band and/or low-frequency seiches band. The frequency composition differed between the seasons as well as between the layers.
- The kinetic energy spectra of currents in the periods of strong wind forcing and weak stratification were dominated by current oscillations coinciding with different modes of seiches.

- During the periods of the two- or three-layer mean flow, also inertial oscillations and probably tides contribute remarkably to the kinetic energy spectrum. In summer, the inertial oscillations were dominating in the upper layer from the surface to either the thermocline or the halocline.
- Reversal events cause movement of the hypoxic salt wedge out from the Gulf. Complete mixing of the water column and saturated oxygen conditions occur in the deep layer during strong reversal and consequent stratification collapse events.
- Hypoxic salt wedge intrusion extending up to 170 km eastward from the entrance of the Gulf was observed during recurrence of estuarine circulation in the Gulf.
- The hypoxic salt wedge water had high phosphate and very low nitrate/nitrite concentrations. Wind-driven circulation modifications in the deep layer cause remarkable fluxes of nutrients between the Gulf of Finland and Northern Baltic Proper.

References

- Alari, V., Staneva, J., Breivik, Ø., Bidlot, JR., Mogensen, K., Janssen, P. 2016. Surface wave effects on water temperature in the Baltic Sea: simulations with the coupled NEMO-WAM model. *Ocean Dyn* 66(8): 917–930. <https://doi.org/10.1007/s10236-016-0963-x>
- Alenius, P., Myrberg, K. and Nekrasov, A. 1998. The physical oceanography of the Gulf of Finland: a review. *Boreal Env. Res.* 3: 97–125.
- Alenius, P., Nekrasov, A. and Myrberg, K. 2003. Variability of the baroclinic Rossby radius in the Gulf of Finland, *Cont. Shelf Res.*, 23, 563–573.
- Allahdadi, M.N. and Li, C. 2017. Effect of stratification on current hydrodynamics over Louisiana shelf during Hurricane Katrina, *Water Science and Engineering* 10(2); 154-165. <https://doi.org/10.1016/j.wse.2017.03.012>
- Andrejev, O., Myrberg, K., Alenius, P. and Lundberg, P.A. 2004. Mean circulation and water exchange in the Gulf of Finland — a study based on three-dimensional modeling. *Boreal Env. Res.* 9: 1–16.
- Arneborg, L. and Liljebladh, B. 2001. The internal seiches in Gullmar Fjord. Part II: Contribution to Basin Water Mixing. *J. Phys. Oceanogr.* 31: 2567–2574.
- Austin, J.A. and Lentz, S.J. 2002. The inner shelf response to wind-driven upwelling and downwelling. *J. Phys. Oceanogr.* 32, 2171–2193.
- Bennet, J.R. 1974. On the dynamics of wind-driven lake currents. *J. Phys. Oceanogr.* 4: 400–414.
- Book, J.W., Perkins, H., Signell, R.P. and Wimbush, M. 2007. *The Adriatic Circulation Experiment winter 2002/2003 mooring data report: A case study in ADCP data processing*. Rep. NRL/MR/7330-07-8999, U.S. Naval Res. Lab., Stennis Space Center, MS.
- Breaker, L.C., Tseng, Y.-H. and Wang, X. 2010. On the natural oscillations of Monterey Bay: Observations, modeling, and origins. *Progress in Oceanography* 86: 380–395.
- Bulczak, A.I., Rak, D., Schmidt, B., Beldowski, J. 2016. Observations of near-bottom currents in Bornholm Basin, Slupsk Furrow and Gdansk Deep. *Deep-Sea Research II*, 128: 96–113, doi: <http://dx.doi.org/10.1016/j.dsr2.2015.02.021>.
- Burchard, H., Hetland, R.D., Schulz, E. and Schuttelaars, H.M. 2011. Drivers of residual estuarine circulation in tidally energetic estuaries: straight and irrotational channels with parabolic cross section. *J. Phys. Oceanogr.* 41: 548–570.
- Butterworth, S. 1930. On the theory of filter amplifiers. *Experimental Wireless and the Wireless Engineer* 7: 536–541.
- Conley, D.J., Humborg, C., Rahm, L., Savchuk, O.P. and Wulff, F. 2002. Hypoxia in the Baltic Sea and basin-scale changes in phosphorus biogeochemistry, *Environ. Sci. Technol.*, 36, 5315–5320.
- Conley, D.J., Björck, S., Bonsdorff, E., Carstensen, J., Destouni, G., Gustafsson, B.G., Hietanen, S., Kortekaas, M., Kuosa, H., Meier, H.E.M., Müller-Karulis, B., Nordberg, K., Norkko, A., Nürnberg, G., Pitkänen, H., Rabalais, N.N., Rosenberg, R., Savchuk, O.P., Slomp, C.P., Voss, M., Wulff, F. and Zillén, L. 2009. Hypoxia-related processes in the Baltic Sea, *Environ. Sci. Technol.*, 43, 3412–3420.
- Csanady, G.T. 1973. Wind-induced barotropic motions in long lakes. *J. Phys. Oceanogr.* 3, 429–438.

- Csanady, G.T. 1977. Intermittent “full” upwelling in Lake Ontario. *J. Geophys. Res.* 82, 397–419.
- Diaz, R.J. 2001. Overview of Hypoxia around the World. *Journal of Environment Quality* 30 (2): 275.
- Diaz, R.J. and Rosenberg, R. 2008. Spreading dead zones and consequences for marine ecosystems, *Science*, 321, 926–929, doi:10.1126/science.1156401.
- Elken, J., Raudsepp, U. and Lips, U. 2003. On the estuarine transport reversal in deep layers of the Gulf of Finland. *J. Sea Res.* 49: 267–274.
- Elken, J., Mälikki, P., Alenius, P. and Stipa, T. 2006. Large halocline variations in the Northern Baltic Proper and associated meso- and basin-scale processes, *Oceanologia*, 48, 91–117.
- Elken, J., Nömm, M. and Lagemaa, P. 2011. Circulation patterns in the Gulf of Finland derived from the EOF analysis of model results. *Boreal Env. Res.* 16: 84–102.
- Elken, J., Raudsepp, U., Laanemets, J., Passenko, J., Maljutenko, I., Pärn, O. and Keevallik, S. 2014. Increased frequency of wintertime stratification collapse events in the Gulf of Finland since the 1990s. *Journal of Marine Systems* 129: 47–55.
- Emery, W.J. and Thomson, R.E. 2004. *Data analysis methods in physical oceanography*. Elsevier, London, UK.
- Geyer, W.R. and MacCready, P. 2014. The estuarine circulation. *Annu. Rev. Fluid Mech.* 46: 175–197.
- Gilbert, D., Sundby, B., Gobeil, C., Mucci, A. and Tremblay, G.H. 2005. A seventy-two-year record of 30 diminishing deep-water oxygen in the St. Lawrence estuary: the northwest Atlantic connection, *Limnol. Oceanogr.* 50, 1654–166.
- Haapala, J. and Alenius, P. 1994. Temperature and salinity statistics for the northern Baltic Sea 1961–1990. *Finnish Marine Research*, 262, pp.51–121
- HELCOM (Helsinki Commission). 2009. Eutrophication in the Baltic Sea: an integrated thematic assessment of the effects of nutrient enrichment in the Baltic Sea region, *Baltic Sea Environment Proceedings*, 115B, 1–152.
- Holtermann, P., Umlauf, L., Tanhua, T., Schmale, O., Rehder, G. and Waniek, J. 2012. The Baltic Sea tracer release experiment. 1. Mixing rates. *J. Geophys. Res.* 117, C01021, doi:10.1029/2011JC007439.
- Janout, M.A., Höltermann, J., Krumpen, T. 2013. Cross-shelf transport of warm and saline water in response to sea ice drift on the Laptev Sea shelf. *Journal of Geophysical Research: Oceans*, Vol., 118, 563-576, doi: 10.1029/2011JC007731.
- Jäntti, H. and Hietanen, H. 2012. The effects of hypoxia on sediment nitrogen cycling in the Baltic Sea, *Ambio*, 41, 161–169, doi:10.1007/s13280-011-0233-6.
- Jönsson, B., Döös, K., Nycander, J. and Lundberg, P. 2008. Standing waves in the Gulf of Finland and their relationship to the basin-wide Baltic seiches. *J. Geophys. Res.* 113, C03004, doi: 10.1029/2006JC003862.
- Keevallik, S. and Soomere, T. 2014. Regime shifts in the surface-level average air flow over the Gulf of Finland during 1981-2010. *Proceedings of the Estonian Academy of Sciences*, 63 (4), 428–437. doi:10.3176/proc.2014.4.08.
- Kikas, V. and Lips, U. 2016. Upwelling characteristics in the Gulf of Finland (Baltic Sea) as revealed by ferrybox measurements in 2007–2013. *Ocean Sci.* 12, 843–859.
- Koue, J., Shimadera, H., Matsuo, T., Kondo, A. 2018. Evaluation of Thermal Stratification and Flow Field Reproduced by a Three-Dimensional Hydrodynamic Model in Lake Biwa, Japan. *Water*, 10(1), 47; <https://doi.org/10.3390/w10010047>.

- Laakkonen, A., Mälkki, P., Niemi, Å. 1981. Studies on the Sinking, Degradation and Sedimentation of Organic Matter off Hanko Peninsula, Entrance to the Gulf of Finland, in 1979 (progress report).
- Laanemets, J., Pavelson, J., Lips, U., Kononen, K. 2005. Downwelling related mesoscale motions at the entrance to the Gulf of Finland: observations and diagnosis. *Oceanological and Hydrobiological Studies*, 34 (2), 15–36.
- Lagemaa, P. 2012. Operational forecasting in Estonian marine waters. (PhD Thesis). Tallinn Univ. Technol., TUT Press, 45 pp.
- Laine, A.O., Andersin, A.-B., Leiniö, S. and Zuur, A.F. 2007. Stratification-induced hypoxia as a structuring factor of macrozoobenthos in the open Gulf of Finland (Baltic Sea), *J. Sea Res.*, 57, 65–77.
- Lappe, C. and Umlauf, L. 2016. Efficient boundary mixing due to near-inertial waves in a nontidal basin: observations from the Baltic Sea. *J. Geophys. Res. Oceans* 121: 8287–8304.
- Lass, H.-U., Prandke, H. and Liljebladh, B. 2003. Dissipation in the Baltic Proper during winter stratification. *J. Geophys. Res.* 108(C6), 3187, doi: 10.1029/2002JC001401.
- Lehmann, A., Myrberg, K., Hoflich, K. 2012. A statistical approach to coastal upwelling in the Baltic Sea based on the analysis of satellite data for 1990–2009. *Oceanologia* 54, 369–393.
- Lehtoranta, J., Savchuk, O.P., Elken, J., Dahlbo, K., Kuosa, H., Raateoja, M., Kauppila, P., Räike, A., Pitkänen, H. 2017. Atmospheric forcing controlling inter-annual nutrient Dynamics in the open Gulf of Finland. *J. Mar. Syst.* doi: 10.1016/j.jmarsys.2017.02.001
- Leppäranta, M. and Myrberg, K. 2009. *The physical oceanography of the Baltic Sea*. Springer-Verlag, Berlin, Heidelberg, New York.
- Li, J., Li, G., Xu, J., Dong, P., Qiao, L., Liu, S., Sun, P. and Z. Fan. 2016. Seasonal evolution of the Yellow Sea Cold Water Mass and its interactions with ambient hydrodynamic system, *J. Geophys. Res. Oceans*, 121, 6779–6792, doi: 10.1002/2016JC012186.
- Liblik, T. and Lips, U. 2011. Characteristics and variability of the vertical thermohaline structure in the Gulf of Finland in summer. *Boreal Env. Res.* 16 (suppl. A): 73–83.
- Liblik, T. and Lips, U. 2012. Variability of synoptic-scale quasi-stationary thermohaline stratification patterns in the Gulf of Finland in summer 2009. *Ocean Science* 8: 603–614.
- Liblik, T. and Lips, U. 2017. Variability of pycnoclines in a three-layer, large estuary: the Gulf of Finland. *Boreal Env. Res.* 22: 27–47.
- Liblik, T., Naumann, M., Alenius, P., Hansson, M., Lips, U., Nausch, G., Tuomi, L., Wesslander, K., Laanemets, J., Viktorsson, L. 2018. Propagation of impact of the recent Major Baltic Inflows from the Eastern Gotland Basin to the Gulf of Finland. *Frontiers in Marine Science*, 5 (222), 1–23.10.3389/fmars.2018.00222.
- Lilover, M.-J. 1989. Тонкая вертикальная структура поля скорости течения в балтийском море. Диссертация на соискание ученой степени кандидата физико-математических наук II.00.08 - океанология. Академия наук Эстонии институт термofизики и электрoфизики.
- Lilover, M.-J., Pavelson J., Kõuts T. 2011. Wind forced currents over the shallow Naissaar bank in the Gulf of Finland. *Boreal Env. Res.* 16: 164–174.

- Lilover, M.-J. 2012. Tidal currents as estimated from ADCP measurements in “practically non-tidal” Baltic Sea. In: *Baltic International Symposium (BALTIC)*, IEEE/OES, Klaipeda, Lithuania, pp. 1–4.
- Lips, U., Lips, I., Liblik, T., Elken, J. 2008. Estuarine transport versus vertical movement and mixing of water masses in the Gulf of Finland (Baltic Sea). *US/EU-Baltic Symposium "Ocean Observations, Ecosystem-Based Management & Forecasting"*, Tallinn, 27-29 May, 2008. IEEE, 1–8. (IEEE Conference Proceedings). Doi: 10.1109/BALTIC.2008.4625535.
- Lips, I., Lips, U., Liblik, T. 2009. Consequences of coastal upwelling events on physical and chemical patterns in the central Gulf of Finland. *Cont. Shelf Res.* 1836–1847.
- Lorke, A., Umlauf, L., Jonas, T. and Wüest, A. 2002. Dynamics of turbulence in low-speed oscillating bottom-boundary layers of stratified basins. *Environmental Fluid Mechanics* 2: 291–313.
- Maas, L.R.M. and Van Haren, J.J.M. 1987. Observations on the vertical structure of tidal and inertial currents in the central North Sea. *J. Mar. Res.* 45: 293–318.
- Matthäus, W. and Franck, H. 1992. Characteristics of major Baltic inflows—a statistical analysis. *Cont. Shelf Res.* 12, 1375–1400. doi: 10.1016/0278-4343(92)90060-W.
- Meier, H.E.M., Feistel, R., Piechura, J., Arneborg, L., Burchard, H., Fiekas, V., Golenko, N., Kuzmina, N., Mohrholz, V., Nohr, C., Paka, V.T., Sellschop, J., Stips, A., Zhurbas, V. 2006. Ventilation of the Baltic Sea deep water: a brief review of present knowledge from observations and models. *Oceanologia* 48 (S), 133–164.
- Mietus, M. (coordinator) 1998. *The Climate of the Baltic Sea Basin, Marine Meteorology and Related Oceanographic Activities*. Report No. 41. World Meteorological Organisation, Geneva.
- Mohrholz, V., Naumann, M., Nausch, G., Krüger, S., Gräwe, U. 2015. Fresh oxygen for the Baltic Sea e an exceptional saline inflow after a decade of stagnation. *J. Mar. Syst.* 148, 152–166.
- Myrberg, K., Andrejev, O. 2003. Main upwelling regions in the Baltic Sea – a statistical analysis based on three-dimensional modelling. *Boreal Environment Research* 8 (2), 97–112.
- Palmén, E. 1930. Untersuchungen über die Strömungen in den Finland umgebenden Meeren. *Soc. Sci. Fenn. Comm. Phys.-Math.* 5: 1–94.
- Pavelson, J., Kononen, K., Laanemets, J. 1999. Chlorophyll distribution patchiness caused by hydrodynamical processes: a case study in the Baltic Sea. *ICES Journal of Marine Science*, 56 (Supplement), 87–99.
- Pitkänen, H., Lehtoranta, J., Räike, A. 2001. Internal nutrient fluxes counteract decreases in external load: the case of the estuarial eastern Gulf of Finland, Baltic Sea. *Ambio* 30, 195–201.
- Pu, X., Shi, J.Z., Hu, G-D. 2017. The effect of stratification on the vertical structure of the tidal ellipse in the Changjiang River estuary, China. *J. Hydro Environ. Res.* 15, 75–94.
- Rasmus, K., Kiirikki, M. and Lindfors, A. 2015. Long-term field measurements of turbidity and current speed in the Gulf of Finland leading to an estimate of natural resuspension of bottom sediment. *Boreal Env. Res.* 20: 735–747.
- Reissmann, J., Burchard, H., Feistel, R., Hagen, E., Lass, H.-U., Mohrholz, V., Nausch, G., Umlauf, L. and Wicczorek, G. 2009. Vertical mixing in the Baltic Sea and consequences for eutrophication: A review. *Progr. Oceanogr.* 82: 47–80.

- Saenko, O.A. 2006. The Effect of Localized Mixing on the Ocean Circulation and Time-Dependent Climate Change. *J. Phys. Oceanogr.* 36: 140–160.
- Sanay, R. and Valle-Levinson, A. 2005. Wind-induced circulation in semienclosed homogeneous, rotating basins. *J. Phys. Oceanogr.* 35: 2520–2531.
- Shivaprasad, A., Vinita, J., Revichandran, C., Reny, P.D., Deepak, M.P., Muraleedharan, K.R. and Naveen Kumar, K.R. 2013. Seasonal stratification and property distributions in a tropical estuary (Cochin estuary, west coast, India). *Hydrol. Earth Syst. Sci.*, 17, 187–199. doi:10.5194/hess-17-187-2013.
- Simpson, J.H., Lucas, N.S., Powel, B. and Maberly, S.C. 2014. Dissipation and mixing during the onset of stratification in a temperate lake, Windermere. *Limnol. Oceanogr.* 60: 29–41.
- Soomere, T. and Keevallik, S. 2001. Anisotropy of moderate and strong winds in the Baltic Proper, *Estonian Acad. Sci. Eng.* 7, 1, 35–49.
- Soomere, T., Keevallik, S. 2003. Directional and extreme wind properties in the Gulf of Finland. *Proc. Estonian Acad. Sci. Eng.* 9, 73–90.
- Stipa, T. 2004. Baroclinic adjustment in the Finnish coastal current. *Tellus* 56A, 79–87.
- Suursaar, Ü. and Aps, R. 2007. Spatio-temporal variations in hydro-physical and -chemical parameters during a major upwelling event off the southern coast of the Gulf of Finland in summer 2006. *Oceanologia* 49, 209–228.
- Talpsepp, L., Nöges, T., Raid, T., Kõuts T. 1994, *Hydrophysical and hydrobiological processes in the Gulf of Finland in summer 1987: characterization and relationship*, *Cont. Shelf Res.*, 14, 749–763.
- Tamminen, T. and Andersen, T. 2007. Seasonal phytoplankton nutrient limitation patterns as revealed by bioassays over Baltic Sea gradients of salinity and eutrophication, *Mar.Ecol. Prog.Ser.* Vol. 340: 121–138.
- Teledyne RD Instruments. 2006. Acoustic Doppler Current Profiler Principles of Operation A Practical Primer. 1–62.
- Troy, C., Cannon, D., Liao, Q., Bootsma, H. 2016. Logarithmic velocity structure in the deep hypolimnetic waters of Lake Michigan, *J. Geophys. Res. Oceans*, 121, 949–965, doi: 10.1002/2014JC010506.
- Tuomi, L., Väha-Piikkiö, O., Alenius, P., Björkqvist, J-V., Kahma, K. 2018. Surface Stokes drift in the Baltic Sea based on modelled wave spectra. *Ocean Dynamics* 68: 17–33. <https://doi.org/10.1007/s10236-017-1115-7>.
- Uiboupin, R. and Laanemets, J. 2009. Upwelling characteristics derived from satellite sea surface temperature data in the Gulf of Finland, Baltic Sea. *Boreal Environment Research* 14, 297–304.
- Vahtera, E., Conley, D.J., Gustafsson, B.G., Kuosa, H., Pitkänen, H., Savchuk, O.P., Tamminen, T., Viitasalo, M., Voss, M., Wasmund, N. and Wulf, F. 2007. Internal ecosystem feedbacks enhance nitrogen-fixing cyanobacteria blooms and complicate management in the Baltic Sea, *Ambio*, 36, 186–194.
- Van Haren, H. 2000. Properties of vertical current shear across stratification in the North Sea. *Journal of Marine Research*, 58 (3), pp. 465–491.
- Viktorsson, L., Almroth-Rosell, E., Tengberg, A., Vankevich, R., Neelov, I., Isaev, R., Kravtsov, V. and Hall, P.O.J. 2012. Benthic Phosphorus Dynamics in the Gulf of Finland, *Aquat. Geochem.* 18, 543–564, doi: 10.1007/s10498-011-9155-y.

- Winant, C., Valle-Levinson, A., Ponte, A., Winant, C., Gutierrez- de-Velasco, G. and Winters, G. 2014. Observations on the lateral structure of wind-driven flows in a stratified, semiarid bay of the Gulf of California. *Estuaries and Coasts*. 37: 1319–1328.
- Wübber, C. and Krauss, W. 1979. The two-dimensional seiches of the Baltic Sea. *Oceanol. Acta* 2: 435–446.
- Zhurbas, V.M., Laanemets, J., Vahtera, E. 2008. Modeling of the mesoscale structure of coupled upwelling/downwelling events and the related input of nutrients to the upper mixed layer in the Gulf of Finland, Baltic Sea. *J. Geophys. Res.* 113, C05004, doi: 10.1029/2007JC004280.

Acknowledgements

I am thankful to my first supervisor Juss Pavelson for the guidance and help throughout the first half of my PhD studies and the advisor Viktor Zhurbas for his help and contribution to the published papers. I am also thankful to my second supervisor Taavi Liblik who accepted me as his student from the half of my PhD project; his advice and support have been really helpful throughout the process. I am also grateful to Urmas Lips for his time, feedback and support during the past years. Also, I take this opportunity to thank all co-authors for the published papers, their time and contribution. I am thankful to Madis-Jaak Lilover and Germo Väli for reviewing the thesis and their helpful comments. Also, I would like to appreciate all the support from all the colleagues in the Department of Marine Systems during the formation of this thesis, especially Sirje, Villu and Nelli. In addition, I would like to express my gratitude to the crew of the research vessel Salme for their helpfulness, cooperation and good company. Finally, I would like to thank my family and friends for continuous support during my studies.

This work was financially supported by the institutional research funding IUT (19-6) of the Estonian Ministry of Education, Estonian Science Foundation (grants 6955, 9023, 9278, 9381, and 9382), Estonian Research Council grant PUT595, Internationalisation Programme DoRa and Doctoral School on Earth Sciences and Ecology.

Abstract

Structure and variability of currents in the stratified Gulf of Finland

The Gulf of Finland is an elongated stratified estuary in the brackish Baltic Sea. Currents are sensitive to wind and play important role in shaping the physical, biogeochemical and biological conditions in the Gulf. The main aim of the present work was to relate observed variability in the vertical structure of currents in various time-scales to the wind forcing and stratification conditions in the Gulf. Secondly, influence of current dynamics on the selected key biogeochemical variables in the deep layer of the Gulf was investigated.

The present work, based on data of 11 ADCP deployments, supports earlier modelling studies, which have suggested that local loops in the mean circulation might exist while the basin-wide residual circulation is cyclonic in the upper layer. The mean current speed was in the range of 9-12 cm s⁻¹ in the upper layer and below 70 m depth; flow was weaker in the intermediate layer. Mean vertical current structure at the thalweg revealed that if airflow from south-west was stronger than the climatic average an ordinary estuarine circulation could be reversed. During the winter period, in extreme cases, strong estuarine circulation reversals led to the vanishing of vertical stratification and creation of the barotropic flow system consisting of an outflow in the open part and inflow along the coast.

The current shear maxima were strongly linked to the seasonal thermocline and halocline. Thus, depending on the presence of the pycnoclines one-, two- or three-layer current structure might occur in the Gulf of Finland. The kinetic energy spectra revealed the energy maxima at a broad semi-diurnal frequency band, broad diurnal frequency band and low-frequency seiches band. During the period of weak stratification and strong wind forcing, different modes of seiches prevailed in spectra. In cases of two- or three- layer flow, the inertial oscillations were dominating from the surface to either thermocline or halocline. Likewise, tides contributed to the kinetic energy of current oscillations during the periods of stratified water column.

The estuarine circulation and associated saltwater wedge intrusion from the Baltic Proper strengthened the vertical stratification and increased remarkably the amount of hypoxic water in the Gulf. The hypoxic saltwater wedge had high phosphate and low nitrate/nitrite concentrations, creating remarkable fluxes of nutrients from the Northern Baltic Proper to the Gulf. Estuarine circulation reversal events caused movement of the hypoxic saltwater wedge out from the Gulf. Thus, wind-driven circulation modifications in the deep layer have strong impact on biogeochemical variables in the Gulf.

Lühikokkuvõte

Hoovuste muutlikkus ja struktuur stratifitseeritud Soome lahes

Soome laht on välja venitatud, stratifitseeritud estuaar riimveelises Läänemeres. Soome lahe hoovused on tundlikud tuule mõjule ning mängivad olulist rolli füüsikaliste, biogeokeemiliste ja bioloogiliste tingimuste kujundamisel. Käesoleva uuringu peamiseks eesmärgiks oli seostada hoovuste vertikaalse struktuuri muutlikkus erinevates ajamastaapides tuule mõju ning stratifikatsiooni tingimustega lahes. Teiseks, uuriti hoovuste dünaamika mõju biogeokeemiliste parameetritele põhjalähedastes kihtides.

Käesolev töö, mis põhineb 11 ADCP mõõtmise aegreal, toetab varasemaid modelleerimisuuringuid, mis on näidanud, et ülemise kihi keskmises tsirkulatsioonis võivad esineda väiksemad tsirkulatsioonipesad, samas kui basseini üldine jäätsirkulatsioon on tsüklonaalne. Keskmine hoovuse kiirus ülemises kihis ja allpool 70 m sügavust oli vahemikus $9\text{--}12\text{ cm s}^{-1}$; aeglasemad kiirused esinesid vahekihis. Hoovuste keskmine vertikaalne struktuur voolunõval näitas, et kui õhuvool edelast oli tugevam kui kliimaatiline keskmine, siis tavaline estuaarne tsirkulatsioon võis olla ümberpööratud. Erakordsetel juhtudel talvel võib tugev estuaarse tsirkulatsiooni ümberpöördumine viia vertikaalse stratifikatsiooni kaoni ja tekitada barotroopse hoovuste süsteemi, mis koosneb väljavoolust lahe keskosas ja sissevoolust piki rannikuid.

Hoovuse kiiruse nihke maksimumid olid tihedalt seotud sesoonse termokliini ja halokliiniga. Sõltuvalt püknokliinide olemasolust võib Soome lahes esineda ühe-, kahe- või kolmekihiline voolamise struktuur. Hoovuste kineetilise energia spektrite maksimumid esinesid perioodidel pool ööpäeva ja ööpäev ning madalsageduslike seiššide perioodidel. Nõrga stratifikatsiooni ja tugeva tuule korral prevaleerisid spektris erinevate perioodidega seišid. Kahe- või kolmekihilise hoovuse struktuuri puhul domineerisid inertsivõnkumised veesamba ülemisest kihist kuni termokliini või halokliini sügavuseni. Stratifitseeritud perioodidel panustasid hoovuste kineetilisse spektrisse ka looded.

Estuaarne tsirkulatsioon ja sellega seotud soolase vee kiilu tungimine Ava-Läänemerest Soome lahte tugevdas stratifikatsiooni ja suurendas hüpoksilise vee kogust lahes märkamisväärselt. Hüpoksilise ja soolase vee kiil oli fosforirikas ja nitraatide/nitrititevaene. Ümberpööratud estuaarse tsirkulatsiooni sündmused põhjustasid hüpoksilise soolase vee kiilu välja surumise lahest. Seega tuule poolt tekitatud tsirkulatsiooni muutused omavad olulist mõju biogeokeemilistele parameetritele Soome lahe süvakihtides.

Appendix

Paper I

Suhhova, I., Liblik, T., Lilover, M.-J. and Lips, U. 2018. A descriptive analysis of the linkage between the vertical stratification and current oscillations in the Gulf of Finland. *Boreal Env. Res.* 23: 83–103.

A descriptive analysis of the linkage between the vertical stratification and current oscillations in the Gulf of Finland

Irina Suhhova*, Taavi Liblik, Madis-Jaak Lilover and Urmas Lips

*Tallinn University of Technology, Department of Marine Systems, Akadeemia 15A, EE-12618 Tallinn, Estonia (*corresponding author's e-mail: irina.suhhova@ttu.ee)*

Received 20 Apr. 2017, final version received 14 Jan. 2018, accepted 16 Jan. 2018

Suhhova I., Liblik T., Lilover M.-J. & Lips U. 2018: A descriptive analysis of the linkage between the vertical stratification and current oscillations in the Gulf of Finland. *Boreal Env. Res.* 23: 83–103.

The data from five ADCP deployments with duration from one to several months in various locations of the Gulf of Finland were analyzed. The observations revealed that the shear maxima of current velocity were strongly linked to the pycnoclines — the seasonal thermocline or vertical salinity gradient. The shear maxima were not detected when the quasi-permanent halocline temporarily vanished in winter due to strong SW winds causing reversed estuarine circulation in the gulf. The kinetic energy spectra of currents revealed the energy maxima at a broad semi-diurnal frequency band, broad diurnal frequency band, and low-frequency seiches band. In the periods of strong wind forcing and weak stratification, the current oscillations coincided with different modes of seiches. During the periods of the two- or three-layer flow in summer, the inertial oscillations were dominating in the upper layer while seiches could be more prominent either in the upper layer or the halocline.

Introduction

The Gulf of Finland is an elongated estuarine basin, located in the northeastern part of the Baltic Sea (Fig. 1). The gulf is about 400-km long and 48–135-km wide, its average and maximum depths are 37 and 123 m, respectively (Alenius *et al.* 1998). Depth decreases from the entrance to the easternmost part. The average riverine discharge to the gulf, concentrated in its eastern part, is about $3500 \text{ m}^3 \text{ s}^{-1}$ (Bergström and Carlson 1994). The surface salinity decreases from the entrance to the east from $5\text{--}7 \text{ g kg}^{-1}$ to $0\text{--}3 \text{ g kg}^{-1}$ while the deep layer salinity exceeds $8\text{--}10 \text{ g kg}^{-1}$ (Alenius *et al.* 1998). The typical estuarine circulation pattern with an outflow of fresher water in the upper layer and inflow of saltier water in the deep layer exists in the gulf. The estuarine

circulation is intensified by the northeasterly and northerly winds (Elken *et al.* 2003, Liblik and Lips 2011), while, in the case of strong westerlies, it can be altered or even reversed (Elken *et al.* 2003). Furthermore, Elken *et al.* (2014) have found that the recent increase in the frequency of circulation reversals could be caused by a shift in the wind regime with increased frequency of westerly–southwesterly winds in wintertime.

Vertical stratification in the gulf is variable and exhibits a clear seasonality. In winter, the water column in deep enough areas has mostly two-layer structure with a well-mixed upper layer extending from the sea surface until the halocline at the depths of 60–80 m (e.g., Alenius *et al.* 1998). However, considerable haline stratification may appear in the upper layer during calm periods (Liblik *et al.* 2013), and intensive rever-

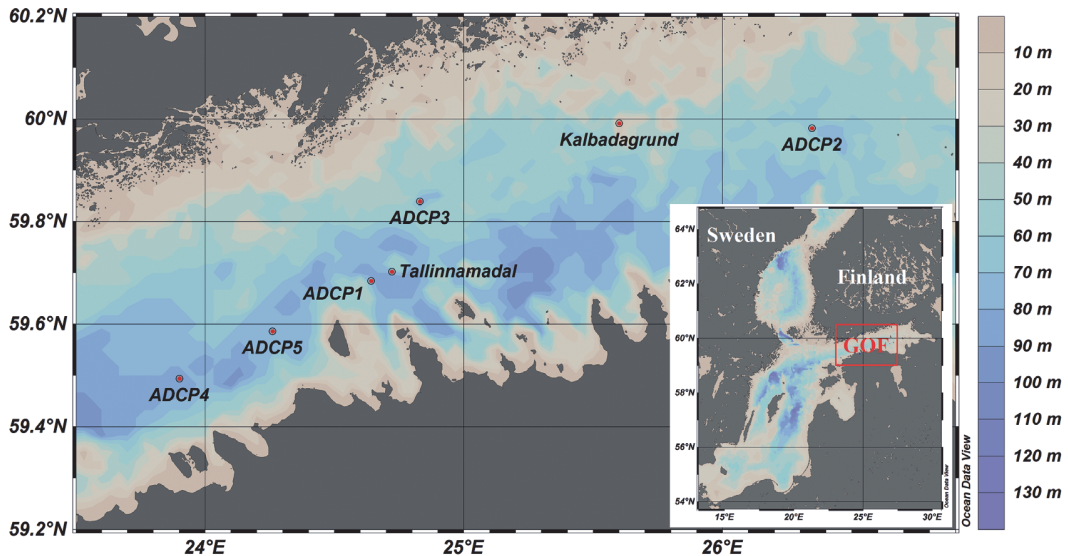


Fig. 1. Map of the study area in the Gulf of Finland. Locations of ADCP deployments (Table 1) and wind measurement locations in Kalbadagrund and Tallinnamadal Lighthouse are shown.

sals of estuarine circulation may cause occasional stratification collapse events (Liblik *et al.* 2013, Elken *et al.* 2014). As a result, three-, two- and one-layer stratification regime may occur in the gulf in winter. In summer, mostly a three-layer vertical structure exists as the seasonal thermocline develops at the depths of 10–30 m (e.g., Alenius *et al.* 1998, Liblik and Lips 2017).

Based on ten series of current profile recordings covering all seasons, Lilover *et al.* (2017) reported that, on average, an inflow with nearly uniform speed throughout the entire water column existed in the deep central part of the gulf in winter, while a layered flow structure was a typical pattern in summer. The vertical structure of currents seems to be linked to the presence and location of the seasonal thermocline (Suhhova *et al.* 2015) and halocline (Liblik *et al.* 2013) while, on the other hand, the changes in circulation are reflected in the variability of vertical stratification (Liblik and Lips 2012). Thus, there should exist a strong interplay between the currents and stratification in the gulf.

Since the gulf is relatively wide, the general circulation may exhibit a transverse structure. As it was suggested already by Palmén (1930) and confirmed by numerical simulations (e.g., Andrejev *et al.* 2004), a quite persistent outflow

exists in the surface and sub-surface layers in the northern gulf. As a result, the general (residual) surface circulation is suggested to be cyclonic, but the occurrence of some sub-cells has been shown by model experiments (e.g., Andrejev *et al.* 2004, Elken *et al.* 2011). Lips *et al.* (2017) suggested that in weakly stratified conditions (in winter), the flow structure might correspond to the circulation pattern either driven by spatially uniform longshore wind in lakes (e.g., Bennet 1974, Winant *et al.* 2014) or formed due to the mixing asymmetry in tidal estuaries (Burchard *et al.* 2011). The three-layer flow observed in some summers could correspond to the flow pattern in the relatively deep fjords where the mixing due to tidal currents does not occupy the whole water column (Valle-Levinson *et al.* 2014). In most of these suggestions, the vertical mixing due to current oscillations is assumed to be involved. Thus, it needs to be studied, what are the most energetic current oscillations in different forcing and stratification conditions.

The energy maxima of current oscillations in the Gulf of Finland are usually revealed at a broad semi-diurnal frequency band (BSD), broad diurnal frequency band (BD) or low-frequency seiches band (LFS) (Wübbler and Krauss 1979, Jönsson *et al.* 2008, Lilover *et al.*

2011). The seiches with periods of 11, 13 and (17) h together with the inertial motions (period 13.9 h) and semi-diurnal tidal constituents S2 (12.0 h) and M2 (12.42 h) contribute to the BSD band kinetic energy. Seiches with periods of 19 (20) h (4th mode), 24 (22) h (3rd mode) and 28 (26) h (2nd mode) and diurnal tidal constituents K1 (23.93 h) and O1 (25.82 h) are the contributors into the BD frequency band. Note that the periods of seiches are cited here according to Wübbler and Krauss (1979) model, without parenthesis, the numbers belong to the entire Baltic and with parentheses to the western Baltic–Gulf of Finland oscillating system. The period of the first mode seiche is 31 hours, and it belongs to the LFS band. Although the occurrence of current oscillations at the listed frequency bands in the Gulf of Finland is known, we lack the knowledge on the vertical distribution of current oscillation energy.

This study aims to examine the concurring variability of currents and thermohaline fields using ADCP (Acoustic Doppler Current Profiler) and CTD (Conductivity, Temperature, and Depth) measurements in the Gulf of Finland. We use five ADCP current profile time series, with duration from one to five month, acquired at different sites of the gulf in 2010–2014. We examined the following hypotheses: (1) one-, two- and three-layer flow regimes can occur in the gulf depending on the wind forcing, (2) strong current shear is linked to the two pycnoclines, and (3) there are differences in the kinetic energy spectra in different layers when a layered flow structure has been realized.

Material and methods

Two out of five current measurement series

analyzed in the present paper were acquired in summers 2010 and 2011 (moorings ADCP1 and ADCP3, respectively). Mooring ADCP2 was deployed during the decay of stratification in autumn 2010. Two last deployments (ADCP4 and ADCP5) describe the conditions with the weak seasonal stratification in winter and its strengthening in spring of 2012 and 2014.

A bottom-mounted ADCP (Workhorse Sentinel, Teledyne RDI, 300 kHz) was deployed at five locations (*see* Fig. 1) for the periods of 29 to 148 days (Table 1). Current velocity profiles were measured over 2-m depth bin with the sampling interval of 10 minutes and 30 minutes (for ADCP4) as averages of 50 pings. The sea depth in the deployment locations varied from 67 to 91 m. Due to the surface side lobe effect and ADCP ringing distance, the current velocities were available in the depth range from 62–86 m to 8–10 m, depending on the depth of deployment locations.

CTD profiles acquired using an Ocean Seven 320plus CTD probe (Idronaut S.r.l.) during several cruises were applied as background data on vertical stratification.

Wind data from the Kalbådagrund meteorological station (Finnish Meteorological Institute) — a lighthouse in the central part of the Gulf of Finland (Fig. 1) were used to describe the local atmospheric forcing conditions from June 2010 until September 2011. The wind speed and direction measured at the height of 32 m were available every third hour as a 10 min average. For the two last measurement periods, wind data from the Tallinnamadal Lighthouse were used. Wind speed and direction were measured at the height of 36 m above the sea level and were reported every hour as a 5 min average. To convert the measured wind speed to the standard 10 m height wind speed, the measured values

Table 1. Mooring positions, deployment periods and depth ranges.

Deployment	Longitude (E)	Latitude (N)	Period	Bin depth range (m)	Sea depth (m)
ADCP1	24°37.5′	59°41.0′	1.06.2010–31.08.2010	9–79	84
ADCP2	26°20.8′	59°58.8′	30.09.2010–28.10.2010	8–62	67
ADCP3	24°49.9′	59°50.3′	13.07.2011–05.09.2011	9–73	78
ADCP4	23°54.1′	59°29.6′	21.12.2011–09.05.2012	10–86	91
ADCP5	24°15.6′	59°35.1′	9.12.2013–06.05.2014	10–82	87

were multiplied by a height correction coefficient (0.91 and 0.90, respectively for Kalbådagrund and Tallinnamadal; Launiainen and Saarinen 1984). The relationship between the wind and current velocity during selected measurement periods is characterized in the paper by the complex vector correlation coefficient according to Kundu (1976).

The quality of the current velocity data was checked following the procedure developed by Book *et al.* (2007). The time-series were smoothed with a 1-h moving average filter to get hourly average values. For the low-frequency analysis, all series were smoothed with a 36-h cutoff Butterworth (1930) filter. Time series of the vertical distribution of current velocity components and polar histograms of currents were analyzed based on the hourly average data. Current shear was calculated between the two nearest velocity horizons over the depth range of 2 m using low-pass filtered data. We defined the following criterion based on the current shear square (S^2): if $S^2 < 2 \times 10^{-4} \text{ s}^{-2}$, a homogeneous flow is present, if $S^2 > 2 \times 10^{-4} \text{ s}^{-2}$, a layered flow is present.

For spectral structure investigations of current oscillations, rotary spectral analysis technique (e.g., Emery and Thomson 2004) was applied to hourly average current data. Dividing time series into two equal-length segments and using 50% overlapping between them the calculated spectrum had 6 degrees of freedom (DoF). To increase the accuracy of the power spectral density at a given depth, an average spectrum over the depth range of 10 m (average of 5 closest spectra) was calculated. As a result, the calculated spectra had 30 DoF. Current speed amplitude was defined as the root mean square of $\sigma^2(f_c) \approx S_c \Delta f$, where $\sigma^2(f_c)$ is the signal variance in a frequency band Δf centered at the frequency f_c , and S_c is the power spectral density (Emery and Thomson 2004).

Power spectral density (PSD) is usually plotted in coordinates $\log S(f)$ versus $\log(f)$, where $S(f)$ is the power spectral density and f the frequency. Such presentation is useful if the spectral slope has to be estimated. We use another spectral plot in the present paper, namely $fS(f)$ versus $\log(f)$ which is a variance-preserving form of spectral presentation. In this presenta-

tion, the energy in every frequency interval is proportional to the corresponding area under the spectral line. The use of the linear scale instead of a logarithmic scale of PSD enables to illuminate the depths and frequencies with elevated kinetic energy.

Results

General description of wind, stratification, and currents

Strong seasonal thermocline was observed at 15–25 depth during both summer deployments in 2010 and 2011. The thermocline weakened and deepened from 25–30 m to 40–50 m depth during the measurement period in September–October 2010 (ADCP2). During both measurement periods in winter–spring 2011/2012 and 2013/2014, weakly stratified conditions prevailed in December–January, but later, vertical stratification developed and three-layer stratification pattern existed by the end of both deployments.

The average wind speed of the first deployment was 5.8 m s^{-1} , and the most frequent wind direction was from the ENE suggesting that summer 2010 was quite exceptional in respect of wind forcing — according to the long-term wind data, the WSW winds prevail in the region (Keevallik and Soomere 2014). Both, the ENE and WSW winds were frequent during the third deployment in summer 2011 while the average wind speed was 5.7 m s^{-1} . The S and NW winds with mean speed of 7.3 m s^{-1} prevailed during the second (autumn) deployment. The last two measurement periods were characterized by variable weather conditions, with an average wind speed of 9.4 m s^{-1} and 8.5 m s^{-1} (2011/2012 and 2013/2014, respectively). Several storms from SW occurred in December–January 2011/2012 and 2013/2014.

The mean current speed during the autumn 2010 and summer 2011 deployments decreased with the depth, while during the summer 2010 and two winter–spring deployments, currents in the upper and deep layers were slightly stronger than in the intermediate layer (Table 2). The maximum current speed (1 h average) for the

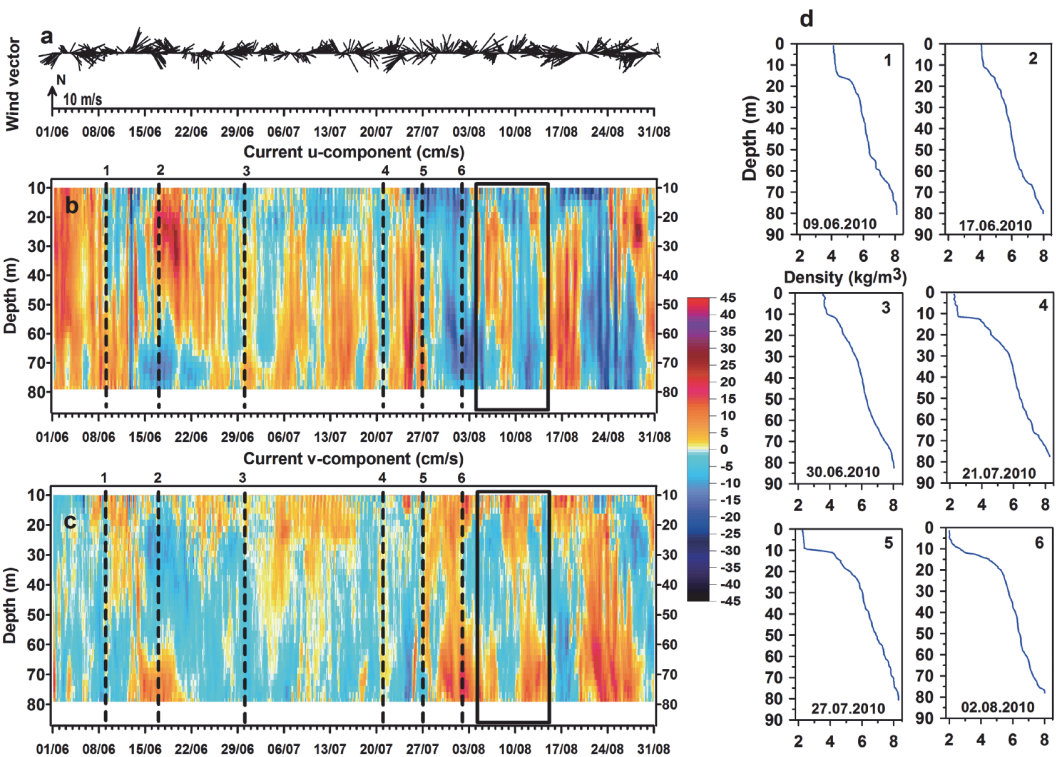


Fig. 2. (a) Time series of wind vectors subsampled every 3 h from 1 June to 31 August 2010. The scale is shown by an arrow on the time axis. Time series of the vertical distribution of (b) east-west current velocity component (u), and (c) north-south current velocity component (v) for the deployment ADCP1. Vertical dashed lines indicate the CTD measurements presented as (d) vertical profiles of density anomaly. The black rectangle indicates the selected period which we analyzed in more detail.

deployments was recorded in the upper layer (the maximum speed was measured in the last week of December 2011) or in the near-bottom layer (the maximum speed was measured on 21 December 2013). An exception was the autumn 2010 measurement period when the maximum current speed was recorded in the intermediate layer.

Summer 2010

Both pycnoclines (the seasonal thermocline and quasi-permanent halocline) were present throughout the first deployment (Fig. 2). A weak barotropic inflow into the gulf (to the east) was observed during the first week of June and a reversal of the estuarine circulation as a reac-

Table 2. Average and maximum values (1 h average) of current speeds (cm s^{-1}) at the five locations.

	Mean speed			Maximum speed		
	Near-bottom layer (m)	Intermediate layer (20–50 m)	Upper layer (8–11 m)	Near-bottom layer (m)	Intermediate layer (20–50 m)	Upper layer (8–11 m)
ADCP1	8.9 (71–79)	8	11.5	34.9	39.7	55.4
ADCP2	5.6 (54–62)	8.4	10.7	25.8	41.7	35
ADCP3	5.0 (65–73)	7.3	11.1	29.3	23.2	41.3
ADCP4	11.2 (78–86)	9.8	12	36.7	48.9	64.6
ADCP5	11.9 (74–82)	9.7	10.7	58.5	50.6	55.1

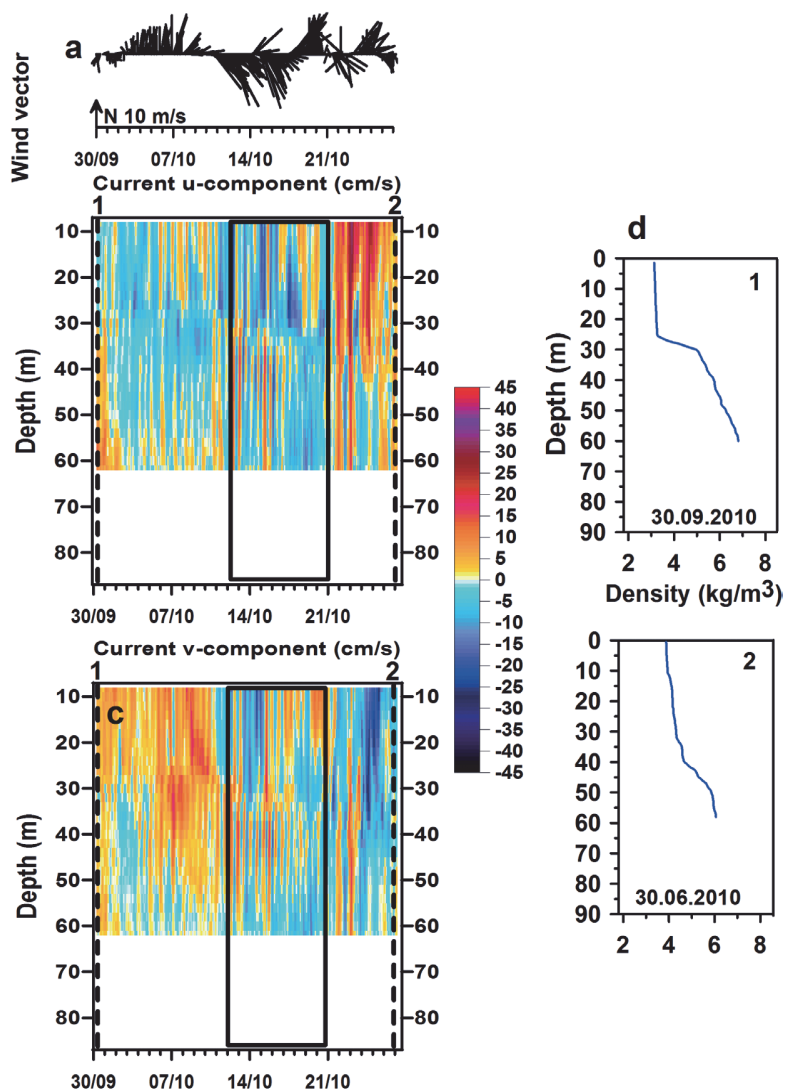


Fig. 3. Same as Fig. 2, but for the deployment ADCP3 from 13 July to 5 September 2011.

tion to the SW wind impulse in mid-June 2010 (Fig. 2). A strong inflow with the current speed exceeding 50 cm s^{-1} in the upper 60 m and an outflow with the maximum speed of 17.2 cm s^{-1} below 60 m depth occurred during this circulation reversal. A relatively weak outflow prevailed in the upper layer, and an inflow was observed beneath the seasonal thermocline in July 2010. Alternating in- and outflow events were observed in the upper and deeper layers in the timescale of about one week as a reaction to the variable wind forcing in August 2010. Strong easterly wind impulses on 23–26 July and 17–19 August 2010

caused strong outflow events (likely upwelling jet along the southern coast) in the upper layer and upwind flow events in the deeper layer.

Summer 2011

Inflow into the gulf dominated in the upper 30 m layer during the second half of July and in the intermediate layer at the beginning of August 2011 (Fig. 3). Starting from 10 August, the flow in the whole water column was rather characterized by an outflow. Current velocities were relatively

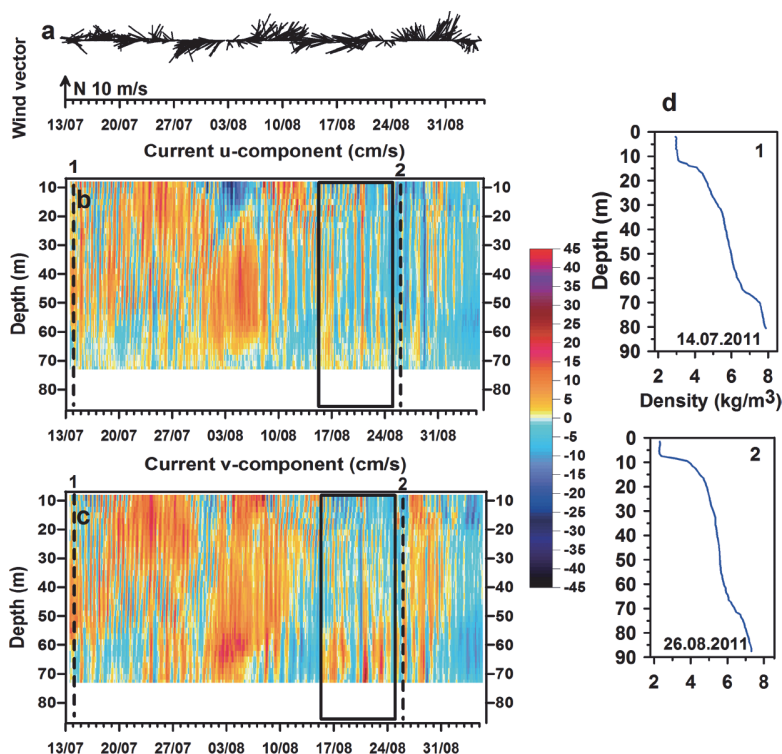


Fig. 4. Same as Fig. 2, but for the deployment ADCP2 from 30 September to 28 October 2010.

weak during this period. A longer period of easterly wind impulse at the end of July caused an outflow from the gulf in the upper 20 m layer at the beginning of August. At the beginning of the observation period and the end of August, both the seasonal thermocline and the quasi-permanent halocline were present in the density profile.

Autumn 2010

The deepest available bin depth (62 m) in the second deployment (Fig. 4) was shallower than the location of the quasi-permanent halocline. However, a strong vertical salinity gradient coincided with the seasonal thermocline. The seasonal thermocline weakened and deepened from the 25–30 m depth to 40–50 m depth during the deployment period. In the first three weeks, an outflow from the gulf prevailed, but rather an inflow dominated during the last week. The flow structure mostly had two layers and the flow separation depth coincided well with the location of the seasonal thermocline.

Winter–spring 2011/2012

The flow during the first month of the fourth observation period had a barotropic structure with alternating in- and outflow events. This structure was a result of the strong south-westerly wind that reversed estuarine circulation and destroyed stratification (Fig. 5). Once stratification vanished, a barotropic flow system formed. In January, the estuarine circulation established due to calm winds and three-layer flow prevailed in the gulf. Another estuarine circulation reversal occurred in February, but in that case, stratification was only weakened, but not collapsed. From March until the end of measurements, a two- or three-layer flow prevailed. Further details of this time-series can be found in the paper by Liblik *et al.* (2013).

Winter–spring 2013/2014

A similar scenario of the variability of the vertical current structure was observed in winter

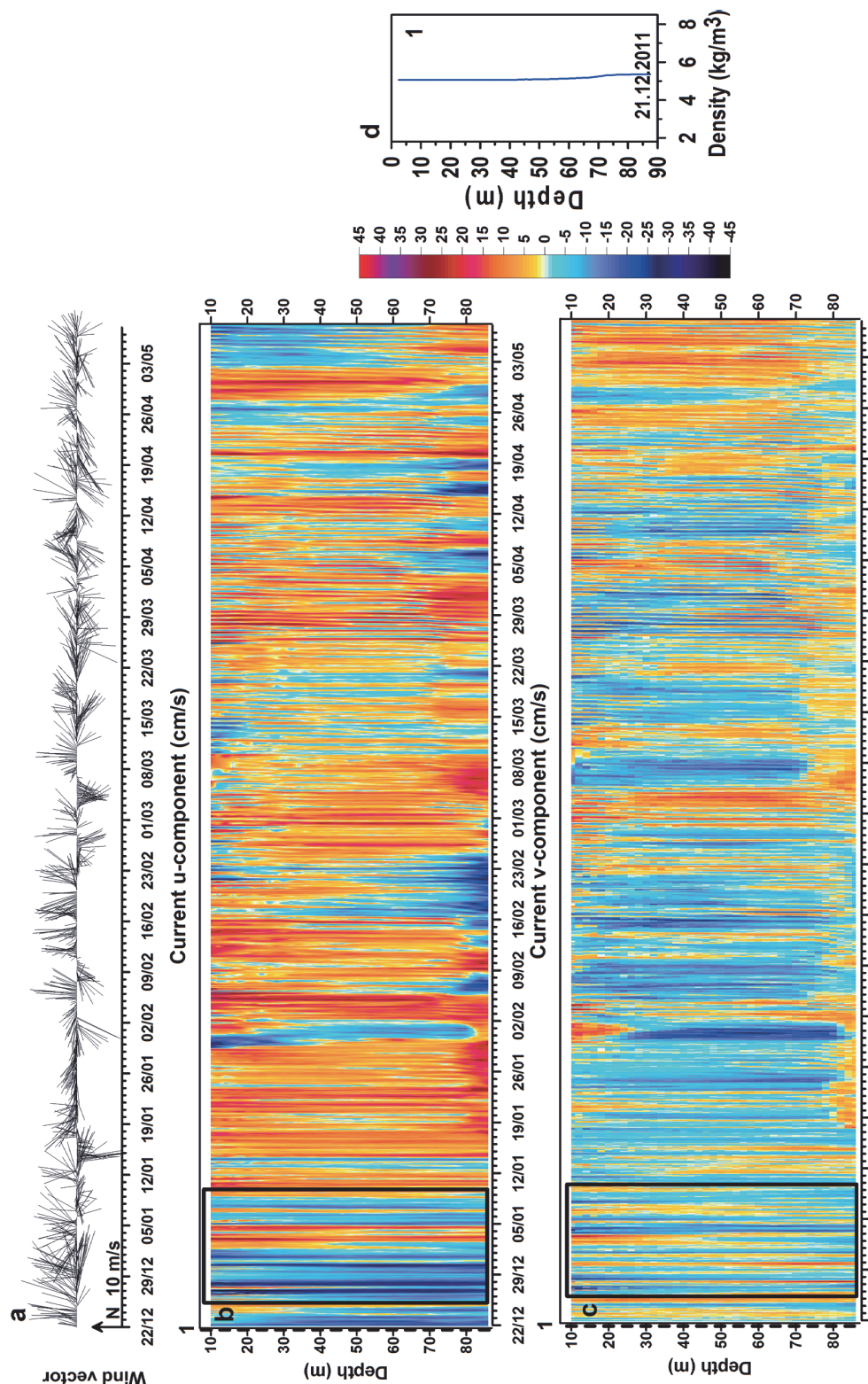


Fig. 5. Same as Fig. 2, but for the deployment ADCP4 from 21 December 2011 to 9 May 2012.

2013/2014. The period from 10 December to 10 January was characterized by a barotropic flow regime due to strong SW-wind domination (Fig. 6). After that, when the wind weakened and turned, first, a barotropic inflow occurred, then a two-layer and later three-layer flow prevailed at the measurement site. Further details can be found in the paper by Lips *et al.* (2017).

Vertical flow structure

Next, we show that one, two or three layers can be distinguished in the vertical current structure in the Gulf of Finland during certain periods. In summer 2010, the current shear was the strongest in the seasonal thermocline (Fig. 7 ADCP1). The other maximum of shear was from time to time observed at the halocline depth, which implies the existence of a three-layer flow in the water column. Similarly to the first observation period, the strongest current shear was observed in the seasonal thermocline in summer 2011 (Fig. 7 ADCP3). The other shear maximum was observed at the depths around 60 m, which was probably associated with the presence of the halocline. Measurements in autumn 2010 showed two-layer flow structure (Fig. 7 ADCP2). During the first half of the observation period, a strong shear maximum was observed at around 25 m depth, and its location deepened due to autumn convection to 40 m by the end of October. The two winter–spring measurements (ADCP4, ADCP5) had a similar pattern of the vertical flow structure (Fig. 7 ADCP4 and ADCP5). The current shear was weak in December and the first half of January. Starting from the second half of January, a strong current shear was present in the halocline. A local shear maximum in the upper layer was associated with the secondary halocline at a depth of 20–25 m.

In order to describe the currents in more detail in the pure one-, two- and three-layer flow cases, periods of 10–17 days were selected (shown by dashed vertical lines in Fig. 7). The number of layers in each period was defined from the period-averaged current shear distribution using the introduced current shear square criterion. The two summer cases (Fig. 8 ADCP1 and ADCP3) revealed a shear minimum in the

intermediate layer and maxima in the seasonal thermocline and quasi-permanent halocline. In autumn (Fig. 8 ADCP2), there was a strong shear maximum at mid-depths (30–40 m) that separated the two layers. In two winter cases (Fig. 8 ADCP4 and ADCP5), no clear maxima could be detected. Thus, the flow was mostly barotropic during the two last selected periods. Available density profiles coincide with the average current shear distributions. Stratification strength parameter — the Brunt-Väisälä frequency shows that the water column was almost mixed during the two winter periods. Vertical locations of stronger density stratification in the three other periods — in summers 2010 and 2011 and autumn 2010 roughly match with the current shear maxima.

The directional distribution of currents in each analyzed period is presented by polar histograms (current roses, Fig. 9) at the three depth horizons (the upper layer, intermediate layer, and deep layer) selected based on the existing stratification and current shear maxima. The wind conditions in both typical summer periods were characterized by a variable along-gulf air flow, but the three polar histograms of currents in these periods were rather dissimilar. Northerly current prevailed in the upper layer during the selected period in summer 2010 (ADCP1). In the intermediate layer, the flow was characterized by weak currents either to ESE or WNW, while in the deep layer, the flow was directed to NE. A uniform directional distribution was revealed in the upper layer during the selected period in summer 2011 (ADCP3). The flow in the intermediate layer and the deep layer was dominated by westward and northward currents, respectively. Complex correlation (r) between wind vectors and current vectors revealed high correlation in the upper 9 m layer, being $r = 0.5$ ($n = 89$, $p < 0.01$) for summer 2010 (ADCP1) and $r = 0.7$ ($n = 80$, $p < 0.01$) for summer 2011 (ADCP3).

The NW and south winds dominated during the selected measurement period in autumn 2010 (Fig. 9 ADCP2). The flow in the upper layer and intermediate layer had a uniform distribution of current directions. The flow in the deep layer was dominated by SW currents. The observed similarity of the upper and intermediate layer current roses in the case of the strong mean shear between the layers is explained by the phase shift of cur-

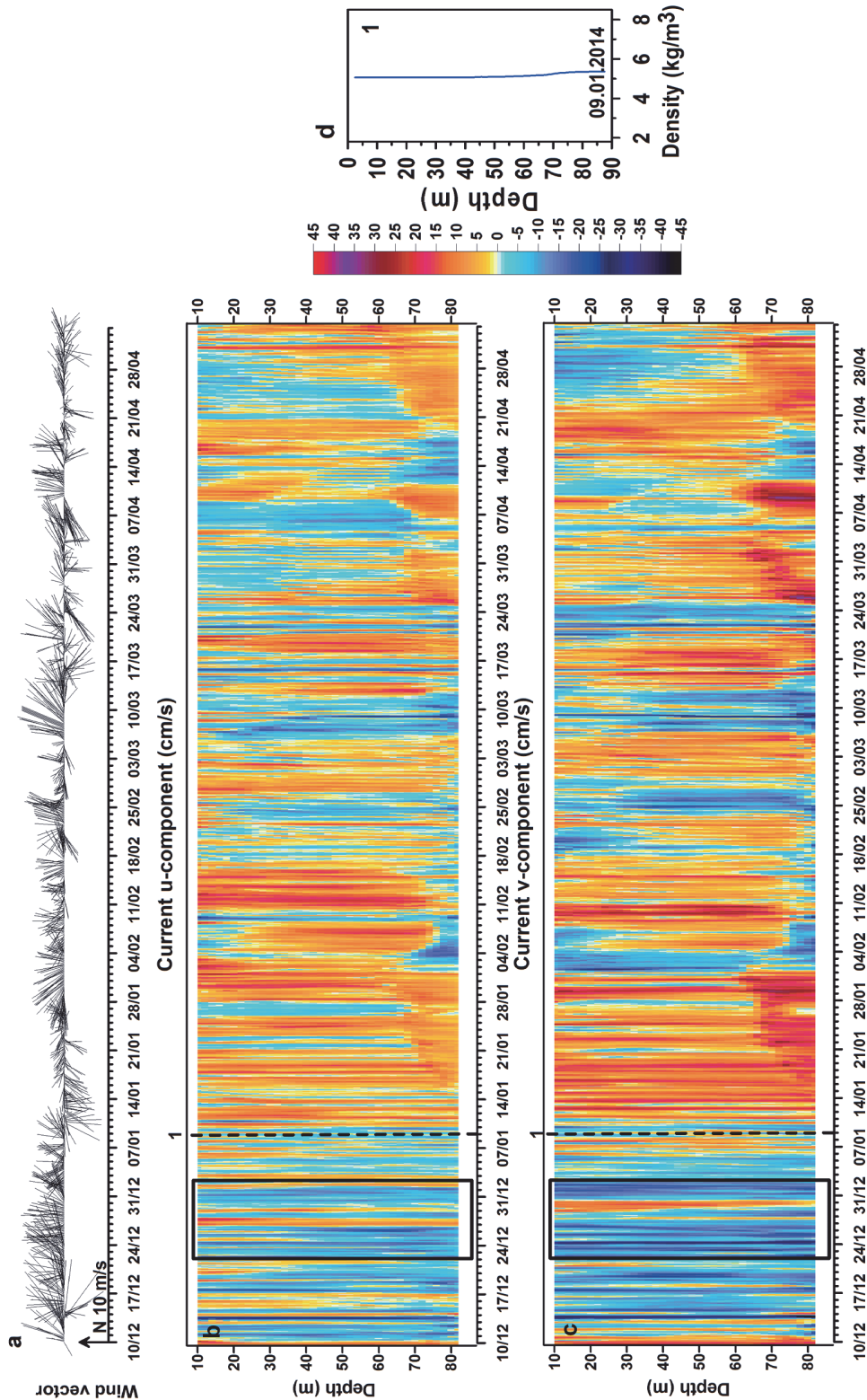


Fig. 6. Same as Fig. 2, but for the deployment ADCP5 from 9 December 2013 to 6 May 2014.

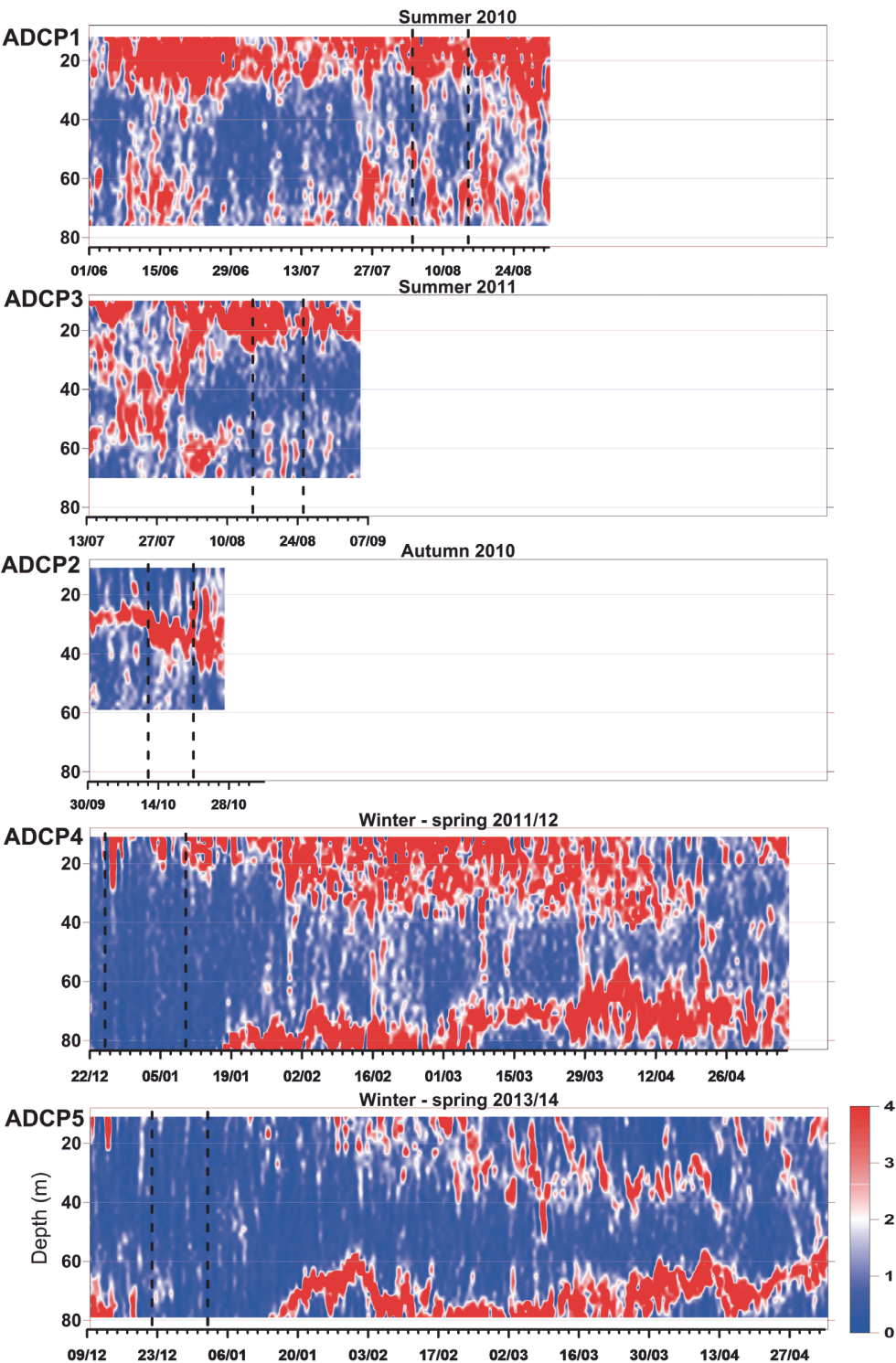


Fig. 7. Low-pass filtered time series of a current shear square (in 10^{-4} s^{-2}) in summer 2010 (ADCP1), summer 2011 (ADCP3), autumn 2010 (ADCP2), winter–spring 2011/2012 (ADCP4), and winter–spring 2013/2014 (ADCP5). Vertical dashed lines indicate the selected periods which we analyzed in more detail.

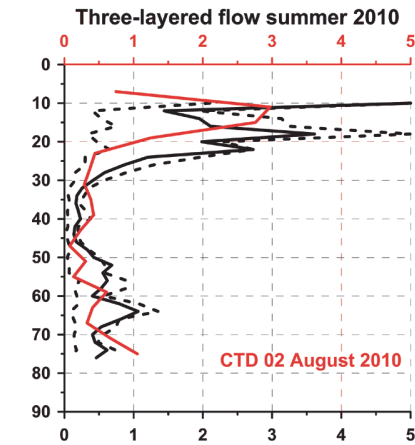
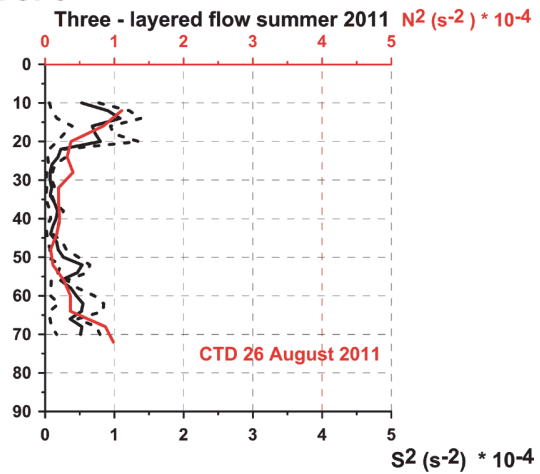
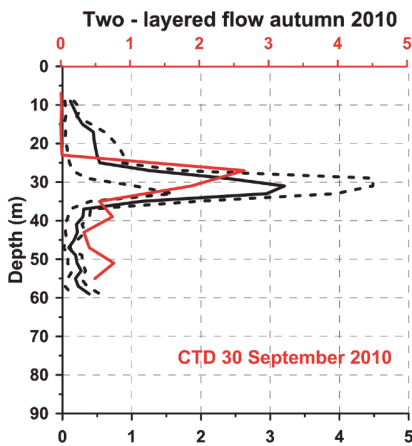
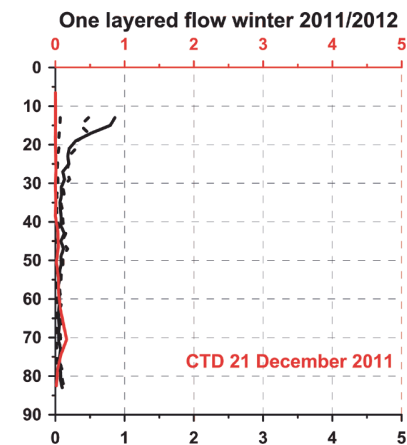
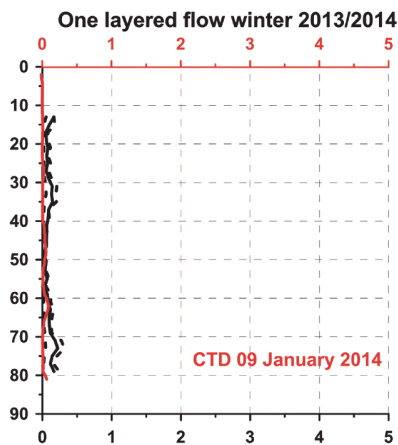
ADCP1**ADCP3****ADCP2****ADCP4****ADCP5**

Fig. 8. Median (solid black lines) current shear square (S^2) distribution and typical Brunt-Väisälä frequency square (N^2) profiles (solid red lines) in summer 2010 (ADCP1), summer 2011 (ADCP3), autumn 2010 (ADCP2), winter-spring 2011/2012 (ADCP4), and winter-spring 2013/2014 (ADCP5). Dashed lines indicate 25- and 75-percentiles of the shear.

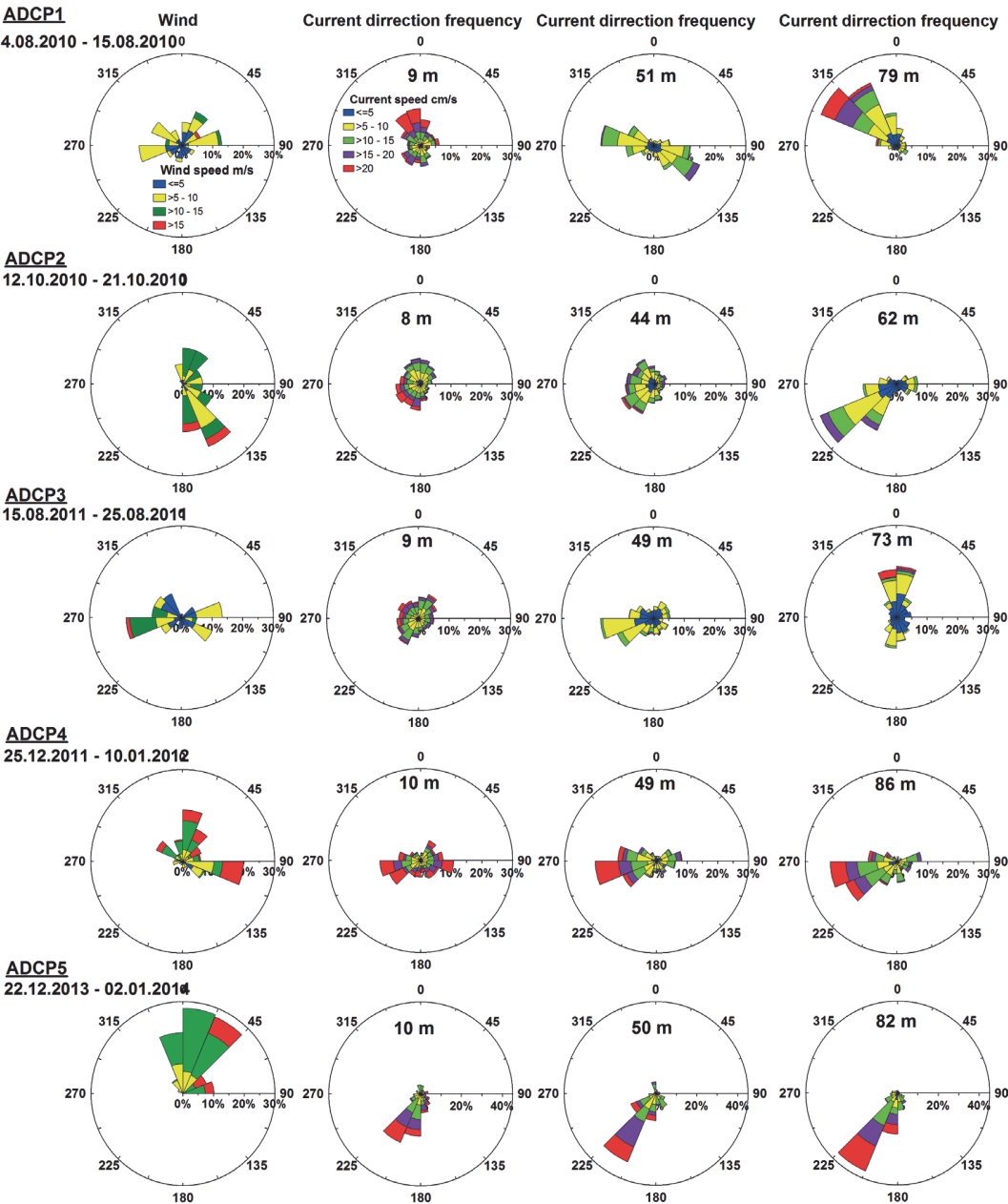


Fig. 9. Wind roses during the five selected periods and current roses at the selected depths in the upper, intermediate, and near-bottom layer. The measured wind direction was turned by 180° to match the wind forcing with the current direction. Colour scales are shown in the first row.

rent oscillations in the pycnocline. Significant vector correlation between the current and wind was found in the sub-surface layer ($r = 0.7$, $n = 73$, $p < 0.001$). The correlation decreased with the depth until it reached a minimum value of $r = 0.5$

($n = 73$, $p < 0.001$) at the depth of 25 m. Below that depth, the correlation started to grow again reaching a value of $r = 0.8$ at a depth of 34 m.

Both selected winter periods were characterized by strong winds from the southwest. The

current roses in the selected period in winter 2011/2012 (Fig. 9 ADCP4) were rather similar at all depths — the currents to the west dominated in all three layers. In the selected period in winter 2013/2014 (Fig. 9 ADCP5), the up-wind flow directed to the SW was present throughout the water column in this site in the central gulf while a down-wind flow existed near the coast (Lips *et al.* 2017). We suggest that the strong currents during the periods of weak stratification were wind induced since a significant correlation between the wind vectors and current vectors was revealed throughout the water column.

Current velocity spectra

The vertical distribution of kinetic energy throughout the water column was examined for five selected current velocity time series. Similarly to the previous studies, the obtained kinetic energy spectra revealed the energy maxima at the broad semi-diurnal frequency band (BSD), the broad diurnal frequency band (BD), and the low-frequency seiches band (LFS). However, these maxima of kinetic energy were not always present in the spectra in all analyzed periods and depth ranges.

During the two selected periods of one-layer (barotropic) flow structure (25 December 2011–10 January 2012 and 22 December 2013–2 January 2014), high kinetic energy bands were assembled in the range from 21 h to 32 h. Significant peaks were revealed throughout the water column close to the periods of the 1st and 3rd mode seiches in 2011/2012 and the 2nd and 3rd mode seiches in 2013/2014 (Fig. 10 ADCP4 and ADCP5). Energy level recorded for the period close to 1st seiche mode for ADCP4 was higher in the upper layer than in the deeper layers corresponding to a current velocity amplitude of 5.6 cm s^{-1} and 4.6 cm s^{-1} , respectively (current spectrum had 30 degrees of freedom (DoF)). During the selected period in winter 2013/2014, the highest energy level was recorded at a period close to the 2nd seiche mode, with the strongest oscillations in the upper layer and slightly weaker in the intermediate layer, with the amplitude of 7.2 cm s^{-1} and 6.3 cm s^{-1} (DoF = 30), respectively. Hence, during both selected winter

periods, strong wind forcing and weak stratification created favorable conditions for the generation of current oscillations with the periods of different mode seiches.

In the selected period of two-layer flow structure from 12 until 21 October 2010, higher spectral energy was concentrated in the broad semi-diurnal frequency band (Fig. 10 ADCP2). The elevated energy was observed from the surface layer to 30 m depth and in the depth range from 36 m to 54 m. Kinetic energy spectra revealed a higher current oscillations amplitude of 8.5 cm s^{-1} (DoF = 30) in the layer below the seasonal thermocline and a lower amplitude of 5.5 cm s^{-1} (DoF = 30) in the upper layer.

Distribution of kinetic energy during the three-layer flow in summer 2010 (4–15 August) showed almost equal energy at the BSD and BD frequencies (Fig. 10 ADCP1). Maximum current oscillations amplitude estimated from the energy spectra in the upper 20-m layer was 5.1 cm s^{-1} for the BSD and 5.5 cm s^{-1} for the BD frequency band (DoF = 30). A prominent BD frequency peak was present in the intermediate layer but was absent at the deepest measurement horizons (at the deepest 20 m). The BSD energy was present throughout the water column, but with very low energy in the depth range from 21 m to 51 m. During the selected period with the three-layer flow structure in summer 2011 (15–25 August), the kinetic energy spectra revealed a clear energy peak in the upper layer at the BSD frequency band and the near-bottom layer at the BD frequency band (Fig. 10 ADCP3) with the current oscillations amplitude of 4.8 cm s^{-1} and 6.1 cm s^{-1} , respectively (DoF = 30). All revealed energy peaks were present in the intermediate layer, but with low energy.

Thus, the current velocity spectra calculated for the selected periods with the quasi-stationary variability of currents revealed clear energy peaks at various frequencies, in the range from BSD to LFS frequencies. During the one-layer flow structure (winter), several modes of seiches close to the 1st, 2nd and 3rd mode were observed. During the two-layer (autumn) and three-layer (summer) flow structure, the temporal variability of currents was influenced by current oscillations belonging to the broad semi-diurnal and broad diurnal frequency bands.

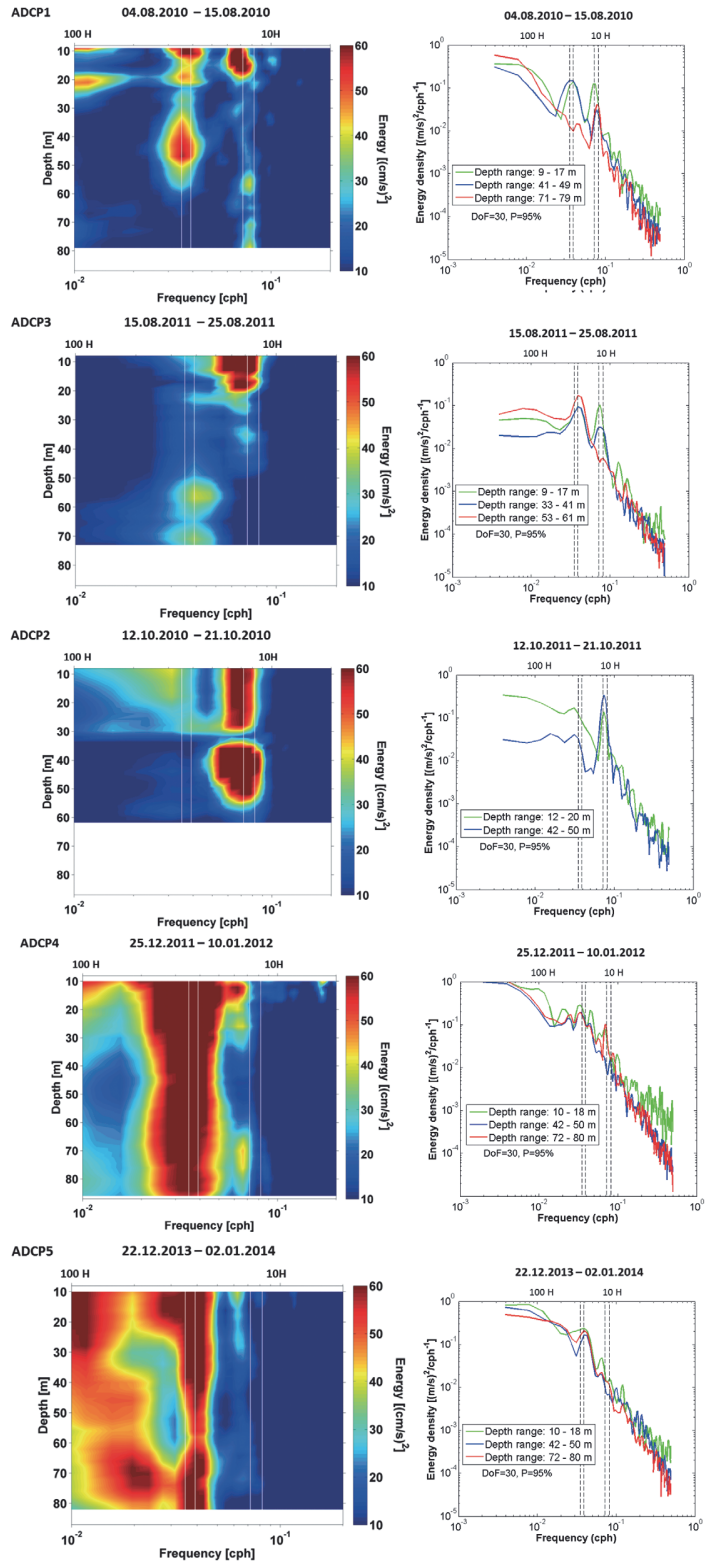


Fig. 10. (Left column) Vertical distributions of kinetic energy spectra during three-layer flow (ADCP1, ADCP3), two-layer flow (ADCP2), and one-layer flow (ADCP4, ADCP5). (Right column) Depth-averaged kinetic energy density for the upper, intermediate, and near-bottom layer. Vertical white lines (left column) and dashed lines (right column) indicate the oscillation periods of 28.6 h, 25.6 h, 13.9 h, and 12.42 h.

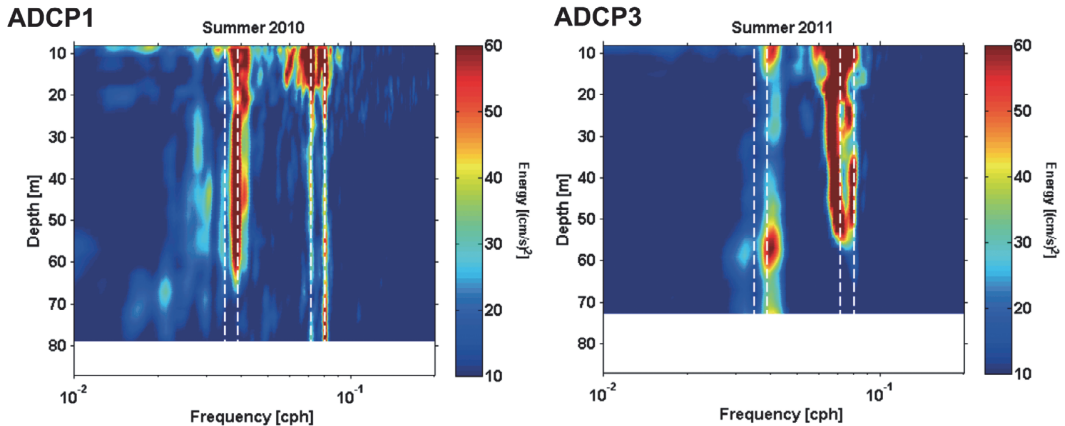


Fig. 11. Vertical distribution of kinetic energy spectra in summer 2010 (ADCP1) and summer 2011 (ADCP3). Vertical dashed lines indicate the oscillation periods of 28.6 h, 25.6 h, 13.9 h, and 12.42 h.

The current velocity spectra for the selected periods from summers 2010 and 2011 revealed the energy peaks at similar frequencies. However, the BD frequencies had higher energy from the surface to 60 m depth in summer 2010, while in summer 2011, these frequencies had a higher energy in the halocline and below it. The second discrepancy between these two summer periods was within the range of BSD frequency. An energy peak at this frequency was present in the whole water column in the selected period from summer 2010 while it was distinguishable only in the upper 50 m in summer 2011. In order to verify if this disparity existed for the whole time-series acquired in summers 2010 and 2011, we calculated the kinetic energy spectra for both full measurement periods.

Current velocity spectra for summer 2010 showed that the most pronounced peaks for the 15-m-thick upper layer were found in the range of oscillation periods from 12 to 27 h (Fig. 11 ADCP1). The M_2 semidiurnal tidal period was present through the whole water column. A prominent spectral maximum at a period close to the local inertial oscillation period (13.9 h) had higher energy in the upper 50 m depth. Energy maxima at the BD frequency band were found in the upper 60 m depth with the almost same energy level, but this peak was not distinguishable in the near-bottom layer.

Similarly, prominent spectral maxima were found for summer 2011 in the period interval from 12.3 to 18 h and at a period close to the 2nd

mode seiches. The broad semi-diurnal frequencies had higher energy in the upper layer if compared to the intermediate layer and did not reveal an energy maximum in the deepest 20-m-thick layer. The prominent peak at a period close to the 2nd mode seiches was present throughout the water column. The kinetic energy spectra revealed more energetic oscillations in the upper layer (upper 10 m) and near-bottom layer, but there was less energy in the layer from 15 to 40 m (Fig. 11 ADCP3).

Thus the two spectra calculated from the full data sets support the mismatch of vertical distributions of kinetic energy spectra between the two selected time-series in summers 2010 and 2011.

Discussion

The analyzed five current measurement time-series revealed that one-, two- or three-layer current structure could occur in the Gulf of Finland depending on the wind forcing and stratification. If we consider the Baltic Sea as an estuarine system, it can be classified as a strongly stratified estuary based on freshwater flow and mixing parameters (Geyer and MacCready 2014). The elongated Gulf of Finland has the main freshwater source at its eastern end and free water exchange with the Baltic Proper through its western border (Alenius *et al.* 1998). Thus, the gulf can be considered as an estuary of the Baltic

Sea. Our results show that the Gulf of Finland is rather extraordinary among world estuaries (Geyer and MacCready 2014) since it can switch from one- to three-layer flow system over time. Likewise, in that respect, the Gulf of Finland is unique in the Baltic Sea. The shallower areas of the Baltic (e.g., the Gulf of Riga and the Belt Sea) operate as one- or two-layer systems (e.g., Lilover *et al.* 1998, Jakobsen and Trebuchet 2000) while in the central Baltic two- and three-layer flow regimes exist (Lass *et al.* 2003).

The most common current structure had two shear maxima and, thus, mostly the three-layer flow occurred in the gulf. As it was also noticed in the earlier studies, the current shear maxima coincide with the two pycnoclines: seasonal thermocline (e.g., Suhhova *et al.* 2015) and quasi-permanent halocline (e.g., Liblik *et al.* 2013). This feature can be confirmed by the time-series acquired during all deployments analyzed in the present study. Strong current shear was also often observed at 10–20 m depth in winter 2011/2012 when the seasonal thermocline did not exist. This shear maximum appeared in the periods of easterly winds that initiated westward transport of fresher water in the upper layer and, in turn, created vertical salinity gradient at the depths of 10–20 m, as also noted by Liblik *et al.* (2013). The advection of fresher water is clearly distinguished in the vertical section of the salinity (e.g., Liblik *et al.* 2013: fig. 3) and current shear (Fig. 7). Similar surface layer current can be detected based on the long-term measurements near the northern coast in the entrance area of the gulf (e.g., Rasmus *et al.* 2015: fig. 5). While the latter observation agrees with the classical concept of the cyclonic circulation scheme in the gulf (Palmén 1930, Alenius *et al.* 1998), we suggest that the fresher surface current can also be observed in the deeper central and southern parts of the gulf (Fig. 5).

The presented current roses confirm that the currents and their variability were similar throughout the water column under conditions of strong up-estuary wind forcing and weak stratification (Fig. 9 ADCP4 and ADCP5). However, the down-estuary current was more persistent in the deeper layers than in the upper layer, as it was expected in the central, deeper part of the gulf where the flow was up-wind. For one of these analyzed winter periods (from winter

2013/2014), a strong down-wind (up-estuary) current was observed along the southern coast at the same time (Lips *et al.* 2017). We assume that two-cell circulation was observed in the study period, which is typical in semi-enclosed basins or lakes (Sanay and Valle-Levinson 2005, Winant *et al.* 2014). During the reversal of estuarine circulation, the up-wind barotropic flow appeared along the thalweg and downwind barotropic flow along the shores (Lips *et al.* 2017).

The current roses qualitatively differed between the layers in the stratified conditions (Fig. 9 ADCP1, ADCP3, and ADCP2). The currents were directionally more equally distributed in the upper layer for the selected summer periods and both the upper and the intermediate layer in autumn. The observed narrow current roses in the deepest layer imply that the currents were topographically steered. A shallow area (Uusmatal) is located to the southeast from the ADCP1 deployment site, and the ADCP3 was deployed in a deeper area between the bottom elevations with the depth of 55–60 m to the east and west from the measurement site. The latter explains the observed discrepancy between the orientation of the gulf and near-bottom currents at ADCP3. This result together with observations by Lilover *et al.* (2017) suggests that channel-like flow in the near bottom layer is a typical feature of the Gulf of Finland.

The prominent spectral peaks at periods from 12.4 h to 26 h (summer measurements) and 14 h to 31 h (winter measurements) indicate the current oscillations due to seiches, tides, and inertial currents. These peaks in the current velocity spectra comprise the local inertial period (13.9 h) and semidiurnal (12.42 h) and diurnal (25.8 h) tidal period (Lilover 2012), as well as seiches-driven current oscillation periods of 16 h (Lilover 2011), 23 h (Jönsson 2008), 26.4 h, and 31 h (Wübbler and Krauss 1979). While prominent peaks close to the inertial frequency were found in the upper and intermediate layers during two-layer flow structure in October 2010, they were almost absent in winter. We assume that the presence of strong seiches and absence of inertial oscillation during one-layer flow can be caused by stormy weather conditions in the study area during our selected periods (Liblik *et al.* 2013, Lips *et al.* 2017).

Wind forcing and disappearance of vertical stratification created favorable conditions for seiche-induced oscillations in the study area (Breaker *et al.* 2010, Simpson *et al.* 2014). Under created conditions, the oscillations are expected to be stronger during winter and autumn periods (Alford *et al.* 2012, Simpson *et al.* 2014). Barotropic flow system was observed during these winter periods, which could cause the absence of inertial oscillations, because of their baroclinic nature (Maas and van Haren, 1987). Furthermore, the kinetic energy spectra revealed the presence of oscillations at the BSD frequencies in the middle of January 2014 after the wind subsided and layered flow structure occurred. The presence of near-inertial oscillations was associated with the re-establishment of stratification (Shearman 2005, Rabinovitch, 2009Castillo *et al.* 2017).

The current velocity spectra for summer periods also showed that the temporal variability of currents (in the range of periods from 12.4 to 26 h) is highly influenced by inertial oscillations, seiches, and tides. In summer 2010, the BD band energy was at a high level from the surface layer to the halocline while this local peak of energy was absent in the near-bottom layer. At the same time, the BSD band energy peak was present in the entire water column from the surface to the near-bottom layer. In summer 2011, the vertical distribution of kinetic energy in these frequency bands were reversed. The BD band energy had high values also in the near bottom layer and BSD band energy being high from the surface to the halocline had no peak in the near-bottom layer (Fig. 11 ADCP1 and ADCP3).

In order to explain the above-mentioned discrepancy between the two summers, we calculated kinetic energy spectra of currents measured in summers 2009 and 2012 at sites very close to the first deployment in 2010. The current velocity spectra showed similar results for the three summer measurements made in the same location (2009, 2010 and 2012 measurements). We suggest that the near-bottom layer was partly disconnected from the above flow structure in summer 2011 due to the topographic peculiarities of the exact measurement site. It can also be qualitatively seen from the current roses (Fig. 9) as an altered orientation of the near-bottom cur-

rents and more persistent current direction in the intermediate layer in summer 2011, which is similar to the persistency of currents in the deep, near-bottom layer during the other measurements in stratified conditions (summer and autumn 2010). However, further studies are needed to see if different current spectra for the 2011 measurements are a sign of regular geographical feature as the measurements were conducted at the rim area 17 km north of the site of the other summer measurements.

The estimated kinetic energy spectra of currents for winter 2013/2014 and both summer measurements revealed significant peaks with the period close to the 2nd seiche mode. This peak could also be related to the diurnal tide period (O_1 25.8 h), as mentioned by Lillover (2011 and 2012). We assume that strong oscillations close to this local energy maximum period could be a combination of these two energy sources. However, the role of tidal forcing in vertical mixing is considered to be low in the Baltic Sea in comparison with the water bodies under tidal influence (Reissmann *et al.* 2009, Valle-Levinson *et al.* 2014). Similarly to the smaller lakes (Lorke *et al.* 2002) and fjords (Arneborg and Liljebladh 2001) with low tidal forcing, seiches, and inertial oscillations have a relatively higher contribution in vertical mixing in the Baltic Sea. It is shown (e.g., Lappe and Umlauf 2016) that the near-inertial waves together with topographic waves are the dominant motions that trigger vertical mixing in the bottom boundary layer in the central Baltic Sea. The contribution of such mixing at the sloping bottoms is suggested to be the main contributor to Baltic deep water mixing (Holtermann *et al.* 2012).

Theoretical studies on the influence of vertical mixing due to current oscillations and its lateral variability (e.g., due to topography) on the transverse structure of residual circulation have mostly considered tidal current oscillations as the energy source (Burchard *et al.* 2011, Winant *et al.* 2014). The comparison of vertical stability and current shear (Fig. 8) indicates that even though the estimated amplitudes of current oscillations at different prevailed frequency bands are relatively low (order of 5 cm s^{-1}), the mixing events might frequently occur. Furthermore, as identified by Lips *et al.* (2017), the average

current speed was clearly higher in the coastal area than in the deepest part of the gulf when the barotropic flow structure was established in winter 2013/2014. Thus, the lateral gradient in mixing effects, which in turn influences the residual flow structure, could exist in the Gulf of Finland. However, further studies are needed to quantify the mixing effects and their impact on the circulation scheme in the gulf.

We showed that the characteristics of kinetic energy spectra are linked to the density structure of the water column. For BSD frequency band, the measurement ADCP2 is a good example of the link between the density field (Fig. 8 ADCP2) and kinetic energy spectrum (Fig. 10 ADCP2 left column). Therefore, the changes in thermohaline structure at different time-scales (decadal, seasonal, and synoptic) should also appear in kinetic energy spectra in different water layers. For instance, one could expect that the vertical distribution of current spectra in the Gulf of Finland before the Major Baltic Inflow in 1993 (Matthäus and Lass 1995) were similar to the two-layer structure due to much weaker stratification through the halocline (Liblik and Lips 2011). It also means that if we observe warmer but stormy winters (as in winter 2014/2015; see Uotila *et al.* 2015) in future, the one-layer flow system realizes more often in the gulf.

Concluding remarks

The analyzed current measurements revealed the occurrence of barotropic and layered flow structures in the Gulf of Finland. The layered flow structure emerged as both the local shear maxima in certain layers and the differences in the kinetic energy spectra of currents between the vertical layers. We confirmed that the location of shear maxima of current velocity is strongly linked to the pycnoclines, including the vertical salinity gradient appearing in the upper 10–20 m layer under certain flow structure in the absence of the seasonal thermocline in winter. The main energy source of the motions in the gulf is wind. The energy maxima of current oscillations occurred at a broad semi-diurnal frequency band, broad diurnal frequency band, and low-frequency seiches band, as it has also been found earlier

in the Gulf of Finland. The frequency composition differed between the seasons mainly due to the vertical stratification, as well as between the layers during a selected period. The kinetic energy spectra of currents in the periods of strong wind forcing and weak stratification were dominated by current oscillations throughout the water column coinciding with different modes of seiches. During the periods of the two- or three-layer residual flow also inertial oscillations and probably tides remarkably contributed to the kinetic energy of current oscillations. We demonstrated that in summer, the inertial oscillations were dominating in the upper layer from the surface to either the thermocline or the halocline. Seiches had higher energy from the surface to 60 m depth in summer 2010, while in summer 2011, they had higher energy in the quasi-permanent halocline and below (it must be noted that the measurements were conducted at different locations).

Acknowledgements: The work was supported by institutional research funding (IUT19-6) of the Estonian Ministry of Education and Research. The measurements and analysis were partly funded by the Estonian Ministry of Environment (Nord Stream construction environmental monitoring) and Estonian Science Foundation grants no. 6955, 9023, and 9382. We thank our colleagues and the crew of the research vessel Salme for their help at sea.

References

- Alenius P., Myrberg K. & Nekrasov A. 1998. The physical oceanography of the Gulf of Finland: a review. *Boreal Env. Res.* 3: 97–125.
- Alford M.H., Cronin M.F. & Klymak J.M. 2012. Annual Cycle and Depth Penetration of Wind Generated Near-Inertial Internal Waves at Ocean Station Papa in the Northeast Pacific. *Journal of Oceanography* 42: 889–909.
- Andrejev O., Myrberg K., Alenius P. & Lundberg P.A. 2004. Mean circulation and water exchange in the Gulf of Finland — a study based on three-dimensional modeling. *Boreal Env. Res.* 9: 1–16.
- Arneborg L. & Liljebladh B. 2001. The internal seiches in Gullmar Fjord. Part II: Contribution to Basin Water Mixing. *J. Phys. Oceanogr.* 31: 2567–2574.
- Bennet J.R. 1974. On the dynamics of wind-driven lake currents. *J. Phys. Oceanogr.* 4: 400–414.
- Bergström S. & Carlsson B. 1994. River runoff to the Baltic Sea: 1950–1990. *Ambio* 23: 280–287.
- Book J.W., Perkins H., Signell R.P. & Wimbush M. 2007. *The Adriatic Circulation Experiment winter 2002/2003*

- mooring data report: A case study in ADCP data processing. Rep. NRL/MR/7330-07-8999, U.S. Naval Res. Lab., Stennis Space Center, MS.
- Burchard H., Hetland R.D., Schulz E. & Schuttelaars H.M. 2011. Drivers of residual estuarine circulation in tidally energetic estuaries: straight and irrotational channels with parabolic cross section. *J. Phys. Oceanogr.* 41: 548–570.
- Butterworth S. 1930. On the theory of filter amplifiers. *Experimental Wireless and the Wireless Engineer* 7: 536–541.
- Breaker L.C., Tseng Y.-H. & Wang X. 2010. On the natural oscillations of Monterey Bay: Observations, modeling, and origins. *Progress in Oceanography* 86: 380–395.
- Castillo I.M., Pizarro O., Ramírez N. & Cáceres M. 2017. Seiche excitation in highly stratified fjord of southern Chile: the Reloncaví fjord. *Ocean Sci.* 13: 145–160.
- Elken J., Raudsepp U. & Lips U. 2003. On the estuarine transport reversal in deep layers of the Gulf of Finland. *J. Sea Res.* 49: 267–274.
- Elken J., Nömm M. & Lagema P. 2011. Circulation patterns in the Gulf of Finland derived from the EOF analysis of model results. *Boreal Env. Res.* 16: 84–102.
- Elken J., Raudsepp U., Laanemets J., Passenko J., Maljutenko I., Pärn O. & Keevallik S. 2014. Increased frequency of wintertime stratification collapse events in the Gulf of Finland since the 1990s. *Journal of Marine Systems* 129: 47–55.
- Emery W.J. & Thomson R.E. 2004. *Data analysis methods in physical oceanography*. Elsevier, London, UK.
- Geyer W.R. & MacCready P. 2014. The estuarine circulation. *Annu. Rev. Fluid Mech.* 46: 175–197.
- Holtermann P., Umlauf L., Tanhua T., Schmale O., Rehder G. & Wanek J. 2012. The Baltic Sea tracer release experiment. 1. Mixing rates. *J. Geophys. Res.* 117, C01021, doi:10.1029/2011JC007439.
- Jakobsen F. & Trébuchet C. 2000. Observations of the transport through the belt sea and an investigation of the momentum balance. *Cont. Shelf Res.* 20: 293–311.
- Jönsson B., Döös K., Nycander J. & Lundberg, P. 2008. Standing waves in the Gulf of Finland and their relationship to the basin-wide Baltic seiches. *J. Geophys. Res.* 113, C03004, doi:10.1029/2006JC003862.
- Keevallik S. & Soomere T. 2014. Regime shifts in the surface-level average air flow over the Gulf of Finland during 1981–2010. *Proceedings of the Estonian Academy of Sciences* 63: 428–437.
- Kundu P.K. 1976. Ekman veering observed near the ocean bottom. *J. Phys. Oceanogr.* 6: 238–242.
- Lappe C. & Umlauf L. 2016. Efficient boundary mixing due to near-inertial waves in a nontidal basin: observations from the Baltic Sea. *J. Geophys. Res. Oceans* 121: 8287–8304.
- Lass H.-U., Prandke H. & Liljebladh B. 2003. Dissipation in the Baltic Proper during winter stratification. *J. Geophys. Res.* 108(C6), 3187, doi:10.1029/2002JC001401.
- Launiainen J. & Saarinen J. 1984. Marine wind characteristics in the northern Baltic Sea. *Finnish Mar. Res.* 250: 52–86.
- Liblik T. & Lips U. 2011. Characteristics and variability of the vertical thermohaline structure in the Gulf of Finland in summer. *Boreal Env. Res.* 16 (suppl. A): 73–83.
- Liblik T. & Lips U. 2012. Variability of synoptic-scale quasi-stationary thermohaline stratification patterns in the Gulf of Finland in summer 2009. *Ocean Science* 8: 603–614.
- Liblik T., Laanemets J., Raudsepp U., Elken J. & Suhhova I. 2013. Estuarine circulation reversals and related rapid changes in winter near-bottom oxygen conditions in the Gulf of Finland, Baltic Sea. *Ocean Science* 9: 917–930.
- Liblik T. & Lips U. 2017. Variability of pycnoclines in a three-layer, large estuary: the Gulf of Finland. *Boreal Env. Res.* 22: 27–47.
- Lilover M.-J., Lips U., Laanearu J. & Liljebladh B. 1998. Flow regime in the Irbe Strait. *Aquat. Sci.* 60: 253–265.
- Lilover M.-J., Pavelson J., Kõuts T. 2011. Wind forced currents over the shallow Naissaar bank in the Gulf of Finland. *Boreal Env. Res.* 16: 164–174.
- Lilover M.-J. 2012. Tidal currents as estimated from ADCP measurements in “practically non-tidal” Baltic Sea. In: *Baltic International Symposium (BALTIC)*, IEEE/OES, Klaipeda, Lithuania, pp. 1–4.
- Lilover M.-J., Elken J., Suhhova I. & Liblik T. 2017. Observed flow variability along the thalweg, and on the coastal slopes of the Gulf of Finland, Baltic Sea. *Estuarine Coastal and Shelf Science*. 195: 23–33.
- Lips U., Laanemets J., Lips I., Liblik T., Suhhova I. & Suursaar Ü. 2017. Wind-driven residual circulation and related oxygen and nutrient dynamics in the Gulf of Finland (Baltic Sea) in winter. *Estuarine Coastal and Shelf Science* 195: 4–15.
- Lorke A., Umlauf L., Jonas T. & Wüest A. 2002. Dynamics of turbulence in low-speed oscillating bottom-boundary layers of stratified basins. *Environmental Fluid Mechanics* 2: 291–313.
- Maas L.R.M. & van Haren J.J.M. 1987. Observations on the vertical structure of tidal and inertial currents in the central North Sea. *J. Mar. Res.* 45: 293–318.
- Matthäus W. & Lass H.-U. 1995. The recent salt inflow into the Baltic Sea. *J. Phys. Oceanogr.* 25: 280–286.
- Palmén E. 1930. Untersuchungen über die Strömungen in den Finland umgebenden Meeren. *Soc. Sci. Fenn. Comm. Phys.-Math.* 5: 1–94.
- Rabinovich A. 2009. Seiches and Harbor Oscillations. In: Kim Y. (ed.), *Handbook of Coastal and Engineering*, World Scientific Publishing Co., California State University, Los Angeles, CA, pp. 193–236.
- Rasmus K., Kiirikki M. & Lindfors A. 2015. Long-term field measurements of turbidity and current speed in the Gulf of Finland leading to an estimate of natural resuspension of bottom sediment. *Boreal Env. Res.* 20: 735–747.
- Reissmann J., Burchard H., Feistel R., Hagen E., Lass H.-U., Mohrholz V., Nausch G., Umlauf L. & Wiczorek G. 2009. Vertical mixing in the Baltic Sea and consequences for eutrophication: A review. *Progr. Oceanogr.* 82: 47–80.
- Sanay R. & Valle-Levinson A. 2005. Wind-induced circulation in semienclosed homogeneous, rotating basins. *J. Phys. Oceanogr.* 35: 2520–2531.
- Shearman R.K. 2005. Observations of near-inertial current variability on the New England shelf. *J. Geophys. Res.*

- 110, C2, C02012, doi:10.1029/2004JC002341.
- Simpson J.H., Lucas N.S., Powel B. & Maberly S.C. 2014. Dissipation and mixing during the onset of stratification in a temperate lake, Windermere. *Limnol. Oceanogr.* 60: 29–41.
- Suhhova I., Pavelson J. & Lagema P. 2015. Variability of currents over the southern slope of the Gulf of Finland. *Oceanologia*. 57: 132–143.
- Uotila P., Vihma T. & Haapala J. 2015. Atmospheric and oceanic conditions and the extremely low Bothnian Bay sea ice extent in 2014/2015. *Geophys. Res. Lett.* 42: 7740–7749.
- Valle-Levinson A., Cacares M.A. & Pizarro O. 2014. Variations of tidally driven three-layer residual circulation in fjords. *Ocean Dyn.* 64: 459–469.
- Winant C., Valle-Levinson A., Ponte A., Winant C., Gutierrez-de-Velasco G. & Winters G. 2014. Observations on the lateral structure of wind-driven flows in a stratified, semiarid bay of the Gulf of California. *Estuaries and Coasts*. 37: 1319–1328.
- Wübbler C. & Krauss W. 1979. The two-dimensional seiches of the Baltic Sea. *Oceanol. Acta* 2: 435–446.

Paper II

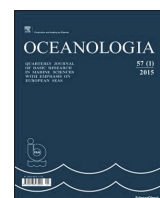
Suuhova, I., Pavelson, J. and Lagemaa, P. 2015. Variability of currents over the southern slope of the Gulf of Finland. *Oceanologia*, 57, 132–143.



Available online at www.sciencedirect.com

ScienceDirect

journal homepage: www.elsevier.com/locate/oceano



ORIGINAL RESEARCH ARTICLE

Variability of currents over the southern slope of the Gulf of Finland[☆]

Irina Suhhova^{*}, Juss Pavelson, Priidik Lagemaa

Marine Systems Institute at Tallinn University of Technology, Tallinn, Estonia

Received 27 November 2014; accepted 19 January 2015

Available online 29 January 2015

KEYWORDS

Slope current;
Stratification;
Up-/downwelling;
The Gulf of Finland

Summary In our intraseasonal variability studies of currents in the coastal sea of the Gulf of Finland northeast of Pakri Peninsula, we compared the observation data from a bottom-mounted ADCP (March–June of 2009, 50 m depth) with the simulation data from High Resolution Operational Model of the Baltic (HIROMB). The structure of the current pattern appeared strongly dependent on the stratification conditions. The flow was quasi-barotropic during the periods of weak inverse thermal stratification at the end of winter season and at transition from the inverse thermal stratification to summer type stratification when the sea was thermally unstratified, but mostly two-layered (baroclinic) when the summer type thermal stratification had developed. The alternation of strong westward (eastward) currents (up to 30 cm s^{-1}) in the upper layer is explained in terms of coastal upwelling (downwelling) due to favourable background winds. The measured and the modelled upper layers along isobath currents showed a noticeable correlation with the correlation coefficient of 0.52 and 0.82 during the periods of winter type and summer type stratifications, respectively, and the absence of a significant correlation during the transition period. The eastward (upwind) current episodes with speeds reaching 18 cm s^{-1} below the seasonal thermocline are likely to reflect the specific circulation response in the elongated basin caused by the easterly wind. The long-term mean (over 3.5 months) current vector (-2.0 cm s^{-1} , -2.9 cm s^{-1}) was westward in the upper sea and eastward, nearly along isobaths (1.1 cm s^{-1} , -0.3 cm s^{-1}) in the deeper layers.

© 2015 Institute of Oceanology of the Polish Academy of Sciences. Production and hosting by Elsevier Sp. z o.o. All rights reserved.

[☆] This study was supported by the Estonian Science Foundation Grant 9381 and institutional research funding IUT19-6 of the Estonian Ministry of Education and Research.

^{*} Corresponding author at: Marine Systems Institute at Tallinn University of Technology, Akadeemia tee 15A, 12618 Tallinn, Estonia.

Tel.: +372 6204309.

E-mail address: irina.suhhova@msi.ttu.ee (I. Suhhova).

Peer review under the responsibility of Institute of Oceanology of the Polish Academy of Sciences.



Production and hosting by Elsevier

1. Introduction

Currents along the continental slope of oceans have been widely studied. Basically, the topographic steering mechanism favours the location of strong flow along the slope, while their maintenance, character, and cross-shelf distribution depend on different forcing factors. Freshwater runoff, along-shore pressure gradient and steady along-shelf wind stress are known as main agents to support coastal currents (e.g., Huthnance, 1995). Similarly, slope currents have been frequently examined in smaller water bodies like the Adriatic Sea (Cushman-Roisin et al., 2001) and the Great Lakes (Rao and Schwab, 2007). At the same time, observational evidence of the current structure along the slopes of the Gulf of Finland, known as the second largest sub-basin of the Baltic Sea, is scarce. Therefore, the objective of the present study is to diminish this gap by using current measurements of a few months' duration at a single site on the southern slope of the western Gulf of Finland.

The Gulf of Finland (Fig. 1a), a relatively shallow and elongated estuarine-like basin, lies in the northeastern part of the tideless Baltic Sea. The gulf is about 400 km long, its width varies between 48 km and 135 km and its total volume is $\sim 1100 \text{ km}^3$. The along-axis depth of the gulf decreases almost monotonically from 80 to 110 m at its entrance to 20–30 m in the eastern part. The coastline and bottom topography as a whole are complex; in the western gulf, a gentle slope on the northern coast and rather steep slope on the southern coast separate the shallow coastal sea from the deep gulf. The long-term mean circulation in the Gulf of

Finland is weak and cyclonic, as evidenced by observations (Alenius et al., 1998; Soomere et al., 2008) as well as by the simulations of numerical models (Andrejev et al., 2004; Elken et al., 2011). Such a mean flow scheme is to a large extent caused by the freshwater discharge of the large Neva River (annual runoff $\sim 110 \text{ km}^3$) in the eastern end of the gulf. As a consequence, the buoyancy-driven Finnish Coastal Current quasi-permanently carries the fresher water westward (Stipa, 2004). In the Estonian coastal sea, an eastward flow of the northern Baltic Proper saltier water is commonly expected. In addition, in the upper layer, pronounced gyre-like currents related to different sub-basins of the gulf are found (Elken et al., 2011; Lagema, 2012). At shorter time-scales, the current system is often more complicated and evidently depends on wind variations. The wind field over the Baltic Sea is influenced by the mostly eastward moving atmospheric cyclones. In the northern Baltic Proper and the western Gulf of Finland, the S-W and to a lesser extent the E winds dominate (Soomere and Keevalik, 2003), which are favourable for forcing coastal up- and downwelling. These wind-forced events are usually accompanied by the strong coastal jet-like currents (Laanemets et al., 2005; Suursaar and Aps, 2007; Zhurbas et al., 2008).

The thermal stratification in the upper gulf has a highly seasonal character (Alenius et al., 1998). By the end of winter season, the water body is characterised by relatively weak inverse thermal stratification with a temperature increase from about 0°C by the sea surface to about 4°C in the depth. The solar heating and wind mixing form a sharp seasonal thermocline/pycnocline starting from May, and in summer it is centred at the depth of 10–15 m (Liblik and Lips, 2011). The haline stratification has weaker seasonality, but changes largely along the gulf because of the Neva River runoff. In the western gulf, as the continuation of the Baltic Proper, a permanent halocline with the salinity difference of 2–3 psu is located at the depth of about 60–70 m. Also, short-term weakening of haline stratification is possible due to the reverse of ordinary estuarine circulation in stronger SW wind conditions (Elken et al., 2003).

In this study, we examine the structure and intraseasonal variability of current over the slope at the north-west coast of Estonia. The questions to be answered are:

- To which extent do the mesoscale (local) coastal processes, e.g., the upwelling/downwelling, modulate the flow?
- To which extent can the locally-observed flow variability be simulated by high-resolution numerical models?
- Is the flow mainly eastward, as expected from the estuarine type general circulation scheme of the Gulf of Finland?

The current velocity measurement period (March–June) is long enough to track the different mesoscale processes (time scale about a week) and its timing enables different stratification conditions. We focus on the forcing factors (wind, sea level) responsible for the nature and variation of the currents. The observational data are combined with hourly forecasts from the operational Baltic Sea circulation model HIROMB-SMHI to include additional parameters (stratification, sea level gradients) and to get some insight to a wider area. The paper is organised as follows. Section 2 presents

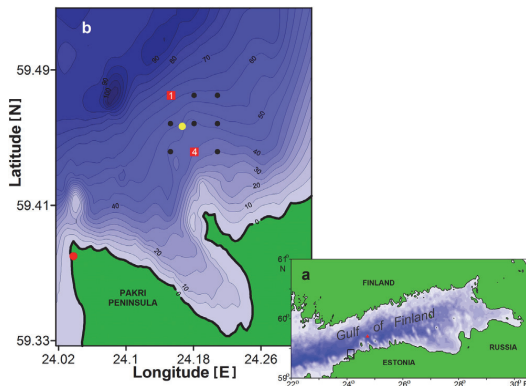


Figure 1 (a) Map of the Gulf of Finland. The study area is indicated by a rectangle and the Tallinnmadal Lighthouse weather station by a red triangle. (b) Bathymetric map of the study area. The location of the bottom-mounted ADCP is shown by a yellow dot and the Pakri weather station by a red dot. Black dots and red squares with labels mark the grid points of the HIROMB model from which data were used. Data from grid point 3 were used for comparison with the ADCP data. Across-isobaths sea level gradients were calculated using data from grid points 1 and 4. Such choice of grid points gives nearly the same rotation of axes (27°) as for the current velocity (30°). (For interpretation of the references to colour in this figure legend, the reader is referred to the web version of this article.)

the observational data used and a brief model description. Section 3 analyses an overall variability of currents with emphasis on the flow regime during up- and downwelling events and compares the data with the model. Section 4 discusses the main findings and presents the conclusions.

2. Data and model

2.1. The ADCP data

Current velocity measurements were carried out at the southern coast of the Gulf of Finland, northeast of the Pakri Peninsula (59°27.4'N, 24°10.0'E) from 13 March to 30 June 2009 (Fig. 1b). In this region of the gulf, the bottom slope is nearly uniform and follows well the coastline. The observation site (50 m depth) is located about 6 km from the coast, i.e., practically in the central part of the slope. The deeper isobaths (>50 m) in the surrounding area are oriented in the direction of approximately 60° from the north, while the shallower ones follow more the complex coastline.

We used a 307.2 kHz broadband ADCP (Workhorse Sentinel, RD Instruments) deployed onto the bottom with a trawl-resistant platform Barnacle 60P. The instrument measured current velocity profiles over 2-m depth bins with the sampling interval of 10 min (average of 50 pings). The two first subsurface bins were truncated from the dataset as contaminated by the surface side lobe effect (~3 m). The quality of the data at each level was then checked using the procedure developed by Book et al. (2007), which is based on certain criteria for the internal quality parameters of the ADCP (error velocity, percentage good, signal correlation). Relying on this analysis, the data from the third upper bin were found partly corrupted (more likely due to sea level variations) and were therefore removed. Thus, the current velocities were available from the depth range between the bins centred at the depths of 6.6 and 44.6 m. The data from the ADCP's pressure sensor were used to estimate the sea level changes. For the assessment of near-bottom water masses, the data from the instrument's temperature sensor (0.6 m above the bottom) were used.

2.2. Wind and sea level data

The wind data were available from the Pakri weather station (59°23.4'N, 24°02.4'E; at 33 m height) and the Tallinnamadal Lighthouse (59°42.7'N, 24°43.9'E; at 31 m height). The former is located at the tip of the Pakri Peninsula, approximately 10 km SW of the ADCP site. The Tallinnamadal Lighthouse is located farther (42 km NE), but represents the open sea wind. Comparison of hourly wind vector series from both stations revealed a good correlation (magnitude of the complex correlation coefficient $R = 0.87$) with a negligible average phase ($\phi \approx 4^\circ$) and lag. This shows that at both stations the wind patterns were quite similar, as might be expected considering the scale of atmospheric cyclones of a few hundred kilometres. However, the mean wind speed at Tallinnamadal was 2.6 m s^{-1} higher than at Pakri, which is likely to reflect the difference between the strength of winds measured above the open sea and mainland. Similar results were obtained by the thorough analysis of sea-measured and land-measured winds with respect to the HIRLAM (High

Resolution Limited Area Model) wind in the same region of the gulf (Keevallik and Soomere, 2010; Keevallik et al., 2010). It was shown that the measured wind speed at Pakri was significantly lower than the speed from the model forecast, while the speeds from the measurements and the forecast at Tallinnamadal were approximately the same. Considering the above arguments, wind data from Tallinnamadal (5 min sampling interval) were used in the present analysis. As the wind was measured at a height of 31 m, its speed was then converted to the speed at the standard 10 m height level for the calculation of wind stress. For that purpose, the logarithmic wind speed profile was applied (Thuillier and Lappe, 1964).

Observational sea level data (1-h interval) from Pakri gauge were involved to verify the ADCP's pressure record in use as a 'sea level' at the measurement site. The contribution from the atmospheric pressure in the ADCP's hourly pressure time-series was removed using the calculated inverse barometric correction. The corrected ADCP pressure data appeared in high correlation with the Pakri sea level data (correlation coefficient $r = 0.97$) collected 10 km apart.

Current, wind, and ADCP's sea level time-series were filtered with a 1-h moving average filter and decimated to obtain hourly values for some descriptive and analysis purposes. For the low-frequency analysis, all series were filtered with a 36-h cutoff Butterworth (1930) filter. Such low-pass filter window was chosen to remove the inertial currents (period 13.9 h), seiche-driven currents with possible periods in the Gulf of Finland up to 31 h (Lilover et al., 2011), as well as other high frequency flow components. An inevitable negative effect of such filtering of the currents and winds is that it will remove some impact of storm and wind forcing from the analysis (e.g., the ocean response to the quickly moving eastward atmospheric cyclones will be more affected than the response to the more sedentary atmospheric anticyclones). Current and wind velocity vectors were rotated counterclockwise by 30° for along- and across-isobath components.

2.3. The model

A state-of-the-art circulation model HIROMB (High Resolution Operational Model for the Baltic Sea) (Funkquist, 2001) is in operational use in Estonia and therefore was used to obtain additional/background data for the analysis of the observed currents. The model with a horizontal grid step of one nautical mile (1.852 km) is run at the Swedish Meteorological and Hydrological Institute (SMHI) and forced by the atmospheric model HIRLAM (SMHI), with a grid step of 22 km. In vertical, the model has a grid step of 4 m between the surface and 12 m, 6 m between 12 m and 30 m, 10 m between 30 m and 60 m and 15 m between 60 m and 90 m. In spite of poor vertical resolution, this model has proved to have a good prediction capability of the sea level (Gästgifvars et al., 2008) and has enabled quite reasonable forecasts of flow in different parts of the Gulf of Finland (Lagemaa et al., 2010). The model includes wind drag coefficient that depends on atmospheric stability (Elken et al., 2011) and the replacement of the Successive Corrections data assimilation scheme by the Optimal Interpolation method (Lagemaa et al., 2010). The HIROMB model used in this study includes assimilation of OSI-SAF SST, Ice, MARNET buoys, in situ measurements from ships and FerryBox for salinity and temperature.

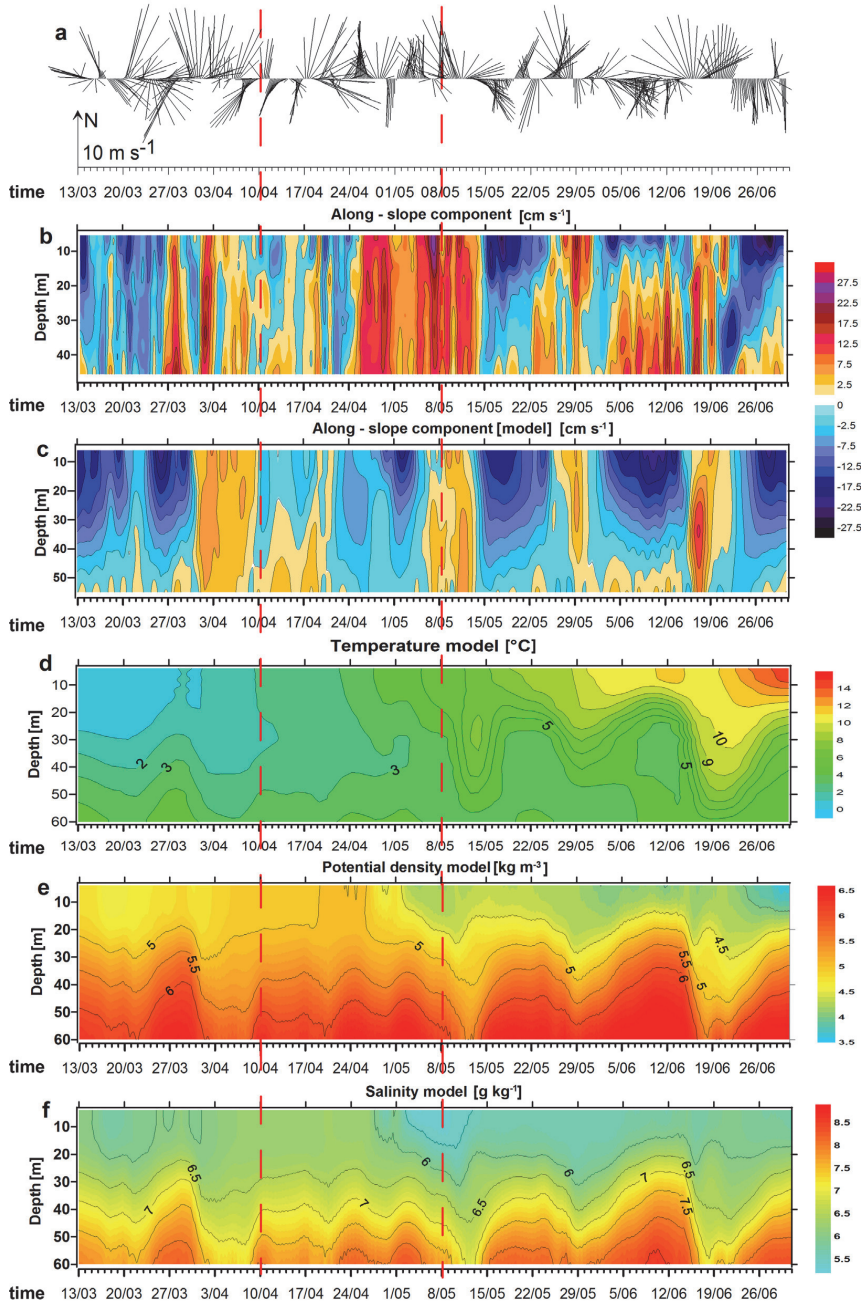


Figure 2 (a) Time series of low-pass filtered wind vectors subsampled every 5 h for visual clarity. An arrow on the time axis shows the scaling of wind vectors. The direction of the arrow approximates the along-coast eastward direction (60° from N). Time series of the low-pass filtered along-isobaths current velocity component in cm s⁻¹ from observations (b) and model (c). Positive velocities (red) display the inflow into the gulf (along-isobaths component) or offshore flow (across-isobaths component), and negative velocities (blue) display the opposite flow respectively ((d) and (e)). Time series of the modelled temperature and the potential density respectively. The vertical dashed lines drawn throughout the panels divide the whole period for three sub-periods. (For interpretation of the references to colour in this figure legend, the reader is referred to the web version of this article.)

In the present study, we used the HIROMB current velocity, sea level, sea level gradients and temperature data (1-h time-series) to compare the measurements and to enhance comprehension of the physical processes involved.

3. Results

3.1. Atmospheric forcing

Wind over the area was promoted by the mainly eastward moving atmospheric cyclones of a few days' duration and by the prolonged sedentary anticyclones. Accordingly, the range of hourly wind speeds was wide, covering light to moderate (68% of the whole period), fresh (23%) and strong (9%) wind speeds. Relatively high percentage of fresh and strong winds ($>8 \text{ m s}^{-1}$) assumes the inducing of the moderate wind-driven current in the upper layer as well as generation of the coastal up- and downwelling events. Altogether six mainly WSW stronger ($>13 \text{ m s}^{-1}$) wind events with the duration of about a day occurred. For example, during the strongest event on 19 April, the WSW wind speeds reached 17 m s^{-1} . The time scale of wind variation was considerably shorter during the first half of observations than within the latter period (see Fig. 2a). The latter was characterised by almost steady wind periods with the duration of 2–7 days.

Unfortunately, our current measurements were not accompanied by the mapping of temperature and salinity. Therefore, to estimate the development of the seasonal vertical stratification, which is an important background condition in the formation of flow structure, we used the courses of air temperature at Pakri and the vertical sea temperature distribution obtained from the model. The winter of 2008/2009 was relatively mild in the Baltic region, which resulted in the practically ice-free western Gulf of Finland. The mean air temperature (January–March) was 1.4°C and slightly higher in the following three weeks in April (3.2°C). After that, the first springtime heat wave with the duration of five days and with maximum temperatures up

to $\sim 20^\circ\text{C}$ hit the region. From the beginning of May, the air temperature gradually rose within the limits of interannual variability. The modelled temporal vertical distribution of sea temperature at the measurement site (Fig. 2d) was in accordance with main tendencies in the course of air temperature. The seasonal stratification started to develop at the end of April and by about mid-May, a moderate thermocline was already present. Thus, in accordance with the modelled sea temperature distribution, the whole observation period was divided into three sub-periods – the weak inverse thermal stratification typical of the end of winter season until 10 April, the summer type stratification from 8 May onwards, and the 'transition' period with negligible thermal stratification between them. The transition period was formally defined as the period when the temperature difference between the surface and the bottom layers, either positive or negative, was less than 2°C in absolute value. Note that the modelled density stratification (Fig. 2c) was weakened but hydrostatically stable even during the transition period, obviously due to the increase of salinity with depth (Fig. 2f).

3.2. Variability of low-frequency current

In general, the low-frequency flow along the isobaths was much stronger than the across-isobaths flow during almost the whole observation period (Figs. 2b and 3a). The alternation of shorter or longer periods of eastward or westward (hereinafter in the frame of rotated coordinates) currents indicating inflow into or outflow from the gulf, respectively, was the most common feature of the temporal flow pattern. However, the structure of the low-frequency current was quite different depending on the strength of density stratification.

During the periods of weak density stratification (i.e., until the summer type stratification is established), the current had quasi-barotropic character with some intensification in the upper about 15-m layer (Fig. 2b). As soon as the summer

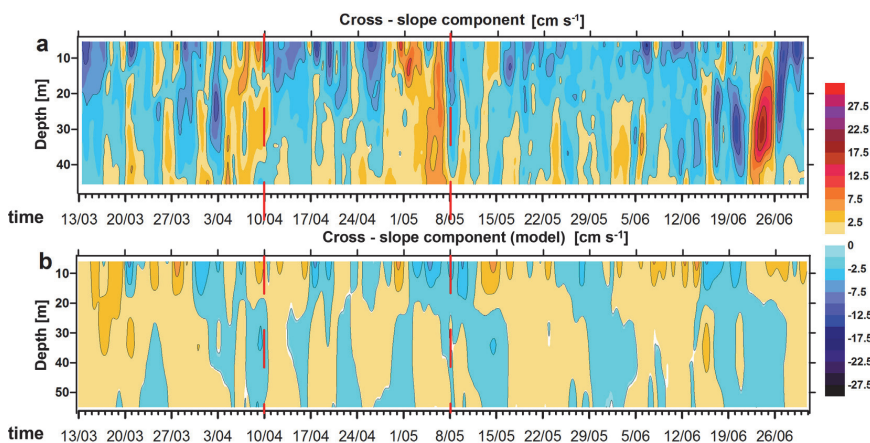


Figure 3 Time series low-pass filtered cross-isobaths current velocity components: (a) observations and (b) model. The vertical dashed lines drawn throughout the panels divide the whole period into three sub-periods.

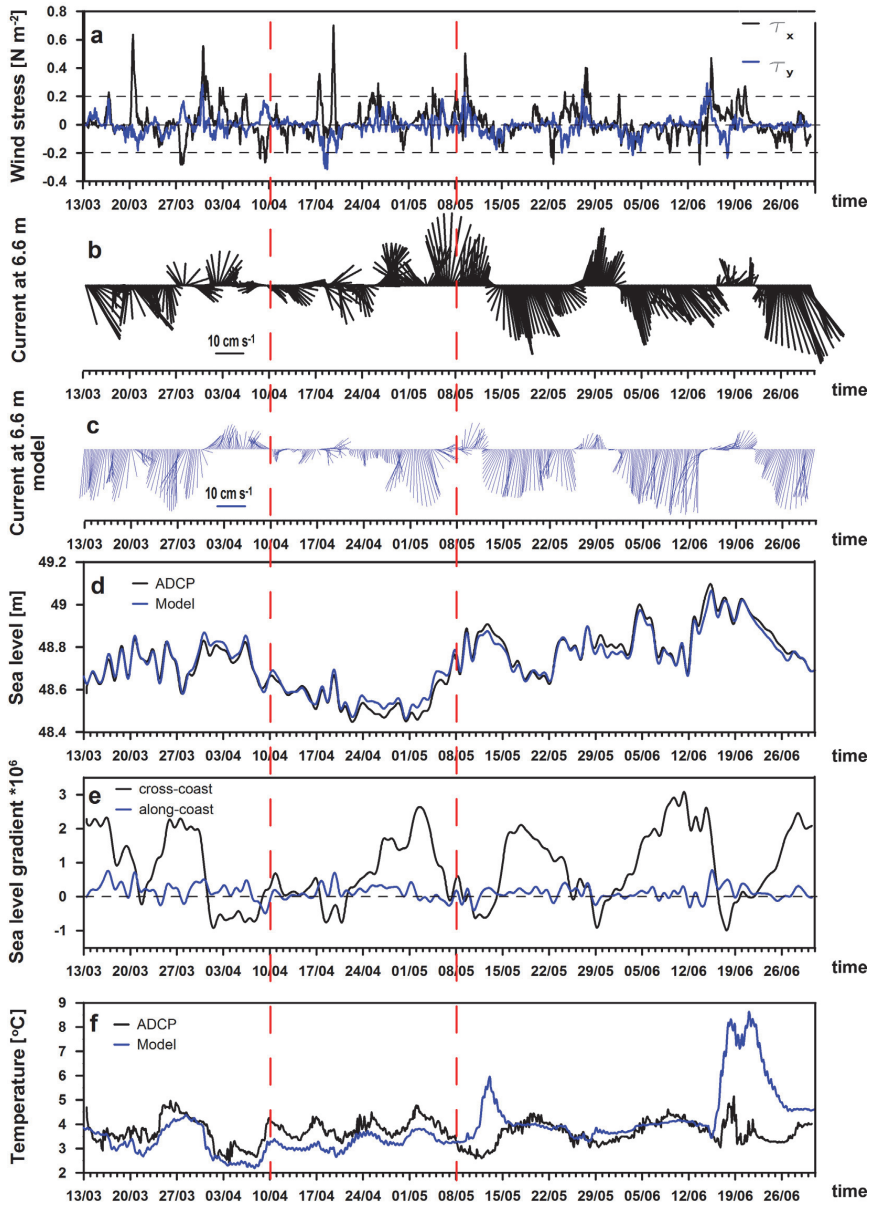


Figure 4 (a) Hourly time series of along-coast (black line) and cross-coast (blue line) wind stress components. ((b) and (c)) Low-pass filtered observed (black line) and modelled (blue line) current vectors at 6.6 m depth (subsamped every 5 h). Straight line on the time axis shows the scaling of current vectors. (d) Low-pass filtered conditional sea level from the ADCP pressure sensor (black line) and from the model (blue line). (e) Low-pass filtered across-isobaths (black line) and along-isobaths (blue line) sea level gradients calculated from the model. (f) Observed (black line) and modelled (blue line) hourly near-bottom temperature. The vertical dashed lines drawn throughout the panels divide the whole period into three sub-periods. (For interpretation of the references to colour in this figure legend, the reader is referred to the web version of this article.)

type stratification is established, the current becomes more baroclinic displaying a two-layer structure for considerable time intervals. Note that the barotropic character was mostly peculiar to the eastward flow when the density stratification weakened due to downwelling. There were periods with minor along-isobaths current component (e.g., 13–15 April), but dominantly the velocities varied around $5\text{--}10\text{ cm s}^{-1}$ in both directions. At times, the stronger current in the upper layer compared to that in the layers below was more likely wind-induced, i.e., it reveals a response to the stronger wind events. This was confirmed by the relatively high correlation between the wind stress and the current vectors ($R = 0.39$, lag 2 h) despite the considerable depth (6.6 m) at which the current was measured. For example, the typical current speeds at 6.6 m depth were $6\text{--}7\text{ cm s}^{-1}$ on 25 March and 12 April. Corresponding excess of the current speed with respect to 20.6 m depth of $\sim 3\text{ cm s}^{-1}$ was in reasonable compliance with that calculated with the classical Ekman model.

The most stable current, barotropic by character, was observed during the period of 25 April–15 May (Fig. 2b). That kind of flow can be explained by relatively stationary W-SW wind (Fig. 2a) and weak density stratification. The resulting inflow (eastward) was evenly distributed over the whole water column, while the typical along-isobaths current velocities were $10\text{--}15\text{ cm s}^{-1}$. Again, similarly to the previous period, the upper 15-m layer was affected by the stronger winds.

The low-frequency flow within the summer type stratification period was mostly two-layered and its along-isobaths component was usually much stronger than during the weakly stratified period (cf. the left- and right-hand sides of Fig. 2b). The flow was most pronounced in the upper 15-m layer, where intense and about 10-days long outflow events with speeds reaching 30 cm s^{-1} alternated with weaker (up to 20 cm s^{-1}) and shorter inflow events. Such high low-frequency current speeds cannot be explained by the wind-driven current and/or barotropic flow due to across-coast sea level gradients alone. Therefore, considering the prevailing along-coast oriented (in both directions) background wind pattern (Figs. 2a and 4a), presumably upwelling and downwelling associated baroclinic currents were involved. We will substantiate that by an analysis in Sections 3.3 and 4.1.

Below the seasonal thermocline (depth $> 15\text{ m}$), the inflow episodes with different extent from the bottom were characteristic of the summer conditions (Fig. 2b). Surprisingly, these eastward flow episodes took place when the wind was explicitly (except on 16–17 June) from eastern directions (Figs. 2a and 4a). The along-isobaths velocities had an evident tendency to increase towards the bottom, and within the most prominent inflow period (3–14 June) they reached up to 18.5 cm s^{-1} . Besides, a clear oscillating character with periods of about 2–3 days during all episodes is rather unconventional for a current in the deeper layers of the gulf. The origin of such upwind current will be discussed in Section 4.2. The strongest westward flow with maximal speeds exceeding 15 cm s^{-1} at about 30 m depth occurred starting from 20 June. This intensification of the along-isobaths current component and the distribution of the enhanced across-isobath component between the depths of 15 and 40 m (19–26 June) with a sign change (Fig. 3a) are more

likely the signatures of an anticyclonic eddy-like structure. The succession of the sign change of both current components reveals that this structure migrated eastward and 'touched' (about a week) our measurement site with its southern periphery. During the rest of the stratified period, the across-isobaths flow component was weak and without firm direction (Fig. 3a).

Finally, permanent, quasi-barotropic undulations of current velocity components with the period of 2–5 days are seen more prominently in the along-isobath component (cf. Figs. 2b and 3a). These undulations are most probably caused by topographic waves (Lilover and Talsepp, 2014).

3.3. Upwelling and downwelling events

Coastal upwelling is usually verified by using the satellite images of the sea surface temperature (SST) or mapping of temperature/salinity fields. In the absence of the latter we explored temporal vertical distribution of the temperature from the model data (Fig. 2d), which revealed qualitatively well the rising (dropping) of thermocline in the study area during easterly (westerly) winds, i.e., supporting occurrence of upwelling (downwelling) events. Because the Gulf of Finland is a narrow basin, an upwelling along one coast is accompanied by a downwelling along the opposite coast. Thus, such a coupled mechanism enables us to conclude the presence of downwelling at the Estonian coast, relying on upwelling signatures at the Finnish coast visible on the satellite SST images. Unfortunately, only a few cloud free SST images covering the periods and the region of our interest were available. These SST images reflected upwelling events on the Estonian coast on 17 May and 29 June and downwelling event on 28 May.

Since upwelling/downwelling events in the southern Gulf of Finland are characterised by a combination of negative/positive along-isobath wind and current pulses and rising/dropping of temperature contours, Figs. 2 and 3 enable clear identification of four upwelling events (23–30 March, 14–24 May, 1–14 June, and 21–30 June), and four downwelling events (31 March–7 April, 8–13 May, 24–30 May, and 15–20 June). Note that the first event of upwelling and downwelling took place during the period of inverse thermal stratification at the end of winter season, while the next three were observed during the period of summer type thermal stratification. Since at the upwelling observed during the period of inverse thermal stratification, the layer of sloping temperature/potential density, 15–45 m, displays a considerable value of the vertical gradient of along-isobath current velocity, we can suggest that the flow, despite a weakened density stratification, is baroclinic. Upwelling/downwelling events during the transition period were not identified because the period under consideration is almost thermally unstratified when the rising/dropping of temperature contours cannot be considered as a signature of upwelling/downwelling processes.

3.4. Comparison with the model

In general, the time series of the observed and modelled vertical distributions of along-isobath current velocity (Fig. 2b and c) display well coordinated intervals of eastward and westward flow in the upper layer. An exception is the

period of 25 April–14 May, which was the longest interval of eastward flow recorded by the ADCP measurements while the model showed the westward transport before 6 May. Unfortunately we could not explain this discrepancy and will leave the issue open. Due to the discrepancy, correlation of the measured and modelled along-isobath current on 6.6 m level (see Fig. 4b and c) was negative for the transition period (-0.39). For the inverse thermal stratification period, the summer-type stratification period, and the whole period of 13 March–30 June, correlation of the measured and modelled along-isobath current on 6.6 m level was positive and relatively high (0.61, 0.52, and 0.82, respectively).

Correlation of the measured and modelled cross-isobath current on 6.6 m level was much lower (0.16 for the whole period). In the deep layers, correlation between the observed and modelled velocities, both along- and cross-isobath, does not exceed 0.2–0.3.

Despite the low correlation of the measured and modelled velocities in the deep layer, a surprisingly high correlation was found between the measured and modelled temperatures in the bottom layer (Fig. 4f): the measured and modelled time series of 44.6 m temperature display almost coherent changes during the whole period of observations except for relatively short intervals of 12–14 May and 17–22 June when the modelled temperature was considerably higher than the measured one. In accordance with Fig. 2b–d, these intervals correspond to well-pronounced downwelling events, when the modelled thermocline deepens to the depth of about 50 m, which results in an excessive increase of the modelled near-bottom temperature. Apart from these intervals, some increase of both the measured and modelled near-bottom temperature is observed during upwelling events, which is explained by the features of typical cross-isobath circulation, when the cross-isobath flow in the near-bottom (near-surface) layer is directed onshore (offshore). With regard to the inverse temperature stratification, the onshore flow in the near-bottom layer results in the increase of the near-bottom temperature. The correlation coefficients between the measured and modelled near-bottom temperature was 0.85, 0.79 and 0.08 for the inverse thermal stratification, transition and summer type stratification periods, respectively. Drastic decrease of correlation in the summer type stratification period is obviously caused by the excessive increase of modelled near-bottom temperature during 12–14 May and 17–22 June downwelling events.

Correlation between the measured and modelled sea level (see Fig. 4d) was extremely high (0.99 for the whole period), which is not surprising – state-of-the-art models are known for excellent prediction of sea level changes. Correlation between the measured (modelled) 6.6 m along-isobath velocity and the modelled cross-isobath sea level gradient (see Fig. 4b, c and e) was -0.45 (-0.86). Note that in the ideal case of a geostrophically-balanced flow, correlation between the along-isobath velocity at the sea surface and the cross-isobath sea level gradient should be -1 .

Finally, we may conclude that the quasi-barotropic oscillations of the velocity current with a 2–5 day period, supposedly caused by topography waves (Lilover and Talsepp, 2014), are less pronounced in the model than in the measurements (cf. Fig. 2b and c, Fig. 3a and b).

4. Discussion and conclusions

The observed low-frequency flow appeared very complex and was strongly dependent on the stratification. Under weak density stratified conditions, the current was almost barotropic whereas at times some intensification occurred in the upper layer due to stronger wind pulses. These results are comparable to observations published by Liblik et al. (2013). The seasonal stratification in combination with wind conditions caused different flow patterns in the upper and deeper layers. In the following, some aspects and nature of the observed currents are discussed.

4.1. Position of upwelling and downwelling related front/current

Taking into account that the eastward flow occupied the whole water column during downwelling events within the summer type stratification period (see Fig. 2b and c), it may be suggested that the ADCP measurements were performed at the onshore periphery of the jet-like current associated with downwelling/upwelling (Zhurbas et al., 2006). Therefore, the displacements of the upwelling and downwelling front from the coast were estimated. A non-linear two-layer model with impulsively exerted wind stress by Csanady (1977) enables us to find the offshore distance (y_0) where the pycnocline surfaces as

$$y_0 = \frac{l}{f\rho_0 h_1} \frac{h_2}{h_1 + h_2} - R, \quad (1)$$

where h_1 and h_2 are the top and bottom layer thicknesses, respectively, l is the cumulative wind stress, $R = f^{-1}[g'h_1h_2/(h_1 + h_2)]^{1/2}$ is the baroclinic radius of deformation, f is the Coriolis parameter, $g' = g(\Delta\rho_1/\rho_0)$ is the reduced gravity, g is the gravitation acceleration (9.8 m s^{-2}), ρ_0 is the reference density (1000 kg m^{-3}), and $\Delta\rho_1$ is the density difference between the two layers. Taking $h_1 = 12 \text{ m}$ and $h_2 = 48 \text{ m}$ (means average cross-gulf depth of 60 m), and assuming $\Delta\rho_1 \approx \Delta\rho$ ($=0.6 \text{ kg m}^{-3}$), formula (1) gives the outcrop of pycnocline 10.4 km from the coast for the upwelling event of 21–30 June ($l = 0.27 \text{ N m}^{-2} \text{ d}$). Note that for the event of 14–24 May ($l = 0.15 \text{ N m}^{-2} \text{ d}$, $\Delta\rho_1 = 0.25 \text{ kg m}^{-3}$), $y_0 = 5.6 \text{ km}$, i.e., practically the distance of the observation site. The offshore displacement of the downwelling front (y_1) according to Austin and Lentz (2002) is scaled as

$$y_1 = \sqrt{\frac{2l}{f\rho_0\beta}}, \quad (2)$$

where β is the bottom slope. Taking $\beta = 0.007$ as characteristic of our study area and $l = 0.60 \text{ N m}^{-2} \text{ d}$ for the downwelling event of 15–20 June, formula (2) gives $y_1 = 10.9 \text{ km}$.

Thus, the estimates of the displacement of the front (centre) from the coast for events of 15–20 June and 21–30 June are both about 10 km. The width of the upwelling/downwelling jet is expected to be a few baroclinic Rossby deformation radii. In the Gulf of Finland the deformation radius is 2–4 km (Alenius et al., 2003) and correspondingly the width of the jet is around 10 km. However, the widths obtained from the model data on the north-south oriented leg (see Fig. 1b) are 15–17 km, thus too large obviously

because of a 'smoothing' effect of the model. On the other hand, the only available (to our knowledge) observational estimate of the width, 8–12 km, for the downwelling jet at the entrance area to the gulf (Laanemets et al., 2005) coincides well with the scaled estimate. Therefore, considering the scaled width of the jet and estimated jet's displacement from the coast, it is highly plausible that our data (about 6 km from the coast) originate from the southern periphery of the jet.

4.2. Upwind current below the thermocline

Next, we examine the eastward current episodes below the seasonal thermocline, which were observed during the easterly winds (Fig. 3a and b). Such an upwind flow is a commonly known phenomenon from the studies focused on the elongated basins and estuaries since the 1970s (e.g., Csanady, 1973), and its essence is as follows. The along-axis wind causes a cross-shore Ekman transport in the upper layers and, as a result, the sea level rises on the right-hand coast looking downwind and drops on the left-hand coast. Due to the corresponding barotropic pressure gradient forces, the downwind jet-like current at both coasts is produced. Besides, the Ekman transport generates upwelling and downwelling at the left- and right-hand coasts, respectively. Therefore, in the presence of stratification, the associated baroclinic downwind current component enhances the jets at both coasts. The transport by these strong downwind jets gives rise to the upwind flow in the central area of the basin, which was predicted by numerous analytical as well as numerical models. However, the Coriolis force (important for larger basins) has been included in the analytical models only since the last decade. The solutions of 'pure' barotropic models (e.g., Winant, 2004) as well as of more general models including baroclinic forcing (e.g., Reyes-Hernandez and Valle-Levinson, 2010) reveal well a bottom intensified upwind flow flanked by the surface intensified downwind jets along the coasts and the sensitivity of this flow pattern on the across-estuary depth variations.

According to our study (at the coastal area of the elongated estuary-like gulf), the most pronounced upwind (eastward) current event occurred on 3–14 June (Fig. 2b) and as was shown in the previous section, it even affected the

downwind flow in the upper layer. The specific features of the current within this period are the intensification towards the bottom and relatively close relation with variations of the along-coast component of wind stress (Fig. 5). The current speed gradually increased down to the depth of 42.6 m and most likely decreased underneath ('untouchable' by the ADCP) due to the bottom stress. The along-isobaths current speeds (low-frequency) were relatively high: 10.6 cm s^{-1} as average and 18.5 cm s^{-1} as maximum (both at 42.6 m depth). Such current speeds are comparable with results presented by Liblik and Lips (2012) and other observations in larger estuaries. For example, subtidal upwind mean inflow speeds up to 19 cm s^{-1} at the entrance to Long Island Sound (Whitney and Codiga, 2011) and in the range of 10–20 cm s^{-1} in the southern (deep) entrance area to Chesapeake Bay (Valle-Levinson et al., 2001, their Fig. 10b and d) were reported. Earlier observations of the deep eastward-directed current during seaward wind in the Gulf of Finland were revealed by Lips et al. (2009) and Liblik et al. (2013). Here we mention that the upwind flow predicted by the HIROMB model was underestimated (mean and maximum speeds of 2.3 and 7.5 cm s^{-1} , respectively at 40 m grid horizon) obviously because of too sparse grid resolution below the seasonal thermocline.

The upwind current was observed relatively close to the coast (6 km), nevertheless above the 50-m bottom. Therefore, it is likely that the flow event occupied at least most of the southern portion of the gulf cross-section (below thermocline). This complies with other observations (e.g., Whitney and Codiga, 2011) as well as predictions of models with stratification (e.g., Reyes-Hernandez and Valle-Levinson, 2010). The latter study also exposed a substantial asymmetry of the lateral distribution of upwind flow (result of possible influence of the Earth's rotation), i.e., a core of the flow was shifted towards the right coast (looking downstream) in the presence of weak and moderate winds. Thus, the relatively high current speeds at our site might in some respects prove the predicted asymmetry.

The reason why the upwind flow developed so strong and lasted over a 10-day period lies obviously in the favourable wind conditions. The recurrent westward, along-coast wind stress component pulses with maximum magnitudes of 0.1–0.25 N m^{-2} dominated (Fig. 5), which was sufficient

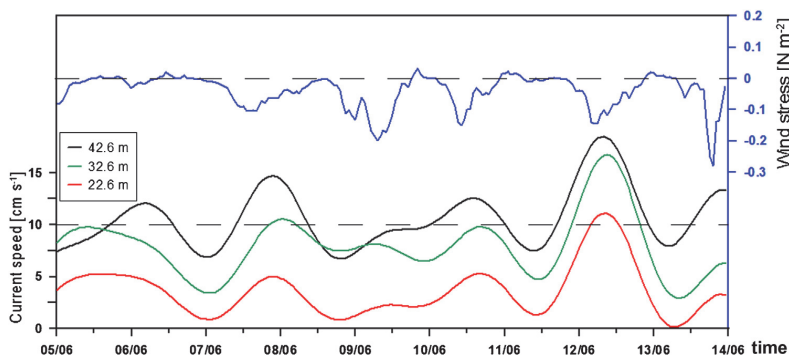


Figure 5 Time series of the low-pass filtered along-isobath current velocity component at 22.6, 32.6, and 42.6 m and the along-isobath wind stress component for the period of 5–14/06.

for the maintenance of the above proposed circulation in the elongated gulf. Moreover, variations of the along-coast wind stress component and correspondingly the changes of the cross-coast sea level gradients ($r = -0.46$, 3 h lag) probably caused the variations in the strength of the eastward current. It is clearly seen that the current strengthened shortly after the wind stress magnitude began to increase and weakened when the wind stress was negligible (Fig. 5). The barotropic response is also confirmed by a significant correlation ($r = -0.28$, 2 h lag) between the components of the cross-coast sea level gradient and the along-isobaths current (at 42.6 m depth). Other eastward, bottom intensified flow events related to periods of 16–25 May and onward from 23 June were considerably weaker and embraced mainly 15–20 m layer above the bottom (Fig. 3b). The upwind current during the period of 16–19 May was very weak, which is likely because of the almost decayed wind (Fig. 4a). However, strong easterly wind pulse on 22 May efficiently enhanced the upwind flow. The full development of the upwind flow event related to period from 23 June onward stayed out of the observation window, but in the initial stage the flow might have been somewhat affected by the eddy-like structure. Thus, at the southern coast of the gulf, the eastward (upwind) flow seems to be a common phenomenon during easterly wind periods, while being very sensitive to the short-term variations of the wind.

4.3. Long-term mean flow

Finally, the mean currents over the whole observation period and those obtained from different multiyear numerical model simulations in the western Gulf of Finland are compared. The five-year forecast by Andrejev et al. (2004) and the three-year forecast (HIROMB model) by Elken et al. (2011) both expose well a cyclonic circulation pattern in the gulf, i.e., a strong westward Finnish Coastal Current and in general eastward flow over almost the whole water column in the southern gulf. Relying on the progressive

vector plots, our data indicate a substantially different current succession in the upper layer (Fig. 6a) and deeper layers (Fig. 6b). In the latter, prevailing along-isobaths inflow occurs during the whole observation period. At the same time, in the upper layer outflow dominates despite stratification conditions, although the flow is considerably inclined toward the coast. Exceptionally, the flow is eastward during the transition period, thus similar to the flow in the deeper layer. In the upper layer, the mean current vector over a 3.5-month period has along- and across-isobaths components of -2.0 and -2.9 cm s^{-1} , respectively. Such mean flows are mostly composed of the westward flow during the inversely thermal stratification period as well as the enhanced westward flow during upwelling events. In the deeper layers the mean current with components of 1.1 and -0.3 cm s^{-1} for along- and across-isobaths directions, respectively, is weaker, and contributed mainly by the stronger barotropic flow within the transition period and the eastward upwind flow events.

Thus, our data reveal the expected mean flow towards the inner gulf only in the deeper layers. For the upper layer the existing models give contrary long-term current directions in the surrounding of the observation site. The mean (1987–1992) flow with speeds ~ 5 cm s^{-1} is eastward (Andrejev et al., 2004, their Fig. 8) and therefore complies with the understanding of the general cyclonic circulation in the gulf. On the other hand, the mean (2006–2008) westward flow of ~ 3 cm s^{-1} as a southern part of relatively large anticyclonic circulation cell (Elken et al., 2011, their Fig. 2) fits well with our estimate. Accordingly, the inflow of open Baltic waters at this longitude takes place over the deepest part of the gulf. A similar result was also obtained using the same model for years 2010–2011 (Lagemaa, 2012, Fig. 7). Our findings contradict the results of earlier coastal numerical circulation, but fit well with recent studies. Therefore, it is highly possible that the processes described in this study will mainly cause the modelled long-term westward flow over the slope. A precondition for such speculation is the timing of our

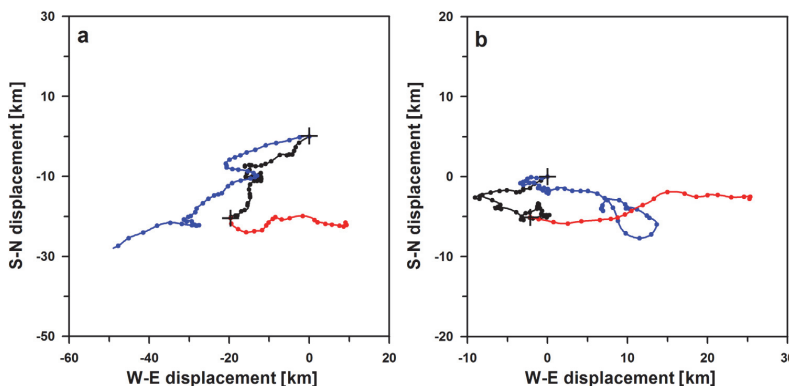


Figure 6 Progressive vector diagrams of low-frequency average current over 6.6–8.6 m layer (a) and 20.6–42.6 m layer (b). Black (red) lines and dots indicate inversely thermal stratification (transition) periods. Blue lines and dots show the summer type stratification period. Dots on the curves are shown after each day. The progressive vector diagram is restarted between the periods; the plus marks the starting point. (For interpretation of the references to colour in this figure legend, the reader is referred to the web version of this article.)

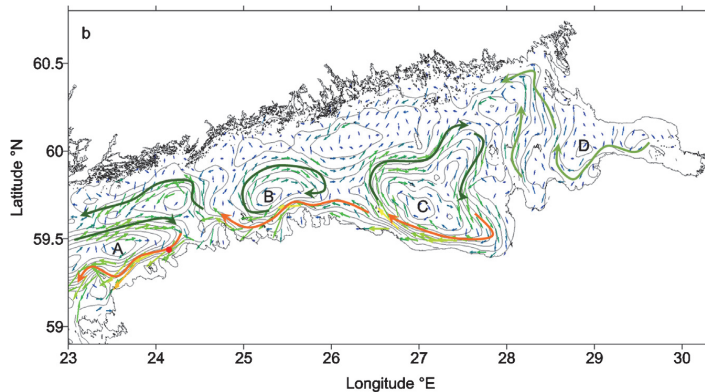


Figure 7 Reprint from [Lagemaa \(2012\)](#) with additional illustrations enhancing the circulation patterns. The location of the bottom-mounted ADCP is shown by a red dot. (For interpretation of the references to colour in this figure legend, the reader is referred to the web version of this article.)

observations, i.e., it partly covers unstratified as well as stratified seasons of the sea. As was shown, the observed westward mean flow results largely from the jet-like currents related to upwelling. However, upwelling at the southern coast of the gulf is not a very common process as follows from the 20-year (1990–2009) statistical analysis of summer satellite SST images, which expose the frequency of occurrence only up to 12% in June ([Lehmann et al., 2012](#)). In spite of rare occurrences of upwelling events in summer, the contribution of related jets (high speeds and duration of about a week) to the long-term mean current may be substantial. The same holds also for the weakly density stratified season when relatively strong westward barotropic currents due to easterly wind impulses may occur. Hence, the mean westward flow in the upper layer (observed and modelled by the HIROMB) at our observation site reflects probably a local coarse-scale feature of the long-term general circulation.

To summarise, our results show that even single point current velocity measurements with a combination of selected data from a relatively coarse numerical circulation model enable acquisition of valuable knowledge about different coastal processes and their contribution to the overall circulation. However, the present understanding of currents over the slopes is still clearly inadequate. Therefore, long-time current measurements together with frequent density mapping covering other seasons and areas of the Gulf of Finland are likely to be in the focus of research in the coming years.

Acknowledgements

We express our gratitude to Viktor Zhurbas for fruitful consultations. We are grateful to Kaimo Vahter for assistance in the deployment of the ADCP and to Rivo Uiboupin for providing satellite SST images. The model data were kindly provided by the Swedish Meteorological Institute under cooperation within BOOS (Baltic Operational Oceanographic System) and HIROMB.

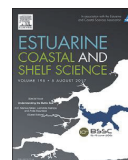
References

- Alenius, P., Myrberg, K., Nekrassov, A., 1998. *Physical oceanography of the Gulf of Finland: a review*. *Boreal Environ. Res.* 3, 97–125.
- Alenius, P., Nekrasov, A., Myrberg, K., 2003. *Variability of the baroclinic Rossby radius in the Gulf of Finland*. *Cont. Shelf Res.* 23, 563–573.
- Andrejev, O., Myrberg, K., Alenius, P., Lundberg, P.A., 2004. *Mean circulation and water exchange in the Gulf of Finland – a study based on three-dimensional modeling*. *Boreal Environ. Res.* 9, 1–16.
- Austin, J.A., Lentz, S.J., 2002. *The inner shelf response to wind-driven upwelling and downwelling*. *J. Phys. Oceanogr.* 32, 2171–2193.
- Book, J.W., Perkins, H., Signell, R.P., Wimbush, M., 2007. *The Adriatic Circulation Experiment winter 2002/2003 mooring data report: A case study in ADCP data processing*. Memo. Rep. NRL/MR/7330-07-8999. U.S. Naval Res. Lab., Stennis Space Center, MS.
- Butterworth, S., 1930. *On the theory of filter amplifiers*. *Exp. Wireless Eng.* 7, 536–541.
- Csanady, G.T., 1973. *Wind-induced barotropic motions in long lakes*. *J. Phys. Oceanogr.* 3, 429–438.
- Csanady, G.T., 1977. *Intermittent “full” upwelling in Lake Ontario*. *J. Geophys. Res.* 82, 397–419.
- Cushman-Roisin, B., Gačić, M., Poulain, P.-M., Artegiani, A. (Eds.), 2001. *Physical Oceanography of the Adriatic Sea: Past, Present, and Future*. Kluwer Academic Publisher, Dordrecht, p. 304.
- Elken, J., Nömm, M., Lagemaa, P., 2011. *Circulation patterns in the Gulf of Finland derived from the EOF analysis of model result*. *Boreal Environ. Res.* 16, 84–102.
- Elken, J., Raudsepp, U., Lips, U., 2003. *On the estuarine transport reversal in deep layers of the Gulf of Finland*. *J. Sea Res.* 49, 267–274.
- Funkquist, L., 2001. *HIROMB, an operational eddy-resolving model for the Baltic Sea*. *Bull. Maritime Inst. Gdansk* 28, 7–16.
- Gästgifvars, M., Müller-Navarra, S., Funkquist, L., Huess, V., 2008. *Performance of operational systems with respect to water level forecasts in the Gulf of Finland*. *Ocean Dyn.* 58, 139–153.
- Huthnance, J.M., 1995. *Circulation, exchange and water masses at the ocean margin: the role of physical processes at the shelf edge*. *Prog. Oceanogr.* 35, 353–431.

- Keevallik, S., Männik, A., Hinnov, J., 2010. Comparison of HIRLAM wind data with measurements at Estonian coastal meteorological stations. *Estonian J. Earth Sci.* 59 (1), 90–99.
- Keevallik, S., Soomere, T., 2010. Towards quantifying variations in wind parameters across the Gulf of Finland. *Estonian J. Earth Sci.* 59, 288–297.
- Laanemets, J., Pavelson, J., Lips, U., Kononen, K., 2005. Downwelling related mesoscale motions at the entrance to the Gulf of Finland: observations and diagnosis. *Oceanol. Hydrobiol. Stud.* 34, 15–36.
- Lagemaa, P., 2012. Operational forecasting in Estonian marine waters. (PhD Thesis). Tallinn Univ. Technol., TUT Press, 45.
- Lagemaa, P., Suhhova, I., Nömm, M., Pavelson, J., Elken, J., 2010. Comparison of current simulations by the state-of-the-art operational models in the Gulf of Finland with ADCP measurements. In: 4th US/EU Baltic Symp., 24–27 August 2010, IEEE Conf. Proc., Riga, <http://dx.doi.org/10.1109/BALTIC.2010.5621656>.
- Lehmann, A., Myrberg, K., Höflisch, K., 2012. A statistical approach to coastal upwelling in the Baltic Sea based on the analysis of satellite data for 1990–2009. *Oceanologia* 54, 369–393.
- Liblik, T., Laanemets, J., Raudsepp, U., Elken, J., Suhhova, I., 2013. Estuarine circulation reversals and related rapid changes in winter near-bottom oxygen conditions in the Gulf of Finland, Baltic Sea. *Ocean Sci.* 10, 727–762.
- Liblik, T., Lips, U., 2011. Characteristics and variability of the vertical thermohaline structure in the Gulf of Finland in summer. *Boreal Environ. Res.* 16A, 73–83.
- Liblik, T., Lips, U., 2012. Variability of synoptic-scale quasi-stationary thermohaline stratification patterns in the Gulf of Finland in summer 2009. *Ocean Sci.* 8, 603–614.
- Lilover, M., Pavelson, J., Köuts, T., 2011. Wind forced currents over the shallow Naissaar Bank in the Gulf of Finland. *Boreal Environ. Res.* 16, 164–174.
- Lilover, M.-J., Talsepp, L., 2014. On the vertical structure of the low-frequency oscillations of currents in the Gulf of Finland. In: *Baltic International Symposium (BALTIC)*, 2014 IEEE/OES. 1–6.
- Lips, I., Lips, U., Liblik, T., 2009. Consequences of coastal upwelling events on physical and chemical patterns in the central Gulf of Finland. *Cont. Shelf Res.* 1836–1847.
- Rao, Y.R., Schwab, D.J., 2007. Transport and mixing between the coastal and offshore waters in the Great Lakes: a review. *J. Great Lakes Res.* 33, 202–218.
- Reyes-Hernandez, C., Valle-Levinson, A., 2010. Wind modifications to density-driven flows in semiencloded rotating basins. *J. Phys. Oceanogr.* 40, 1473–1487.
- Soomere, T., Keevallik, S., 2003. Directional and extreme wind properties in the Gulf of Finland. *Proc. Estonian Acad. Sci. Eng.* 9, 73–90.
- Soomere, T., Myrberg, K., Leppäranta, M., Nekrasov, A., 2008. The progress in knowledge of physical oceanography of the Gulf of Finland: a review for 1997–2007. *Oceanologia* 50, 287–362.
- Stipa, T., 2004. Baroclinic adjustment in the Finnish coastal current. *Tellus* 56A, 79–87.
- Suursaar, Ü., Aps, R., 2007. Spatio-temporal variations in hydro-physical and -chemical parameters during a major upwelling event off the southern coast of the Gulf of Finland in summer 2006. *Oceanologia* 49, 209–228.
- Thuillier, R.H., Lappe, U.O., 1964. Wind and temperature profile characteristics from observations on a 1400 ft tower. *J. Appl. Meteor.* 3, 299–306.
- Valle-Levinson, A., Wong, K.-C., Bosley, K.T., 2001. Observations of the wind-induced exchange at the entrance to Chesapeake Bay. *J. Mar. Res.* 59, 391–416.
- Whitney, M.M., Codiga, D.L., 2011. Response of a large stratified estuary to wind events: observations, simulations, and theory for Long Island Sound. *J. Phys. Oceanogr.* 41, 1308–1327.
- Winant, C.D., 2004. Three-dimensional wind-driven flow in an elongated, rotating basin. *J. Phys. Oceanogr.* 34, 462–476.
- Zhurbas, V., Laanemets, J., Vahtera, E., 2008. Modeling of the mesoscale structure of coupled upwelling/downwelling events and the related input of nutrients to the upper mixed layer in the Gulf of Finland, Baltic Sea. *J. Geophys. Res. Oceans* C113, 1–8.
- Zhurbas, V., Oh, I.S., Park, T., 2006. Formation and decay of a longshore baroclinic jet associated with transient coastal upwelling and downwelling: a numerical study with applications to the Baltic Sea. *J. Geophys. Res. Oceans* 111, C04014, <http://dx.doi.org/10.1029/2005JC003079>.

Paper III

Lilover, M.-J., Elken, J., Suhhova, I., Liblik, T. 2017. Observed flow variability along the thalweg, and on the coastal slopes of the Gulf of Finland, Baltic Sea. *Estuarine Coastal and Shelf Science*, 195, 23–33.



Observed flow variability along the thalweg, and on the coastal slopes of the Gulf of Finland, Baltic Sea



Madis-Jaak Lilover*, Jüri Elken, Irina Suhhova, Taavi Liblik

Marine Systems Institute, Tallinn University of Technology, Tallinn, Estonia

ARTICLE INFO

Article history:

Received 21 March 2016

Received in revised form

24 October 2016

Accepted 3 November 2016

Available online 5 November 2016

Keywords:

Gulf of Finland

ADCP measurements

Flow patterns

Estuarine circulation

ABSTRACT

Bottom-mounted ADCP measurements from 10 installations, collected between 2009 and 2014 and each lasting several months, are analysed in order to distinguish between different flow regimes, and to detect variability (a) along the thalweg of the elongated basin, with different regimes in summer and in winter, and (b) on the coastal slopes. In the deep thalweg area the mean flow speed amounts to 6–13 cm s⁻¹, whereas the maximum speeds appear in winter near the bottom of the basin, and in summer within the halocline (around 70 m depth). The mean zonal flow component reveals a nearly depth uniform inflow during winter, and a layered inflow-outflow during summer. In years where up-estuary (W to SW) winds are stronger during the summer, inflow dominates in upper layers, and anti-estuarine outflow dominates in deeper layers. This causes the export of a salt wedge, and the weakening of haline stratification. Inflow frequency zonal currents (i.e. excluding topographic waves etc. with periods of less than 10 days) have a structure which is uniform with depth for 53% of the time in winter; in summer, a layered structure is present 65% of the time. However, during both periods the reversed estuarine flow (inflow in upper layers and outflow in the bottom layer) appears, on average, for 30% of the time. The deep flow zonal component is well correlated with westward winds during summer ($r = 0.84$), and south-westward winds during winter ($r = 0.77$). On the coastal slopes, the speed of the currents are lower than in the thalweg region, and they decay with depth. In the vertical the flow exhibits a layered structure in both the winter and summer seasons.

© 2016 Elsevier Ltd. All rights reserved.

1. Introduction

The Gulf of Finland is an elongated estuarine-like sub-basin of the Baltic Sea (Fig. 1, about 400 km long, 48–135 km wide, with a mean depth of 37 m) characterised by strong along-basin and vertical gradients of salinity and water density. The latter is a result of large fresh water input from the River Neva into the eastern end of the Gulf, and saline water inflow from the Baltic Proper into the western entrance area. The along-axis depth of the Gulf decreases from 100 m at the entrance to 20 m at the eastern end. The variable coastline and bottom topography play an important role in developing a complex circulation. The salinity in the entrance area is typically in the range 5–7 at the surface, and 8–10 in the bottom layers, whereas at the eastern end of the Gulf salinity is in the range 0–3 (Alenius et al., 1998). In the western part of the Gulf a quasi-permanent halocline exists at depths of 60–80 m. However, both

salinity and stratification vary strongly with season (Haapala and Alenius, 1994).

Water dynamics in the Gulf of Finland are not sufficiently well quantified or understood on the time scales of several months or greater. For example, both cyclonic (Alenius et al., 1998) and anti-cyclonic (Soomere et al., 2011) circulation schemes can be found in the literature. Mechanisms for the prevalence of a particular flow type are not firmly established. Variable winds in concurrence with barotropic and baroclinic forcing from neighbouring sea areas result in different temporal and spatial scales of current variability. Previous studies in the Gulf of Finland (Lilover et al., 2011) and in the Gotland Basin (Holtermann and Umlauf, 2012) reported that shorter periodic processes like tides, inertial oscillations, and seiches contain minor components of the total kinetic energy (25% and 36% respectively), and that the major component of the energy is in the low-frequency band.

Density-driven flow in an elongated, semi-enclosed rotating basin exhibits outflow in the upper layer and inflow in the bottom layer. Wind stress variations enhance, inverse, or reduce the

* Corresponding author.

E-mail address: madis-jaak.lilover@msi.ttu.ee (M.-J. Lilover).

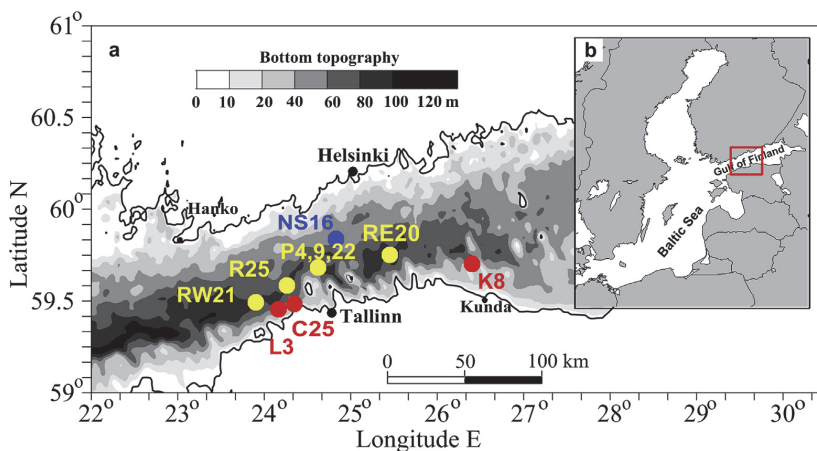


Fig. 1. Map of the study area in the Gulf of Finland with grey-scale bathymetry, and its location in the Baltic Sea (right upper corner). The locations of the bottom-mounted ADCP measurements along the thalweg are indicated by yellow dots (4 locations), along the southern coast by red dots (3 locations), and close to the northern coast by a blue dot. (For interpretation of the references to colour in this figure legend, the reader is referred to the web version of this article.)

density-driven flow by altering the barotropic and baroclinic pressure gradients, and by momentum transfer from wind drag (Reyes-Hernández and Valle-Levinson, 2010). Palmen (1930) conducted intensive measurements of surface currents in the central part of the Gulf of Finland from 1923 to 1927. Measurements revealed the wind-modified general circulation scheme—weak cyclonic circulation in the surface layers of the Gulf, inflow along the southern coast, and outflow on the northern side. Measurements of the current close to the northern coast (Haapala et al., 1990) supported the idea of outflow on the northern side of the Gulf of Finland. In general, the proposed scheme (Palmen, 1930) was found to be in agreement with the results from simulations using numerical models (Andrejev et al., 2004; Elken et al., 2011). The empirical orthogonal function analysis of modelled current data for the period 2006–2008 revealed both the barotropic (unidirectional over the whole section) and two-layer (surface Ekman transport with deeper compensation flow) flow patterns (Elken et al., 2011) in the western region of the Gulf. Measurements of the current showed that strong westerly winds can turn the currents to the opposite, eastward direction along the Finnish coast within several weeks (Haapala et al., 1990).

Recent studies reported relatively strong, low-frequency currents (on time scales longer than 36 h) in the bottom layers of the Gulf of Finland (Liblik et al., 2013; Lilover and Talpsepp, 2014; Suhhova et al., 2015; Rasmus et al., 2015). Earlier, it was found that the currents in the bottom layers of the Gulf responded to forcing by the wind (Elken et al., 2006; Liblik and Lips, 2012). South-westerly winds resulted in an estuarine circulation reversal – inflow into the Gulf in the surface layer and outflow in the bottom layer (Elken et al., 2003, 2014; Liblik et al., 2013) – together with a rise in sea level at the eastern end of the Gulf. The subsequent basin-scale barotropic flows over a variable topography were converted into mesoscale hydrophysical phenomena like strong eddies and topographic waves. Consequently, both the aperiodic (estuarine circulation reversals and eddies as well as upwelling/downwelling and related jet currents, and deep compensating flows) and periodic (topographic waves) currents contributed to the flow variability in the water column.

Due to the high variability of currents, short period records provide quite fragmented knowledge of the mean patterns and

variations of low-frequency flows. More detailed knowledge is urgently needed in the context of enhanced uses of the sea, and the necessity of studying the responses of the sea to a changing climate and human activity. The aim of this study was to obtain reliable knowledge of the observed flow variability along the thalweg, and on the coastal slopes of the Gulf of Finland. For this purpose, 10 multi-month ADCP measurement series were collected between 2009 and 2014.

This paper is organised into the following sections. Section 2 presents the observational material and the methods used for data processing. Section 3 presents the results of analyses of different aspects of the collected observations, including: mean flow speeds, horizontal patterns of mean currents, vertical profiles of mean current vectors and their persistence, mean zonal current components, statistics of deep estuarine circulation, and the relation of zonal flow to wind forcing. Section 4 discusses the observed findings. Section 5 closes with a summary and the conclusions of this study.

2. Materials and methods

2.1. ADCP measurements

Multi-monthly current measurements were conducted in the Gulf of Finland within different research projects using bottom-mounted ADCPs. In the period 2009–2014 a total of ten long-term (with a duration of at least two months) current profile time series were measured at different locations and time periods, as shown in Fig. 1 and Table 1. Six out of the ten ADCP time series (one series at stations RW21, R25, and RE20, and three series at central station P – P4, P9 and P22) were performed along the thalweg of the Gulf. Among them, the westernmost station (RW21) and easternmost station (RE20) were installed during the same period in winter/spring 2011/2012. Another pair of synchronous measurements is from winter/spring of 2013/2014 at the thalweg station R25 and coastal station C25. Stations P9 and P22 occupied the same location in the central part of the study area, but covered different observation periods—the summers of 2010 and 2012, respectively. One thalweg time series, P4, was rather short in comparison with others – only 2 months instead of the usual 4–5

Table 1
Characteristics of the ADCP measurement series.

ID	Observation Time		D ^b	Season/type	Coordinates		Depth ^a (m)
	from	to			Lat.	Lon.	
L3	13.03.2009	30.06.2009	3.5	Spring/coastal	59° 27.40'	24° 09.96'	45
K8	12.01.2010	27.04.2010	3.5	Winter/coastal	59° 42.10'	26° 24.23'	58
NS16	13.07.2011	05.09.2011	2	Summer/rim	59° 50.34'	24° 49.9'	73
C25	09.12.2013	28.04.2014	5	Winter/coastal	59° 28.98'	24° 20.82'	19
RE20	21.12.2011	9.05.2012	4.5	Winter/thalweg	59° 45.05'	24° 27.19'	82
RW21	21.12.2011	9.05.2012	4.5	Winter/thalweg	59° 29.60'	23° 54.10'	86
R25	09.12.2013	06.05.2014	5	Winter/thalweg	59° 35.13'	24° 15.64'	82
P4	23.07.2009	24.09.2009	2	Summer/thalweg	59° 41.2'	24° 37.4'	80
P9	14.04.2010	31.08.2010	4.5	Summer/thalweg	59° 41.02'	24° 37.45'	79
P22	28.05.2012	9.10.2012	4	Summer/thalweg	59° 41.00'	24° 37.50'	80

^a Deepest depth measured.^b Duration in months.

months. Therefore, those data were considered to be complementary to, and were used to check the findings in, the long-term measurements. Three ADCP time series measurements at stations L3, K8, and C25 had a duration of at least of 3.5 months on the southern coastal slope of the Gulf. Finally NS16, which was located out of the thalweg and closer to the northern coastal slope, had a duration of 2 months. All of these ADCPs were deployed at different times. Seasonally, data pertaining to the currents in the thalweg area covers 14 months of winter/spring and 10.5 months of summer; in the coastal area data covers 12 months of winter/spring and 2 months of summer (Table 1).

Most of the current data were recorded using bottom-mounted 300 kHz ADCP by Teledyne RD Instruments; in one location – C25 (Lips et al., 2017) – an RDCP 600 was used. The profilers were configured to measure the currents with a vertical increment of 2 m. The lowest readings were obtained at 5–9 m above the seabed; the uppermost readings were reliable from 5 m to 10 m from the surface, depending on the depth of the location. Data with original sampling intervals, from 10 min to 1 h, were converted to hourly current vector components. For the low-frequency analysis, the time series were filtered with a 36 h cut-off Butterworth filter. Such low-pass filtering almost removed the inertial, tidal and seiche-related current components (Lilover et al., 2011). In order to remove the effect of bottom-trapped topographic waves with a period of a few days, which are evident in the region (Talpepp, 2006), further infra-low-pass filtering of time series, with a cut-off period 10 days, was carried out for EOF (empirical orthogonal functions) and wind forcing analyses.

The one- or two-layered vertical structure of the flow was examined using EOF analysis. From the profile data two depth levels – one near the surface and another near the bottom – were selected to form the time series. After calculating the correlations between the time series of a station, eigenvalues, two-point eigenvectors, and mode amplitude time series were found using the standard EOF procedures (Von Storch and Zwiers, 2001). This analysis reveals how much of the total kinetic energy is explained by the first mode in different measurements. The first mode can have both a one-layer and a two-layer vertical structure. The structure of the first mode indicates the dominant structure.

2.2. Historical observations of currents

In order to deal with the high temporal variability and relatively small average speeds of current vectors, lengthy measurements are needed to accurately establish mean current characteristics. A summary of historical long-term current measurements is presented in Table 2, including Palmen's 5 year and Hela's subsequent 11 and 12 year (Palmen, 1930; Hela, 1952) current measurement

results. Also included are more recently published results of observations conducted in 1979 near Hanko (Laakkonen et al., 1981). Palmen (1930) defined the current direction persistence of the mean circulation as the ratio of vector-averaged current speed to scalar-averaged speed, multiplied by 100% (see also Andrejev et al., 2004). If the current direction does not change, then persistence is 100%—in the case of rotating flow, persistence reaches zero and the net transport of water is also equal to zero. Very low persistence values may also show equal contributions of eastward and westward flows. As discussed by Kundu (1976), determination of the direction of the mean motion is uncertain if the mean current components are small, and their fluctuations are large. The distribution of current directions ("current roses") may then be used to make the general current pattern visible.

2.3. Meteorological data

The analysis of the atmospheric conditions during the measurement campaigns was performed using the data from Utö and Kalbådagrund weather stations, which were provided by the Finnish Meteorological Institute. Incorporation of more spatially detailed meteorological data was not considered necessary at this stage of the analysis, since the time-varying spatially uniform wind represents more than 90% of the wind velocity variance in the Gulf of Finland (Elken et al., 2011). Thus these two stations are generally representative of the large-scale wind conditions in the Gulf of Finland.

The monthly mean zonal wind stress showed large variability during the six years 2009–2014 (Fig. 2). Mean eastward wind stress was evident in 7 out of 10 measurements. Summer series NS16 and winter series K8 showed mean westward wind stress. Summer series P9 had a mean value close to zero.

2.4. On the dynamical analysis of observed currents

The main axis of the western and central part of the Gulf of Finland is oriented 12° anticlockwise from the zonal (west to east) direction. Several modelling studies, such as Andrejev et al. (2004) and Elken et al. (2011), used meridional sections in order to interpret the cross-section zonal flows as longitudinal (nearly along the main axis) flows. Since the cross-section presented by Andrejev et al. (2004) is outside of the current study area, the 2006–2008 results of Elken et al. (2011), who used the operational HIROMB-SMHI model, are used. This model has a horizontal resolution of about one nautical mile, and a vertical resolution of 4 m down to 12 m, then increasing with depth to give a total of 16 vertical layers (Funkquist, 2001; Gästgifvars et al., 2008). The model mean flow includes the effects of several processes that have been studied in

Table 2
The resultant surface current at the north and south sides of the Gulf of Finland (historical data).

Station	Coordinates	Years	The resultant surface current			The resultant current at 10 m		
			Current direction (°)	Current Magnitude (cm/s)	Persistence of current direction (%)	Current direction (°)	Current Magnitude (cm/s)	Persistence of current direction (%)
¹⁾ Kalbadagrund	59° 58' N, 25° 36' E	1923–1927	238, WSW	1.3	14	236, WSW	1.9	22
¹⁾ Årandsgrund/	59° 57' N,	1923–1927	266, W	2.2	16	266, W	2.2	18
²⁾ Helsinki	24° 57' E	1928–1939	290, W	0.9	9			
¹⁾ Revalstein/	59° 43' N,	1923–1927	63, ENE	3.2	26	64, ENE	3.4	27
²⁾ Tallinn	24° 44' E	1924–1934	57, ENE	3.4	28			
³⁾ Tvärminne	59° 47' N, 23° 16' E	1979 m: 5,6,7,8,9				238, WSW	1.5	
³⁾ Hanko	59° 45' N, 23° 37' E	1979 m: 5,6,7,8,9				237, WSW	5.4	

¹⁾Prepared according to [Palmen, 1930](#), ²⁾[Hela, 1952](#), ³⁾[Laakkonen et al., 1981](#) papers.

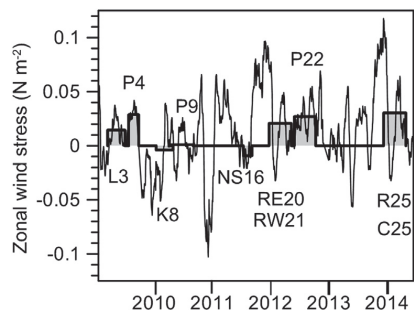


Fig. 2. Monthly mean zonal wind stress for the measurement campaign from 2009 to 2014. Shaded columns show the corresponding measurement series ([Table 1](#)) zonal wind stress mean values.

simplified special cases: estuarine flow according to the Knudsen budget, flows of an elongated basin forced by the mean density gradients without wind forcing (e.g. [Kasai et al., 2000](#)) and with uniform wind stress without density gradients ([Winant, 2004](#)), and wind modifications to the density-driven flows ([Reyes-Hernández and Valle-Levinson, 2010](#)). The dominance of density stratification over wind forcing at a specific basin aspect ratio can be estimated using the Wedderburn number ([Monismith, 1986](#)):

$$W = \frac{\rho g' h^2}{\tau L} \tag{1}$$

where $g' = g \Delta \rho / \rho$ is reduced gravity, g is gravitational acceleration, $\Delta \rho$ is the density change through the pycnocline of depth h , ρ is the mean density of seawater in the basin, τ is the wind stress acting on the basin, and L is the basin length. Wind dominates over density gradients when $W < 10$ ([Reyes-Hernández and Valle-Levinson, 2010](#)) and in the case of landward (up-estuary) winds the flows will be reversed.

3. Results

3.1. Mean flow speeds

The mean current speed is a basic flow property which describes the energetics of motion, transport capacity in the water column, resuspension potential near the bottom, etc. In many sea areas, there are marked differences in mean speed between the coastal and offshore regions, and between the surface, intermediate and

deep layers, with higher speeds usually found near the coast and at the surface.

The mean profiles of low-frequency current speed (current variations with a period of less than 36 h removed) are shown in [Fig. 3](#). Along the thalweg all six time series revealed the mean current speed to be about 9 cm s^{-1} in the uppermost measured layer, irrespective of the year, season and location. In winter the flow speed in the thalweg was almost uniform down to a depth of 50 m ([Fig. 3b](#)), while the speed decreased with depth in summer ([Fig. 3c](#)). In summer, below 50 m depth in the halocline the flow speed increased to a maximum at 70 m. The maximum speed values at stations P22 and P4 were very high, being about 13 cm s^{-1} . Simultaneous wintertime measurements at the westernmost (RW21) and easternmost (RE20) stations showed similar high speeds of about 9 cm s^{-1} in the surface layer. Below this the current speed decreased with depth at station RE20, while at the westernmost station RW21 it remained nearly constant in the depth interval of 20 m–70 m and then increased with depth, reaching values of 11 cm s^{-1} five metres above the sea floor ([Fig. 3b](#)). Calculating the average of six series' (total recording length about 2.2 years) current speeds revealed minimum values in the middle of the water column (30–50 m layer, current speed about 7.5 cm s^{-1}) and maximum values in the halocline at around 70 m (9.5 cm s^{-1}).

While in the thalweg area there was an increase in flow speed with depth (mainly down to 70 m), at the coastal stations L3, C25 and K8 located in the shallower depths, the current speeds showed the highest values in the near-surface layer and decreased with depth ([Fig. 3a](#)). Such a current speed pattern is similar to that described on the northern coastal slopes by [Rasmus et al. \(2015\)](#).

It is interesting to note that all of the observations used here gave scalar mean current speeds of about 9 cm s^{-1} in the uppermost layer of reliable ADCP measurements (about 10 m depth). This estimate was obtained with a record length as short as two months, and it was the same irrespective of location and timing. During the three years of uninterrupted current observations on the northern slope of the Gulf, [Rasmus et al. \(2015\)](#) obtained the same value of 9 cm s^{-1} for the current speed in the uppermost observation layer.

The vertical profiles of the standard deviations of current speed ([Fig. 3d, e, f](#)) comprised 50–70% of the mean current speed and showed similar variations in depth.

3.2. Horizontal pattern of mean currents

Resultant (vector average) current vectors of the measurements are presented in [Fig. 4a](#), together with the results from historical observations ([Fig. 4b](#)). Of the observations carried out on the thalweg, five measurement series out of six showed an eastward

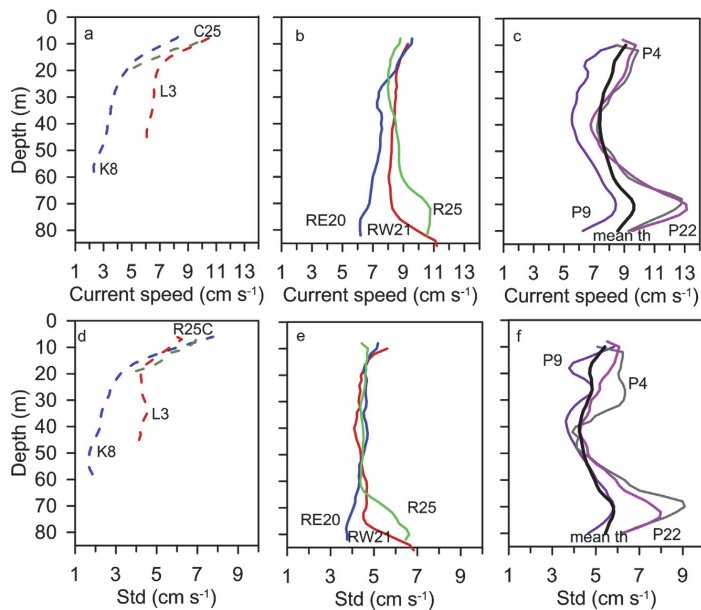


Fig. 3. Mean profiles of current speed at coastal stations (a) and along the thalweg stations during winter season (b) and summer season (c). Corresponding standard deviations of current speed are given in d, e and f, respectively. The along-thalweg averaged values are shown by the black line (averaged over 768 days, Table 1).

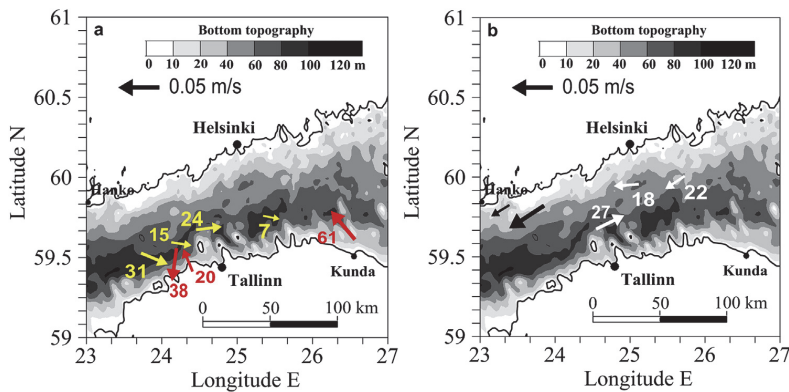


Fig. 4. Maps of resultant vectors of current at 10 m depth level overlaid with (a) new ADCP measurements and (b) historical measurements. Numbers close to each vector indicate the corresponding flow persistence (%). Arrows are centred on the measurement sites. Station names are given in Fig. 1. Yellow indicates new measurements along the thalweg (4 locations, at central location P22 data were used), red indicates new measurements along the southern coast (3 locations). The historical data are marked by white (years 1923–1927) and black arrows (year 1997) (Table 2). (For interpretation of the references to colour in this figure legend, the reader is referred to the web version of this article.)

resultant current vector (inflow into the Gulf) in the uppermost (8 m–10 m depth) layer. This pattern corresponds in general to the known mean cyclonic circulation of the Gulf of Finland (Palmen, 1930; Andrejev et al., 2004), but the inflow of near-surface waters (outside the thin surface layer of direct Ekman drift) is located further offshore from the southern coast. One time series measured at central station P9 during summer (not shown because its location overlaps with that of P22) revealed a westward current with relatively high persistence (40%). Current measurements close to the southern coast (3 stations) revealed that the westward component was dominant over the eastward component. Two out

of three measurement series (L3 and K8) had high persistence—38% and 61% respectively.

3.3. Vertical profiles of mean current vectors

Vertical profiles of mean current vectors and corresponding persistence are shown in Fig. 5. During the summer (Fig. 5c, f), the resultant current at the central station P (with different time series named as P4, P9 and P22) had a two-layer structure in the vertical (inflows changed to outflows with depth, series P22 and P4) or even a three-layer structure (P9). In the deeper layers the mean currents

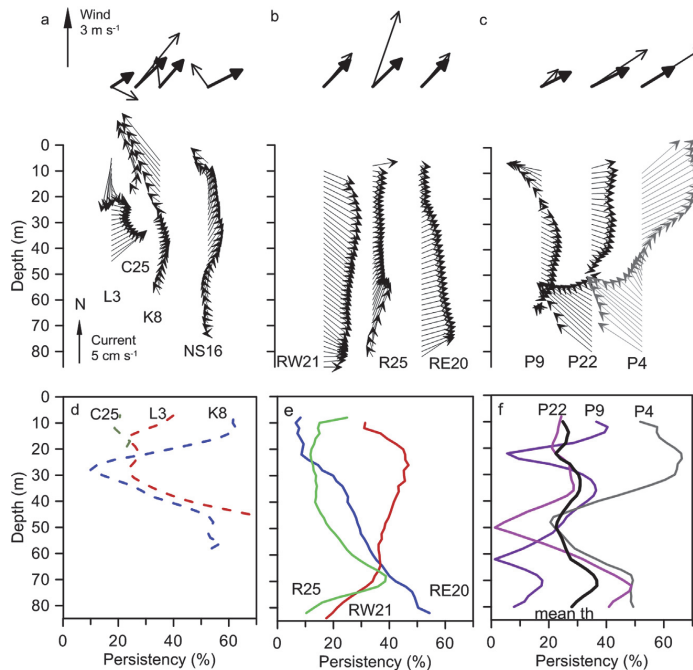


Fig. 5. The resultant vectors of wind (upper arrows) and currents (a) at coastal stations and along the thalweg stations (b) in winter and (c) in summer. The thin wind vectors are the measurement period mean and bold are the measurement period long-term (1981–2015) mean wind vectors respectively. Two time series (RW21 and R25) were measured towards the west from central station P (where three series were performed) and one (RE20) towards the east. The lower panels d, e, f show the corresponding persistence of the currents, and a black line depicts an averaged persistence over the six series measured along the thalweg.

were directed towards the northwest—in correspondence with the anti-estuarine outflow. The persistence of current direction varied across a large range, being mostly between 10% and 60%. Remarkably high persistence (up to 50%) was found within the deep outflow in series P4 (2009) and P22 (2012).

It should be noted that the wind conditions during the observations at station P9 were rather different from the observations at P4 and P22 (namely in the latter cases strong south-westerly winds were present, in contrast to the weak southerly winds observed during P9). South-westerly winds agreed more closely with the long-term winds (Fig. 5c, upper panel). Based on the similarity of the shorter period wind forcing to the long-term mean forcing, measurement series P22 was chosen for further analysis of the summer period and RW21 for the winter period (Fig. 5c and b, upper panels).

During the winter the resultant current had nearly unidirectional vertical distribution over the entire depth of the basin (Fig. 5b), revealing inflow in all three locations along the thalweg. The smallest mean flows were observed at station R25; simultaneous observations at the westernmost station RW21 and easternmost station RE20 showed maximum resultant current speeds of 4 cm s^{-1} around a depth of 26 m, and of 3 cm s^{-1} near the bottom, respectively. Note that the stations RW21 and RE20 were located in different deep basins of depths greater than 80 m, separated by moderate sills of 70 m–80 m depth. The persistence of the flow directions (Fig. 5e) was rather variable with depth and had maxima in the upper layers (RW21), in the halocline (R25), and near the bottom (RE20). The mean persistence profile taken over the summer and winter observations had minima around depths of

20 m and 50 m (both about 22%) and maxima around 30 m–40 m (31%) and 70 m (37%).

On the southern coastal slopes, at stations L3, C25 and K8, the resultant current revealed a westward outflow in the upper layer (Fig. 5a). At station NS16, northward from the thalweg, the resultant upper layer current was also westward. A remarkable offshore current component was found at station K8 and an onshore component at station L3. The resultant current revealed a two- or three-layered vertical structure. The persistence of the current direction (Fig. 5d) varied over a wide range—mostly between 10% and 70%. In the upper layer the highest persistence was found at station K8.

3.4. Mean zonal current components

During winter observed zonal (longitudinal) flows revealed a unidirectional with depth inflow in the thalweg area (Fig. 6c), as described by the above model results (a model example is given in Fig. 6a). During summer the mean flows are of two-layer origin (Fig. 6d), exposing an inflow above 50 m depth and anti-estuarine outflow in deeper layers. Setting $L = 300 \text{ km}$ for the wider part of the Gulf and describing the mean summer stratification with $\Delta\rho = 3 \text{ kg m}^{-3}$, $h = 40 \text{ m}$ (based on the data by Liblik and Lips, 2011), the value of the Wedderburn number was calculated using the time series of wind observations, which gave $W = 3$ for the data from P4 ($\tau = 0.046 \text{ N m}^{-2}$, strong anti-estuarine wind forcing), $W = 5$ for the data from P22 ($\tau = 0.028 \text{ N m}^{-2}$, strong anti-estuarine wind forcing), and $W = 12$ for the data from P9 ($\tau = 0.011 \text{ N m}^{-2}$, moderate wind forcing). Hence the flow reversal in the cases of P4

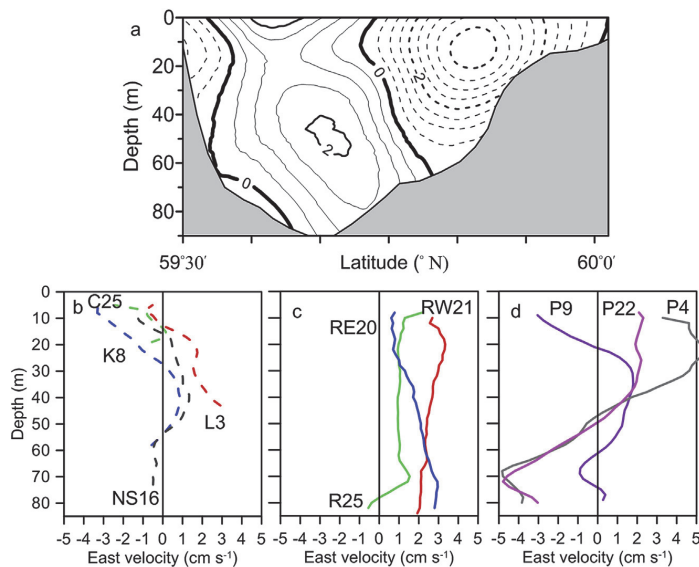


Fig. 6. (a) Mean zonal current velocity (mean of the period 2006–2008; positive towards east; the contours for currents are cm s^{-1}) through a cross section of the Gulf of Finland (model data redrawn from Elken et al., 2011), mean zonal current velocity (b) in the coastal stations, along the thalweg (c) in winter and (d) in summer.

and P22 can be explained by the appropriate wind forcing. In the case of moderate wind forcing (P9) the outflow in the near-surface layer (characteristic of density-driven flow) was observed. This observed outflow in the location of the thalweg was in agreement with FerryBox data from summer 2010 (Kikas and Lips, 2016) that showed the detachment of low-saline waters from the northern coast, spreading to the west near the central axis of the Gulf.

On the coastal slopes, mean outflow was observed in the surface layers of both the southern and northern coasts (Fig. 6b).

3.5. Statistics of deep estuarine circulation vs reverse estuarine circulation

In the following section, the statistics that could explain the formation of either estuarine or reverse mean flows in deep layers are examined.

Polar histograms of current direction presented in Fig. 7 show that motions in the near-bottom layers were characterised by a narrow band of directions, steered by local bottom topography. In most of the cases there were back-and-forth motions along specific lines. The main angles (counted clockwise from a northerly direction) for eastward motion components were 120° – 130° at the central stations (P4, P9, P22) irrespective of the timing of the observations. At other thalweg locations, the main angles were 70° for the westernmost station (RW21), 25° for R25, and 50° for the easternmost station (RE20). In the eastern local sub-basin (separated in the west by a sill of moderate height) around RE20, westward motions were nearly absent and eastward flows clearly dominated. All the other thalweg stations exhibited higher speeds during westward outflow, especially in the cases of P4 and P22 during summer, and RW21 during winter. On the coastal slopes the near-bottom currents were oriented in only one dominant direction: towards 50° at L3, 40° at C25 and 320° at K8. In the upper layer (not shown) current directions were more widely dispersed across different directions, but still the structure observed in the bottom

layer was generally visible.

The distribution of the dispersion (kinetic energy) of zonal (west-east) flow components between unidirectional and two-directional flows was also studied. Prior to the analyses, infra-low-pass filtering was implemented (with cut-off period of 10 days). EOF analysis of near-surface and near-bottom zonal currents revealed a bidirectional structure of the most energetic 1st mode during summer (series P22, P9) and during winter/spring (series R25) with kinetic energy contributions of 75%, 67%, and 66% respectively. The unidirectional 1st mode was observed during winter/spring (series RW21 and RE20 with kinetic energy contributions of 79% and 92% respectively) when the resultant wind of the particular measurement period was close in magnitude and direction to the long-term (1981–2015) mean resultant wind (Fig. 5b, upper panel).

During the winter/spring period (series RW21) the vertical normalised amplitude had a maximum value on the bottom for the 1st unidirectional mode (maximum 0.98 out of 1.0) and on the surface for the 2nd bidirectional mode (maximum also 0.98). Thus the 1st mode time evolution very closely resembled the original bottom layer current (Fig. 8b), whereas the 2nd mode resembled the upper layer current (not shown). During the summer period the dispersion at P22 was more evenly distributed in the vertical. Nevertheless, the most energetic mode describes the original observations well (Fig. 8a). Simultaneous current measurements along the thalweg (R25) and at coastal station C25 revealed opposite flow directions (Lips et al., 2017). The EOF analysis, including the near-surface zonal current velocity at those two stations, revealed the bidirectional structure of the most energetic 1st mode, with a kinetic energy contribution of 81%.

There are four different flow regimes corresponding to the sign combinations of zonal current speed near the surface u_s and near the bottom u_b : estuarine circulation (EC, $u_s < 0$, $u_b > 0$), reverse estuarine circulation (REC, $u_s > 0$, $u_b < 0$), unidirectional inflow (UIN, $u_s > 0$, $u_b > 0$) and unidirectional outflow (UOUT, $u_s < 0$,

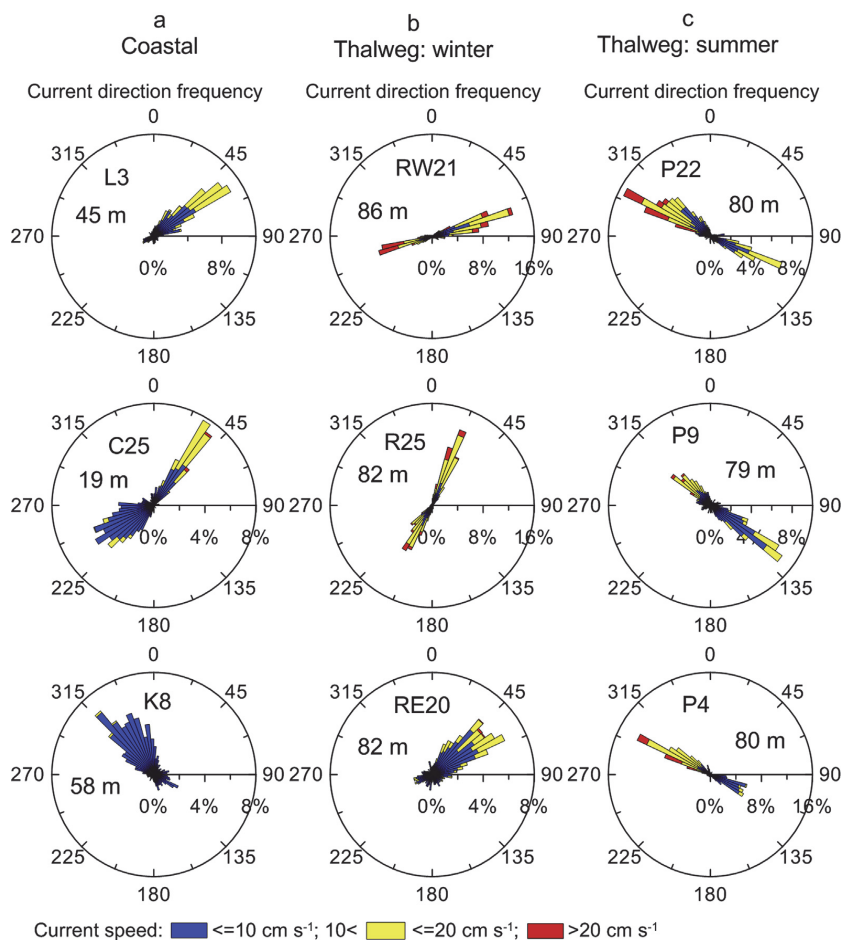


Fig. 7. Polar histograms of current direction with scaled current speed in the bottom layer along (a) the coastal and (b) thalweg stations during winter and (c) during summer seasons. The meter value in each figure shows the depth of current velocity data.

$u_b < 0$). Results of the analysis presented in Table 3 show that during the summer observation period in 2012, when the mean zonal wind stress was 0.028 N m^{-2} ($W = 5$), the prevailing flow type at P22 was bidirectional flow (70% of the time) where EC took place 26% and REC 44% of the time, UIN and UOUT took place 15% and 15% of the time respectively. During the summer of 2010 when mean zonal wind stress was lower (0.011 N m^{-2} , $W = 12$), observations at P9 also revealed dominant bidirectional flows, but EC prevailed over REC (43% vs 17%). As a summer mean EC prevailed slightly over REC (34% vs 31% respectively). For winter/spring period the unidirectional and two-directional flows were roughly in balance. Among four flow sub-regimes, UIN clearly prevailed at RW21 (41% of the time), as a winter mean EC took place 17% and REC 30% of the time. The summer and winter periods had approximately equal percentages of salty water inflows in the bottom layer (EC + UIN). However, there were key differences in the flow regimes: in winter UIN prevailed over EC and in summer EC prevailed over UIN by a similar amount (Table 3).

3.6. Relation of zonal flow to wind forcing

In the theories of wind-forced motions of elongated basins (e.g. Winant, 2004), downwind flows develop on the coastal shoals and on the thin surface Ekman layer of the basin interior, but compensating upwind flows take place in the deeper parts of the basins because the sea level is piled up in the downwind end of the basin. Such mechanisms have been confirmed by the analysis of results from numerical models (Krauss and Brüggemann, 1991; Elken et al., 2003), but there is little observational evidence during winter seasons (Liblik et al., 2013; Lips et al., 2017). Liblik et al. (2013) have found the best correlation ($r^2 = 0.44$, $p < 0.01$) between the low-pass filtered (36 h) NNE wind and an easterly longitudinal inflow current in the deep layer when a time lag of 18 h was taken into account.

The wind data observed at Kalbådagrund weather station were processed with the same filters used for the currents, excluding the variations with periods of less than 10 days. Later, the angle at which to project the wind velocity values, in order to obtain

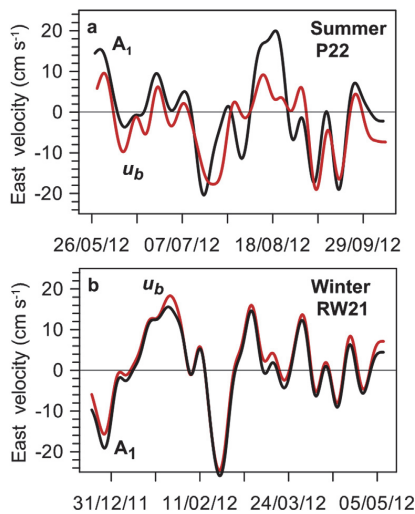


Fig. 8. Low-pass-filtered zonal flow velocities (periods of less than 10 days excluded) in the bottom layer of (a) station P22 during summer 2012 and (b) station RW21 during winter 2012 are indicated by the red lines. The black lines depict the 1st EOF mode amplitudes (A_1) of zonal flow velocities (a) for summer season 2012 and (b) for winter/spring season 2012. (For interpretation of the references to colour in this figure legend, the reader is referred to the web version of this article.)

Table 3

Frequency of occurrence (%) of different vertical flow structures: bidirectional estuarine (EC) and reversed estuarine (REC) flow, unidirectional inflow (UIN) and outflow (UOUT).

Station	EC (%)	REC (%)	UIN (%)	UOUT (%)
Winter (RW21)	14	28	45	13
Winter (R25)	21	31	24	24
Winter mean	17	30	34	19
Summer (P22)	26	44	15	15
Summer (P9)	43	17	15	25
Summer mean	34	31	15	20
Mean	26	30	25	19

maximum correlation between the projected wind velocity and the deep zonal current velocities, was sought. Results of the analysis presented in Fig. 9 show slightly different relationships: during summer (P22) the zonal near-bottom velocity revealed the maximum correlation $r = 0.84$ with wind projected to the west (wind direction 90°), but during winter (RW21) $r = 0.77$ was obtained with wind projected to the south-west (direction 45°).

During winter 2012 (RW21) (Fig. 9b) the largest deviations of currents from the simple wind dependence occurred at the end of January. This is when the salt wedge (Fig. 10b) intruded, due to baroclinic pressure gradients, into the Gulf after the earlier full decay of stratification (Liblik et al., 2013). At the end of February, when strong south-westerly winds blew again, zonal outflow contributed to the salinity decrease (Figs. 9b and 10b). During the summer observations at P22, the periods of decreasing salinity coincided with the strong outflows (Fig. 10a). Thus the decreasing salinity in the bottom layer, due to strong outflows, substantially weakened water column stratification in both summer and winter periods. During the winter (because of the lack of a thermocline) this could lead to a vertically mixed water column (Lips et al., 2017; Liblik et al., 2013; Elken et al., 2003). Note that more detailed analysis of baroclinic and wind forcing of deep flows is out of the

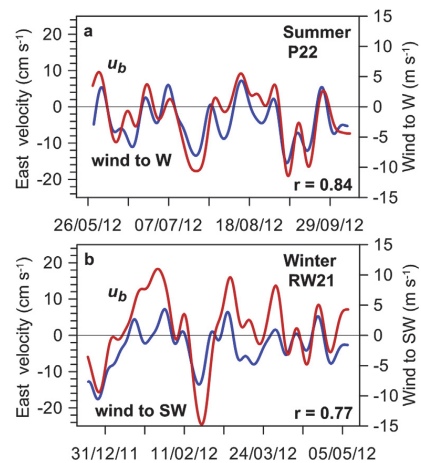


Fig. 9. Low-pass-filtered zonal flow velocities (periods of less than 10 days excluded) in the bottom layer of (a) station P22 during summer 2012 and (b) station RW21 during winter 2012 are indicated by the red lines. The blue lines depict the low-pass-filtered wind (a) projected to the west for the summer season 2012 (correlation between current and wind $r = 0.84$) and (b) projected to the south-west for the winter/spring season 2012 ($r = 0.77$). (For interpretation of the references to colour in this figure legend, the reader is referred to the web version of this article.)

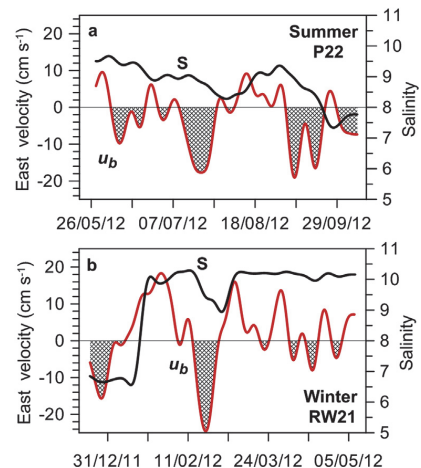


Fig. 10. Low-pass-filtered zonal flow velocities (periods of less than 10 days excluded) in the bottom layer of (a) station P22 during summer 2012 and (b) station RW21 during winter 2012 are indicated by the red lines. The black lines depict the salinity (a) for summer season 2012 and (b) for winter/spring season 2012. The shaded time periods corresponding to outflow in the bottom layer coincide with the periods of salinity decrease. (For interpretation of the references to colour in this figure legend, the reader is referred to the web version of this article.)

scope of the present paper.

4. Discussion

The first maps of the currents in the Gulf of Finland, based on the observational data, were drawn by Palmén (1930) and complemented by Hela (1952). To the north of the main axis of the Gulf,

it was found that the resultant current flowed to the WSW at Kalbådgrund, and to the W at the Årandsgrund/Helsinki station with relatively low current direction persistence (Fig. 4b). To the south of the main axis, at the Revalstein/Tallinn station, the resultant current was found to flow in the opposite direction, towards the ENE with relatively high persistence (26–28%). The new measurements presented here revealed a flow pattern which corresponds in general to the known mean cyclonic circulation in the Gulf of Finland (Palmen, 1930; Andrejev et al., 2004). However, the inflow of near-surface waters (outside the thin surface layer of direct Ekman drift) is located further offshore from the southern coast, with outflow dominating closer to the coast. The latter result is in line with recent observations (for the details of station L3, see Suhhova et al., 2015) and is independent from the model results shown in Fig. 5a (Soomere et al., 2011; Suhhova et al., 2015).

The steady water exchange of the Gulf of Finland can be estimated using the Knudsen theorem, which yields a yearly inflow of 480 km³ and an outflow of 600 km³, in addition to 120 km³ of river discharge (Alenius et al., 1998). In the western part of the Gulf, the cross-sectional area is about 4 km² (Elken et al., 2011). Dividing the areas of inflow and outflow in proportion to their volume transports, a mean velocity of 1.1 cm s⁻¹ over the inflow and outflow areas was obtained. Assuming continuous flow distribution over the cross-section, maximum steady flows in the inflow and outflow cores can be estimated as 2–3 cm s⁻¹. The long-term wintertime observations reveal mean zonal inflow (Fig. 5c) with speeds of 1–3 cm s⁻¹ in the thalweg area, perfectly matching the estimates from the steady Knudsen budget. The Knudsen estimates are also in agreement with the model results (e.g. Andrejev et al., 2004; Elken et al., 2011).

The summertime observations (P9 and P22) showed layered mean zonal flows, with outflow dominating in the deep layer, with an average speed of about 3 cm s⁻¹ at 70 m depth during the summer periods (Fig. 5d). This finding may be discussed in the context of the seasonal pattern of salinity stratification: Haapala and Alenius (1994) have identified that, on average for 1961–1990, salinity below 40 m has a maximum value in summer during the second half of June. Until that time the isohaline 9 rises from 90 m to 65 m depth within two months, beginning in the second half of April. After the maximum stratification, the same isohaline is found back at a depth of 90 m within four months of the second half of October. According to the hypsographic curves (e.g. Leppäranta and Myrberg, 2009), the volume of the Gulf of Finland between the depths of 65 m and 90 m is about 280 km³. An average cross-sectional area of 0.5 km² was adopted for the flow between 65 m and 90 m depth. Assuming that seasonal changes of isohaline depths are solely due to the kinematic import and export of the salt wedge in the deep layers (mean salinity profiles are nearly linear, suggesting a small average vertical mixing, Liblik and Lips, 2011), a mean outflow velocity of 5.4 cm s⁻¹ for the period July–October was obtained. This value is above the observed mean value of 3 cm s⁻¹. This probably indicates the role of vertical mixing in changes to the isohaline depth.

The average estuarine budget of the Gulf of Finland is maintained by quite low flow speeds, of the order of a few cm s⁻¹. In order to explain the seasonal salinity variations, deep water inflow speeds must be larger during the spring salt wedge import phase. The decay of stratification between July and October may be described as primarily due to the kinematic export of the salt wedge. In this case, temporary deep water outflow (reverse estuarine circulation), with a velocity larger than the “Knudsen” speed, fits well into the above qualitative concept of a seasonal water exchange and mixing pattern. However, such seasonal knowledge is largely missing, and further studies are urgently needed, first of all in order to explain and predict the environmental conditions in

the Gulf.

Earlier observations reported estuarine circulation reversals with a duration of a couple of weeks, both in summer and winter (Elken et al., 2003; Liblik et al., 2013 respectively). Based on the model results, Elken et al. (2003) concluded that stronger than average SW winds can lead to reverse estuarine transports; this was calculated by the integration of current velocities over the cross-section. In the case of current profile observations at isolated points, it was only possible to carry out temporal filtering in order to remove or suppress the effects of mesoscale eddies, topographic waves, fronts etc. with time scales of less than 10 days. After this filtering, the topographic influence on flow directions was still clearly visible in the changes in infra-low frequency deep currents. The analysis presented in this paper, based on time series P22 and P4, showed that deep outflows were the prevailing circulation type during the summer season in the years of stronger WSW winds, whereas they occurred about half of time during the whole observation period. Observational evidence that, irrespective of the season, deep along-basin current velocities depend on the wind velocity was also found, with correlations above 0.7. Maximum deep inflows occur in winter during north-easterly winds and in summer during easterly winds, with outflows occurring during winds from the opposite direction. This relation is in agreement with the results of calculations (not shown) of longitudinal (along the channel axis) wind forced flows, using the analytical model by Winant (2004). For the estuarine flow reversal in real conditions, the W or SW wind speed must be greater than some critical value that depends on the stratification, including the density difference between the Northern Baltic Proper and the Gulf of Finland. There may also be a direct dependence of critical wind speed on the freshwater fluxes to the sea, although the fluxes first of all affect the salinity and density fields, keeping the mean estuarine gradients restored against water exchange and mixing. A rough estimate of the critical value of the wind speed may be obtained by analysis of the Wedderburn number. It is considered that the further examination of the effects of wind and salinity/density variations on the water exchange and mixing in elongated basins like the Gulf of Finland is important.

5. Conclusions

Ten long-term records of bottom-mounted ADCPs deployed in the elongated part of the Gulf of Finland were analysed to distinguish between different flow regimes and variability (a) on the coastal slopes and along the thalweg (b) in summer and (c) in winter. Deep thalweg areas are characterised by mean scalar flow speeds of 6–13 cm s⁻¹, with a maximum either near the bottom during winter, or within the halocline at around 70 m depth during summer. Seasonally, there is a mean inflow along the thalweg which is near-constant with depth during winter, but during summer in years with stronger WSW winds the layered flow regime reveals inflow above 50 m depth and anti-estuarine outflow in deeper layers. Such anti-estuarine flow was evident during the periods when the Wedderburn number was smaller than 10. The latter corresponds to the export of the salt wedge, and to the weakening of seasonal saline stratification after its maximum in June–July.

EOF analysis showed that temporal variations in infra-low frequency (time scales of longer than 10 days) zonal (nearly longitudinal) currents have a depth-uniform or layered structure during winter and a layered structure during summer. The 1st modes explain 66%–92% of the total variance in zonal flows near the surface and near the bottom. Wind-induced deep inflow is caused by easterly wind during summer and north-easterly wind during winter, and outflow occurs during the opposite wind directions. On

the coastal slopes the current speeds are smaller than in the thalweg region and decay with depth. The flow vectors exhibit a layered vertical structure during both winter and summer. In winter the near-surface zonal flow along the thalweg and at coastal stations revealed a bidirectional flow structure with a 1st mode kinetic energy contribution of 81%.

During the winter period, the unidirectional inflow was the prevailing flow structure feeding the bottom layers with salty water, while during the summer period the bidirectional estuarine flow prevailed over unidirectional inflow. In both periods the reversed estuarine flow, leading to the weakening of stratification, took place on average 30% of the time.

Acknowledgements

This study was partly supported by institutional research funding IUT 19–6 from the Estonian Ministry of Education and Research, and partly by the Estonian Science Foundation grants 9278, 9381 and 9382. ADCP stations were installed within the following projects: base funding of Marine Systems Institute (L3, RE20, RW21), IUT 19–6 (R25, C25), Estonian Science Foundation grants G6955 (P4, P9) and G9023 (P22), EEA grant GEMP53 (K8), Nord Stream gas pipeline construction monitoring contract LMIN10079 (NS16). We are grateful to the crew and the scientific team of R/V Salme for assistance in the deployment of the ADCP, to Ülo Suursaar for providing RDCP current measurements data (C25). The comments from reviewers helped to improve the quality of the paper.

References

- Alenius, P., Myrberg, K., Nekrasov, A., 1998. The physical oceanography of the Gulf of Finland: a review. *Boreal Environ. Res.* 3 (2), 97–125.
- Andrejev, O., Myrberg, K., Alenius, P., Lundberg, P.A., 2004. Mean circulation and water exchange in the Gulf of Finland—a study based on three-dimensional modelling. *Boreal Environ. Res.* 9 (1), 1–16.
- Elken, J., Raudsepp, U., Lips, U., 2003. On the estuarine transport reversal in deep layers of the Gulf of Finland. *J. Sea Res.* 49 (4), 267–274.
- Elken, J., Malkki, P., Alenius, P., Stipa, T., 2006. Large halocline variations in the Northern Baltic Proper and associated meso- and basin-scale processes. *Oceanologia* 48 (S), 91–117.
- Elken, J., Nomm, M., Lagema, P., 2011. Circulation patterns in the Gulf of Finland derived from the EOF analysis of model results. *Boreal Environ. Res.* 16, 84–102.
- Elken, J., Raudsepp, U., Laanemets, J., Passenko, J., Maljutenko, I., Pärn, O., Keavallik, S., 2014. Increased frequency of wintertime stratification collapse events in the Gulf of Finland since the 1990s. *J. Mar. Syst.* 129, 47–55.
- Funkquist, L., 2001. HIROMB, an operational eddy-resolving model for the Baltic Sea. *Bull. Marit. Inst. Gdansk* 28, 7–16.
- Gästgifvars, M., Müller-Navarra, S., Funkquist, L., Huess, V., 2008. Performance of operational systems with respect to water level forecasts in the Gulf of Finland. *Ocean. Dyn.* 58 (2), 139–153.
- Haapala, J., Alenius, P., 1994. Temperature and salinity statistics for the northern Baltic Sea 1961–1990. *Finn. Mar. Res.* 262, 51–121.
- Haapala, J., Launiainen, J., Keynäs, K., Pokki, J., 1990. Hankoniemen edustan virtaustutkimus. Loppuraportti. *Hels. Yliop. Geofys. laitos* 59.
- Hela, I., 1952. Drift Currents and Permanent Flow. In: *Societas Scientiarum Fennica*.
- Holtermann, P.L., Umlauf, L., 2012. The Baltic Sea tracer release experiment: 2. Mixing processes. *J. Geophys. Res. Oceans* (1978–2012) 117 (C1).
- Kasai, A., Hill, A.E., Fujiwara, T., Simpson, J.H., 2000. Effect of the Earth's rotation on the circulation in regions of freshwater influence. *J. Geophys. Res. Oceans* (1978–2012) 105 (C7), 16961–16969.
- Kikas, V., Lips, U., 2016. Upwelling characteristics in the Gulf of Finland (Baltic sea) as revealed by ferrybox measurements in 2007–2013. *Ocean Sci.* 12, 843–859.
- Krauss, W., Brügge, B., 1991. Wind-produced water exchange between the deep basins of the Baltic Sea. *J. Phys. Oceanogr.* 21 (3), 373–384.
- Kundu, P.K., 1976. Ekman veering observed near the ocean bottom. *J. Phys. Oceanogr.* 6 (2), 238–242.
- Laakkonen, A., Mälikki, P., Niemi, Å., 1981. Studies on the Sinking, Degradation and Sedimentation of Organic Matter off Hanko Peninsula, Entrance to the Gulf of Finland, in 1979 (progress report).
- Leppäranta, M., Myrberg, K., 2009. *Physical Oceanography of the Baltic Sea*. Springer Science & Business Media.
- Liblik, T., Lips, U., 2011. Characteristics and variability of the vertical thermohaline structure in the Gulf of Finland in summer. *Boreal Environ. Res.* 16, 73–83.
- Liblik, T., Lips, U., 2012. Variability of synoptic-scale quasi-stationary thermohaline stratification patterns in the Gulf of Finland in summer 2009. *Ocean Sci.* 8 (4), 603–614.
- Liblik, T., Laanemets, J., Raudsepp, U., Elken, J., Suhhova, I., 2013. Estuarine circulation reversals and related rapid changes in winter near-bottom oxygen conditions in the Gulf of Finland, Baltic Sea. *Ocean Sci.* 9 (5), 917–930.
- Lilover, M.J., Talpsepp, L., 2014. On the vertical structure of the low-frequency oscillations of currents in the Gulf of Finland. *Baltic International Symposium (BALITIC), 2014 IEEE/OES* (pp. 1–6). IEEE.
- Lilover, M.J., Pavelson, J., Kõuts, T., 2011. Wind forced currents over the shallow Naissaar bank in the Gulf of Finland. *Boreal Environ. Res.* 16, 164–174.
- Lips, U., Laanemets, J., Lips, I., Liblik, T., Suhhova, I., Suursaar, Ü., 2017. Wind driven residual circulation and related oxygen and nutrient dynamics in the Gulf of Finland (Baltic Sea) in winter. *Estuar. Coast. Shelf Sci.* 195, 4–15.
- Monismith, S., 1986. An experimental study of the upwelling response of stratified reservoirs to surface shear stress. *J. Fluid Mech.* 171, 407–439.
- Palmen, E., 1930. Untersuchungen über die Strömungen in den Finland umgebenden Meeren. *Soc. Sci. Fenn. Comm. Phys.-Math.* 5, 1–94.
- Rasmus, K., Kiirikki, M., Lindfors, A., 2015. Long-term field measurements of turbidity and current speed in the Gulf of Finland leading to an estimate of natural resuspension of bottom sediment. *Boreal Environ. Res.* 20, 735–747.
- Reyes-Hernández, C., Valle-Levinson, A., 2010. Wind modifications to density-driven flows in semiencloded, rotating basins. *J. Phys. Oceanogr.* 40 (7), 1473–1487.
- Soomere, T., Delpeche, N., Viikmae, B., Quak, E., Meier, H.E., Doos, K., 2011. Patterns of current-induced transport in the surface layer of the Gulf of Finland. *Boreal Environ. Res.* 16, 49–63.
- Suhhova, I., Pavelson, J., Lagema, P., 2015. Variability of currents over the southern slope of the Gulf of Finland. *Oceanologia* 57 (2), 132–143.
- Talpsepp, L., 2006. Periodic variability of currents induced by topographically trapped waves in the coastal zone in the Gulf of Finland. *Oceanologia* 48 (S), 75–90.
- Von Storch, H., Zwiers, F.W., 2001. *Statistical Analysis in Climate Research*. Cambridge University Press.
- Winant, C.D., 2004. Three-dimensional wind-driven flow in an elongated, rotating basin. *J. Phys. Oceanogr.* 34 (2), 462–476.

Paper IV

Liblik, T., Laanemets, J., Raudsepp, U., Elken, J., Suhhova, I. 2013. Estuarine circulation reversals and related rapid changes in winter near-bottom oxygen conditions in the Gulf of Finland. Baltic Sea. *Ocean Science*, 9, 917–930.



Estuarine circulation reversals and related rapid changes in winter near-bottom oxygen conditions in the Gulf of Finland, Baltic Sea

T. Liblik, J. Laanemets, U. Raudsepp, J. Elken, and I. Suhhova

Marine Systems Institute, Tallinn University of Technology, Akadeemia Road 15a, 12618 Tallinn, Estonia

Correspondence to: T. Liblik (taavi.liblik@msi.ttu.ee)

Received: 25 March 2013 – Published in Ocean Sci. Discuss.: 12 April 2013

Revised: 13 September 2013 – Accepted: 26 September 2013 – Published: 30 October 2013

Abstract. The reversal of estuarine circulation caused by southwesterly wind forcing may lead to vanishing of stratification and subsequently to oxygenation of deep layers during the winter in the Gulf of Finland. Six conductivity, temperature, depth (CTD)+oxygen transects (130 km long, 10 stations) were conducted along the thalweg from the western boundary to the central gulf (21 December 2011–8 May 2012). Two bottom-mounted ADCP were installed, one near the western border and the second in the central gulf. A CTD with a dissolved oxygen sensor was deployed close to the western ADCP. Periods of typical estuarine circulation were characterized by strong stratification, high salinity, hypoxic conditions and inflow to the gulf in the near-bottom layer. Two circulation reversals were observed: one in December–January and one in February. The first reversal event was well developed; it caused the disappearance of the stratification and an increase in the oxygen concentration from hypoxic values to $270\ \mu\text{mol L}^{-1}$ (to $6\ \text{mL L}^{-1}$) throughout the water column along the thalweg and lasted approximately 1.5 months. Shifts from estuarine circulation to reversed circulation and vice versa were both associated with strong longitudinal (east–west) gulf currents (up to $40\ \text{cm s}^{-1}$) in the deep layer. The change from oxygenated to hypoxic conditions in the western near-entrance area of the gulf occurred very rapidly, within less than a day, due to the intrusion of the hypoxic salt wedge from the NE Baltic Proper. In the eastern part of the gulf, good oxygen conditions caused by reversals remained for a few months.

1 Introduction

The bottom of the Baltic Sea is the largest dead zone in the world (Diaz and Rosenberg, 2008). Hypoxia (oxygen concentration of less than $90\ \mu\text{mol L}^{-1}$ or $2\ \text{mL L}^{-1}$) has been present during the last 8000 yr in the Baltic Sea (Zillén et al., 2008). The present extent of hypoxia in the Baltic Sea may be partly connected to the anthropogenic nutrient load and concurrent eutrophication (Conley et al., 2009). Eutrophication leads to increased sedimentation of organic material, thus increasing the area of anoxic bottoms and internal phosphorus loading. In addition, the hypoxic water volume displays a negative correlation with the total dissolved inorganic nitrogen pool: greater overall nitrogen removal with increased hypoxia (Vahtera et al., 2007). Hypoxia-related effects on the benthic ecosystem (e.g., Laine et al., 2007) and biogeochemical cycles of nutrients (e.g., Jäntti and Hietanen, 2012) are evident in the Gulf of Finland.

Deep layers of the Baltic Proper are supplied with oxygen only during the time of major inflows, when advecting highly saline, oxygen-rich water enters from the North Sea. Recently, such inflow events occurred in 1993 (Matthäus and Lass, 1995) and 2003 (Feistel et al., 2003). A significant ventilation of the Baltic Proper deep layers was observed after the major inflow in 1993, when the oxygen concentration in the Gotland deep rose to $90\ \mu\text{mol L}^{-1}$ ($2\ \text{mL L}^{-1}$); however, the oxygen had disappeared by 1998 (Fonselius and Valderrama, 2003). The next ventilation event due to a major inflow occurred in 2003, when a near-bottom oxygen concentration of up to $180\ \mu\text{mol L}^{-1}$ ($4\ \text{mL L}^{-1}$) was measured in the central Gotland Basin. Between the sporadic major inflows, stagnation periods have been observed, when a lack of deep advection decreased the near-bottom salinity

and oxygen concentrations. During the period 1961–2005, the deep hypoxic zone extended on average across an area of approximately 50 000 km² in the Baltic Sea (Savchuk, 2010), despite temporary oxygenation during and after the major inflows. Higher oxygen concentrations have been observed in the intermediate depths (80–120 m) of the water column during periods of stagnation (Conley et al., 2002).

Because the deep water of the Gulf of Finland originates near the halocline of the Baltic Proper, a stronger and shallower halocline in the Baltic Proper induces stronger stratification and increased hypoxia in the Gulf of Finland; the opposite change takes place when the halocline is weaker and deeper (Conley et al., 2009). It has been demonstrated that the halocline was stronger (Liblik and Lips, 2011) and oxygen depletion increased (Laine et al., 2007) in the Gulf of Finland after the major inflows of North Sea waters in 1993 and 2003.

Elken et al. (2003) concluded, based on summer CTD measurements, that halocline weakening that cannot be explained by vertical mixing alone may occur in the gulf. They suggested that southwesterly (generally up-estuary) wind forcing caused the reversal of estuarine circulation in the gulf: the surface-layer flows into the estuary, and the deep layer flows out (i.e., the opposite of normal estuarine circulation). In contrast, northeasterly and northerly winds support standard estuarine circulation, resulting in stronger stratification (Elken et al., 2003; Liblik and Lips, 2011) and import of phosphorus-rich waters from the deeper sub-halocline layers of the Baltic Proper (Lips et al., 2008). Elken et al. (2013) analyzed routine CTD measurements and wind data over several decades to investigate possible changes in the frequency of wintertime stratification collapse events. They found that the bottom-to-surface density difference becomes close to zero (note that the winter is already characterized by the weakest stratification in the Gulf, see Haapala and Alenius, 1994) during wind-induced strong estuarine circulation reversal events caused by up-estuary (southwesterly) wind forcing. They also found that since the 1990s, the frequency and duration of such stratification collapse events have increased due to the shift in the wind regime (i.e., the considerable increase in the west-southwesterly wind impulse in December–January). It is commonly understood that mixing of the entire water column will improve the near-bottom oxygen conditions either (1) by direct vertical stirring processes only or (2) by stirring in combination with wind-induced straining (differential lateral advection), with the latter factor dominating. These two types of mixing may result in various rates of change in the near-bottom salinity and oxygen content, perhaps also resulting in various release rates of phosphorus from the sediments (e.g., Viktorsson et al., 2012), but these rates of change remained unknown because of a lack of purposeful observations.

The primary aim of the present study was to observe and map details of winter stratification changes in the Gulf of Finland (as a model for the larger non-tidal estuary) to identify

the conditions under which the stratification collapse events occur. Specific goals were to determine whether these events are caused primarily by estuarine circulation reversals or if the vertical stirring dominates and to estimate the effect of these events on the spatiotemporal variability of the oxygen concentration in the deep layer of the gulf. When planning these studies, we hypothesized that a reversal of the estuarine circulation and concurrent disappearance of the salt wedge may rapidly and remarkably alter the oxygen conditions in the deep layer of the Gulf of Finland.

Following a description of the study area and the methods used, this paper presents an analysis of (1) a regular time series of wind conditions, (2) repeated transects of CTD and O₂ along the thalweg, and (3) time-series observations at two deep mooring locations: ADCP (acoustic Doppler current profiler) recording of current profiles and near-bottom point-recording of CTD and O₂. The presentation and analysis of observational results is followed by discussion and conclusions.

2 Study area, data and methods

2.1 Study area and surveys

The Gulf of Finland lies in the northeastern part of the Baltic Sea (Fig. 1). Due to the near isolation of the Baltic Sea from the ocean, tidal oscillations of the sea level are of minor importance in the dynamics of the gulf (e.g., Kullenberg, 1981), which is unique among the world's estuaries (Hansen and Rattray, 1966; MacCready and Geyer, 2010). The gulf is approximately 400 km long and varies from 48 to 135 km wide. The maximum depths exceed 100 m in the central and western areas. River discharge is concentrated in the eastern part of the gulf, where the inflow from the Neva River averages 77.6 km³ yr⁻¹, which constitutes approximately two thirds of the freshwater inflow to the gulf (Bergström and Carlsson, 1994). As a result, the surface-layer salinity varies from approximately 1 g kg⁻¹ in the easternmost area up to 6–7 g kg⁻¹ at the entrance (e.g., Haapala and Alenius, 1994). The deep layer is characterized by a slight westward salinity increase (e.g., Liblik and Lips, 2011). The seasonal thermocline forms at the beginning of May, develops during the summer and starts to erode by the end of August (e.g., Alenius et al., 1998). The thermocline is usually situated at a depth of 10–15 m and is strongest in July–August, when the surface-layer temperature rises to an average of 17 °C in the open gulf (Liblik and Lips, 2011). During the winter, the water masses are rather well mixed down to a depth of 60 m (Haapala and Alenius, 1994; Alenius et al., 2003). The gulf has a free connection to the NE Baltic Proper; a sill is lacking, and the salinity may therefore increase below the halocline (located at a depth of 60–70 m, Alenius et al., 1998) in the western part of gulf to as much as 10 g kg⁻¹, (i.e., values typical of the open sea). Greater sea depths and steeper

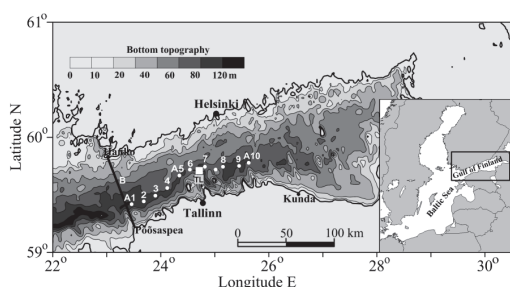


Fig. 1. Map of the study area in the Gulf of Finland. The solid white circles represent the locations of the CTD stations (A1–A10) along the thalweg of the gulf. The two bottom-mounted ADCPs were located at CTD stations A3 and A9. The bottom-mounted ADCP at location A3 was equipped with a CTD and dissolved oxygen sensor. The solid white square represents the location of the wind measurements at Tallinnamadal Lighthouse (TL). The bottom topography is drawn from the gridded topography in meters (Seifert et al., 2001). The western border of the gulf is defined as a line between the peninsulas of Põõsaspea and Hanko (line B).

bottom slopes are present along the southern coast (Fig. 1). The line connecting the greatest depths in cross sections (i.e., the thalweg) is located closer to the southern coast. A slight (less than 10 m) cross-gulf bottom rise between Tallinn and Helsinki separates the two (western and central) deeper basins.

We performed six surveys along the thalweg of the gulf during the winter of 2011–2012 and the spring of 2012 onboard the R/V *Salme*, which belongs to the Marine Systems Institute at Tallinn University of Technology. Specifically, these six surveys were performed on 21 December (2011), 24–25 January, 7–8 February, 29 February, 15–16 March and 8 May (2012). The ten sampling stations, designated A1 through A10, were located in the western and central parts of the gulf (Fig. 1). The westernmost station, A1, was located near the western end of the gulf, and station A10 was located approximately 130 km east of station A1, exceeding the bottom elevation near Tallinn–Helsinki. The distances between the stations varied within a range of 10–17 km.

At all of the stations, vertical profiles of the temperature, salinity and dissolved oxygen were recorded, using a Sea-Bird SBE 19*Plus* V2 CTD SEACAT profiler equipped with the dissolved oxygen sensor SBE43. No dissolved oxygen profiles were recorded on 8 May; only the bottom oxygen concentrations were acquired during that cruise. The quality of the salinity data was checked against the water sample analyses using a high-precision salinometer, the 8410A Portasal (Guildline). The Sea-Bird SBE 19*Plus* CTD profiler overestimated the salinity by an average of 0.041 g kg^{-1} . The dissolved oxygen sensor was calibrated against water sample analyses. The dissolved oxygen concentration in bottle samples was measured using the OX 4000 L meters (WWR

International, LLC). In all, 60 data pairs were used to find the best linear fit between the dissolved oxygen (DO) values obtained using the SBE43 and those obtained from the sample analyses. That linear fit is given by the equation $\text{DO} = \text{DO}_{\text{SBE}} \times 1.41$ ($r^2 = 0.99$), where DO_{SBE} is the dissolved oxygen recorded using SBE43 sensor. The accuracy of SBE43 is 2 % of saturation. The OX 4000 L meter has accuracy of 0.5 % of the measured value within the temperature range +5 to +30 °C. Measurements for lower temperatures can be less precise.

2.1.1 Autonomous recording

We installed two buoy stations with acoustic Doppler current profilers (ADCP, 300 kHz; Teledyne RD Instruments) on the seafloor at the locations of stations A3 and A9; the seafloor at those locations was at depths of 91 m and 87 m, respectively. These current profilers were set to collect measurements in 40 and 38 vertical bins, respectively, in 2 m depth increments. The shallowest bin was at a depth range of 7–9 m, and the deepest was at a range of 85–87 m and 81–83 m. A Seabird SBE 16*Plus* V2 CTD SEACAT conductivity and temperature recorder with the SBE43 dissolved oxygen sensor was also deployed at station A3. The recorder was set at a depth of 86 m (5 m above the seafloor). The current profilers were set to take measurements at intervals of 30 min, and the SBE 16 recorded data at 1 h intervals. The dissolved oxygen sensor was calibrated against the results of the water sample analyses ($r^2 = 0.99$).

2.1.2 Wind and sea level data, NAO index

The wind data were obtained near the thalweg at Tallinnamadal Lighthouse (Fig. 1). The wind speed and direction were measured at an elevation of 36 m above the sea surface and were reported as hourly averages. The wind speed was multiplied by a height correction coefficient of 0.91 (Lau-niainen and Saarinen, 1984) to reduce the recorded wind speed to that of the reference height of 10 m during neutral atmospheric stratification. In addition, we used the wind data time series (1981–2012) from the Kalbådagrund weather station (Finnish Meteorological Institute), because the time series at Tallinnamadal was too short for certain analyses. The wind speed and direction data from Kalbådagrund was available every third hour as a 10 min average. Keevallik and Soomere (2010) found slight differences, both in wind direction and speed, between Tallinnamadal and Kalbådagrund. In the present study, we used the data from the Tallinnamadal station as the primary descriptor of the wind characteristics in the western gulf during the study period. The wind velocity components were calculated along the axis from SSW to NNE, with positive values corresponding to NNE. The winds from the SSW are most favorable for estuarine circulation reversal, and those from the NNE the most favorable for estuarine circulation (Liblik and Lips, 2011).

Hourly sea level data were obtained from the Kunda coastal station (Estonian Hydrological and Meteorological Institute), located on the southern coast of the Gulf of Finland. The sea level values in Estonia are relative to the long-term mean (0 cm).

The NAO index (Jones et al., 1997) data (<http://www.cru.uea.ac.uk/~timo/datapages/naoi.htm>) were used to characterize the airflow during the study period and compare it with the long-term data.

2.2 Calculation procedures

The acquired salinity data expressed as values on the practical salinity scale (Fofonoff and Millard Jr., 1983) were multiplied by 1.0047 (Millero et al., 2008) and presented as values of absolute salinity (g kg^{-1}).

The ADCP velocity, sea level and wind data were filtered using a 36 h cutoff Butterworth filter (Butterworth, 1930).

The areas and volumes of hypoxic near-bottom waters (oxygen concentration $\leq 90 \mu\text{mol L}^{-1}$) were estimated from the O_2 profiles taken on the transect located along the thalweg, assuming that cross-transect changes are small. Using the gridded topography by Seifert et al. (2001), the observed upper boundaries of the hypoxic layer were extrapolated across the transect and interpolated along the transect. The area of sea used in the numerical integration was bounded by the western border of the Gulf of Finland and the easternmost station, A10. This region has a surface area of approximately $10\,000 \text{ km}^2$ and volume of approximately 450 km^3 . In a similar manner we also calculated the bottom area and volume of the water with a salinity of $\geq 9.3 \text{ g kg}^{-1}$.

3 Results

3.1 Wind conditions

Prior to the start of our observation campaign on 21 December 2011, weak to moderate winds from various directions blew during the first 20 days of November (Fig. 2). From the last 10 days of November until the end of December, the wind conditions in the study area were shaped by strong air flow from south and southwest, reaching a maximum wind speed of 25 m s^{-1} on 26 December. Variable and weaker winds prevailed during the first half of January. The second half of January was shaped by a high atmospheric pressure system, resulting in low air temperatures and calm wind conditions. Southeasterly and southwesterly winds prevailed in February, and southwesterly winds prevailed in March. However, the prevailing winds in February–March were frequently interrupted by northerly winds or calm periods. Only in mid-February was there a long period of continuous southeasterly and southwesterly winds. As is typical of the spring, variable and weaker winds were observed from April until the end of the study period.

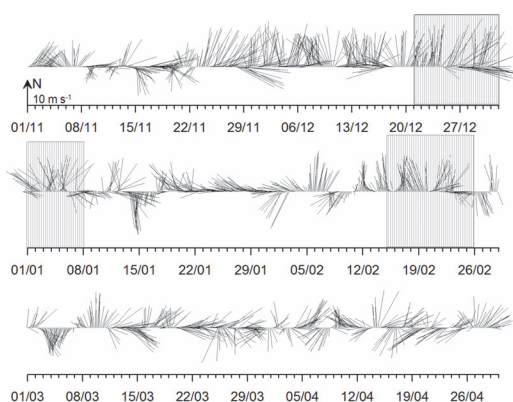


Fig. 2. Time series of the 10 m level Tallinnmadal wind vector from 1 November 2011 to 30 April 2012. Shaded areas mark time intervals when estuarine circulation reversals prevailed.

3.2 CTD and O_2 transects along the thalweg

A weakly stratified water column was observed on 21 December (Fig. 3). The density difference between the near-bottom and surface water did not exceed 0.7 kg m^{-3} along the thalweg. At stations A2–A7, the density difference was 0.3 kg m^{-3} or less. The salinity along the entire section was relatively low: it exceeded 7.0 g kg^{-1} only in the near-bottom layer at the westernmost station, A1, and at stations A8–A10. The east–west salinity gradient in the surface layer was relatively weak, and the salinity varied from 6.2 – 6.3 g kg^{-1} in the easternmost part to 6.4 – 6.5 g kg^{-1} in the westernmost part. The temperature clearly exceeded the maximum density temperature in the entire section and varied in the range of 5.8 – 7.1°C . The water column in the entire section was well oxygenated, and even near the seafloor the oxygen concentration at all stations exceeded $220 \mu\text{mol L}^{-1}$ (5 mL L^{-1}).

On 24–25 January, a well-defined deep saltwater wedge was observed at stations A1–A6, separated from the upper mixed layer by a strong halocline. The salinity above the halocline varied in the range of 6.4 – 6.8 g kg^{-1} , while salinity up to 9.9 g kg^{-1} was observed in the deep layer. This halocline was relatively sharp: for example, a salinity increase from 6.8 to 9.8 g kg^{-1} was observed between depths of 75 and 76.5 m at station A4. The vertical salinity distribution at the eastern stations (A7–A10) was clearly more uniform. The temperature varied in the range of 3.1 – 6.0°C , increasing with depth and decreasing eastward. The oxygen conditions in the section were strongly related to the extent of the salt wedge. The water column above the salt wedge was well oxygenated: the oxygen concentrations were $> 360 \mu\text{mol L}^{-1}$ (8 mL L^{-1}). As a result of the salt water intrusion, the bottom water was hypoxic at stations A1–A6, while the water was nearly fully saturated with oxygen at stations A7–A10.

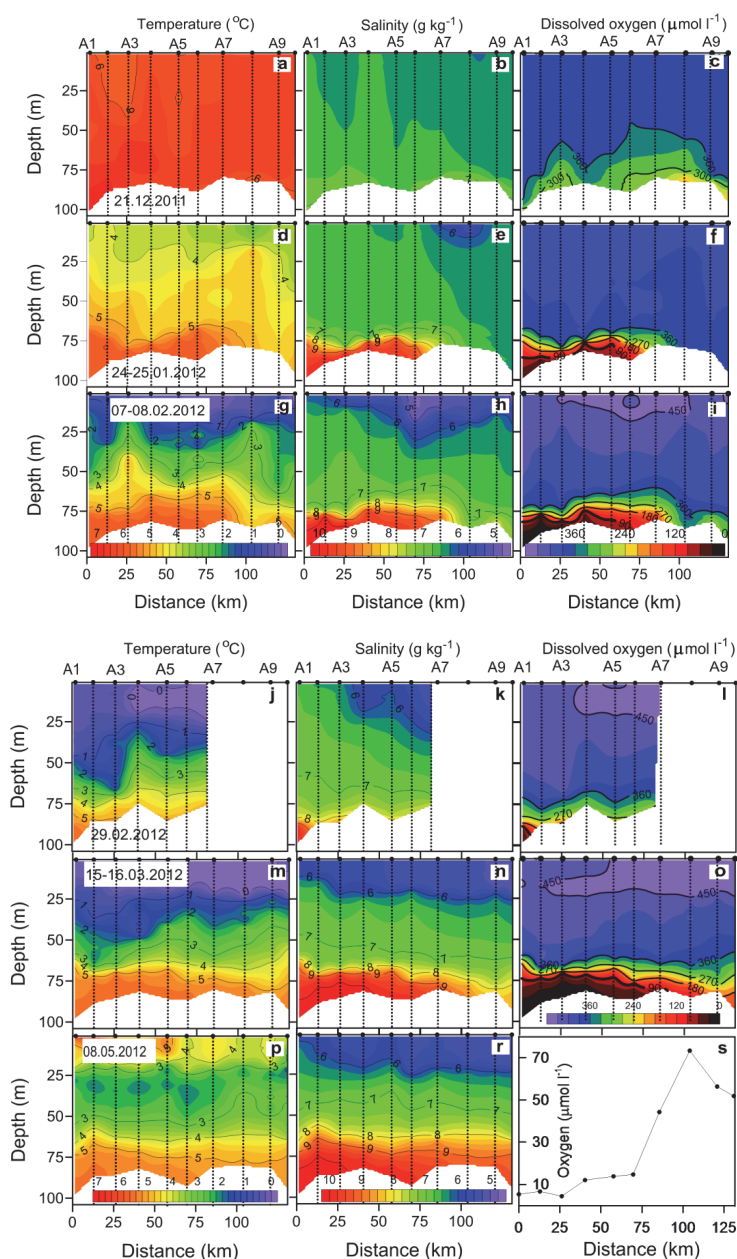


Fig. 3. Vertical sections of temperature (interval 0.25°C), salinity (interval 0.25 g kg^{-1}) and dissolved oxygen (interval $30\text{ }\mu\text{mol L}^{-1}$) on 21 December 2011 (a, b, c), 24–25 January 2012 (d, e, f), 7–8 February (g, h, i), 29 February (j, k, l), 15–16 March (m, n, o) and 8 May (p, r) measured along the thalweg of the gulf. A thick contour line marks the dissolved oxygen concentration of $90\text{ }\mu\text{mol L}^{-1}$. On 8 May, only near-bottom layer dissolved oxygen concentrations were available (s). Values on the x axis indicate distance from the westernmost station (see Fig. 1).

Consequently, the near-bottom oxygen levels were higher even at the easternmost stations compared to levels recorded during the previous survey.

Two weeks later, by 7–8 February, the deep saltwater wedge was observed approximately 15 km east of its former position. A slight increase in salinity was also observed at the three easternmost stations. The development of a near-surface halocline was observed in the upper part of the water column at a depth of 10–20 m at all of the stations. The surface-layer water temperature varied in the range of -0.2 – 0.8 °C. Its salinity was in the range of 4.7 – 5.5 g kg $^{-1}$ at stations A3–A10, while the temperature and salinity were 0.8 – 0.9 °C and 6.0 g kg $^{-1}$, at the two westernmost stations. The oxygen content of the near-bottom layer was slightly depressed along the entire section, but the oxygen concentrations still exceeded 270 $\mu\text{mol L}^{-1}$ (6 mL L $^{-1}$) throughout the water column in the eastern part of the study area.

On 29 February, the section was not fully surveyed, due to heavy ice conditions. The available data from the western part of the section indicated westward movement of a deep layer salt wedge. The halocline was still evident at the westernmost station, A1, where the salinity exceeded 9 g kg $^{-1}$. The density difference between the bottom and surface water exceeded 1 kg m $^{-3}$ at all of the stations where measurements were taken. Similar to conditions in the deeper layer, the near-surface halocline had weakened and was absent from the upper part of the water column at certain stations. The surface-layer salinity still exhibited a strong decrease toward the east, decreasing from 6.8 g kg $^{-1}$ at station A1 to 5.2 g kg $^{-1}$ at station A7. The surface-layer temperature was below 0 °C at stations A4–A7, while it was slightly over 0 °C at the westernmost stations, A1–A3. With the exception of the near-bottom layer at station A1, the oxygen concentration exceeded 90 $\mu\text{mol L}^{-1}$ at all of the stations.

By 15–16 March, both of the haloclines had reformed. The saltwater wedge in the deep layer and the fresher water in the upper layer were evident at all of the stations. The salinity decreased eastward from 5.8 (station A1) to 5.0 g kg $^{-1}$ (station A10) in the upper layer and from 10.2 to 8.4 g kg $^{-1}$ in the near-bottom layer, respectively, at those two stations. The temperature increased from 0 °C near the surface to 5.5 °C in the near-bottom layer. The reappearance of the hypoxic salt wedge affected the deep water oxygen content across the entire section. However, at the easternmost stations, A8–A10, the water in the bottom layer still contained oxygen at a concentration over 90 $\mu\text{mol L}^{-1}$. Compared to the situation on 7–8 February, the hypoxic water layer above the bottom was thicker. In the western half of the section, the oxygen concentration had decreased below 90 $\mu\text{mol L}^{-1}$ below a depth of 71–74 m.

The water with oxygen saturation up to 107 % was observed on 7–8 February, 29 February and 15–16 March in the upper layer where temperature was ≤ 0 °C. The observed high saturation was likely caused by the growth of phytoplankton. Chlorophyll *a* fluorescence (data not shown) was

also higher in the same layer. High fluorescence values were not observed throughout the whole water column in previous cruises.

The last survey along the thalweg was conducted at the end of the study period, on 8 May. The upper layer temperature has increased to 4 – 5 °C. The cold intermediate layer was positioned between depths of 20 and 50 m. In comparison to the previous survey, the salinity in the upper 35 m layer exhibited minor changes. The upper layer halocline was positioned at a depth of 25 m. The deep layer of saline water had extended across the entire section, such that the deep water halocline was observed between depths of 65 and 75 m. The isohaline of 7 g kg $^{-1}$ had risen from a depth of 50–60 m to 40–50 m depth between the two surveys, which indicates the eastward transport of the lower layer water. The density difference between the surface and bottom layers exceeded 3 kg m $^{-3}$ at all of the stations. The oxygen distribution was consistent with a deep water salinity distribution, and the near-bottom water was hypoxic at all of the stations. Nevertheless, a slight eastward increase in oxygen, from 4 – 9 $\mu\text{mol L}^{-1}$ (0.1 – 0.2 mL L $^{-1}$) at the three westernmost stations to 54 – 71 $\mu\text{mol L}^{-1}$ (1.2 – 1.6 mL L $^{-1}$) at the three easternmost stations, was still evident.

3.3 Time series of current profiles, temperature, salinity and oxygen

At both of the current measurement sites, the currents were variable and occasionally very strong (Figs. 4 and 5). The average current speeds in the eastern part of study area (station A9) varied from 7.5 cm s $^{-1}$ at an 82 m depth (deepest measured bin) to 11.6 cm s $^{-1}$ at an 8 m depth (shallowest measured bin), while the maximum recorded speeds were in the range of 40 – 56 cm s $^{-1}$ in the upper 30 m and 33 – 40 cm s $^{-1}$ below that depth. At station A3, the average current speed was stronger in the deep layer and upper layer (11 – 13 cm s $^{-1}$) and slightly weaker in the intermediate layer (9 – 11 cm s $^{-1}$). The highest recorded speeds were in the range of 35 – 49 cm s $^{-1}$ at a depth of 26–86 m, while the speeds exceeded 52 cm s $^{-1}$ in the upper part (8–26 m) of the water column. The strongest current, 88 cm s $^{-1}$, was recorded at a depth of 12 m during a southwesterly storm event on 26 December.

The temporal progression of cumulative wind stress indicated that reversal-favorable winds (from the SSW) started on 25 November and lasted until 5 January (Fig. 6). The cumulative wind stress was approximately 11 N m $^{-2}$ d during that period. At the onset of winds, the sea level at Kunda rose from -10 cm to 66 cm (36 h low-pass filtered). The last 18 days of flow reversal (21 December to 8 January) were covered by measurements. The vertical flow structures at both measurement sites were dominated by barotropic outflow opposite to the wind direction from the last 10 days of December through the first half of January (Figs. 4 and 5): during the period of weak haline stratification

(Fig. 3b). During the reversal period beginning on 21 December, the temperature, salinity and dissolved oxygen concentration varied in a relatively narrow range: 5.0–6.6 °C, 6.5–6.8 g kg⁻¹ and 326–380 µmol L⁻¹ (7.3–8.5 mL L⁻¹), respectively. A temperature decrease was evident throughout this period, however, and shorter-period fluctuations with simultaneous changes in salinity were observed: a temperature increase of 0.5 °C was accompanied by a salinity increase of approximately 0.1 g kg⁻¹.

Beginning on 8 January, short-term variations in the wind direction from the south to the northeast were well reflected in the deep layer current, in which the earlier prevailing outflow was temporary replaced by inflow. This period of a variable flow regime ended on 14 January with the help of 1.5 days of a northerly wind impulse and a subsequent period of weaker winds (Fig. 2). The re-establishment of estuarine circulation caused a deep salt wedge intrusion extending to station A3 (Fig. 3e) and an interruption of barotropic flow (Fig. 4). However, the haline stratification and current shear at station A9 (Fig. 5) still remained weak. Inflow prevailed throughout the water column until mid-February and was particularly strong in the deep layer. The re-establishment of estuarine circulation coincided closely with the drop in the sea level in the gulf. In the near-bottom layer, the dissolved oxygen levels during the period of estuarine circulation rarely exceeded 45 µmol L⁻¹ (1 mL L⁻¹), while the salinity varied in a range of 9.4–10.3 g kg⁻¹ (Fig. 6). In contrast with the previous period, the increases in salinity were accompanied by slight decreases in temperature.

The second reversal event was induced by southerly winds beginning in mid-February and peaked after southerly winds prevailed for 12 days; the cumulative wind stress during that period was 2 N m⁻² d. The reversal-favorable winds raised the sea level and altered the estuarine flow in the deep layer. Strong outflow in the deep layer that extended to a 30–40 m depth and simultaneous inflow in the upper layer were observed in the second half of February at station A3, located near the west end of the section (Fig. 4). This event was also evident at station A9, near the east end of the section (Fig. 5), where inflow prevailed in the upper 20 m and outflow prevailed in the rest of the water column. Compared to the strong near-bottom outflow at location A3, the outflow was at a maximum in the middle of the water column and was much weaker at location A9. The second reversal event was not as strong as the one observed in December–January. This reversal event peaked with a dissolved oxygen concentration of 210 µmol L⁻¹ (4.7 mL L⁻¹), while the salinity simultaneously decreased to 8.2 g kg⁻¹. The dissolved oxygen concentration and salinity fluctuated in a relatively wide range during this event and correlated strongly.

As a consequence of a short-duration wind impulse from the north at the beginning of March, inflow reappeared in the deep layer, the sea level dropped and the salt wedge was re-established simultaneously at the buoy station on 3 March. The flow structure at location A3 was multi-layered, with

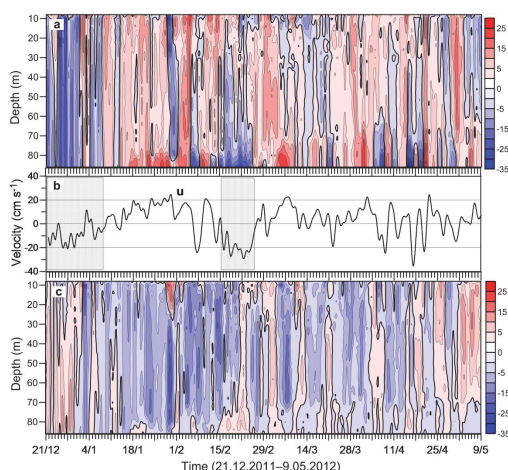


Fig. 4. (a) Temporal progression of vertical distribution of low-pass filtered along-gulf axis current velocity component (u) and (c) cross-gulf axis current velocity component (v) in cm s⁻¹ at the location of mooring station A3 from 21 December 2011 to 9 May 2012. Positive velocities (red) denote the inflow into the gulf or northward flow, and negative velocities (blue) denote the opposite, respectively. (b) Temporal course of along-gulf axis current velocity component (u) at the depth of 85 m. Shaded areas mark time intervals when estuarine circulation reversals were observed at location A3.

the strongest current shear in the deep halocline. The mean flow, however, was to the east over the entire water column. Although we observed short periods of outflow in the deep layer and simultaneous slight decreases and increases in the salinity and oxygen concentration, respectively; the oxygen concentration remained below 45 µmol L⁻¹ (1 mL L⁻¹) until the end of the study period on 8 May. At the same time that the flow was weaker but more persistent at station A9, outflow prevailed in the upper layer and inflow in the deep layer, which, on average, resulted in typical estuarine flow in the eastern part of study area.

3.4 Effects of reversal events on oxygen conditions in the gulf

A hypoxic near-bottom salt wedge, originating in the NE Baltic Proper, penetrated the gulf in the middle of January after a reversal event that had lasted since the end of November. The salt wedge had reached station A6 by 24–25 January, and a similar situation was observed on 7–8 February. On 29 February, during a weaker reversal event, hypoxic water was present only at the westernmost station. It reappeared at station A3 on 3 March. By 15–16 March, the salty and hypoxic water reappeared along the thalweg at stations A1–A7, while the near-bottom oxygen concentration still exceeded

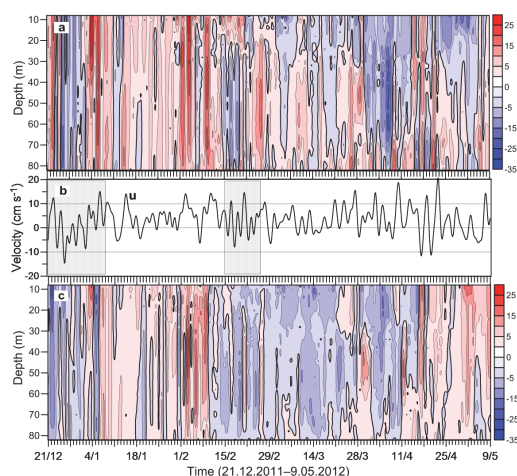


Fig. 5. (a) Temporal course of the vertical distribution of low-pass filtered along-gulf axis current velocity component (u) and (c) cross-gulf axis current velocity component (v) in cm s^{-1} at the location of mooring station A9 from 21 December 2011 to 9 May 2012. Positive velocities (red) denote the inflow into the gulf or northward flow, and negative velocities (blue) denote the opposite, respectively. (b) Temporal course of along-gulf axis current velocity component (u) at a depth of 85 m. Shaded areas mark time intervals when estuarine circulation reversals prevailed.

$90 \mu\text{mol L}^{-1}$ at the three easternmost stations. The thickness of the hypoxic water column had increased compared to the situation during previous cruises. On 8 May, hypoxic water was present at all of the stations, but the oxygen concentrations were still slightly higher in the eastern part of the study area than in the western part.

The oxygen concentrations within and below the halocline were strongly related to the salinity: the estimated areas and volumes occupied by hypoxic water and water with a salinity $\geq 9.3 \text{ g kg}^{-1}$ showed correlations with values of $r^2 = 0.99$ and $r^2 = 0.98$, respectively ($n = 5$; $p < 0.01$). The estimated bottom area covered by hypoxic water (Table 1) was $> 1300 \text{ km}^2$ on 15–16 March (the case of normal estuarine circulation), whereas the area was nearly hypoxic-free even during the relatively weak reversal event in February. The hypoxic area and volume were even greater after the spring bloom on 8 May.

4 Discussion

The surveying along the thalweg and the time-series observations of the near-bottom layer revealed high variability in the thermohaline structure and oxygen concentration in the Gulf of Finland. We found that the vertical flow structure, particularly the bottom current, is the most important fac-

Table 1. Estimated hypoxic bottom areas and hypoxic water volumes. On 8 May hypoxic values were calculated on the basis of bottom oxygen concentrations and salinity profiles: linear regression between sea areas and volumes occupied by hypoxic water and by water with salinity $\geq 9.3 \text{ g kg}^{-1}$ was used in estimation. Area under consideration (approximately $10\,000 \text{ km}^2$) was between the western border of the Gulf of Finland and the easternmost station, A10 (Fig. 1).

Cruise	Hypoxic area (km^2)	Hypoxic water volume (km^3)
21 Dec	0	0
24–25 Jan	510	2.6
7–8 Feb	770	4.9
29 Feb	130	0.8
15–16 Mar	1380	12.0
8 May	1650	14.6

tor shaping the deep water characteristics in the winter: the oxygen conditions in the bottom layer of the gulf can be explained by spatiotemporal variability of the salt wedge. We observed two estuarine circulation reversal events with durations of 1.5 and 0.5 months, in December–January and February, respectively. As a consequence, the stratification was greatly weakened, the current structure was altered and the hypoxic salt wedge disappeared during those events. Our observations revealed that differential advection in case of temporary estuarine reversal (anti-estuarine straining) is an important factor for the stratification disappearance, as suggested earlier by Elken et al. (2003) and Elken et al. (2013). Unfortunately, within the present study it was not possible to establish the balance of different advection and diffusion terms during rapid changes of stratification because of the long time interval between the along-thalweg mappings and missing information on transverse flow and density structures.

These halocline disappearance and reappearance events coincided with the presence of strong near-bottom currents. The re-establishment of a deep layer salt wedge may occur very rapidly, within 12 h. The reactivations of estuarine circulation were associated with a strong inflow and reversal event in February that began with strong outflow in the deep layer. However, when the reversal drastically weakened the stratification (as in December–January) upwind barotropic flow along the thalweg was also observed, and the current shear maximum disappeared together with the halocline. The current structure in the deep layer of the gulf has not been rigorously studied, but strong near-bottom currents appear to be a common feature of the gulf (Almroth et al., 2009; Lagemaa et al., 2010; Liblik and Lips, 2012). Strong wind-induced currents in the deep layer have also been observed in other estuaries, such as in the Long Island Sound (Whitney and Codiga, 2011). The observed upwind barotropic flow along the thalweg allowed for us to assume a temporary wind-induced

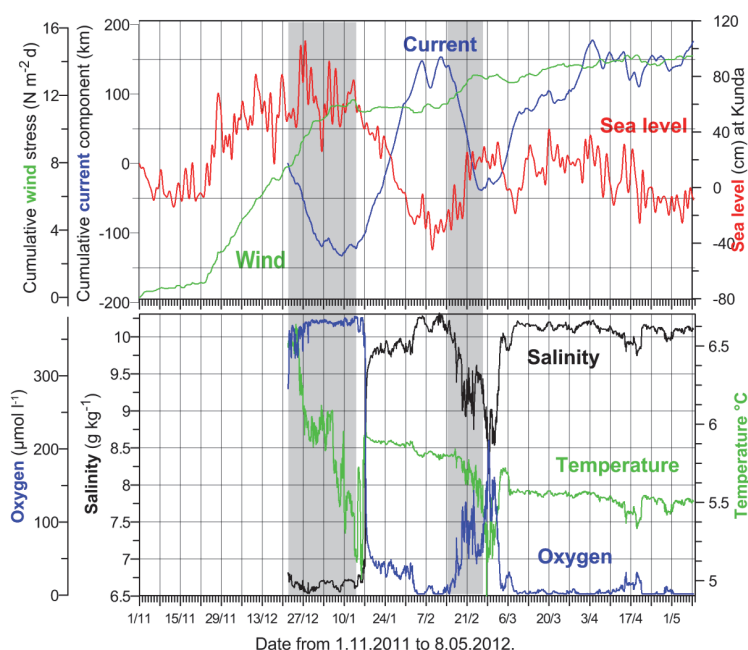


Fig. 6. Cumulative along-gulf axis current velocity component (km, blue line), cumulative wind stress ($\text{N m}^{-2} \text{d}$, green line) and low-pass filtered sea level (cm) time series in the upper panel. Hourly time series of salinity (g kg^{-1} , black line), temperature ($^{\circ}\text{C}$, green line) and dissolved oxygen ($\mu\text{mol L}^{-1}$, blue line) in the lower panel. Temperature, salinity, dissolved oxygen and current were measured at location A3 from 21 December 2011 to 8 May 2012 at a depth of 85 m (approximately 5 m above the seafloor). Wind and sea level measurements were obtained at Tallinnamadal Lighthouse and Kunda coastal station, respectively. Shaded areas mark time intervals when estuarine circulation reversals prevailed.

two-cell circulation in the Gulf: a well-developed reversal event resulted in downwind barotropic flow along the shores and upwind barotropic compensation flow along the thalweg, as is typical in semi-enclosed homogeneous basins (e.g., Sanay and Valle-Levinson, 2005). Further investigation of this theory is warranted.

The shifts in the flow regime of the deep layer were highly dependent on wind forcing. We found the best correlation ($r^2 = 0.44$, $p < 0.01$, $n = 3323$) between the low-pass filtered (36 h) NNE wind and an easterly longitudinal inflow current in the deep layer when a time lag of 18 h was taken into account. This lag is slightly longer than the lag used by Elken et al. (2003), who applied a 15 h offset in their experimental model. Cumulative wind stress of approximately $1 \text{ N m}^{-2} \text{d}$ was required to start the second reversal event, but weak wind ($-0.2 \text{ N m}^{-2} \text{d}$) preceded both estuarine circulation reactivation events. Once estuarine circulation was established, it was well maintained by gravitational forcing without the supporting wind forcing: e.g. the period between two reversal events from mid-January to mid-February (see Fig. 6). Moreover, the estuarine circulation is able to withstand the reversal of

favorable winds to a certain extent. Elken et al. (2003) found that the estuarine circulation may be altered if the southwesterly wind component exceeds the mean value by at least $4\text{--}5.5 \text{ m s}^{-1}$.

The strength of the stratification depended primarily on the presence of the halocline in the deep layer due to the salt wedge intrusion and on the presence of a near-surface halocline in the upper layer due to relatively fresher water in the surface layer. The simultaneous appearance of salty water in the deep layer and fresher riverine water in the surface layer has been observed in a transverse (north–south) section in the summer (Lips et al., 2009). However, in the summer the effect of this phenomenon on the stratification is not as drastic (Liblik and Lips, 2012), because the water column is also thermally stratified. The wind-driven impact on estuarine circulation and respective changes in stratification were also observed in Liverpool Bay (Simpson et al., 1990), in Chesapeake Bay (Scully et al., 2005; Li and Li, 2011) and in the Rio de la Plata estuary (Meccia et al., 2013). In our study, during the reversal events the density difference between the near-bottom and surface water declined below 0.3 kg m^{-3} ,

whereas it exceeded 3 kg m^{-3} when estuarine circulation prevailed. Thus, a well-developed reversal event may result in the complete mixing of the water column. The reversal event most likely peaked, and complete mixing occurred between the two cruises on 22 December and 24–25 January. The water column was completely mixed and saturated with oxygen (98 %) at the two easternmost stations on 24–25 January while the salt wedge was already present at the rest of the stations. To our knowledge, with the exception of the sill-separated Gulf of Bothnia (Håkansson et al., 1996), such a complete mixing event has never been observed in the deep basins of the Baltic Sea.

Based on the wind statistics and analysis of routine CTD measurements in the Gulf of Finland, the winter reversal events occur often and have been occurring with increasingly greater frequency since the 1990s (Elken et al., 2013). However, the approximately 1.5 month-long reversal event observed in December–January was an unusually large event. To evaluate the probability of such a reversal event, we briefly analyzed the NAO index data since 1822 and the autumn–winter Kalbådgrund wind data since 1981. The NAO index of 3.20 in December 2011 clearly exceeded the long-term mean of 0.31 for December. The monthly NAO index in December has exceeded 3.20 only seven times since 1822, most recently in December 1986. Monthly NAO index values ≥ 3.20 in January and February have been more common; 15 and 25 such instances were recorded during January and February, respectively, since 1822. The mean monthly NAO index of 1.72 in September–November 2011 was clearly higher than the long-term mean of -0.31 . Only in five years since 1822 has the mean NAO index been higher than 1.72, indicating that airflow from the southwest was exceptionally intense in autumn 2011. The strong relationship between NAO and oxygen conditions has also been detected in the eastern part of the gulf (Eremina et al., 2012). Temperature and salinity profiles developed in the study area (stations A1 and A6, unpublished data) have suggested that the haline stratification was already weakened in September–October. The monthly averages of the wind component from SSW to NNE in Kalbådgrund in November 2011 and January–April 2012 were close to the long-term means (1981–2012) and varied in a range from -0.3 m s^{-1} to 2.2 m s^{-1} . However, December 2011 was extraordinary, when the monthly mean wind component was 7.6 m s^{-1} , which exceeds by far the long-term mean of 2.0 m s^{-1} for that month and indicates a clearly dominant SSW wind. Until December 2011, the highest monthly mean SSW wind speed favorable for reversal since 1981 was 6.2 m s^{-1} , which was recorded in November of 1982 and 1986.

The oxygen content and salinity were strongly related, as clearly revealed by a coinciding halocline and oxycline. The longitudinal excursions of the salt wedge defined the strength of the vertical stratification and near-bottom oxygen content locally (Fig. 7). During the first reversal event, the stratification was weak and the near-bottom water was well

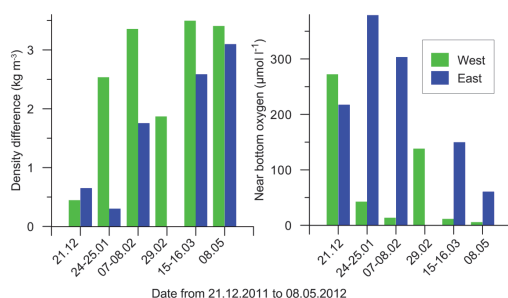


Fig. 7. Average density difference between near-bottom and surface water (kg m^{-3} , left panel) and oxygen concentration in the near-bottom layer ($\mu\text{mol L}^{-1}$, right panel) at westernmost stations A1–A3 (green) and easternmost stations A8–A10 (blue) from 21 December to 8 May. On 29 February, only the western part of the section was visited.

oxygenated ($366 \mu\text{mol L}^{-1}$ or 8.2 mL L^{-1} on average) in the deep layer in the western part of the study area. The same tendency was observed in the case of the relatively weak reversal event observed in February. During periods of estuarine circulation, the stratification increased and the oxygen concentration was clearly under $90 \mu\text{mol L}^{-1}$. The estimated bottom area covered by hypoxic water was $> 1300 \text{ km}^2$, and the volume of this water was approximately 12 km^3 in mid-March (Table 1, Fig. 8). The near-bottom oxygen concentrations were even lower and the estimated hypoxic area and volume were greater on 8 May. With respect to the cross-gulf inclination of the halocline (Lips et al., 2009), our hypoxic area estimations are slightly underestimated rather than overestimated, given the fact that the thalweg of the gulf (our study section) is closer to the southern coast.

The intensification of estuarine circulation often causes improvement in the near-bottom oxygen conditions in estuarine environments due to the import of oxygen-rich ocean waters (e.g., Sato et al., 2012). In this respect, the Gulf of Finland is an unusual marine system, because the imported open sea waters are often depleted of oxygen and the intensification of estuarine circulation leads to an increase in the hypoxic water area and volume. A similar estuarine system is found in the lower St. Lawrence estuary, where the bottom water, isolated from the upper layer by a permanent halocline, has to travel several years before it arrives at the estuary (Gilbert et al., 2005). Because the hypoxic water originates in the intermediate layer of the Baltic Proper, the oxygen conditions there often determine the oxygen conditions in the Gulf of Finland as well. Conley et al. (2002) found that so-called stagnation periods lead to oxygen deficiency in the deep layer of the Baltic Proper, whereas the intermediate layer contains more oxygen during such periods. The long-duration period of stagnation in the 1980s caused a weaker halocline (Liblik and Lips, 2011) and higher deep

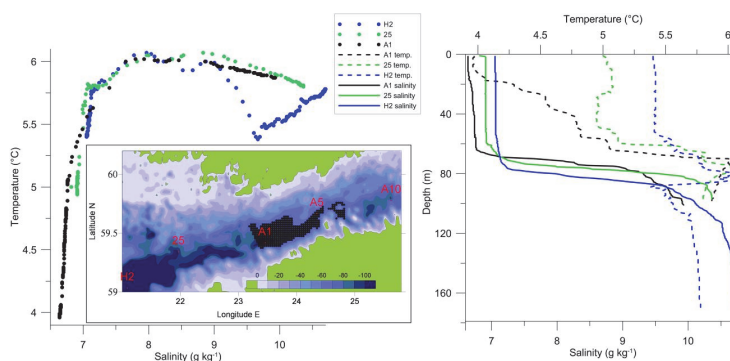


Fig. 8. TS-diagrams (dots on left panel), temperature ($^{\circ}\text{C}$, dashed lines on right panel) and salinity profiles (g kg^{-1} , solid lines on right panel) on 24–25 January and hypoxic area (black area on left panel) on 15–16 March. TS-diagrams and profiles at station H2 (blue), 25 (green) and A1 (black). Hypoxic area was estimated only between the western border of the Gulf of Finland and the easternmost station, A10 (Fig. 1). The bottom topography is drawn from the gridded topography in meters (Seifert et al., 2001).

layer oxygen concentrations (HELCOM, 2009) in the Gulf of Finland, while the oxygen conditions in the deep layer of the Baltic Proper deteriorated during the same period. The inflow from the North Sea therefore has an oxygenation effect opposite to that of the deep layer of the Gulf of Finland and the Baltic Proper.

The reversal events had longer-lasting effects on the oxygen conditions in the deep layer in the eastern part of the study area (Fig. 7). On 15–16 March, two months after the reappearance of the hypoxic salt wedge in the western part of the gulf, the three easternmost stations in the study area were still hypoxic-free. Elken et al. (2013) found that the stratification collapse events occur frequently in the central part of the gulf in the winter. Our results indicate that relatively weak stratification and well-oxygenated water in the central part of the gulf may occur simultaneously with a hypoxic salt wedge in the deep layer in the western part of the gulf (Fig. 7). This pattern may be related to the topography of the gulf: a slight (up to 10 m) bottom rise located in the area around station A7 (Fig. 1). This slightly shallower section of the thalweg impeded the eastward spread of the salt wedge. However, if the thickness of the salt wedge was sufficient, as on 8 May, then it penetrated farther to the east and occupied the bottom layer along the entire thalweg. Furthermore, the eastward advection of the salt wedge can lead to hypoxic conditions even in the eastern part of the gulf (i.e., the Russian waters of the gulf between Kotlin and the Hogland Islands) (Eremina et al., 2012).

During the cruise of 24–25 January, we also acquired CTD profiles at two stations in the northern Baltic Proper: estonian National Monitoring Station 25, at a depth of 100 m, and the international 170 m-deep monitoring station H2 (Fig. 8). The hypoxic saltwater wedge at station 25 was approximately 20 m thick and was situated in a depth range from 80 m to

the bottom. The hypoxic water there seemed to be a mixture of two waters: saltier and slightly colder water originating from the area of station H2 at a depth range of 110–115 m and warmer water from the upper part of the halocline. The hypoxic deep layer found at westernmost station A1 was a mixture of salty near-bottom water from station 25 and fresher, warmer water. This fresher, warmer water evidently also originated outside the Gulf of Finland, as the water column temperature was below 6°C in the gulf at that time. Thus, the deep water salt wedge observed in the study area on 24–25 January after a major reversal event originated in the northern Baltic Proper at a depth range of 110–115 m. This depth most likely was deeper than normal due to the seasonal weakening and descent of the halocline in the northern Baltic Proper (Matthäus, 1984). In addition, Elken et al. (2006) found that the counter-estuarine transport in the Gulf of Finland reduces the vertical stability and decreases the halocline in the NE Baltic Proper.

The current structure in the deep layer during development of the second reversal event (Fig. 4) indicated that the weakening of the halocline and oxygenation of the bottom water were most likely related to the horizontal advection. For confirmation, we plotted salinity–oxygen diagrams and profiles before the reversal event (7–8 February) and during the reversal event (29 February) at station A3 (Fig. 9). Based on the consecutive salinity and oxygen profiles, the saltier and hypoxic water disappeared from the deep layer at A3 station by 29 February, whereas an increase in the salinity and decrease in oxygen were not observed in the layer above (10–70 m). Thus, pure vertical mixing could not have caused this disappearance. This fresher, oxygenated bottom water originated from the eastern part of the thalweg: the deep layer water at station A3 on 29 February had an oxygen content and salinity similar to that of the deep layer water observed

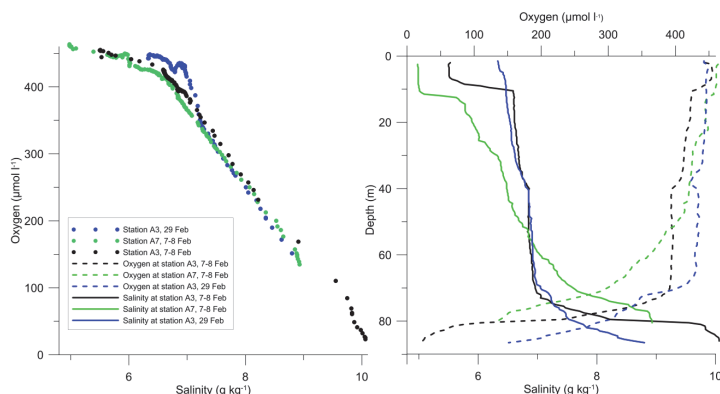


Fig. 9. Salinity–oxygen diagrams (dots on left panel) and salinity (g kg^{-1} , solid lines on right panel) and dissolved oxygen ($\mu\text{mol L}^{-1}$, dashed lines on right panel) profiles on 7–8 February (black) and 29 February (blue) at station A3 and on 7–8 February (green) at station A7.

at A7 station on 7–8 February (see oxygen–salinity plot in Fig. 9). An opposite change in the salinity occurred simultaneously in the upper 10 m layer, but most likely a minor amount of vertical mixing was also involved, as the 10–30 m layer had become fresher. Similar changes in the upper layer salinity were observed in the summer when the southwesterly winds were dominant (Liblik and Lips, 2012). Therefore, the halocline disappearance and oxygenation of the bottom water may be related to the advection of oxygen-rich water from the eastern part of the study area. However, when eastward transport of relatively salty water in the upper layer and westward transport of relatively fresher water in the deep layer last long enough, complete mixing of the water column may occur. The homogenous water column observed at the two easternmost stations on 24–25 January most likely was the consequence of such an event.

The effects related to oxygen depletion clearly impact the biogeochemical cycles in the Baltic Sea (HELCOM, 2009). At the same time as our cruise of 24–25 January, the Estonian national monitoring survey was conducted, and near-bottom water samples were collected for nutrient analysis near the thalweg. The nutrient concentrations clearly differed between the hypoxic and well-oxygenated deep layer waters. The concentrations of NH_4 , $\text{NO}_2 + \text{NO}_3$ and PO_4 in water affected by the hypoxic salt wedge were in the range of 4.2–6.4, 0.1–2.3 and 2.7–4.0 $\mu\text{mol L}^{-1}$, respectively, while the concentrations in the well-oxygenated near-bottom water were in the range of 0.1–0.2, 6.8–8.1 and 0.9–1.0 $\mu\text{mol L}^{-1}$, respectively. These findings confirm earlier conclusions that hypoxic conditions in the near-bottom layer cause the release of phosphorus from the sediment (e.g., Viktorsson et al., 2012), the interruption of the nitrification–denitrification chain and enrichment in ammonium (e.g., Jäntti et al., 2012) in the Gulf of Finland. In these respects, the reversal events affect the nutrient pool in the Gulf of Finland in three ways:

(1) interrupting estuarine transport of phosphate-rich waters from the Baltic Proper (Lips et al., 2008), (2) allowing more efficient diapycnal mixing (Elken et al., 2003) and nutrient transport to the euphotic zone due to weaker stratification (Reissmann et al., 2009), and (3) altering the benthic nutrient dynamics in the gulf (Hietanen and Lukkari, 2007). Thus, the reversal events potentially have an effect on the entire ecosystem of the gulf.

5 Conclusions

The winter temporary reversals of the standard estuarine circulation clearly influence the stratification and oxygen conditions in the Gulf of Finland. As a result of two circulation reversals in winter 2011–2012, the stratification was greatly weakened, the current structure was altered and the hypoxic salt wedge disappeared during the reversal events. The well-developed reversal event (December–January) lasted approximately 1.5 months and caused the complete disappearance of stratification, barotropic flow along the thalweg and nearly homogenous oxygen concentrations throughout the water column. The shifts from estuarine circulation to reversed circulation and vice versa were both associated with strong currents (up to 40 cm s^{-1}) in the deep layer. The vertical stratification and oxygen conditions in the deep layer were defined by longitudinal east- and westward migrations of the salt wedge. The hypoxic salt wedge originated from the NE Baltic Proper at a depth range of 110–115 m. Thus, the deterioration of the deep layer oxygen conditions was solely related to the advective transport of hypoxic water from the NE Baltic Proper. Likewise, the weakening of the halocline and oxygenation of the near-bottom water was most likely related to westward advection along the thalweg. However, long-duration counter-advective transport in the upper and

deep layer most likely caused convection and complete mixing of the entire water column.

The change from oxygenated to hypoxic conditions at the entrance to the gulf occurred very rapidly (within 12 h).

The near-bottom layer of the gulf was nearly hypoxic-free even in instances of relatively weak reversal during February. However, during estuarine circulation periods the estimated bottom area covered by hypoxic water was $> 1300 \text{ km}^2$. Reversal events had longer-lasting effects on the near-bottom oxygen conditions in the eastern part of the study area, where hypoxic-free conditions remained two months after the reappearance of the hypoxic salt wedge in the western part of the Gulf. These conditions most likely were related to the topography of the Gulf: the shallower area between Tallinn and Helsinki along the thalweg may have prevented the salt wedge from spreading farther east. However, if estuarine circulation prevailed long enough, then the salt wedge was able to penetrate farther east and occupy the bottom layer along the entire thalweg.

Acknowledgements. This study was supported by the Estonian Science Foundation (grant Nos. 9278 and 9382) and the EstKliima project, funded by Environmental Protection and Technology Programme No. 3.2.0802.11-0043 of the European Regional Fund. The Finnish Meteorological Institute kindly provided Kalbådagrund wind data, and the Estonian Meteorological and Hydrological Institute the sea level data. We are thankful to A. Trei and F. Buschmann for performing oxygen measurements, T. Kõuts for providing Tallinnamadal wind data and S. Stjopin for providing nutrient data. Likewise, we thank the crew of R/V *Salme*. We thank Urmas Lips for his comments on the methodology. We would like to thank the two reviewers and the editor for their valuable comments.

Edited by: M. Hoppema

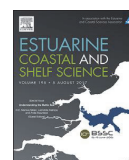
References

- Alenius, P., Myrberg, K., and Nekrasov, A.: The physical oceanography of the Gulf of Finland: a review, *Boreal Environ. Res.*, 3, 97–125, 1998.
- Alenius, P., Nekrasov, A., and Myrberg, K.: Variability of the baroclinic Rossby radius in the Gulf of Finland, *Cont. Shelf Res.*, 23, 563–573, 2003.
- Almroth, E., Tengberg, A., Andersson, J. H., Pakhomova, S., and Hall P. O. J.: Effects of resuspension on benthic fluxes of oxygen, nutrients, dissolved inorganic carbon, iron and manganese in the Gulf of Finland, *Baltic Sea, Cont. Shelf Res.*, 29, 807–818, 2009.
- Bergström, S. and Carlsson, B.: River runoff to the Baltic Sea: 1950–1990, *Ambio*, 23, 280–287, 1994.
- Butterworth, S.: On the theory of filter amplifiers, *Experimental Wireless and the Wireless Engineer*, 7, 536–541, 1930.
- Conley, D. J., Humborg, C., Rahm, L., Savchuk, O. P., and Wulff, F.: Hypoxia in the Baltic Sea and basin-scale changes in phosphorus biogeochemistry, *Environ. Sci. Technol.*, 36, 5315–5320, 2002.
- Conley, D. J., Björck, S., Bonsdorff, E., Carstensen, J., Destouni, G., Gustafsson, B. G., Hietanen, S., Kortekaas, M., Kuosa, H., Meier, H. E. M., Müller-Karulis, B., Nordberg, K., Norkko, A., Nürnberg, G., Pitkänen, H., Rabalais, N. N., Rosenberg, R., Savchuk, O. P., Slomp, C. P., Voss, M., Wulff, F., Zillén, L.: Hypoxia-related processes in the Baltic Sea, *Environ. Sci. Technol.*, 43, 3412–3420, 2009.
- Diaz, R. J. and Rosenberg, R.: Spreading Dead Zones and Consequences for Marine Ecosystems, *Science*, 321, 926–929, doi:10.1126/science.1156401, 2008.
- Elken, J., Raudsepp, U., and Lips, U.: On the estuarine transport reversal in deep layers of the Gulf of Finland, *J. Sea Res.*, 49, 267–274, 2003.
- Elken, J., Mälikki, P., Alenius, P., and Stipa, T.: Large halocline variations in the Northern Baltic Proper and associated meso – and basin-scale processes, *Oceanologia*, 48, 91–117, 2006.
- Elken, J., Raudsepp, U., Laanemets, J., Passenko, J., Maljutenko, I., Pärn, O., and Keevallik, S.: Increased frequency of winter-time stratification collapse events in the Gulf of Finland since the 1990s, *J. Marine Syst.*, doi:10.1016/j.jmarsys.2013.04.015, 2013.
- Eremina, T. R., Maximov, A. A., and Voloshchuk, E. V.: The influence of climate's variability on the deep-water oxygen conditions in the east of the Gulf of Finland, *Oceanologia*, 52, 771–779, 2012.
- Feistel, R., Nausch, G., Matthäus, W., and Hagen, E.: Temporal and Spatial Evolution of the Baltic Deep Water Renewal in Spring 2003, *Oceanologia*, 45, 623–642, 2003.
- Fofonoff, N. P. and Millard, Jr., R. C.: Algorithms for computation of fundamental properties of seawater, *Unesco Tech. Pap. Mar. Sci.*, 44, 1–58, 1983.
- Fonselius, S. and Valderrama, J.: One hundred years of hydrographic measurements in the Baltic Sea, *J. Sea Res.*, 49, 229–241, 2003.
- Gilbert, D., Sundby, B., Gobeil, C., Mucci, A., and Tremblay, G. H.: A seventy-two-year record of diminishing deep-water oxygen in the St. Lawrence estuary: the northwest Atlantic connection, *Limnol. Oceanogr.*, 50, 1654–1666, 2005.
- Haapala, J. and Alenius, P.: Temperature and salinity statistics for the northern Baltic Sea 1961–1990, *Finnish Mar. Res.*, 262, 51–121, 1994.
- Håkansson, B., Alenius, P., and Brydsten, L.: Physical environment in the Gulf of Bothnia, *Ambio Spec. Rep.*, 8, 5–12, 1996.
- Hansen, D. V. and Rattray, M.: New dimensions in estuary classification, *Limnol. Oceanogr.*, 11, 319–326, 1966.
- HELCOM (Helsinki Commission): Eutrophication in the Baltic Sea: an integrated thematic assessment of the effects of nutrient enrichment in the Baltic Sea region, *Baltic Sea Environment Proceedings*, 115, 2009.
- Hietanen, S. and Lukkari, K.: Effects of short-term anoxia on benthic denitrification, nutrient fluxes and phosphorus forms in coastal Baltic sediment, *Aquat. Microb. Ecol.*, 49, 293–302, doi:10.3354/ame01146, 2007.
- Jäntti, H. and Hietanen, H.: The Effects of Hypoxia on Sediment Nitrogen Cycling in the Baltic Sea, *AMBIO*, 41, 161–169, doi:10.1007/s13280-011-0233-6, 2012.
- Jones, P. D., Jonsson, T., and Wheeler, D.: Extension to the North Atlantic Oscillation using early instrumental pressure observa-

- tions from Gibraltar and South-West Iceland, *Int. J. Climatol.*, 17, 1433–1450, 1997.
- Keevallik, S. and Soomere, T.: Towards quantifying variations in wind parameters across the Gulf of Finland, *Est. J. Earth Sci.*, 59, 288–297, 2010.
- Kullenberg, G.: Physical oceanography, in: *The Baltic Sea*, Elsevier Publishing Company, Amsterdam, 135–182, 1981.
- Lagemaa, P., Suhhova, I., Nõmm, M., Pavelson, J., and Elken, J.: Comparison of current simulations by the state-of-the-art operational models in the Gulf of Finland, in: *IEEE Conference Proceedings, IEEE/OES Baltic 2010 International Symposium*, 25–27 August 2010, Riga, Latvia, 1–11, 2010.
- Laine, A. O., Andersin, A.-B., Leiniö, S., and Zuur, A. F.: Stratification-induced hypoxia as a structuring factor of macrozoobenthos in the open Gulf of Finland (Baltic Sea), *J. Sea Res.*, 57, 65–77, 2007.
- Launiainen, J. and Saarinen, J.: Marine wind characteristics in the northern Baltic Sea, *Finnish, Mar. Res.*, 250, 52–86, 1984.
- Li, Y. and Li, M.: Effects of wind on stratification and circulation in a partially mixed estuary, *J. Geophys. Res.*, 116, C12012, doi:10.1029/2010JC006893, 2011.
- Liblik, T. and Lips, U.: Characteristics and variability of the vertical thermohaline structure in the Gulf of Finland in summer, *Boreal Environ. Res.*, 16, 73–83, 2011.
- Liblik, T. and Lips, U.: Variability of synoptic-scale quasi-stationary thermohaline stratification patterns in the Gulf of Finland in summer 2009, *Ocean Sci.*, 8, 603–614, doi:10.5194/os-8-603-2012, 2012.
- Lips, I., Lips, U., and Liblik, T.: Consequences of coastal upwelling events on physical and chemical patterns in the central Gulf of Finland (Baltic Sea), *Cont. Shelf Res.*, 29, 1836–1847, 2009.
- Lips, U., Lips, I., Liblik, T., and Elken, J.: Estuarine transport versus vertical movement and mixing of water masses in the Gulf of Finland (Baltic Sea), in: *IEEE Conference Proceedings, US/EU-Baltic Symposium “Ocean Observations, Ecosystem-Based Management & Forecasting”*, Tallinn, 27–29 May, 2008, IEEE, 2008, (IEEE Conference Proceedings), 1–8, 2008.
- MacCready, P. and Geyer, W. R.: Advances in estuarine physics, *Annual Reviews of Marine Science*, 2, 35–58, 2010.
- Matthäus, W.: Climatic and seasonal variability of oceanological parameters in the Baltic Sea, *Beiträge zur Meereskunde*, 51, 29–49, 1984.
- Matthäus, W. and Lass, H. U.: The recent salt inflow into the Baltic Sea, *J. Phys. Oceanogr.*, 25, 280–286, 1995.
- Meccia, V. L., Simonato, C. G., and Guerrero, R. A.: The Rio de la Plata estuary response to wind variability in synoptic timescale: salinity fields and salt wedge structure, *J. Coastal Res.*, 29, 61–77, 2013.
- Millero, F. J., Feistel, R., Wright, D. G., and McDougall, T. J.: The composition of Standard Seawater and the definition of the Reference-Composition Salinity Scale, *Deep-Sea Res. Pt. I*, 55, 50–72, doi:10.1016/j.dsr.2007.10.001, 2008.
- Reissmann, J. H., Burchard, H., Feistel, R., Hagen, E., Lass, H. U., Mohrholz, V., Nausch, G., Umlauf, L., and Wiczorek, G.: Vertical mixing in the Baltic Sea and consequences for eutrophication – A review, *Prog. Oceanogr.*, 82, 47–80, 2009.
- Sanay, R. and Valle-Levinson, A.: Wind-induced circulation in semiencloded homogeneous, rotating basins, *J. Phys. Oceanogr.*, 35, 2520–2531, 2005.
- Sato, C., Nakayama, K. and Furukawa, K.: Contributions of wind and river effects on DO concentration in Tokyo Bay, *Est. Coast. Shelf Sci.*, 109, 91–97, 2012.
- Savchuk, O. P.: Large-scale dynamics of hypoxia in the Baltic Sea, in: *Chemical Structure of Pelagic Redox Interfaces: Observation and Modelling*, Hdb., Springer Verlag, Berlin Heidelberg, Germany, *Env. Chem.*, 22, 137–160, 2010.
- Scully, M. E., Friedrichs, C., and Brubaker, J.: Control of estuarine stratification and mixing by wind-induced straining of the estuarine density field, *Estuaries*, 28, 321–326, 2005.
- Seifert, T., Tauber, F., and Kayser, B.: A high resolution spherical grid topography of the Baltic Sea – 2nd edition, *Baltic Sea Science Congress*, Stockholm 25–29 November 2001, Poster #147, www.io-warnemuende.de/iowtopo, 2001.
- Simpson, J. H., Brown, J., Matthews, J., and Allen, G.: Tidal straining, density currents, and stirring in the control of estuarine stratification, *Estuaries*, 13, 125–132, 1990.
- Vahtera, E., Conley, D. J., Gustafsson, B. G., Kuosa, H., Pitkänen, H., Savchuk, O. P., Tamminen, T., Viitasalo, M., Voss, M., Wasmund, N., and Wulf, F.: Internal ecosystem feedbacks enhance nitrogen-fixing cyanobacteria blooms and complicate management in the Baltic Sea, *Ambio*, 36, 186–194, 2007.
- Viktorsson, L., Almroth-Rosell, E., Tengberg, A., Vankevich, R., Neelov, I., Isaev, R., Kravtsov, V., and Hall, P. O. J.: Benthic Phosphorus Dynamics in the Gulf of Finland, *Aquat. Geochem.*, 18, 543–564, doi:10.1007/s10498-011-9155-y, 2012.
- Whitney, M. M. and Codiga, D.: Response of a large stratified estuary to wind events: observations, simulations, and theory for Long Island Sound, *J. Phys. Oceanogr.*, 41, 1308–1327, 2011.
- Zillén, L., Conley, D. J., Andrén, T., Andrén, E., and Björck, S.: Past occurrences of hypoxia in the Baltic Sea and the role of climate variability, environmental change and human impact, *Earth-Sci. Rev.*, 91, 77–92, 2008.

Paper V

Lips, U., Laanemets, J., Lips, I., Liblik, T., Suhhova, I., Suursaar, Ü. 2017. Wind-driven residual circulation and related oxygen and nutrient dynamics in the Gulf of Finland (Baltic Sea) in winter. *Estuarine Coastal and Shelf Science*, 195, 4–15.



Wind-driven residual circulation and related oxygen and nutrient dynamics in the Gulf of Finland (Baltic Sea) in winter

Urmas Lips^{a,*}, Jaan Laanemets^a, Inga Lips^a, Taavi Liblik^a, Irina Suhhova^a, Ülo Suursaar^b

^a Marine Systems Institute at Tallinn University of Technology, Akadeemia Road 15a, 12618 Tallinn, Estonia

^b Estonian Marine Institute, University of Tartu, Mäealuse 14, 12618 Tallinn, Estonia



ARTICLE INFO

Article history:

Received 1 February 2016

Received in revised form

7 July 2016

Accepted 4 October 2016

Available online 6 October 2016

Keywords:

Gulf of Finland
Estuarine circulation
Saltwater wedge
Oxygen content
Nutrients

ABSTRACT

Establishment of distinct circulation patterns in the Gulf of Finland was observed by a targeted measurement campaign in winter 2013–2014. Strong and long enough up-estuary wind events caused a collapse of vertical stratification and development of a barotropic flow system consisting of an outflow in the open part and inflow along the coasts. In the periods without such unidirectional wind forcing, but when the water column remained weakly stratified, the residual barotropic inflow in the open gulf and outflow along the coasts was observed. In the case of moderate wind forcing, the three-layer vertical stratification and flow structure developed in the gulf. It is shown that the along-gulf expansion of the fresher water tongue in the surface layer as well as the up-estuary penetration of the saltwater wedge in the near-bottom layer followed well the long-term (monthly) changes in the cumulative along-gulf wind stress. The dynamics of the near-bottom saltwater wedge determined the extent of hypoxic bottoms and, as suggested by the firm correlation between the near-bottom phosphate concentration and salinity, the nutrient conditions in the near-bottom layer. The lateral transport of phosphorus, strengthened vertical stratification in the Northern Baltic Proper and suggested increase in the frequency of stratification collapses in the Gulf of Finland in winter predict that the eutrophication effects would not diminish significantly in this estuary in the nearest future.

© 2016 Elsevier Ltd. All rights reserved.

1. Introduction

The Baltic Sea is a semi-enclosed sea with restricted water exchange with the North Sea. High freshwater runoff from the catchment area and sporadic inflows of saline waters through the Danish Straits maintain vertical stratification in the Baltic Sea (e.g. Leppäranta and Myrberg, 2009). Stratification effectively blocks the direct ventilation of the deeper layers below the quasi-permanent halocline at 60–70 m depth. The deep water is renewed and, thus, the oxygen conditions in the near-bottom layer are improved by spreading of dense waters from saline inflow events (e.g. Matthäus and Franck, 1992). Since the 1980s, the frequency of inflow events has dropped drastically from five–seven to only one major inflow per decade. Widespread anoxic conditions in the deep layers became the usual state in the central Baltic (Mohrholz et al., 2015).

The Gulf of Finland lies in the northeastern part of the Baltic Sea

(Fig. 1). This shallow (mean depth 37 m) and elongated (length about 400 km, width varies 48–135 km) gulf is often considered as an estuary in the Baltic Sea multi-basin brackish water system where tidal oscillations of the sea level are of minor importance (e.g., Kullenberg, 1981). Greater sea depths (exceeding 100 m in the western part) and steeper bottom slopes are characteristic along the southern coast. Therefore, the line connecting the deepest depths on cross-sections (thalweg) is located closer to the southern coast. Slightly shallower depths at the thalweg in the sea area between Tallinn and Helsinki (Fig. 1) separate the western and the central deeper basins of the gulf.

Freshwater is mostly discharged into the eastern part of the gulf through the Neva River with an average runoff of $77.6 \text{ km}^3 \text{ yr}^{-1}$, which is about two-thirds of the freshwater inflow to the Gulf of Finland (Bergström and Carlsson, 1994). As a result, the surface layer salinity (expressed in the present paper according to the Practical Salinity Scale, 1978) increases from about 1 in the easternmost area up to 6–7 at the entrance area (e.g. Haapala and Alenius, 1994). The gulf has a free connection to the Northern Baltic Proper and therefore salinity may increase below the quasi-permanent halocline (located

* Corresponding author.

E-mail address: urmas.lips@msi.ttu.ee (U. Lips).

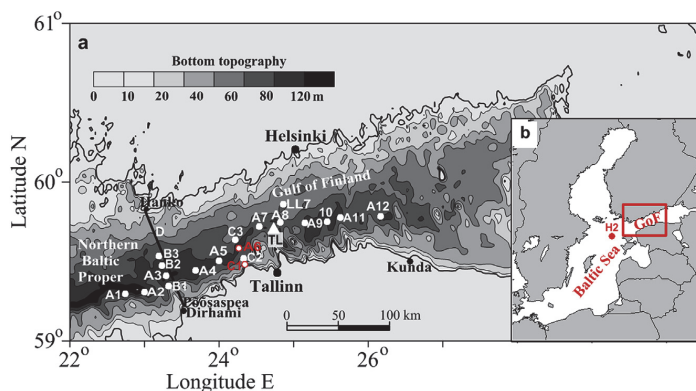


Fig. 1. (a) Map of the study area in the Gulf of Finland with bottom topography (based on Seifert et al., 2001). White dots represent the locations of the CTD stations along the thalweg (A1–A12) and across it (B1–B3 and C1–C3). Red circles coinciding with CTD stations A6 and C1 show the locations of the two bottom-mounted ADCP-s. White triangle marked as TL represents the location of the wind measurements at Tallinnamadal Lighthouse. The western border of the gulf is defined as the line from Pöösaspea–Hanko (bold black line D). (b) A map of the Baltic Sea and location of the HELCOM monitoring station H2 (59.03° N, 21.08° E). (For interpretation of the references to colour in this figure legend, the reader is referred to the web version of this article.)

at a depth of 60–70 m; Alenius et al., 1998) in the western part of gulf up to 10. The seasonal thermocline forms at the beginning of May, develops at the depths of 10–20 m during the summer and starts to erode by the end of August (e.g. Alenius et al., 1998; Liblik and Lips, 2011). During the winter, the water body is well mixed down to the depth of the quasi-permanent halocline (Haapala and Alenius, 1994; Alenius et al., 2003).

Although the physical processes, which control stratification and the renewal of oxygen in bottom waters in the Baltic Sea, have been extensively studied over the decades, there are still some poorly understood issues, including the spreading of hypoxic waters from one sub-basin to another. The inflows of saline water from the North Sea are the main governing factor for the spatial extent and duration of hypoxia in the Baltic Sea as a whole (Conley et al., 2009). However, the sub-halocline oxygen and nutrient conditions in the Gulf of Finland depend also on the dynamics of the saltwater wedge and vertical stratification in this estuarine basin.

Wintertime convection due to the surface cooling, turbulent erosion from surface towards deeper layers and turbulent shear mixing are usually considered as important ventilation processes in the Gulf of Finland (Meier et al., 2006). Elken et al. (2003) showed on the basis of summer CTD measurements in the Gulf of Finland that the significant weakening of haline stratification could occur when the southwesterly (up-estuary) wind forcing causes the reversal of estuarine circulation: the surface layer flows into the gulf and the deep layer flows out. On the contrary, northeasterly and northerly winds support estuarine circulation, resulting in stronger stratification (Elken et al., 2003; Liblik and Lips, 2011) and transport of phosphorus-rich waters from the deeper sub-halocline layers of the Northern Baltic Proper into the gulf (Lips et al., 2008).

Liblik et al. (2013) showed that reversal of the estuarine circulation in the winter 2011–2012 caused the vanishing of stratification and improvement of oxygen conditions (oxygen concentrations over 6 ml l^{-1}) in the entire water column along the thalweg in the western and central gulf. Good oxygen conditions did last more than a month in the deep layer of the western gulf; however, a fast change to hypoxia and strong haline stratification occurred after re-establishment of estuarine circulation due to intrusion of saline and hypoxic water from the Northern Baltic Proper. Elken et al. (2014) found that since the 1990s the frequency and duration of estuarine circulation reversals in the Gulf of Finland have increased due to the shift in wind regime, i.e., the considerable

increase of westerly-southwesterly wind impulse in December–January.

The eutrophication of the Baltic Sea is to a large extent driven by anthropogenic nutrient enrichment. However, it has been noted that despite inputs of nutrients have decreased since the late 1980s, the concentrations of nutrients in the sea have not declined accordingly (HELCOM, 2009). It has been argued that the long residence time of water in the Baltic Sea, the release of phosphorus from anoxic sediments and the blooms of nitrogen-fixing cyanobacteria slow down the recovery from the eutrophied state (Vahtera et al., 2007; HELCOM, 2014). Lukkari et al. (2009) estimated the long-term lower limit of P release as $19 \text{ kg P km}^{-2} \text{ yr}^{-1}$ from poorly oxygenated bottom areas in the Gulf of Finland. Furthermore, Jäntti and Hietanen (2012) showed that nitrogen removal has decreased since the mid-1990s in the Gulf of Finland likely due to the increase of bottom water hypoxia.

The main aim of this study is to describe the wintertime estuarine dynamics in the Gulf of Finland and the changes in the near-bottom oxygen and nutrient conditions induced by the dynamic saltwater wedge. The specific objectives were:

- (1) to describe the vertical and lateral structure of the along-gulf flow in the Gulf of Finland from autumn 2013 to spring 2014 and relate the observed variability to the atmospheric forcing;
- (2) to describe the temporal changes in the along-gulf salinity (density) distribution and vertical stratification and link the observed changes with the alterations in the flow regime (and atmospheric forcing);
- (3) to reveal the changes in the near-bottom oxygen and nutrient conditions caused by the saltwater wedge dynamics;
- (4) to relate the changes in the nutrient concentrations in the surface layer of the gulf to the alterations in flow regime, vertical mixing and other factors.

2. Methods

2.1. CTD surveys and nutrient sampling

Six surveys onboard the RV Salme were performed in the Gulf of

Finland from December 2013 to May 2014: on 9–10 December 2013, and on 9–10 January, 3–4 February, 4–5 March, 3–4 April and 5–6 May 2014. Twelve stations (A1–A12), ten of which were located along the thalweg in the western and central part of the gulf, were sampled six times (Fig. 1). The westernmost stations A1 and A2 were located in the Northern Baltic Proper. The overall length of the along-thalweg transect was approximately 200 km and the distance between the stations varied within a range of 10–30 km. The cross-thalweg transects C (stations C1, C2, A6 and C3) and B (stations B1, B2, A3 and B3) were sampled four (surveys 3–6) and three (surveys 3–5) times, respectively. The distance between the stations on transects B and C varied within a range of 4–7 km.

At all stations, the vertical profiles of temperature, salinity, dissolved oxygen (DO) and chlorophyll *a* (Chl *a*) fluorescence were recorded using an Ocean Seven 320plus CTD probe (Idronaut S.r.l.) equipped with a Seapoint Chl *a* fluorometer. The quality of the salinity data was checked against the water sample analyses using a high-precision salinometer 8410A Portasal (Guildline). Comparison of measured values by CTD and salinometer gave the mean and standard deviation of the difference of salinity measurements of 0.009 ± 0.009 (in total 33 data pairs were used). Thus, we concluded that the Ocean Seven 320plus CTD profiler estimated the salinity with an accuracy of 0.02. The dissolved oxygen sensor was calibrated before each survey and the data quality was checked against water sample analyses using an OX 4000 L DO meter (WWR International, LLC). During each survey from 32 to 52 water samples were analyzed for oxygen content and linear regression line between the results of laboratory analyses and the readings of the oxygen sensor attached to the CTD probe were found. The linear regression line equations varied from $DO_{cal}=DO_{Idronaut} \times 0.978$ to $DO_{cal}=DO_{Idronaut} \times 1.052$ with r^2 varying between 0.990 and 0.997.

During the surveys, water samples for nutrient analyses were collected at each CTD station from 3 to 5 depths – in the surface layer (5 m depth), in the near-bottom layer (about 3–4 m above the seabed), at the depth about 13–14 m above the seabed and in the intermediate layer (1–2 samples). In the shallow areas, water samples were collected in the surface, intermediate and near-bottom layer – one sample in each layer. Dissolved inorganic nutrients PO_4^{3-} and $NO_2^-+NO_3^-$ (NO_x) were determined with the automatic nutrient analyzer Lachat QuikChem 8500 Series 2 (Lachat Instruments, Hach Company) according to the recommendations made by USEPA, ISO, and DIN standards – method 31-107-04-1-D NO_3^- (Egan, 2000) and 31-115-01-1-I PO_4 (Ammerman, 2001). The analyses of NH_4^+ were done manually according to Grasshoff et al. (1999). The lower detection range for PO_4^{3-} and $NO_2^-+NO_3^-$ was 0.03 and 0.07 μM , respectively, and for NH_4^+ it was 0.2 μM .

2.2. Autonomous measurements

The bottom-mounted acoustic Doppler current profilers (ADCP, 300 kHz, Teledyne RD Instruments and RDCP 600, 600 kHz, Aanderaa Data Instruments) were deployed at stations A6 and C1 (Fig. 1). The depths at the mooring locations were 86 m and 21 m, respectively. The current profilers were set to collect measurements in 40 and 10 vertical bins, respectively, with 2-m depth increments. The ADCP sampling interval was 10 min and the RDCP sampling interval was 1 h. The center of the shallowest correct bin was at depths of 8 and 7 m and the center of the deepest correct bin was at depths of 82 and 19 m, respectively. To remove inertial oscillations from the data series, the velocity data were filtered using a 36-h cutoff Butterworth filter (Butterworth, 1930). ADCP current velocity vectors were rotated counter clockwise by 65° to estimate the velocity components corresponding to the along-thalweg and

cross-thalweg flow directions. RDCP current velocity vectors were rotated counter clockwise by 50° to estimate the velocity components corresponding to the along-coast and cross-coast flow directions.

The RDCP deployed in the shallow area (station C1) was equipped with temperature, conductivity, dissolved oxygen and turbidity sensors. A Seabird conductivity and temperature recorder SBE 16Plus V2 CTD SEACAT with a SBE43 dissolved oxygen sensor was deployed about 5 m above the ADCP at station A6, i.e. approximately at the depth of the deepest correct ADCP bin. The SBE 16 recorded data at 1-h intervals. The SBE43 dissolved oxygen (DO_{SBE43}) was calibrated using calibrated Ocean Seven 320plus CTD profiler oxygen (DO) data. The linear fit is given by the equation $DO_{cal} = DO_{SBE43} \times 1.05$ ($r^2 = 0.95$).

2.3. Wind data

We used the wind data measured at Tallinnamadal Lighthouse (Fig. 1). The wind speed and direction were measured at the height of 36 m above the sea level and were reported with 1-h interval (5 min averages). The wind speed was multiplied by a height correction coefficient of 0.91 (neutral atmospheric stratification) to reduce the recorded wind speed to that at the height of 10 m (Launiainen and Saarinen, 1984).

2.4. Hypoxic area and phosphate-phosphorus content

The area of hypoxic near-bottom water (using oxygen concentration ≤ 2.9 mg l^{-1} as the threshold concentration for hypoxia) was estimated from the oxygen profiles measured at the sampling stations along the thalweg, assuming that the cross-transect changes were small. The measured upper boundaries of the hypoxic layer were interpolated between the stations along the transect and then extrapolated across the transect to find the lateral extent of the hypoxic area using the gridded topography (Seifert et al., 2001). Phosphate-phosphorus amount in the near-bottom layer was estimated by calculating the mean measured concentration below the 60 m depth. The mean value of phosphate-phosphorus in each survey was multiplied by the water volume (53 km³) in the selected area below 60 m depth. The western border of the gulf and the longitude corresponding to the sampling station A11 were selected as boundaries when estimating the hypoxic area and volume, and phosphate-phosphorus amount (Fig. 1).

3. Results

3.1. Wind conditions

Weather conditions in winter 2013–2014 were extremely variable. November and December 2013 were unusually stormy. Warm and moist air was brought to the Baltic Sea area by a series of extra-tropical cyclones (including winter storms Hilde, Ivar, Xaver and some others). Based on wind data at the Tallinnamadal Lighthouse, variable winds with speed up to 20 m s^{-1} and along-gulf and cross-gulf components of wind stress varying from -0.5 to 0.8 N m^{-2} and from -0.8 to 0.4 N m^{-2} were observed prior to the first field measurements on 9–10 December 2013 (Fig. 2a). Strong winds (the maximum measured gust wind speed of 25.5 m s^{-1}) with corresponding along-gulf and cross-gulf wind stress of 1.4 and -0.9 N m^{-2} , respectively, were recorded on 13 December. On the same day at the meteorological station Põõsaspea (Estonian Environment Agency; see Fig. 1), the 1-h sustained W-NW wind speed peaked at 20.7 m s^{-1} and wind-gusts exceeded 30 m s^{-1} .

On the second half of December 2013, along-gulf wind impulses

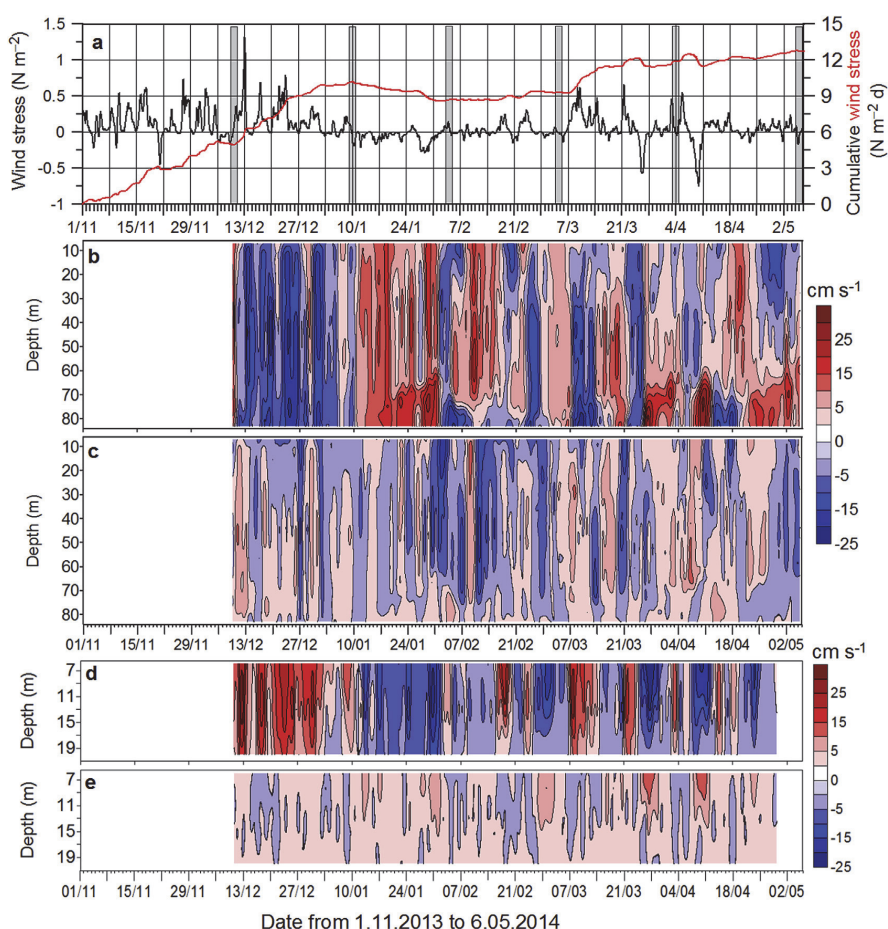


Fig. 2. (a) Time series of along-gulf component of wind stress (black curve, positive eastward) and cumulative along-gulf wind stress (red curve) based on wind data from 1 November 2013 to 9 May 2014 at Tallinnamadal Lighthouse in the Gulf of Finland. Time series of vertical distribution of low-pass filtered (b) along-thalweg and (c) cross-thalweg current velocity component at station A6 from 9 December 2013 to 6 May 2014 and (d) along-coast and (e) cross-coast current velocity component at station C1 from 9 December 2013 to 28 April 2014. Positive values (red) display the inflow to the gulf for the along-gulf component and north-northwestward flow for the cross-gulf (cross-coast) component.

up to 0.75 N m^{-2} were observed. The weather settled to much calmer winter conditions in the middle of January, which brought along sub-zero (-17°C) air temperatures and anti-cyclonic weather conditions with mild or moderate easterly-northerly winds. The along-gulf and cross-gulf wind stresses varied between -0.3 and 0.3 N m^{-2} until the 10 March, whereas the easterly winds prevailed. From the second half of March until the middle of April, strong wind impulses with along-gulf component of wind stress varying between -0.8 and 0.75 N m^{-2} were recorded. Variable and weaker winds prevailed from the middle of April until the end of the study period on 6 May 2014.

3.2. Flow regime

Time series of the vertical distributions of low-pass filtered current velocity displayed high variability and at times very high current speeds at both measurement sites (Fig. 2). From the beginning of measurements until the second half of January, outflow in the whole water column dominated (Fig. 2b) at the

thalweg while the current direction was opposite in the coastal zone of the southern gulf (Fig. 2d). During the next three weeks, inflow dominated in the whole water column at the thalweg and outflow in the coastal zone. Onwards, the highest values of inflow/outflow were observed mainly in the deep layer below 70 m depth reflecting the alternation of estuarine and reverse circulation. In the case of estuarine circulation, maximum inflow current speed in the deep layer was 36 cm s^{-1} and, in the case of its reversal, maximum outflow speed was 29 cm s^{-1} . In the cross-thalweg current velocity component, speeds less than 5 cm s^{-1} prevailed in the deep layer (Fig. 2c). Maximum along-coast current speed in the coastal zone was 27 cm s^{-1} in both directions. In the cross-coast current velocity component, speeds less than 5 cm s^{-1} prevailed in the whole water column (Fig. 2e). The occurrence of currents in opposite directions at the thalweg and in the coastal zone was typical for the flow regime from 9 December 2013 to 31 January 2014. The estimated coefficient of determination for the along-thalweg velocity component in the surface layer at the deep station and the along-coast velocity component at the shallow station was $r^2 = 0.51$.

3.3. Along-gulf distributions of salinity, oxygen and nutrients

On 9–10 December, a near-bottom saltwater wedge (salinity >9) was observed at stations A1–A7 (Fig. 3). Accordingly, stratification was stronger in the western gulf where at station A3 (the western border of the gulf) the bottom to surface density difference was 2.7 kg m^{-3} while in the eastern part the density difference was about 0.9 kg m^{-3} . Fresher water mass, with surface salinities of 5.7–6.0, extended down to 50 m depth at stations A10–A12. The oxygen and nutrient conditions in the deep layer were related to

the extent of the hypoxic saltwater wedge (Fig. 4a). Phosphate concentrations in the hypoxic layer varied around $4 \text{ }\mu\text{M}$ while concentrations $<2 \text{ }\mu\text{M}$ were observed in the near-bottom layer at the easternmost stations. In the surface layer, phosphate concentrations increased from $0.3 \text{ }\mu\text{M}$ at station A1 to $0.7 \text{ }\mu\text{M}$ in the eastern part of the transect (Fig. 4e). NO_x concentrations were very low in the hypoxic water and were the highest, up to $10 \text{ }\mu\text{M}$, in the near-bottom layer at stations A8 and A9 (Fig. 4c). In the surface layer, NO_x concentrations increased from $2 \text{ }\mu\text{M}$ to $5 \text{ }\mu\text{M}$ from west to east.

The saltwater wedge almost moved out from the gulf by the

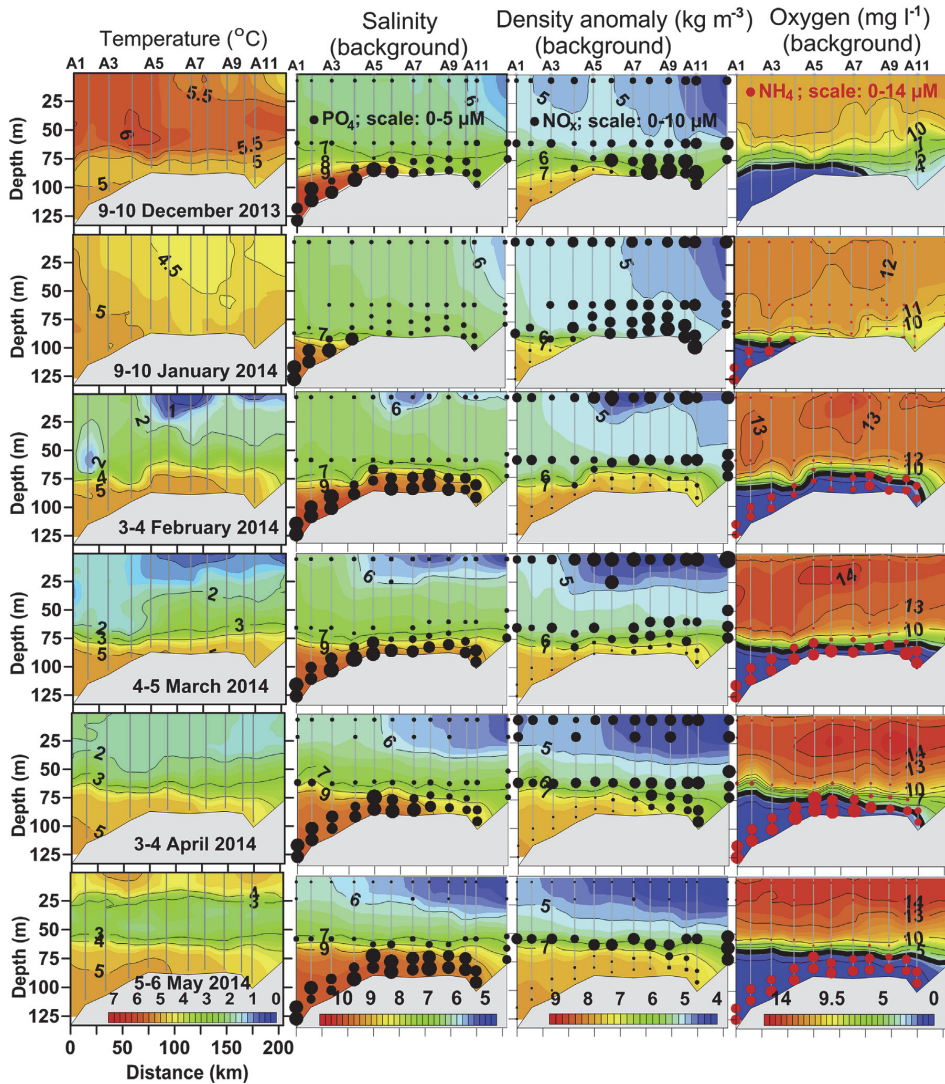


Fig. 3. Vertical sections of temperature, salinity, density anomaly and dissolved oxygen concentration on 9–10 December 2013 and on 9–10 January, 3–4 February, 4–5 March 3–4 April and 5–6 May 2014 along the thalweg of the Gulf of Finland from station A1 to station A12 (see Fig. 1). Color scales are shown in the lower panels. A black bold contour line (panels in the right column) marks the dissolved oxygen concentration of 2.9 mg l^{-1} (threshold concentration for hypoxia). Concentrations of PO_4^{3-} and NO_x are indicated as black dots and concentrations of NH_4^+ as red dots varying in size; scales are shown in the upper panels. Note that concentrations of NH_4^+ were not measured on 9–10 December 2013. Values on the x-axis indicate the distance from the westernmost station A1.

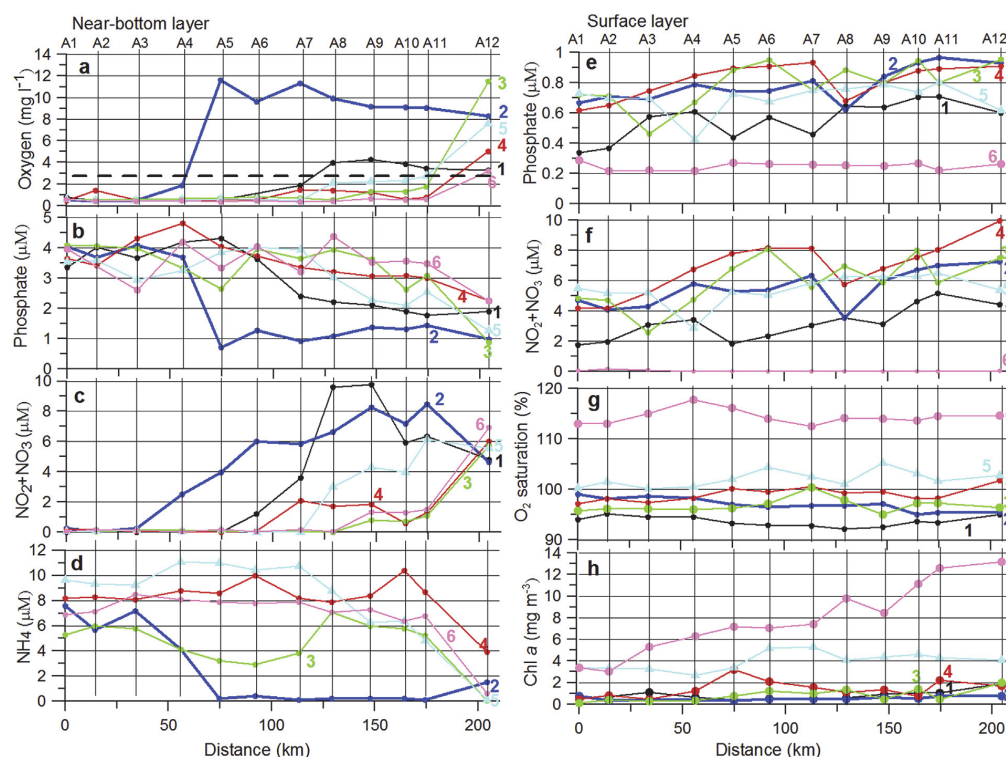


Fig. 4. Temporal variability of (a) dissolved oxygen, (b) phosphate, (c) NO_x , and (d) NH_4^+ concentrations in the near-bottom layer and (e) phosphate and (f) NO_x concentrations, (g) O_2 saturation and (h) Chl *a* content in the surface layer along the thalweg (A1–A12). Numbers 1–6 and corresponding colors indicate the numbers of the surveys.

second survey and was observed in the near-bottom layer only at stations A1–A4 on 9–10 January (Fig. 3). In the saltwater wedge, high NH_4^+ (up to 8 μM) and phosphate (up to 4 μM) and low oxygen ($<1 \text{ mg l}^{-1}$) and NO_x ($<0.3 \mu\text{M}$) concentrations were measured. A weakly stratified water column was observed at stations A5–A12, where the bottom to surface density difference varied between 0.1 and 0.4 kg m^{-3} . Oxygen concentrations varied from 8 to 12 mg l^{-1} , phosphate concentrations around 1 μM and NO_x concentrations from 4 to 8 μM while NH_4^+ concentrations were very low in the near-bottom layer (Fig. 4a–d). In general, phosphate and NO_x concentrations in the surface layer along the thalweg had increased by 0.2–0.3 μM and by 2–3 μM , respectively, if compared to the previous survey (except at station A8; Fig. 4e and f).

By 3–4 February, the saltwater wedge has filled the near-bottom layer in the gulf resulting in re-establishment of the halocline at the depths of 75–80 (Fig. 3). Patches of fresher water (salinity <6) were observed in the surface layer. In the saltwater wedge, oxygen concentrations were clearly below the threshold concentration for hypoxia (2.9 mg l^{-1}) and high concentrations of NH_4^+ (3–7 μM) and phosphates (2.5–4 μM) were measured (Fig. 4b and d) while NO_x concentrations were $<1 \mu\text{M}$. The water column above 75 m was well oxygenated, phosphate and NO_x concentrations at 60 m depth varied in the range of 0.7–1.0 μM and 3.5–6.5 μM , respectively. In the surface layer, phosphate and NO_x concentrations varied in a wide range from 0.4 to 1 μM and from 2 to 8 μM , respectively.

In the period between the third and fourth survey, outflow dominated in the near-bottom layer (Fig. 2b) and the halocline deepened by 4–5 March (Fig. 3). Fresher water appeared in the

25 m thick surface layer at stations A5–A12 resulting in the horizontal salinity gradient – the surface layer salinity decreased from 6.1 at station A4 to 4.7 at station A12. Hypoxic conditions and low NO_x concentrations ($<1 \mu\text{M}$) remained in the saltwater wedge. Concentrations of NH_4^+ (8–10 μM) and phosphates (3–5 μM) were increased in comparison with the previous survey (Fig. 4a–d). In the surface layer, phosphate and NO_x concentrations were increased and varied in the ranges from 0.6 to 1.0 μM and from 4 to 10 μM , respectively.

In March 2014, periods of outflow alternated with the periods of inflow in the near-bottom layer (Fig. 2b) and by 3–4 April, the halocline was observed in the western part of the gulf but it was almost absent at the easternmost stations (Fig. 3). Fresher surface layer was thicker (about 35 m) and had smaller horizontal extent covering stations from A12 to A6. The saltwater wedge observed at stations A1–A7, the concentrations of oxygen and NO_x remained very low, while concentrations of NH_4^+ increased (9–11 μM) and concentrations of phosphate decreased (3.3–4 μM) if compared with the previous survey (Fig. 4a–d). The decrease in phosphate and NH_4^+ concentrations and increase in NO_x concentrations in the near-bottom layer in the eastern part of the transect occurred most likely due to the temporary outflow between the surveys. In the surface layer, phosphate and NO_x concentrations, varying in the range of 0.6–0.8 μM and 3–6 μM , respectively, were decreased if compared with the previous survey.

On 5–6 May, the near-bottom saltwater wedge had the largest horizontal extent and vertical thickness resulting in a strong halocline at depths about 60 m at stations A1–A11. The fresher

surface layer had extended to station A3 forming a secondary halocline at depths about 25 m. The bottom to surface density difference exceeded 3 kg m^{-3} at all stations. In the saltwater wedge, oxygen concentrations were $<0.6 \text{ mg l}^{-1}$ and very low NO_x concentrations ($<0.2 \text{ }\mu\text{M}$) were measured at stations A1–A8. Concentrations of NH_4^+ varied within $7\text{--}8 \text{ }\mu\text{M}$ and concentrations of phosphates within $2\text{--}4.5 \text{ }\mu\text{M}$ (stations A1–A11). The surface layer was depleted of NO_x while phosphate concentrations varied between 0.2 and $0.3 \text{ }\mu\text{M}$ along the thalweg.

Oxygen concentrations in the surface layer increased from 11 mg l^{-1} , measured during the first survey, up to 14.5 mg l^{-1} by the end of observation period. A similar trend was observed in the oxygen saturation (Fig. 4g); during the first three surveys oxygen saturation was below 100% but increased from March to May 2014 to 115%. The observed high saturation was likely caused by the development of the spring bloom, clearly seen from the increase of chlorophyll *a* content in the surface layer (Fig. 4h).

Notably lower temporal variability of all measured parameters in the near-bottom layer was observed at the westernmost and easternmost stations in comparison with variability at stations A4–A11. At the westernmost stations A1–A3, the hypoxic conditions with very low oxygen concentrations ($<1 \text{ mg l}^{-1}$), low NO_x concentrations ($<0.3 \text{ }\mu\text{M}$), and high phosphate ($3.4\text{--}4.1 \text{ }\mu\text{M}$) and NH_4^+ ($5.3\text{--}9.5 \text{ }\mu\text{M}$) concentrations in the deep layer were observed during the whole measurement period. In the near-bottom layer at the easternmost station A12, oxygen concentrations ($3.3\text{--}11.5 \text{ mg l}^{-1}$) were above the threshold level of hypoxia and coincided with relatively high NO_x ($4.8\text{--}6.9 \text{ }\mu\text{M}$) and low phosphate ($0.9\text{--}2.3 \text{ }\mu\text{M}$) and NH_4^+ ($0.4\text{--}3.9 \text{ }\mu\text{M}$) concentrations during the whole study period.

Before the onset of the spring bloom, phosphate and NO_x concentrations increased from west to east in the surface layer varying from 0.35 to $0.73 \text{ }\mu\text{M}$ and $1.7\text{--}5.5 \text{ }\mu\text{M}$ at station A1 to $0.62\text{--}0.95 \text{ }\mu\text{M}$ and $4.4\text{--}9.9 \text{ }\mu\text{M}$ at station A12, respectively.

3.4. Temporal variability at the mooring stations

Time series of along-thalweg current velocity component, salinity and dissolved oxygen concentration revealed migrations of the near-bottom saltwater wedge at the deep mooring station A6 (Fig. 5c and d). Due to the migration of saltwater wedge out from the gulf, the near-bottom salinity decreased and oxygen concentration increased from the beginning of the measurements until 27 December 2013. The following about three-week period until 13 January corresponded to the situation with well-mixed water column (see Fig. 3). During the next week, the saltwater wedge moved back to the east over the measurement site and hypoxic conditions re-established in the near-bottom layer. It is interesting that during this period of saline water inflow in the near-bottom layer (until 3 February), the sea level dropped about 1 m in the gulf (Fig. 5a); thus, in general the outflow from the gulf prevailed. During the next month (until 3 March), the outflow with variable speed dominated in the near-bottom layer and as a result salinity decreased and oxygen concentration increased.

Oscillations of the boundary of the saltwater wedge were reflected in short-term variations of salinity and oxygen concentration at the depth of 5 m above the seabed, i.e. the CTD with oxygen sensor was located close to the upper boundary of the saltwater wedge. However, the temperature time series at about 1 m above the seabed showed that the saltwater wedge remained at the station A6 (Fig. 5e). Since 3 March, inflow with large variations of the near bottom velocity dominated and, by the end of March, the high saline hypoxic water covered the area. The oxygen and salinity changes at the mooring station were strongly correlated ($r^2 = 0.94$) during the whole measurement period.

4. Discussion

4.1. Along-gulf flow structure

The typical estuarine circulation pattern consists of an outflow in the surface layer and an inflow into the estuary in the deeper layers governed by the down-estuary barotropic pressure gradient and up-estuary baroclinic pressure gradient. Results of the present study show that different flow and stratification patterns could exist in the Gulf of Finland depending on the forcing characteristics. In the long-term, the core of outflow is located in the subsurface layer of the northern gulf and inflow in the deeper layers of the southern gulf (e.g. Andrejev et al., 2004) while in the signal of temporal variability, a two-layer structure with opposite flows in the surface and deeper layers arise (Elken et al., 2011). The latter imply that the estuarine circulation could often be reversed as a response to the strong westerly-southwesterly wind events (Elken et al., 2003). In extreme cases, especially in winter, vertical stratification could collapse in the central part of the gulf (Liblik et al., 2013) while, in summer, mostly three-layer stratification exists in the deep areas (Liblik and Lips, 2011).

Based on the measurement results from winter 2011–2012, Liblik et al. (2013) noticed that in the case of reversals of the estuarine circulation, a barotropic flow system was developed in the central, deep area of the gulf. Within the periods of shorter-term alterations from the estuarine to the reversed circulation, the layered flow with opposite directions in the surface and deeper layers prevailed. Similar general conclusions could also be made on the basis of the measurements in winter 2013–2014. Current measurements in the shallow area of the gulf during the latter study period revealed that in the case of the barotropic flow in the deep area, currents in opposite direction prevailed in the shallow area near the southern coast. Two periods with barotropic flow system could be identified – from the beginning of the study period until 10 January 2014 and from 11 January until 31 January. Within these two periods, the average along-thalweg current speed in the surface layer at the deep mooring was -4.7 cm s^{-1} and 12.4 cm s^{-1} , respectively; while the average along-coast current had opposite direction with a speed of 9.8 cm s^{-1} and -8.3 cm s^{-1} , respectively, at the shallow mooring. Thus, the flow structure in the first period was similar to the circulation pattern driven by spatially uniform longshore wind in lakes with up-wind flow in the center and down-wind flow along the coasts (Benet, 1974; Winant et al., 2014). The flow pattern in the second period agrees with the lateral structure of the along-estuary flow in weakly stratified tidal estuaries where the mixing asymmetry and lateral advection could play a significant role in the estuarine dynamics (Burchard et al., 2011).

Although tidal currents do not play a major role in the Baltic (Kullenberg, 1981; Lilover, 2012), there exist energetic self-oscillations of the system Baltic Sea – Gulf of Finland in the current velocity field (Lilover et al., 2011). The presence of current oscillations with the periods from 24 to 26 h, which correspond to the frequency band of seiches (Lilover et al., 2011), was confirmed by spectral analysis of non-smoothed current velocity time series at both mooring stations during the mentioned periods in December 2013–January 2014. It is interesting to underline that within the first period (until 10 January 2014), the amplitude of self-oscillations up to 20 cm s^{-1} was found while later, and as it is in general (Lilover et al., 2011), the characteristic speed of such oscillations was about 5 cm s^{-1} . When the saltwater wedge has reached the central gulf (the area where the mooring was deployed), the flow structure converted first to two-layer flow pattern and later, when also the fresher surface layer appeared at this measurement site, to three-layer flow pattern. The three-layer residual flow structure has also been shown for the relatively deep

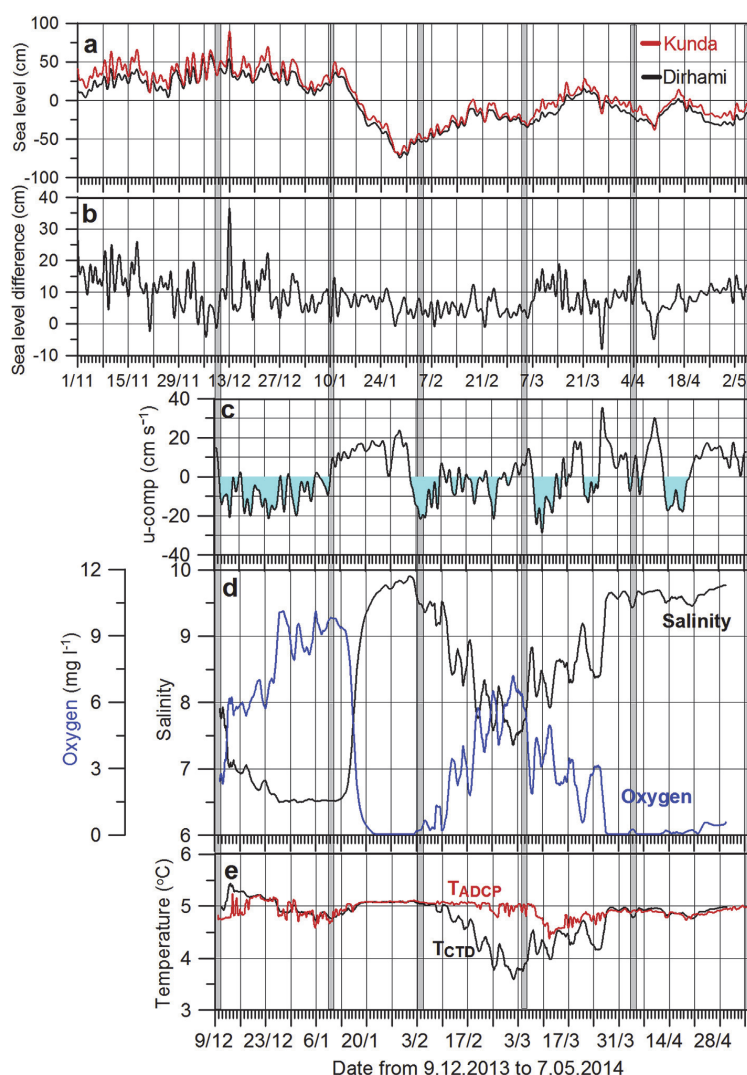


Fig. 5. Time series of (a) sea level at Kunda and Dirhami coastal stations and (b) sea level difference between these two stations. Time series of (c) along-thalweg current velocity component (blue shaded areas mark the outflow periods), (d) salinity (black line) and dissolved oxygen concentration (blue line) at the mooring station A6 (see Fig. 1) at the depth of 82 m (about 5 m above the seabed). (e) Time series of ADCP temperature (red line) at about 1 m above the seabed and CTD temperature (black line) at about 5 m above the seabed. All parameters are low-pass (36 h) filtered. (For interpretation of the references to colour in this figure legend, the reader is referred to the web version of this article.)

fjords where the mixing due to tidal currents does not occupy the whole water column (Valle-Levinson et al., 2014). We suggest that in winter 2013–2014, the shift from the barotropic to layered flow structure occurred due to a decrease in energy of oscillatory currents and re-stratification of the water column (further decreasing the mixing effect) when the wind forcing weakened and the relative role of baroclinic (buoyancy) forcing increased.

4.2. Along-gulf salinity (density) distribution patterns

Not much attention has been paid to the along-estuary distribution patterns of salinity (density) although the oxygen and nutrient conditions could largely be related to the transport and

retention of fresher and saltier waters inside the estuarine basin (e.g. Codiga, 2012). Data collected in the Gulf of Finland in winter 2013–2014 revealed large excursions of the boundaries between the different water masses in the near-bottom layer and the surface layer in response to the changing wind forcing. In the extreme case, the strong up-estuary wind event in December 2013–January 2014 flushed the fresher surface layer and the near-bottom saltwater wedge away from the central gulf. We estimated the positions of the isohaline 6.0 in the surface layer (5 m depth) and isohaline 9.0 in the deep layer (80 m depth) based on gridded salinity fields from each survey. It was found that the distance of isohalines 6.0 and 9.0 from the westernmost station A1 correlated well with the cumulative wind stress within a month before the survey. The monthly

time window was used since it has been shown earlier that the best correlation between the deep layer stratification (strength of the halocline) and along-gulf wind stress is achieved when 3–6 weeks average wind is applied (Liblik and Lips, 2011). The found coefficients of determination were as high as 0.62 for fresher surface layer extent and 0.76 for the near-bottom saltwater wedge extent. A similar impact of the along-estuary wind straining on layered flow and vertical stratification has been reported in the case of two-layer estuaries (Scully et al., 2005) while in the Gulf of Finland the water column could be better approximated by a three-layer structure.

In many theoretical studies of estuarine circulation, the along-estuary buoyancy (salinity) gradient has been assumed as a given (forcing) parameter related to the river discharge although it has been shown that the horizontal buoyancy gradient itself depends on other forcing factors as well as on the realized flow regime (e.g. Geyer and MacCready, 2014). As shown in the present study, the along-gulf horizontal gradient of salinity varied a lot from survey to survey with the high spatiotemporal variability in the surface and near-bottom layer while the variability stayed clearly lower in the intermediate layer (Fig. 6a). If taking into account the part of the study area, which could be considered as a channel with a roughly constant width extending from station A3 to station A11, the following parameters were estimated. The standard deviation of salinity along the constant depth decreased from 0.36 to 0.40 in the surface layer (1–10 m) to a minimum of 0.11 in the intermediate layer (42–48 m) and to the highest value of 1.20 in the deep layer (79 m; maximum analyzed depth was 82 m, where data at all stations during all surveys were available). The largest horizontal salinity differences along the thalweg were found for the surveys after the major stratification collapse when the near-bottom saltwater and fresher surface water moved back to the study area – in February and March 2014, respectively. The survey-based estimates of the average vertical difference of salinity between the 80 and 5 m depths (salinity stratification) were correlated with the cumulative wind stress ($r^2 = 0.58$) as it was also found between the positions of certain isohalines and cumulative wind stress.

Since the stratification and flow structure observed in the Gulf of Finland varied in large ranges, a comparison of this basin with other estuaries using the estuarine parameter space introduced by Geyer and MacCready (2014) was performed. The freshwater Froude number and mixing parameter were estimated as:

$$Fr_f = \frac{U_R}{(\beta g S_{BS} H)^{\frac{1}{2}}}$$

and

$$M^2 = \frac{C_D U_T^2}{\omega N_0 H^2}$$

respectively, where U_R is the river volume flux (value of $110 \text{ km}^3 \text{ yr}^{-1}$ was used) divided by the cross-section area, S_{BS} is the maximum bottom-to-surface salinity difference in the gulf, H is the depth, U_T is the amplitude of the depth-averaged velocity (self-oscillations in the gulf), ω is the frequency of oscillations, and N_0 is the buoyancy frequency for the maximum bottom-to-surface salinity difference. The following constants were used: $\beta = -7.7 \cdot 10^{-4}$, $g = 9.81 \text{ m s}^{-2}$ and $C_D = 1.2 \cdot 10^{-3}$.

The estimated freshwater Froude number for the Gulf of Finland of about 0.02 was higher than that referred by Geyer and MacCready (2014) for the Baltic Sea. It is in accordance with the knowledge that the Gulf of Finland receives more freshwater per a volume unit than the Baltic Sea (Bergström and Carlsson, 1994). The estimated mixing parameter varied in the range from 0.25 to 1.0 if the amplitude of oscillation velocity from 0.05 to 0.20 m s^{-1} was applied. Thus, the gulf should belong to the stratified estuaries, as expected, except when energetic self-oscillations are generated by atmospheric forcing (see Fig. 6 by Geyer and MacCready, 2014).

4.3. Oxygen and nutrient conditions in the near-bottom layer related to saltwater wedge dynamics

Earlier studies by Liblik et al. (2013) and Elken et al. (2014) showed that in the winter months, when the saline and thermal stratification is seasonally decreased in the gulf (e.g. Haapala and Alenius, 1994), the estuarine circulation reversal forced by westerly-southwesterly wind might lead to the temporary mixing of the whole water column along the thalweg. Thus, besides of high wintertime variability in salinity and current velocity, oxygen concentrations in the near-bottom layer could change dramatically due to the alternation between the stratified and mixed conditions (Liblik et al., 2013). The present study also documented the high

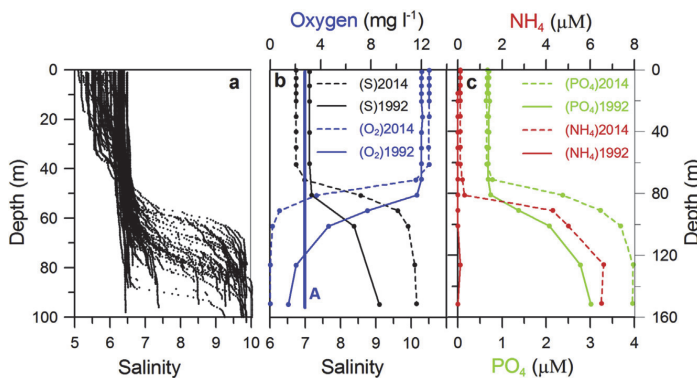


Fig. 6. (a) Vertical profiles of salinity measured at stations A3–A11 in the Gulf of Finland from December 2013 to May 2014. (b) Vertical profiles of salinity (black curves; solid curve indicates a profile from February 1992 and dashed curve from February 2014) and dissolved oxygen (blue curves). (c) Vertical profiles of phosphates (green curves) and ammonia (red curves). The profiles in the panels (b) and (c) are measured at the monitoring station H2 in the Northern Baltic Proper (see Fig. 1b). (For interpretation of the references to colour in this figure legend, the reader is referred to the web version of this article.)

variability of near-bottom nutrient conditions whereas the major changes in nutrient concentrations were associated with the along-gulf movements of the hypoxic saltwater wedge. This relationship between the dynamics of saltwater wedge, oxygen and nutrients is well seen in the graphs where oxygen and phosphate concentration are plotted against salinity in the near-bottom layer (Fig. 7; only data from the deepest horizon were used). Similar high linear correlation was found if data from the two deepest horizons (3–4 and 3–14 m above the seabed) were analyzed – $r^2 = 0.88$ between salinity and dissolved oxygen concentration and $r^2 = 0.86$ between salinity and phosphate concentration. This very high correlation of oxygen and phosphate concentration with salinity suggests that the enhanced phosphorus level in the near-bottom layer was mostly controlled by the saltwater wedge dynamics.

The changes in the phosphorus content in the deep layer between the consecutive surveys were calculated and compared with the estimates of sediment release of phosphorus in anoxic conditions and total riverine input of phosphorus to the gulf. The amount of phosphate-phosphorus in the near-bottom layer varied in large ranges from survey to survey with a maximum monthly change of about 2000 tons (Table 1). If assuming that the phosphorus flux in the hypoxic areas of the central gulf was between $19.0 \text{ kg P km}^{-2} \text{ yr}^{-1}$ (Lukkari et al., 2009) and $13 \text{ kg P km}^{-2} \text{ day}^{-1}$ (Pitkänen et al., 2001), one can estimate the amount of released phosphorus by multiplying these values by the average hypoxic area extent between the two consecutive surveys (Table 1). These estimates gave very different results with a lower limit much smaller than but a higher limit comparable to the observed changes of the phosphate-

phosphorus amount in the near-bottom hypoxic layer between the surveys. Nevertheless, since the correlation between the near-bottom salinity and phosphate concentration was very strong, the real fluxes should be between the obtained limit values and observed changes should mostly be related to the movements of the saltwater wedge, i.e. lateral transport between the Northern Baltic Proper and the Gulf of Finland. In the context of the external load of phosphorus to the gulf, which was estimated as 6370 tons per year based on the data from 2010 (HELCOM, 2015), the observed changes in the near-bottom layer were very high – these could be several times higher than the monthly load to the entire gulf.

4.4. Wintertime estuarine dynamics and eutrophication effects

Transport of hypoxic waters from the Northern Baltic Proper into the near-bottom layer of the Gulf of Finland has a major impact on the environmental conditions in the gulf causing an increase in phosphate content directly via horizontal advection and indirectly by creating favorable conditions for sediment release of phosphorus. Since the lateral transport of phosphorus in the near-bottom layer could be larger than the internal and external load, the conditions in the Northern Baltic Proper determine the conditions in the near-bottom layer of the Gulf of Finland. In the 1980s and early 1990s, when the stagnation of deep waters of the Baltic Proper had occurred, lower salinity and phosphate concentrations than in 2014 were observed in the Northern Baltic Proper (Fig. 7b and c). Thus, at present, the lateral transport of phosphorus to the

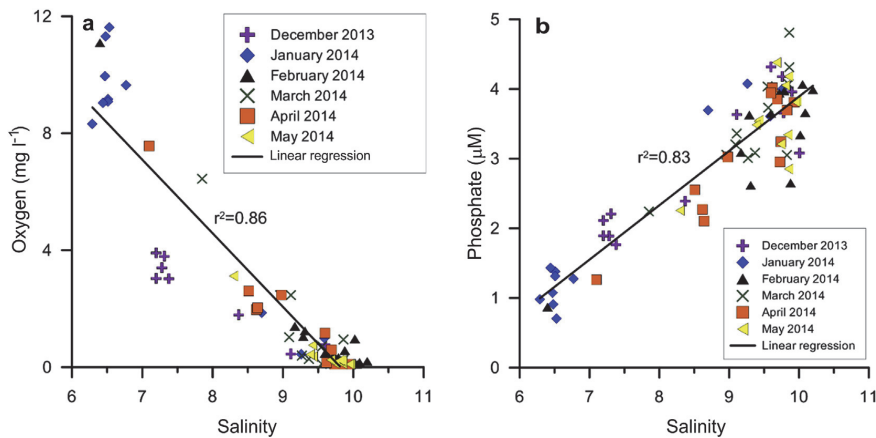


Fig. 7. (a) Near-bottom oxygen concentration versus salinity and (b) near-bottom phosphate concentration versus salinity with corresponding linear regression lines based on the measurements at stations A1–A12 (see Fig. 1) in the Gulf of Finland during six surveys from December 2013 to May 2014.

Table 1

Estimated area and volume of hypoxic waters, amount of phosphorus in the deep layer below 60 m depth and estimates of sediment phosphorus release from the hypoxic area in the Gulf of Finland (between stations A3 and A11, see Fig. 1) based on the six surveys from December 2013 to May 2014. For the phosphorus release estimates the flux intensities of $19 \text{ kg P km}^{-2} \text{ yr}^{-1}$ (Lukkari et al., 2009) and $13 \text{ kg P km}^{-2} \text{ day}^{-1}$ (Pitkänen et al., 2001) were applied.

Survey no	Dates	Area of hypoxic waters (km ²)	Volume of hypoxic waters (km ³)	Amount of phosphorus (tons)	Estimates of phosphorus release (tons/month)
1	9–10 December 2013	760	4.8	2990	
2	9–10 January 2014	100	0.4	1990	0.7/168
3	3–4 February 2014	1550	11.0	4010	1.3/322
4	4–5 March 2014	1070	6.1	3740	2.1/511
5	3–4 April 2014	1610	13.9	3630	2.1/523
6	5–6 May 2014	2620	31.3	4540	3.4/825

Gulf of Finland is potentially higher than 25 years ago. If also taking into account the increased frequency of complete mixing in the Gulf of Finland in winters (Elken et al., 2014), which creates vertical fluxes of phosphate-phosphorus, the impact is amplified further. Wintertime collapses of stratification could temporarily improve the near-bottom oxygen conditions, but the deep layer phosphorus will be mixed upward in the water column, thus, likely intensifying the effects of eutrophication and probability of occurrence of cyanobacterial blooms (Pitkänen et al., 2001; Vahtera et al., 2007).

Indirectly the influence of the lateral transport in the near-bottom layer and vertical mixing during the stratification collapses can be seen from the temporal courses of phosphate concentration in the surface layer of the study area (Fig. 5e). Between the first and the second survey, phosphate concentrations increased significantly along the transect and in February–March (before the spring bloom) concentrations in the central part of the transect were as high as at the easternmost stations. Furthermore, the hypoxic area formed by May 2014 in the Gulf of Finland had very large extent – it was estimated as 2620 km² that is about twice as large as the area estimated based on similar measurements in 2011–2012 (Liblik et al., 2013). According to the environmental monitoring data (not presented here), the hypoxic layer below 60–70 m depth remained in the gulf until early November 2014.

Nevertheless, the recent major Baltic inflow (Mohrholz et al., 2015), which has resulted in distinct changes in the oxygen and nutrient conditions in the deep layers of the Gotland Deep, could also influence the oxygen conditions in the deep layers of the Northern Baltic Proper and the near-bottom phosphorus flux into the Gulf of Finland. The impact of the major Baltic inflows, as well as more accurate quantification of nutrient fluxes between the Baltic sub-basins and through the sediment–water interface, could be the topics of future studies.

5. Conclusions

Targeted measurement campaign from December 2013 to May 2014 revealed the establishment of distinct residual circulation patterns, large variations in vertical stratification and along-thalweg salinity distribution as well as dramatic changes in oxygen and nutrient conditions in the Gulf of Finland. In the case of strong and long enough up-estuary wind event, resulting in a collapse of vertical stratification, the residual circulation was established as a barotropic flow system consisting of outflow in the open gulf and inflow along the coasts. Such flow structure is similar to the circulation pattern occurring in large lakes with up-wind flow in the deep areas and down-wind flow in the shallow coastal areas (Bennet, 1974; Winant et al., 2014). In the periods without such unidirectional wind forcing, but when the water column remained weakly stratified, the residual barotropic inflow in the open gulf (in the deep area) and outflow along the coasts was established in accordance with the estuarine circulation pattern largely influenced by mixing asymmetry and lateral advection in weakly stratified estuaries (Burchard et al., 2011). In the case of moderate wind forcing, the three-layer vertical stratification and flow structure developed in the deeper part of the gulf most probably due to the shift to buoyancy controlled flow in the surface and near-bottom layer.

We showed that the along-gulf expansion of the fresher water tongue in the surface layer as well as the up-estuary penetration of the saltwater wedge in the near-bottom layer followed well the long-term changes in the cumulative along-gulf wind stress. The dynamics of the near-bottom saltwater wedge determined the extent of hypoxic bottoms in the gulf and the nutrient conditions in the near-bottom layer, which potentially affected the winter pool of nutrients available for the phytoplankton growth in the next

spring–summer. The firm correlation of both the near-bottom oxygen content and the near-bottom phosphate concentration with the near-bottom salinity suggests that the transport of phosphorus from the Northern Baltic Proper overruled possible local fluxes of phosphorus from the sediments in the Gulf of Finland in winter. The estimated flux of phosphorus by the saltwater wedge could be higher than the present monthly waterborne input of phosphorus into the gulf from all sources (HELCOM, 2015). Taking into account this amount of transported phosphorus, strengthened vertical stratification in the Northern Baltic Proper and suggested increase in the frequency of stratification collapses in the Gulf of Finland (Elken et al., 2014), we predict that the eutrophication effects would not diminish significantly in this estuary in the nearest future.

Acknowledgements

This work was supported by institutional research funding IUT 19-6 of the Estonian Ministry of Education, Estonian Science Foundation grant No. 9382 and Estonian Research Council grant PUT595. We are thankful to Fred Buschmann for performing oxygen measurements; to Aet Meerits, Kati Lind and Anne-Ly Sirel for performing nutrient and chlorophyll analyses; Tarmo Kõuts for providing Tallinnamadal wind data. Likewise, we thank the crew of RV Salme and our colleagues (Villu Kikas, Andres Trei, Germa Väli and others) for their help during field measurements and sampling.

References

- Alenius, P., Myrberg, K., Nekrasov, A., 1998. The physical oceanography of the Gulf of Finland: a review. *Boreal Environ. Res.* 3, 97–125.
- Alenius, P., Nekrasov, A., Myrberg, K., 2003. Variability of the baroclinic Rossby radius in the Gulf of Finland. *Cont. Shelf Res.* 23, 563–573.
- Andrejev, O., Myrberg, K., Alenius, P., Lundberg, P.A., 2004. Mean circulation and water exchange in the Gulf of Finland – a study based on three-dimensional modeling. *Boreal. Environ. Res.* 9, 1–16.
- Ammerman, J., 2001. QuikChem® Method 31-115-01-1-I – Determination of Orthophosphate by Flow Injection Analysis. Lachat Instruments.
- Bennet, J.R., 1974. On the dynamics of wind-driven lake currents. *J. Phys. Oceanogr.* 4, 400–414.
- Bergström, S., Carlsson, B., 1994. River runoff to the Baltic Sea: 1950–1990. *Ambio* 23, 280–287.
- Burchard, H., Hetland, R.D., Schulz, E., Schuttelaars, H.M., 2011. Drivers of residual estuarine circulation in tidally energetic estuaries: straight and irrotational channels with parabolic cross section. *J. Phys. Oceanogr.* 41, 548–570.
- Butterworth, S., 1930. On the theory of filter amplifiers. *Exp. Wirel. Eng.* 7, 536–541.
- Codiga, D.L., 2012. Density stratification in an estuary with complex geometry: Driving processes and relationship to hypoxia on monthly to inter-annual timescales. *J. Geophys. Res.* 117. <http://dx.doi.org/10.1029/2012JC008473>. C12004.
- Conley, D.J., Björck, S., Bonsdorff, E., Carstensen, J., Destouni, G., Gustafsson, B.G., Hietanen, S., Kortekaas, M., Kuosa, H., Meier, H.E.M., Müller-Karulis, B., Nordberg, K., Norkko, A., Nürnberg, G., Pitkänen, H., Rabalais, N.N., Rosenberg, R., Savchuk, O.P., Slomp, C.P., Voss, M., Wulff, F., Zillen, L., 2009. Hypoxia related processes in the Baltic Sea. *Environ. Sci. Technol.* 43, 3412–3420.
- Egan, L., 2000. QuikChem® Method 31-107-04-1-D – Determination of Nitrate and/or Nitrite in Brackish Waters by Flow Injection Analysis. Lachat Instruments.
- Elken, J., Raudsepp, U., Lips, U., 2003. On the estuarine transport reversal in deep layers of the Gulf of Finland. *J. Sea Res.* 49, 267–274.
- Elken, J., Nömm, M., Lagamaa, P., 2011. Circulation patterns in the Gulf of Finland derived from the EOF analysis of model results. *Boreal Environ. Res.* 16, 84–102.
- Elken, J., Raudsepp, U., Laanemets, J., Passenko, J., Maljutenko, I., Pärn, O., Keevallik, S., 2014. Increased frequency of wintertime stratification collapse events in the Gulf of Finland since the 1990s. *J. Mar. Syst.* 129, 47–55.
- Geyer, W.R., MacCready, P., 2014. The estuarine circulation. *Annu. Rev. Fluid Mech.* 46, 175–197.
- Grasshoff, K., Ehrhardt, M., Kremling, K., 1999. *Methods of Seawater Analysis*, third ed. Wiley-VCH, Weinheim.
- Haapala, J., Alenius, P., 1994. Temperature and salinity statistics for the northern Baltic Sea 1961–1990. *Finn. Mar. Res.* 262, 51–121.
- HELCOM, 2009. Eutrophication in the Baltic Sea – an integrated thematic assessment of the effects of nutrient enrichment and eutrophication in the Baltic Sea region. *Balt. Sea Environ. Proc.* No. 115B, 148, 148 pp.
- HELCOM, 2014. Eutrophication status of the Baltic Sea 2007–2011 – a concise

- thematic assessment. *Balt. Sea Environ. Proc.* No. 143, 41 pp.
- HELCOM, 2015. Updated fifth Baltic Sea pollution load compilation (PLC-5.5). *Balt. Sea Environ. Proc.* No. 145, 142 pp.
- Jäntti, H., Hietanen, H., 2012. The effects of hypoxia on sediment nitrogen cycling in the Baltic Sea. *Ambio* 41, 161–169. <http://dx.doi.org/10.1007/s13280-011-0233-6>.
- Kullenberg, G., 1981. Physical oceanography. In: Voipoi, A. (Ed.), *The Baltic Sea*, vol. 30. Elsevier Oceanography Series, pp. 135–218.
- Launiainen, J., Saarinen, J., 1984. Marine wind characteristics in the northern Baltic Sea, Finnish. *Mar. Res.* 250, 52–86.
- Leppäranta, M., Myrberg, K., 2009. *Physical Oceanography of the Baltic Sea*. Praxis publishing, Chester, UK.
- Liblik, T., Lips, U., 2011. Characteristics and variability of the vertical thermohaline structure in the Gulf of Finland in summer. *Boreal Environ. Res.* 16 (A), 73–83.
- Liblik, T., Laanemets, J., Raudsepp, U., Elken, J., Suhhova, I., 2013. Estuarine circulation reversals and related rapid changes in winter near-bottom oxygen conditions in the Gulf of Finland, Baltic Sea. *Ocean Sci.* 9, 917–930.
- Lilover, M.-J., 2012. Tidal currents as estimated from ADCP measurements in “practically non-tidal” Baltic Sea. In: *Baltic International Symposium (BALTIC)*, 2012. IEEE/OES, pp. 1–4. <http://dx.doi.org/10.1109/BALTIC.2012.6249181>.
- Lilover, M.-J., Pavelson, J., Kouts, T., 2011. Wind forced currents over the shallow Naissaar bank in the Gulf of Finland. *Boreal Environ. Res.* 16 (A), 164–174.
- Lips, U., Lips, I., Liblik, T., Elken, J., 2008. Estuarine transport versus vertical movement and mixing of water masses in the Gulf of Finland (Baltic Sea). In: *US/EU-Baltic International Symposium*, 2008. IEEE/EOS, pp. 1–8. <http://dx.doi.org/10.1109/BALTIC.2008.4625535>.
- Lukkari, K., Leivuori, M., Kotilainen, A., 2009. The chemical character and behaviour of phosphorus in poorly oxygenated sediments from open sea to organic-rich inner bay in the Baltic Sea. *Biogeochemistry* 96, 25–48.
- Matthäus, W., Franck, H., 1992. Characteristics of major Baltic inflows — a statistical analysis. *Cont. Shelf Res.* 12, 1375–1400.
- Meier, H.E.M., Feistel, R., Piechura, J., Arneborg, L., Burchard, H., Fiekas, V., Golenko, N., Kuzmina, N., Mohrholz, V., Nohr, C., Paka, V.T., Sellschop, J., Stips, A., Zhurbas, V., 2006. Ventilation of the Baltic Sea deep water: a brief review of present knowledge from observations and models. *Oceanologia* 48 (5), 133–164.
- Mohrholz, V., Naumann, M., Nausch, G., Krüger, S., Gräwe, U., 2015. Fresh oxygen for the Baltic Sea — an exceptional saline inflow after a decade of stagnation. *J. Mar. Syst.* 148, 152–166.
- Pitkänen, H., Lehtoranta, J., Räike, A., 2001. Internal nutrient fluxes counteract decreases in external load: the case of the estuarial eastern Gulf of Finland, Baltic Sea. *Ambio* 30, 195–201.
- Scully, M.E., Friedrichs, C., Brubaker, J., 2005. Control of estuarine stratification and mixing by wind-induced straining of the estuarine density field. *Estuaries* 28, 321–326.
- Selfert, T., Tauber, F. and Kayser, B., 2001. A high resolution spherical grid topography of the Baltic Sea. second ed., *Baltic Sea Science Congress*, Stockholm, 25–29 November 2001, Poster No. 147, Abstr. Vol., [<http://www.iowarnemuende.de/iowtopo>].
- Vahtera, E., Conley, D.J., Gustafsson, B.G., Kuosa, H., Pitkänen, H., Savchuk, O.P., Tamminen, T., Viitasalo, M., Voss, M., Wasmund, N., Wulff, F., 2007. Internal ecosystem feedbacks enhance nitrogen-fixing cyanobacteria blooms and complicate management in the Baltic Sea. *Ambio* 36, 186–194.
- Valle-Levinson, A., Cacares, M.A., Pizarro, O., 2014. Variations of tidally driven three-layer residual circulation in fjords. *Ocean. Dyn.* 64, 459–469.
- Winant, C., Valle-Levinson, A., Ponte, A., Winant, C., Gutierrez-de-Velasco, G., Winters, G., 2014. Observations on the lateral structure of wind-driven flows in a stratified, semiarid bay of the Gulf of California. *Estuaries Coasts* 37, 1319–1328.

Curriculum vitae

Personal data

Name: Irina Suhhova
Date of birth: 30 July 1984
Place of birth: Russia
Citizenship: Estonian

Contact data

E-mail: irina.suhhova@taltech.ee

Education

2010–2018 Tallinn University of Technology – PhD
2008–2010 Tallinn University of Technology, Natural Sciences and Engineering;
Geosciences – MSC,
2003–2007 Estonian Maritime Academy, Hydrometeorology – BSC
2000–2003 High school

Language competence

Russian – Native
Estonian – Fluent
English – Fluent

Professional employment

2013–present Tallinn University of Technology, Department of Marine Systems,
Junior researcher.
2010–2013 Tallinn University of Technology, Department of Marine Systems,
Engineer.

Scientific work

Publications according ETIS

1.1.

- Suhhova, I.; Liblik, T.; Liloover, M.-J.; Lips, U. (2018). A descriptive analysis of the linkage between the vertical stratification and current oscillations in the Gulf of Finland. *Boreal Environment Research*, 23, 83–103.
- Liloover, M.-J.; Elken, J.; Suhhova, I.; Liblik, T. (2017). Observed flow variability along the thalweg, and on the coastal slopes of the Gulf of Finland, Baltic Sea. *Estuarine, coastal and shelf science*, 195, 23–33.10.1016/j.ecss.2016.11.002.
- Lips, Urmas; Laanemets, Jaan; Lips, Inga; Liblik, Taavi; Suhhova, Irina; Suursaar, Ülo (2017). Wind-driven residual circulation and related oxygen and nutrient dynamics in the Gulf of Finland (Baltic Sea) in winter. *Estuarine Coastal and Shelf Science*, 195, 4–15.10.1016/j.ecss.2016.10.006.
- Suhhova, Irina; Pavelson, Juss; Lagemaa, Priidik (2015). Variability of currents over the southern slope of the Gulf of Finland. *Oceanologia*, 132–143.
- Liblik, Taavi; Laanemets, Jaan; Raudsepp, Urmas; Elken, Jüri; Suhhova, Irina. (2013). Estuarine circulation reversals and related rapid changes in winter near-bottom oxygen conditions in the Gulf of Finland, Baltic Sea. *Ocean Science*, 9, 917–930.10.5194/os-9-917-2013.

3.1.

- Erm, Ants; Maljutenko, Ilja; Buschmann, Fred; Suhhova, Irina; Meerits, Aet (2014). Stormwater impact on the coastal area of the Tallinn Bay. *2014 IEEE/OES Baltic International Symposium (BALTIC 2014): 2014 IEEE/OES Baltic International*

- Symposium, 24-27.04.2014, Tallinn. Institute of Electrical and Electronics Engineers (IEEE), 308–321.10.1109/BALTIC.2014.6887867.*
- Lagemaa, Priidik; Suhhova, Irina; Nõmm, Marden; Pavelson, Juss; Elken, Jüri (2010). Comparison of Current Simulations by the State-of-the-Art Operational Models in the Gulf of Finland with ADCP Measurements. *IEEE/OES Baltic 2010 International Symposium: IEEE/OES Baltic 2010 International Symposium, 25-27 August 2010, Riga. IEEE, 1–11. (IEEE Conference Proceedings).10.1109/BALTIC.2010.5621656.*
- 3.2.
- Talsepp, L.; J. Elken, T. Kõuts, M.-J.Lilover, I.Suhova (2010). Hydrophysical processes in the gulf of Finland inferred from bottom-mounted ADCP measurements. In: H. O. Andrassdottir (Ed.). Proceedings of the 14th International Workshop on Physical Processes in Natural Waters, June 28 - July 1, Reykjavik, Iceland (138–139). Reykjavík, Iceland: University of Iceland.
- 3.4.
- Erm, Ants; Buschmann, Fred; Maljutenko, Ilja; Kolesova, Natalja; Suhhova, Irina (2013). Investigation of pollution sources and transport mechanisms along the south-east coast of Tallinn Bay. *Finnish, Estonian and Russian researchers planned joint research for the Gulf of Finland Year 2014: The Gulf of Finland Scientific Forum, Tallinn, 16 - 17 Oct 2013. Suomen Ympäristökeskus.*
- 5.2.
- Lagemaa, Priidik; Suhhova, Irina; Pavelson, Juss; Elken, Jüri (2014). Current Simulations and observations in the Gulf of Finland. *Ocean Sciences Meeting 2014, Honolulu, Hawaii USA, 23-28 February 2014. <http://www.sgmeet.com/osm2014/viewabstract.asp?abstractid=15881>.*
- Erm, Ants; Buschmann, Fred; Maljutenko, Ilja; Suhhova, Irina; Kolesova, Natalja; Voll, Martin; Listak, Madis (2013). Algae Blooms on a Tallinn City Beach: a Case Study. *BSSC 9th Baltic Sea Science Congress 2013 : New Horizons for Baltic Sea Science, 26-30 August, 2013, Klaipeda, Lithuania, Abstract Book: BSSC 9th Baltic Sea Science Congress, Klaipeda, Lithuania, 26-30 August, 2013. Coastal Research and Planning Institute of Klaipeda University (KU CORPI), 38.*
- Suhhova, I.; Liblik, T.; Lips, U.; Pavelson, J. (2013). Temporal patterns of vertical mixing in the stratified Gulf of Finland. *Baltic Sea Science Congress 2013 New Horizons for Baltic Sea Science; 26-30 August 2013; Klaipeda, Lithuania: Abstract book Baltic Sea Science Congress 2013. 115–115.*

Elulookirjeldus

Isikuandmed

Nimi: Irina Suhhova
Sünniaeg: 30 Juuli 1984
Sünnikoht: Venemaa
Kodakondsus: Eesti

Kontaktandmed

E-post: irina.suhhova@taltech.ee

Hariduskäik

2010–2018 Tallinna Tehnikaülikool – PhD
2008–2010 Tallinna Tehnikaülikool, Matemaatika-Loodusteaduskond – MSC
2003–2007 Eesti Mereakadeemia, Hüdro meteoroloogia – BSC
2000–2003 Keskharidus

Keelteoskus

Vene keel – Emakeel
Eesti keel – Kõrgtase
Inglise keel – Kõrgtase

Teenistuskäik

2013 – tänaseni TTÜ Meresüsteemide Instituut, Nooremteadur
2010 – 2013 TTÜ Meresüsteemide Instituut, insener

Teadustegevus

Publikatsioonid Eesti Teadusinfosüsteemi klassifikaatori järgi

1.1.

Suhhova, I.; Liblik, T.; Liloover, M.-J.; Lips, U. (2018). A descriptive analysis of the linkage between the vertical stratification and current oscillations in the Gulf of Finland. *Boreal Environment Research*, 23, 83–103.

Liloover, M.-J.; Elken, J.; Suhhova, I.; Liblik, T. (2017). Observed flow variability along the thalweg, and on the coastal slopes of the Gulf of Finland, Baltic Sea. *Estuarine, coastal and shelf science*, 195, 23–33.10.1016/j.ecss.2016.11.002.

Lips, Urmas; Laanemets, Jaan; Lips, Inga; Liblik, Taavi; Suhhova, Irina; Suursaar, Ülo (2017). Wind-driven residual circulation and related oxygen and nutrient dynamics in the Gulf of Finland (Baltic Sea) in winter. *Estuarine Coastal and Shelf Science*, 195, 4–15.10.1016/j.ecss.2016.10.006.

Suhhova, Irina; Pavelson, Juss; Lagemaa, Priidik (2015). Variability of currents over the southern slope of the Gulf of Finland. *Oceanologia*, 132–143.

Liblik, Taavi; Laanemets, Jaan; Raudsepp, Urmas; Elken, Jüri; Suhhova, Irina. (2013). Estuarine circulation reversals and related rapid changes in winter near-bottom oxygen conditions in the Gulf of Finland, Baltic Sea. *Ocean Science*, 9, 917–930.10.5194/os-9-917-2013.

3.1.

Erm, Ants; Maljutenko, Ilja; Buschmann, Fred; Suhhova, Irina; Meerits, Aet (2014). Stormwater impact on the coastal area of the Tallinn Bay. *2014 IEEE/OES Baltic International Symposium (BALTIC 2014): 2014 IEEE/OES Baltic International Symposium, 24-27.04.2014, Tallinn*. Institute of Electrical and Electronics Engineers (IEEE), 308–321.10.1109/BALTIC.2014.6887867.

- Lagemaa, Priidik; Suhhova, Irina; Nõmm, Marden; Pavelson, Juss; Elken, Jüri (2010). Comparison of Current Simulations by the State-of-the-Art Operational Models in the Gulf of Finland with ADCP Measurements. *IEEE/OES Baltic 2010 International Symposium: IEEE/OES Baltic 2010 International Symposium*, 25-27 August 2010, Riga. IEEE, 1-11. (IEEE Conference Proceedings).10.1109/BALTIC.2010.5621656.
- 3.2.
- Talsepp, L.; J. Elken, T. Kõuts, M.-J.Lilover, I.Suhova (2010). Hydrophysical processes in the gulf of Finland inferred from bottom-mounted ADCP measurements. In: H. O. Andradottir (Ed.). *Proceedings of the 14th International Workshop on Physical Processes in Natural Waters*, June 28 - July 1, Reykjavík, Iceland (138-139). Reykjavík, Iceland: University of Iceland.
- 3.4.
- Erm, Ants; Buschmann, Fred; Maljutenko, Ilja; Kolesova, Natalja; Suhhova, Irina (2013). Investigation of pollution sources and transport mechanisms along the south-east coast of Tallinn Bay. *Finnish, Estonian and Russian researchers planned joint research for the Gulf of Finland Year 2014: The Gulf of Finland Scientific Forum*, Tallinn, 16 - 17 Oct 2013. Suomen Ympäristökeskus.
- 5.2.
- Lagemaa, Priidik; Suhhova, Irina; Pavelson, Juss; Elken, Jüri (2014). Current Simulations and observations in the Gulf of Finland. *Ocean Sciences Meeting 2014, Honolulu, Hawaii USA, 23-28 February 2014*. <http://www.sgmeet.com/osm2014/viewabstract.asp?abstractid=15881>.
- Erm, Ants; Buschmann, Fred; Maljutenko, Ilja; Suhhova, Irina; Kolesova, Natalja; Voll, Martin; Listak, Madis (2013). Algae Blooms on a Tallinn City Beach: a Case Study. *BSSC 9th Baltic Sea Science Congress 2013 : New Horizons for Baltic Sea Science, 26-30 August, 2013, Klaipeda, Lithuania, Abstract Book: BSSC 9th Baltic Sea Science Congress, Klaipeda, Lithuania, 26-30 August, 2013*. Coastal Research and Planning Institute of Klaipeda University (KU CORPI), 38.
- Suhhova, I.; Liblik, T.; Lips, U.; Pavelson, J. (2013). Temporal patterns of vertical mixing in the stratified Gulf of Finland. *Baltic Sea Science Congress 2013 New Horizons for Baltic Sea Science; 26-30 August 2013; Klaipeda, Lithuania: Abstract book Baltic Sea Science Congress 2013*. 115-115.